Climate Monitoring and Diagnostics Laboratory

No. 22

Summary Report 1993

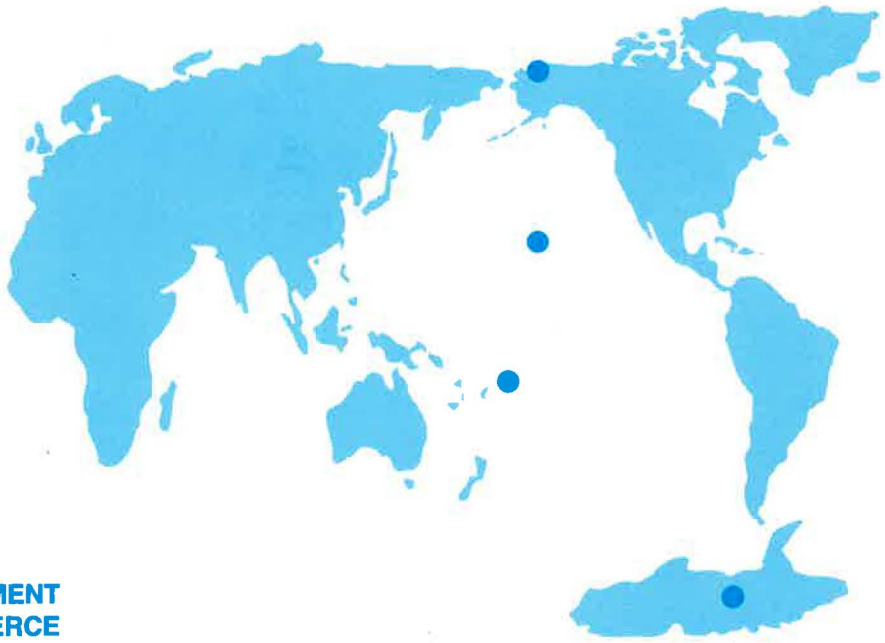

U.S. DEPARTMENT
OF COMMERCE

NATIONAL
OCEANIC AND
ATMOSPHERIC
ADMINISTRATION

ENVIRONMENTAL
RESEARCH
LABORATORIES

Climate Monitoring and Diagnostics Laboratory No. 22

Summary Report 1993

James T. Peterson, Editor
Rita M. Rosson, Assistant Editor

Boulder, Colorado

December 1994

U.S. DEPARTMENT OF COMMERCE
Ronald H. Brown, Secretary

National Oceanic and Atmospheric Administration
D. James Baker, Under Secretary for Oceans and Atmosphere/Administrator

Environmental Research Laboratories
James L. Rasmussen, Director

NOTICE

Mention of a commercial company or product does not constitute an endorsement by NOAA Environmental Research Laboratories. Use for publicity or advertising purposes of information from this publication concerning proprietary products or the tests of such products is not authorized.

For sale by the National Technical Information Service, 5285 Port Royal Road
Springfield, VA 22161

Contents

CMDL Organization, 1993

The CMDL organization structure features five divisions organized according to scientific discipline as follows: (1) Carbon Cycle; (2) Nitrous Oxide and Halocarbons; (3) Aerosols, Radiation, Ozone and Water Vapor; (4) Acquisition and Data Management; and (5) Observatory Operations. The Office of the Director includes administrative and special project staff. At the end of 1993, the laboratory staff consisted of 47 civil service personnel (excluding part-time student assistants), 30 CIRES/University of Colorado personnel, and two NOAA Corps officers as well as several visitors and people on special appointments.

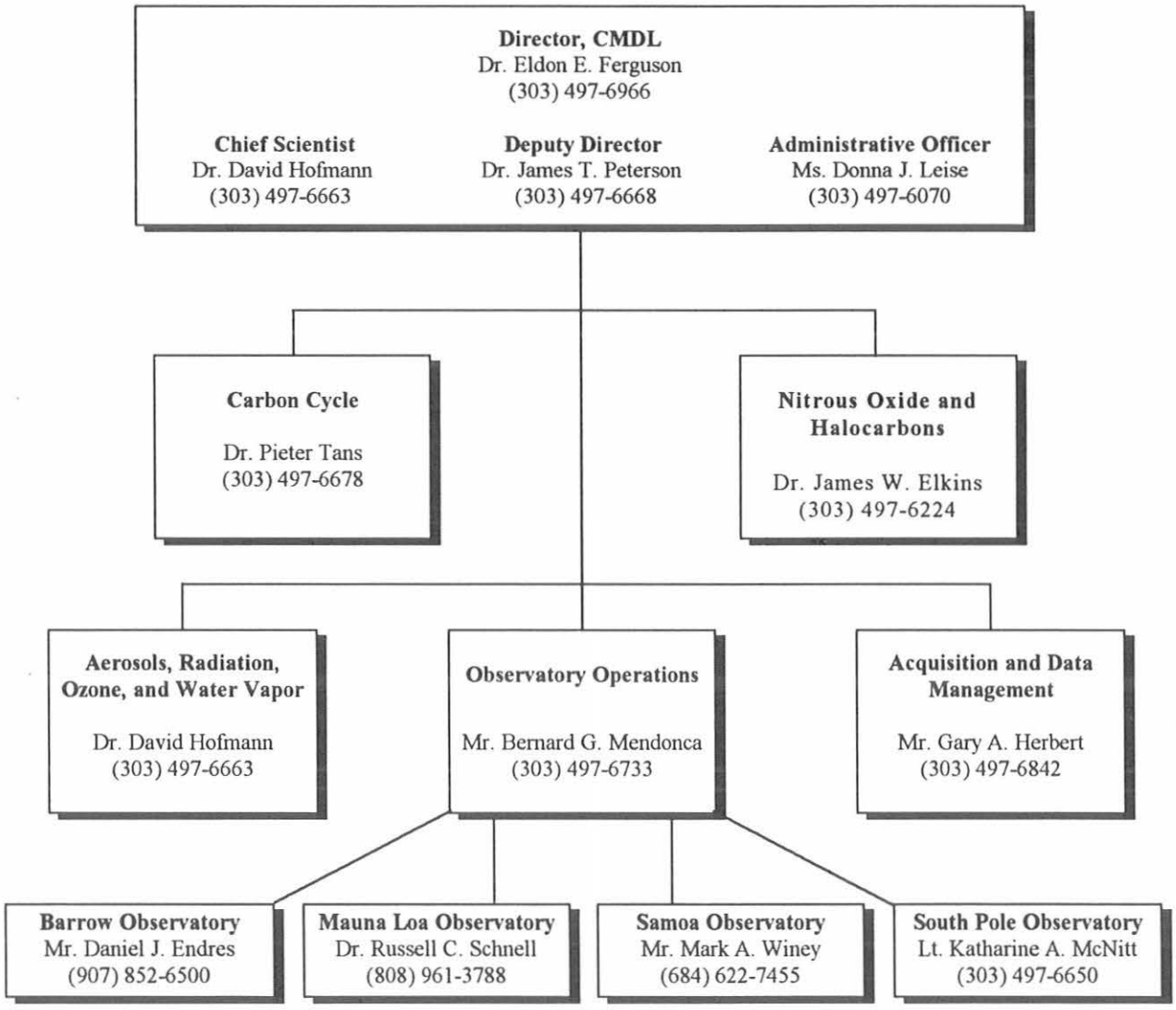

CMDL Staff, 1993

Director's Office

Eldon Ferguson, Director
James T. Peterson, Deputy Director
Donna Leise, Administrative Officer
Sandra Howe, Administrative Assistant
Carole Brandes, Secretary
Rita Rosson, Editorial Assistant
Denise Theede, Program Support Technician

Special Projects

Shuji Aoki, Visiting Scientist
Howard Bridgman, Visiting Scientist
Xing Sheng Li, Visiting Scientist
Craig Quincy, Contractor
Patrick Sheridan, CIRES

Aerosols, Radiation, Ozone & Water Vapor Division

David Hofmann, Chief
Jill Foose, Secretary
Jennifer Barnett, Physical Science Aid
Barry Bodhaine, Meteorologist
Paul Chilson, Physical Science Aid
Mark Clark, CIRES
John DeLuisi, Meteorologist
Sean Dougherty, Physical Science Aid
Ellsworth Dutton, Meteorologist
Robert Evans, CIRES
Douglas Garcia, Summer Aid
Jason Gingerich, Physical Science Aid
Helena Gonzalez-Jorge, Guest Worker
Jason Gump, CIRES Student
Robert Grass, CIRES
Rudy Haas, Mathematician
Bradley Halter, CIRES
Joyce Harris, Physical Scientist
Gloria Koenig, Physical Scientist
Walter Komhyr, CIRES
Thomas Kotsines, Engineering Technician
Jeffrey Lathrop, Physical Scientist
Kent Leonard, CIRES
David Longenecker, CIRES
Charles Myers, Engineering Aid
Donald Nelson, Meteorologist
John Ogren, Physical Scientist
Samuel Oltmans, Physicist
Micheal O'Neill, CIRES
Greg Orleans, Phyical Science Aid
Gina Palmer, Physical Science Aid
Frank Polacek, III, Engineering Technician
Dorothy Quincy, CIRES
Scott Sanberg, Electronic Technician
Herman Sievering, Guest Worker
Robert Stone, CIRES
David Theisen, Physical Science Aid
Holger Vömel, CIRES
Byron Wells, Physical Science Aid
James Wendell, Electronic Technician

Atmospheric Radiation Monitoring Division

Gary Herbert, Chief
Linda (Craig) Sachetti , Secretary
Mark Bieniulis, CIRES
Thomas Mefford, CIRES
Kenneth Thaut, Electronic Technician

Carbon Cycle Division

Pieter Tans, Chief
Debra Hansen , Secretary
Peter Bakwin, Physicist
Phillipe Ciais, NRC
Thomas Conway, Research Chemist
Wyatt Coy, CIRES
Mario DiCino, Physical Science Aid
Ed Dlugokencky, Research Chemist
Laurie Geller, CIRES Student
Douglas Guenther, CIRES
Korie Handwerger, CIRES Student
Duane Kitzis, CIRES
Patricia Lang, Physical Scientist
Lisa Lindstrom, CIRES Student
Kenneth Masarie, CIRES
Mark Ohan, CIRES Student
Paul Novelli, CIRES
Zhiqing Shao, Visiting Scientist
Norman Sitter, Physical Science Aid
Michael Stavish, CO-OP
Kirk Thoning, Physicist
Michael Trolier, INSTAAR
Aaron Troyer, CIRES Student
Jennifer Vaughan, CIRES Student
Lee Waterman, Research Chemist
Ni Zhang, CIRES
Conglong Zhao, CIRES

Nitrous Oxide and Halocarbons Division

James Elkins, Chief
Debra Hansen, Secretary
Hans Auer, CIRES Student
Thomas Baring, CIRES
Diana Barnes, Guest Worker
James Butler, Research Chemist
Scott Cummings, CIRES
Jeannie Dolan, C.U. Work Study
Geoffrey Dutton, CIRES
Fahim Ghafoori, C.U. Work Study
Jonathan Gilligan, CIRES
Arnold Hayden, CIRES Student
Dale Hurst, NRC Associate
Bryan Jordan, C.U. Work Study
Kristen Kauffman, C.U. Work Study
Jürgen Lobert, CIRES
Loreen Lock, C.U. Work Study
Angelo Madonna, Physical Science Aid
Steve Montzka, Research Chemist
Richard Myers, Physical Science Technician
Phuong Nguyen, CIRES Student
Matthew Nowick, CIRES Student
William Sturges, CIRES
Thomas Swanson, CIRES
Thayne Thompson, Physicist
Joshua Trought, CCHE Student
Jennifer Vaughn, C.U. Work Study
Michael Volk, CIRES

Observatory Operations Division

Bernard Mendonca, Chief
Linda (Craig) Sachetti , Secretary

Daniel Endres, Station Chief, **Barrow**
Bradley Halter, Physical Scientist

Russell Schnell, Director, **Mauna Loa**
Judith Pereira, Program Support Technician
John Barns, Physical Scientist
John Chin, Physicist
Thomas DeFoor, Electronic Engineer
Melody Keaunui, Clerk
Darryl Kuniyuki, Electronic Engineer
Steven Ryan, Physical Scientist
Robert Uchida, Electronic Technician
Alice Wall, Physical Science Aid
Alan Yoshinaga, Chemist

Carl Farmer, Station Chief, **Samoa**
Mark Winey, Electronic Engineer/Staiton Chief

Dale Tysor, NOAA Corps, **South Pole**
Katherine, McNitt, NOAA Corps
Raymond Dunn, Electronic Engineer
Carl Groeneveld, NOAA Corps
Thomas Jacobs, NOAA Corps
Donald Neff, Physicist

CMDL Station Information

Name:	**Barrow (BRW)**	**Mauna Loa (MLO)**
Latitude:	71.323	19.539
Longitude:	156.609	155.578
Elevation:	8 m 3397 m	
Time Zone:	GMT -9	GMT -10
Office Hours:	8:00 am-5:00 pm	8:00 am-5:00 pm
Telephone		
Office hours:	(907) 852-6500	(808) 961-3788
Fax:	(907) 852-4622	(808) 961-3789
Postal Address:	Officer in Charge	U.S. Dept. of Commerce
	NOAA/ERL/CMDL	NOAA - Mauna Loa Observatory
	Pouch 8888	P.O. Box 275
	Barrow, AK 99723	Hilo, HI 96720
Freight Address:	Same as above	U.S. Dept. of Commerce

NOAA - Mauna Loa Observatory
154 Waianuenue Ave.
Hilo, HI 96720

Name:	**Samoa (SMO)**	**South Pole (SPO)**
Latitude:	-14.232	-89.997
Longitude:	170.563	-102.0
Elevation:	77 m	2841 m
Time Zone:	GMT -11	GMT +12
Office Hours:	8:00 am-5:00 pm	8:00 am - 5:00 pm
Telephone:		
Office hours:	011 (684) 622-7455	Relayed through CMDL Boulder
After hours:	011 (684) 699-9953	
Fax:	011 (684) 699-4440	
Postal Address:	U.S. Dept. of Commerce NOAA - CMDL Samoa Observatory Pago Pago, American Samoa 96799 PSC 468 Box 402 FPO AP 96598-5402	Officer in Charge NOAA/CMDL Clean Air Facility S-257 South Pole, Antarctica
Freight Address:	Same as above	Same as above

Preface

This report presents the major accomplishments of the National Oceanic and Atmospheric Administration/Climate Monitoring and Diagnostics Laboratory (NOAA/CMDL) for calendar year 1993. This is the 22nd consecutive annual report issued by this organization and its ARL/GMCC predecessor since formation in 1972.

CMDL is located in Boulder, Colorado, with observatories at Barrow, Alaska; Mauna Loa, Hawaii; Cape Matatula, American Samoa; and South Pole, Antarctica. It is one of twelve components of the Environmental Research Laboratories within NOAA's Office of Oceanic and Atmospheric Research. The collected plans and accomplishments of all Environmental Research Laboratories are jointly published in two separate volumes: the *ERL Programs and Plans* document and the *ERL Publication Abstracts*. This CMDL document supplements the two ERL publications by providing a more detailed view of the CMDL programs during 1993.

This report is organized into six major sections: Observatory Operations; Carbon Cycle Division; Aerosol, Radiation, Ozone, and Water Vapor Division; Acquisition and Data Management Division; Nitrous Oxide and Halocarbons Division; and Cooperative Programs. The body of the report is followed by a list of Publications and Presentations of CMDL personnel for 1993.

Inquires and/or comments are welcomed and should be addressed to:

Director, R/E/CG
Climate Monitoring and Diagnostics Laboratory
U.S. Department of Commerce/NOAA
325 Broadway
Boulder, Colorado 80303-3328
(303) 497-6074

1. Observatory Operations Division

1.1. Mauna Loa Observatory

R.C. Schnell

1.1.1. Operations

MLO is undergoing an evolution in data gathering and data transmission brought on by the availability of inexpensive and reliable PCs and the Internet. In 1993 MLO continued the process of expanding the number of measurements accessible in essentially real time via Internet and/or telephone modems. With the planned connection of the carbon cycle measurements to Internet in late 1994 and the halocarbons in 1995, the process will be near completion. Thus, by the end of 1995 all the continuous, automatic MLO measurements will be monitored (and in some cases, instruments adjusted) by PIs from their office computers wherever in the world they may be. Because of this movement to PC-based data monitoring systems at MLO, the venerable CAMS units are being replaced. With the upgrading of the carbon cycle CO_2 systems, the CAMS era at MLO will come to an end.

Early in the year, the MLO outdoor electrical upgrade was completed and accepted coincident with a major upgrade of Hawaiian Electric's Hawaii Island generating capacity. Together, these new facilities reduced the number of power interruptions at MLO from 25 in January to 2 in February. Power problems were thought to be bad memories until July 24 when a lightning strike traveled backward through the now well-grounded MLO system and burned out about a dozen instruments. On a positive note, the breakers on the hot side worked in this lightning strike. The situation is now being monitored and isolating some sections of the grounding network should lightning damage occur again may be considered.

A major staff change occurred in June when the electronic engineer, who ran the MLO lidar program for 13 years, moved to a management position with the NOAA Space Environment Laboratory in Boulder. He was replaced in July by a physical scientist from the University of Michigan, Ann Arbor, in a smooth transition.

The JPL ozone lidar measurement system (part of the NDSC program) arrived on site in July in two 13-m (40 ft) trailers that were installed on a cement pad immediately east of the AEC building. The lidar is operated by one of a rotating crew of three from JPL, Pasadena, California, who spend 3-4 weeks per shift in Hawaii. The JPL lidar group works closely with the NOAA lidar group in conducting coincident aerosol and temperature profiles. The JPL ozone profiles are compared with the weekly MLO ozonesonde profiles with generally excellent agreement.

Electrical power with 14 separate circuits (including 2 RV and 2 at 220 V) has been installed at the base of the Cape Kumukahi lighthouse tower, and four air lines run to the top of the 18-m (60-ft) tower. Air Cadet pumps (one of which is pumping continuously) are mounted under a movable metal cover at the tower base and are used for the URI and SIO oxygen flask sampling programs. A 15 m × 15 m fenced enclosure is planned for construction just south of the tower to protect trailers and containers brought to Cape Kumukahi for future marine boundary layer measurement programs.

Through an arrangement with Western Pacific Communications, Hilo, a radio telephone transceiver station was installed at MLO. This provides MLO, JPL, and HAO vehicles with uninterrupted telephone communications on the Saddle and Observatory Roads, including the portion of the Saddle Road down to the Kona Coast. This communication link will be a valuable safety asset during the NDSC building construction phase.

The transfer of the NDSC land from the state of Hawaii to NOAA was approved by the Department of Land and Natural Resources. Complete and clear title to the 4-acre parcel should occur in 1994 or early 1995.

In September, commercial bike tours began operating on the Observatory Road. The tours consist of a van depositing mountain bikes and riders at MLO from where they coast approximately 51 km down to Kona. MLO is working with these companies (now numbering two) to make their riders visible to Observatory Road vehicle traffic. Early groups were riding black bikes, wore black T-shirts and helmets, and coasted head-down in the center of the road. Now at least they wear orange vests, white helmets, and are told to be aware of vehicle traffic.

MLO was host to 399 signed-in visitors in 1993. Countries represented were Canada, Japan, China, Germany, Burkina-Faso, Switzerland, France, Togo, Australia, Brazil, Russia, Iran, England, Denmark, American Samoa, Mexico, Singapore, Italy, Holland, New Zealand, Norway, and Sweden. This was in addition to visitors from 26 states. Most of the visiting scientists were given a tour and reprints of the most up-to-date CMDL data plots MLO had available. MLO keeps a store of color plots on hand for such occasions.

1.1.2. Programs

Table 1.1 summarizes the programs in operation at MLO during 1993. Relevant details of note on the respective programs are as follows:

Carbon Dioxide

The CMDL Siemens Ultramat-3 IR CO_2 analyzer and the SIO Applied Physics IR CO_2 analyzer were operated in parallel without major problems throughout the year.

TABLE 1.1. Summary of Measurement Programs at MLO in 1993

Program	Instrument	Sampling Frequency
Gases		
CO_2	Siemens Ultramat-3 IR analyzer	Continuous
	0.5-L glass flasks, through analyzer	1 pair wk^{-1}
CO	Trace Analytical RGA3 reduction gas analyzer no. R5	Continuous (5/92)
CO_2, CH_4, CO, ^{13}C, ^{18}O of CO_2	2.5-L glass flasks, MAKS pump unit*	1 pair wk^{-1}
	3-L evacuated (KUM)	1 pair wk^{-1}
CH_4	Carle automated GC no. 6	1 sample $(24\ min)^{-1}$
Surface O_3	Dasibi ozone meter	Continuous
Total O_3	Dobson spectrophotometer no. 76	3 day^{-1}, weekdays
O_3 profiles	Dobson spectrophotometer no. 76 (automated Umkehr method)	2 day^{-1}
	Balloonborne ECC sonde	1 wk^{-1}
N_2O, CFC-11, CFC-12, CFC-113, CH_3CCl_3, CCl_4	300-mL stainless steel flasks	1 sample wk^{-1}
N_2O, CFC-11, CFC-12, CFC-113, CH_3CCl_3, CCl_4, HCFC-22, HCFC-141b, HCFC-142b, CH_3Br, CH_3Cl, CH_2Cl_2, $CHCl_3$, C_2HCl_3, C_2Cl_4, H-1301, H-1211	850-mL stainless steel flasks	1 sample mo^{-1}
CFC-11, CFC-12, CFC-113, N_2O, CCl_4, CH_3CCl_3,	HP5890 automated GC	1 sample h^{-1}
N_2O	Shimadzu automated GC	1 sample h^{-1}
Radon	Two-filter system	Continuous integrated 30-min samples
Aerosols		
Condensation nuclei	Pollak CNC	1 day^{-1}
	TSI CNC†	Continuous
Optical properties	Four-wavelength nephelometer†: 450, 550, 700, 850 nm	Continuous
Stratospheric and upper tropospheric aerosols	Lidar, 694.3 nm	1 profile wk^{-1}
Black carbon	Aethalometer	Continuous
Solar Radiation		
Global irradiance	Eppley pyranometers with Q, OG1, and RG8 filters	Continuous
Direct irradiance	Eppley pyrheliometer (2) with Q filter	Continuous
	Eppley pyrheliometer with Q, OG1, RG2, and RG8 filters	3 day^{-1}
	Eppley/Kendall active cavity radiometer	1 mo^{-1}
Diffuse irradiance	Eppley pyrgeometer with shading disk and Q filter†	Continuous
Terrestrial (IR) radiation	Global downwelling IR pyrgeometer	Continuous (11/93)
Turbidity	J-202 and J-314 sunphotometers with 380-, 500-, 778-, 862-nm narrowband filters	3 day^{-1}, weekdays
	PMOD three-wavelength sunphotometer†: 380, 500, 778 nm; narrowband	Continuous
Column water vapor	Two wavelength tracking sunphotometer: 860-, 940-nm	Continuous (4/92)
Meteorology		
Air temperature	Aspirated thermistor†, 2- and 40-m heights (removed October 1993)	Continuous
	Aspirated thermistor†, 2-, 9-, 37-m heights (added October 1993)	Continuous
	Max.-min. thermometers, 2-m height	1 day^{-1}

TABLE 1.1. Summary of Measurement Programs at MLO in 1993—Continued

Program	Instrument	Sampling Frequency
Meteorology - Continued		
Temperature gradient	Aspirated thermistors†, 2- and 40-m heights (removed October 1993)	Continuous
	Aspirated thermistors†, 2-, 9-, 37-m heights (added October 1993)	Continuous
Dewpoint temperature	Dewpoint hygrometer†, 2-m height	Continuous
Relative humidity	TSL 2-m height	Continuous
Pressure	Capacitance transducer†	Continuous
	Mercurial barometer	5 wk^{-1}
Wind (speed and direction)	Bendix Aerovane†, 8.5- and 40-m heights (40-m Aerovane removed October 1993)	Continuous
Wind (speed and direction)	8.5-, 10-, and 38-m heights (added October 1993)	Continuous
Planetary boundary layer meteorology (PBL MET)	Wind vane, cup anemometer, and aspirated RTD thermometer (direction, speed, temperature at 3-, 5-, 10-, 20-, 30-, and 40-m levels) (removed October 1993)	Continuous
Precipitation	Rain gauge, 20-cm	5 wk^{-1}
	Rain gauge, 20-cm‡	1 wk^{-1}
	Rain gauge, tipping bucket†	Continuous
Total precipitable water	Foskett IR hygrometer†	Continuous
Precipitation Chemistry		
pH	pH meter	Daily
Conductivity	Conductivity bridge	Daily
Cooperative Programs		
CO_2 (SIO)	Applied Physics IR analyzer	Continuous
CO_2, ^{13}C, N_2O (SIO)	5-L evacuated glass flasks*	1 pair wk^{-1}
CO_2, CO, CH_4, $^{13}C/^{12}C$ (CSIRO)	Pressurized glass flask sample	1 mo^{-1}
CH_4, CH_3CCl_3, CH_3Cl, F-22, F-12, F-11, F-113 CO, CO_2, N_2O, $CHCl_3$, CCl_4 (OGIST)	Pressurized stainless steel flasks	3 wk^{-1}
O_2 analyses (SIO)	5-L glass flasks through tower line and pump unit* (started June 1993)	3 $(2\ mo)^{-1}$
O_2 analyses (URI)	3-L glass flasks through tower line and pump unit (started June 1993 at KUM)	2 $(2\ mo)^{-1}$
CH_4 ($^{13}C/^{12}C$) (Univ. of Washington)	35-L evacuated flask	1 mo^{-1}
Total suspended particles (DOE)	High-volume sampler (1 filter wk^{-1})	Continuous
Ultraviolet radiation (Smithsonian)	Eight-wavelength UV radiometer: 290-325 nm; narrowband	Continuous
Ultraviolet radiation (ARL)	Robertson-Berger UV radiometer (erythema)	Continuous
UV solar radiation (ARL)	Yankee Environmental UVB pyranometer (280-320 nm)	Continuous (10/92)
Ultraviolet radiation (Univ. of Hawaii)	Robertson-Berger UV radiometer (erythema) (started June 1993)	Continuous
Solar aureole intensity (CSU)	Multi-aperture tracking photometer: 2, 5, 10, 20, 30° fields of view	Continuous
Precipitation collection (DOE)	Exposed collection pails	Integrated monthly sample
Precipitation collection for organic acid analysis (Univ. of Virginia)	Aerochemetric automatic collector (terminated August 1993)	Collection after each rain event
Wet-dry deposition (ISWS, NADP)	Aerochemetric automatic collector and weighing-bucket rain gauge	Integrated 7-day sample
Aerosol chemistry (Univ. of Calif.-Davis)	Programmed filter sampler	Integrated 3-day sample 1 continuous and 1 down-slope sample $(3\ days)^{-1}$
Various trace gases (OGIST)	Stainless steel flasks*	1 set wk^{-1} (3 flasks)
Sulfate, nitrate, aerosols (URI)	Filter system	Daily, 2000-0600 LST

TABLE 1.1. Summary of Measurement Programs at MLO in 1993—Continued

Program	Instrument	Sampling Frequency
Cooperative Programs - Continued		
Radon (ANSTO)	Aerosol scavenging of Rn daughters	Continuous; integrated 30-min samples
Solar spectra (Univ. of Denver)	FTIR spectrometer	1 wk^{-1}

All instruments are at MLO unless indicated.
*MLO and Kumukahi
†Data from this instrument recorded and processed by microcomputers.
‡Kulani Mauka

Routine maintenance and calibrations were undertaken on both instruments as scheduled. An SIO electronic engineer upgraded the SIO CO_2 data acquisition system on March 24-26. Data are now recorded on a Brown strip chart recorder and stored on a PC hard disk. Hourly average CO_2 values are printed out at MLO.

The preliminary average MLO CO_2 concentration for 1993 was 356.8 ppm. The CO_2 annual growth rate between 1992 and 1993 was approximately 0.6 ppm. Compared with the 1990-1991 growth rate of 1.3 ppm per year, and the 1991-1992 growth rate of 0.8 ppm per year, this indicates a continued slowdown in the CO_2 growth rate measured at MLO.

Outgassing from the volcanic vents at the Mauna Loa caldera and along the northeast rift zone at Mauna Loa continued to cause periodic observable disturbances in some of the CO_2 data record. As in prior years, these venting events occurred mostly between midnight and 0800 LST of the following day, during the downslope wind regime. The erratic CO_2 concentration data resulting from these venting events were easily identified by visually scanning chart records or by utilizing a computerized data-screening procedure, and thus they have been separated from the clean-air record without difficulty. Such venting episodes were detected mainly on the basis of criteria for CO_2 concentration, CO_2 variability, and wind sector. The criterion for the CO_2 standard deviation screening was 1.0 ppm, which is the value suggested by *Thoning et al.* [1989].

The frequency of monthly occurrences of observable outgassing from volcanic vents on Mauna Loa for 1993 are listed in Table 1.2, and the annual number of events for the past 6 years are listed in Table 1.3.

The weekly CO_2, CH_4, and other gas sampling programs, using flasks at MLO and at Cape Kumukahi, were carried out according to schedule throughout the year, without major problems.

The flask sampling procedure at MLO was changed as of November 19, 1993:

- For the through analyzer sampling, the 0.5-L greased-type flasks were replaced with 0.5 L Teflon O-ring-type flasks.
- For the MAKS sampling, the 0.5-L Teflon O-ring flasks were replaced with 2.5-L Teflon O-ring flasks.

Carbon Monoxide

A Trace Analytical RGA3 Reduction Gas Analyzer for the continuous measurement of CO mixing ratios was installed in May 1992 and continues to work well. System operations and chromatographic data logging are handled by an HP3396A integrator.

Methane

The Carle automated GC system, Carle 6, was in continuous operation throughout the year providing CH_4 data on the basis of a grab air sample being taken every 24 minutes. The instrument functioned well during the year.

The CH_4 data continued to show clearly defined cycles of varying frequencies. The typical diurnal cycle was well correlated with upslope and downslope winds, with the marine boundary layer air having the higher CH_4 concentrations. There were also multiday or synoptic-scale CH_4 cycles observed that apparently

TABLE 1.2. Estimated Mauna Loa Venting Episodes (Total Time in Hours) at MLO in 1993*

Jan.	Feb.	March	April	May	June	July	August	Sept.	Oct.	Nov.	Dec.	Year
1	0	4	1	0	1	1	4	4	2	0	10	28

*Criteria: CO_2 SD ≥1.0 ppm; wind direction sector 135°-225°; wind speed ≥1.35 m s^{-1}.

TABLE 1.3. CO_2 Venting Events From 1988 Through 1993

Year	Total Time (Hours)
1988	200
1989	84
1990	48
1991	26
1992	23
1993	28

relate to different air mass source regions. The average MLO CH_4 concentration for 1993 was ~1728 ppb with the maximum occurring in November (~1750 ppb) and minimum in August (~1720 ppb).

Ozone Monitoring

The 1993 MLO ozone monitoring program consisted of three measurement foci: continuous surface ozone monitoring using a Dasibi model 1003-AH UV absorption ozone monitor; total and Umkehr ozone profile measurements using computer-based automated Dobson instrument 76; and ozone profile measurements based on weekly ascents of balloonborne ECC ozonesondes released from the NWS station at the Hilo Airport. In addition to the daily automated Umkehr measurements and 5-day-a-week total ozone measurements, five special early-morning AD-CD direct sun observations were completed in 1993. The Dasibi ozone monitor performed in a fully satisfactory manner and provided a continuous, high-quality record of station-level ozone concentrations for the entire year.

Halocarbons and Nitrous Oxide

The RITS system had its annual major maintenance in September 1993. During this time, shutoff solenoid assemblies and regulator warmers were added to the CAL1 and CAL2 tanks. Persistent leaks necessitated the replacement of various valves in the stream select unit and a brass actuator in the HP-GC. A new air compressor was installed to replace one that burned out because of the leaks.

In general, the RITS computer continued to experience hangups throughout the year. A bad power supply was replaced in May. Program editing to cut down printing and data handling problems have not solved the computer "glitches."

Radon

The CMDL-DOE radon program completed its third year of operation and collected the first full year of improved data since the instrument background was reduced by applying epoxy over welds inside the instrument. The current background is 8 counts per 30 minutes. A re-examination of the 1991-1992 data suggests that the background was 26 counts per 30 minutes over that period. The 1993 data show excellent agreement with the ANSTO radon monitor data.

Radon concentrations on January 6 reached their highest levels in the 3 years of radon monitoring at MLO, with half-hour averages greater than 2800 mBq m^{-3}. This coincided with the high post-frontal wind flows from a storm on January 4-6.

Aerosol Monitoring

The TSI unit is a continuous expansion CNC in which condensation occurs in butyl alcohol vapor in a chamber and single particle counting statistics are used as a basis for the CN concentration calculations. The instrument has continued to display higher counts than the Pollak counter since its return from the manufacturer in 1991.

The aethalometer performed satisfactorily collecting black carbon data. There was some local contamination of the data during the early part of the year when the observatory electrical upgrade contractor was using diesel equipment on site.

The four-wavelength nephelometer went down on January 17 because of a faulty automatic air/filter valve. While awaiting arrival of a replacement valve from Boulder, maintenance was performed on the circuitry. The system was brought back into service on February 26. The system performed without any problems the remainder of the year.

Solar Radiation

With the inclusion of the EKO sunphotometer on the spar in March, MLO is now measuring turbidity in more channels than ever before. The EKO is at MLO on a test basis and will be removed in 1994. Using two handheld sunphotometers, the PMOD sunphotometer, two water vapor meters with two channels each, and the EKO sunphotometer, MLO monitors in three channels at 380 nm, three channels at 500 nm, one channel at 675 nm, two channels at 778 nm, one channel at 862 nm, two channels at 870 nm, and two channels at 940 nm. This is a total of 14 channels at 7 separate wavelengths.

Diffuse pyranometer no. 12562, which had developed a negative offset, was replaced with no. 8031 on January 26. A pyrgeometer (global downwelling IR) began operation for the first time at MLO on November 1. Thirty-five handheld sunphotometer instrument calibrations were performed during the year.

A new data acquisition system was installed on October 12 based on Campbell Scientific modules that allow for direct access via a phone modem or RS232 port. All the solar radiation instruments on the radiation tower, the diffuse pyranometer, the CN counter, and the nephelometer are now being monitored with this system at a 3-min time resolution. When instruments are accessed remotely by phone, data are sent at 3-s intervals and plotted using Campbell Scientific software.

Meteorology

The standard meteorological monitoring equipment was down for a few days after the observatory took a

direct lightning hit on July 24. It took about a week for all meteorological systems to become fully restored.

There were no changes in the meteorological program other than the data system changes noted under the Computer/Network heading. The PBL system functioned without problems through 1993. The system measures wind speed, wind direction, and temperature at the 3-, 5-, 10-, 20-, 30-, and 40-m levels.

Precipitation Chemistry

The MLO modified program of precipitation chemistry collection and analyses was continued throughout 1993 within the basic MLO operational routine. This program consists of collection of a weekly integrated precipitation sample from the Hilo NWS station and collection of precipitation event samples at MLO. Analyses of these samples are undertaken in the Hilo laboratory for pH and conductivity.

Computers/Network

This is the year that Internet access was established, and it is rapidly transforming MLO operations. There is a direct link from the Hilo office to the University of Hawaii, and then to MLO via microwave. The PBL system was the first instrument to send data to Hilo and Boulder via the Internet. Other projects that followed included sending the JPL and CMDL lidar data through fiber optic links to the main MLO building. Ozonesonde data are also sent over the Internet on a weekly basis. With direct toll-free E-mail access available on Internet, this powerful form of communication is heavily utilized by MLO staff, thus cutting down on long-distance toll charges. MLO does not have access to FTS.

The Hilo office has networked all of its PCs and uses Windows for Workgroups for its main operating system. For connection to the VAX, the PCs also run Decnet (Pathworks) and TCP/IP protocols. The VMS operating system on the VAX was upgraded to version 6.

October was the last month of operation for the MO3 CAMS. It was removed on November 1 and replaced by the new PC-based meteorology data system. October was also the last month in which CAMS recorded solar radiation data; the ASR CAMS was replaced by a Campbell Scientific data system on November 1. The ASR CAMS is still connected to the aerosol instruments as a backup to the CSI system and will operate at least through 1994.

Lidar

Lidar operations continued on a regular weekly basis from February 1, 1993, through the end of the year. During January the repair of the laser power supply was completed. In October and November a new computer system (Gateway 80486 DX, 33 MHz) for controlling the laser and the data acquisition electronics replaced the old computer. The laser power supply was modified to accept a trigger from the new computer. A new digital I/O board provides this trigger and is the interface with the data acquisition electronics. The instrument now runs automatically but still requires the operator to monitor the laser power and adjust it periodically. The raw data are displayed in real time and can be used to adjust the laser. The control and analysis software has been written in Turbo Pascal to run on the new computer.

Observations of the decay of the Mount Pinatubo aerosols continued, allowing comparisons to be made with the El Chichon eruption. In Figure 1.1 the integrated aerosol backscatter is shown for the period from 1980 to present. The complete ruby lidar record at MLO extends back to December 1974. The backscatter is integrated from slightly below the tropopause to well above the stratospheric aerosol layer.

The period from 1989 to 1991 would appear to show measurements of the stratospheric background level. No significant eruptions took place during that time, and the level appears constant. The average integrated aerosol backscatter is 0.69×10^{-4} sr^{-1}. After subtracting this level from the data, decay lifetimes of 7.4 months and 11.5 months were calculated for Pinatubo and El Chichon aerosols, respectively.

Outgassing of Mauna Loa Volcano

Trace gas and aerosol measurements made at MLO have been analyzed in a special study aimed at characterizing the quiescent volcanic plume coming from the 6-km-distant summit of Mauna Loa volcano. The volcano has long been recognized as a source of CO_2 and aerosols. Previous studies have been concerned with identifying and eliminating this contamination from the climatological baseline record.

In this study, minute-scale variability in the atmospheric CO_2 concentration was used to identify the presence of the volcanic plume at night in the

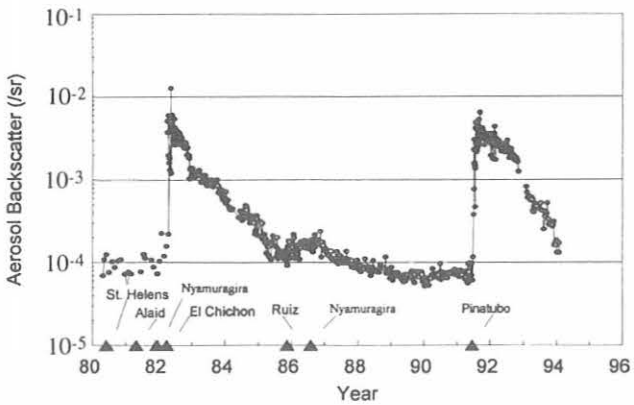

Fig. 1.1. Stratospheric column integrated aerosol backscatter measured with the MLO ruby lidar since 1980. Between 1980 and 1982 the data are monthly averages; after 1982 each observation is shown.

downslope wind. The excess concentration of gases and aerosols above background levels was calculated for each hour in which the plume was present. The frequency of night-time hours in which the plume was detected varied between 50% and about 5%. In the months after the 1984 eruption, the plume CO_2 occasionally saturated the analyzer output; an extrapolation model suggests that hourly excess CO_2 may have reached levels greater than over 600 ppm above baseline. The excess CO_2 was greatest when winds blew from the direction of the summit (180° to 190°), with a small, sympathetic peak when winds came from east of 130° (Figure 1.2). The plume was frequently trapped beneath the night-time surface temperature inversion and had a scale height of tens of meters. The average strength of the plume at MLO followed the evolution of the temperature inversion, forming after sunset, gradually intensifying, and reaching a stable maximum between 0100 and 0600 LST.

Excess CO_2 was measured in the plume throughout the 1958-1993 period of record. The amount of CO_2 was greatest shortly after eruptions (1950, 1975, 1984) and decreased exponentially in the following years, as may be observed in Figure 1.3. The rate of decrease following the 1984 eruption was about 6 times greater than that after the 1975 eruption. The post-1958 rate of decrease was similar to that after 1975. The onset of enhanced outgassing was delayed by 65 days following the 1975 eruption and by less than 20 days following the 1984 eruption. Neither eruption was preceded by any outgassing activity that could have been used to predict the eruption.

Excess aerosol particles were present throughout the 1974-1993 period of record as shown in Figure 1.4. In the post-1975 period, high CN levels were present. After the 1984 eruption, CN levels dropped by a factor of 5 and continued to fall through 1993. Two brief dips that occurred in 1986-1987 and 1990-1991 coincided with periods when geodetic observations showed that

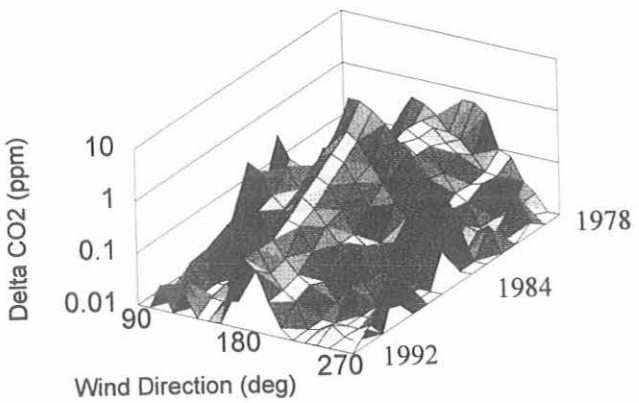

Fig. 1.2. Yearly average excess CO_2 between 2000 and 0759 LST in 10° wind direction bins between 1978 and 1992. Excess CO_2 was normalized to a standard sampling height of 23 m. Winds outside of 10° to 260° blew too infrequently to yield statistically signficant excess CO_2 values.

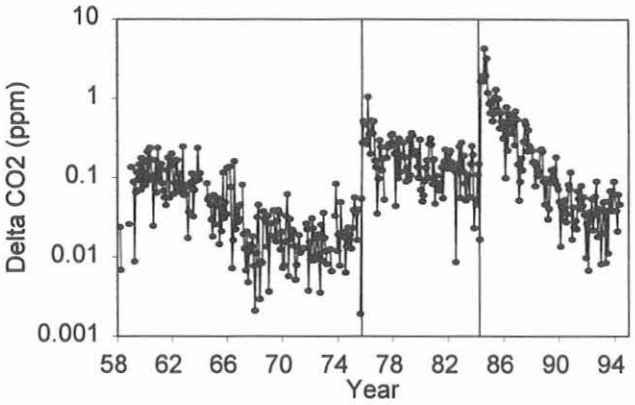

Fig. 1.3. Monthly average excess CO_2 between 2000 and 0759 LST normalized to a standard sampling height of 23 m. The 1975 and 1984 eruptions are denoted by vertical lines. Data prior to 1976 were derived from hand-scaled data obtained by the SIO; the rest were derived from computer-digitized NOAA data.

the gradual inflation of the summit either halted or was temporarily reversed. Light scattering aerosols were detectable only between 1977 and 1980 and to a lesser degree in 1983. The magnitude of large aerosols in the plume was consistent with the visual thickness of the plume at the vent (Figure 1.4).

Seven additional MLO data sets were examined for a volcanic plume component: H_2O (1974-1993), CH_4 (1987-1993), SO_2 (1988-1992), Aerosol black carbon (1990-1993), radon (1991-1993), CO (1992-1993), and H_2 (1992-1993). None of these species were present in the plume down to the detection limits of the analysis technique.

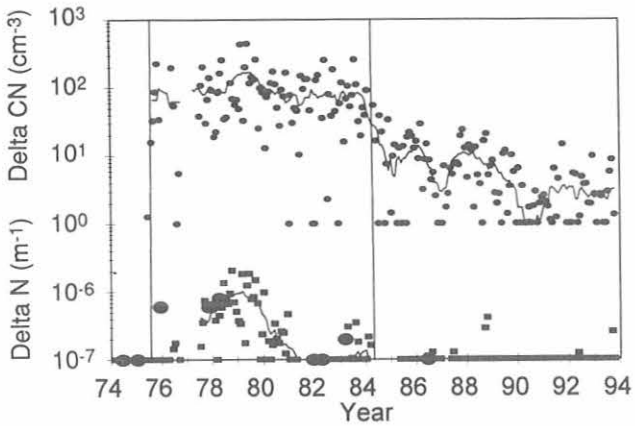

Fig. 1.4. Monthly average excess aerosols between 0000 and 0759 LST measured from a sampling height of 13 m. The fits are 12-mo running means. Excess CN are shown by small ovals with a lower limit of detection of 1 cm^{-3}. Excess 550 nm light scattering (squares) less than 1×10^{-7} m^{-1} is plotted as 1×10^{-7} m^{-1}. The large solid ovals within the light scattering data indicate the visual thickness of the fume at the caldera vent estimated from aerial photographs (on a scale of 0 to 5) and then linearly scaled between 1×10^{-7} and 10^{-6} m^{-1}.

Cooperative Programs

MLO cooperative programs are listed last in Table 1.1; new programs and changes in existing programs are presented below.

The only major new program instituted at the MLO mountain site in 1993 was the University of Hawaii UV radiation measurement (Robertson-Berger meter) installed on June 18, 1993. This instrument has telephone access, and the data are also available on the MLO VAX through Internet.

At the MLO Cape Kumukahi lighthouse tower site, SIO and URI staff installed four Dekobon 6-mm (1/4 in) air sampling lines up to the top of the 18-m tower on June 25-27. Individual Air Cadet pumps are used to draw air through the air intake lines. The sample air will be used for the new SIO and URI oxygen flask sampling programs initiated in June 1993.

SIO upgraded the SIO CO_2 data acquisition system at MLO on March 24-26. The data are now recorded on a Brown stripchart recorder and stored in a PC hard disk. The hourly average CO_2 values are printed out on the PC printer at the observatory.

The formation of ^3He (WHOI), O_2/N_2 flask sampling (NCAR), and University of Washington aerosol chemistry programs were discontinued in 1993.

1.2. Barrow Observatory

D. Endres

1.2.1. Operations

It was a relatively quiet year for CMDL programs at the BRW Observatory during 1993. Cooperative programs experienced some minor changes with the addition of new programs and changes in continuing programs. Barrow continues to serve as a training center for SPO personnel. This year the NOAA Corps officer was in Barrow for training during May and June. The SPO technician was in SMO for training because of scheduling conflicts.

The biggest problem during the winter months involved access to the station. Once the road drifted over with snow, it received no maintenance due to the high cost of snow removal. Access was accomplished by snowmachine, skiing, or walking. There were fewer polar bear sightings this year than last. During the summer months, a gate was installed across the road to keep the amount of local traffic to a minimum.

Plans for a new observatory building were completed during 1992 and are on site. NOAA facilities funding has not yet been secured for construction.

Both GSA vehicles continued to run well. An agreement with the DEW Line allows us use of one stall in the garage to park vehicles. The stall is used for the truck during the day and snowmachines overnight. The Skandic snow machine had the engine rebuilt after it blew a piston.

Water pipes in the bathroom at the house froze and had to be repaired this year. All the plumbing was moved so that all the pipes are now inside the house or in heated channels and no further freeze-ups are expected. In December the NWS hired a Seattle contractor to hook up the NOAA housing compound to the local utility system. The plans called for several hundred meters of unheated pipe with 10 mm of insulation to be installed and water to be circulated through it. The pipe froze two times in the first 24 hours and was disconnected. Future plans call for an upgrade sometime in 1995.

A tape back-up was installed in the station computer to save on the number of disks used in backing up the hard drive. A storm with westerly winds caused several power outages during the fall. It was an unusual storm with wet, heavy snow.

During 1993, BRW was visited by 88 registered guests. This list included guided tours, researchers, and interested individuals. Visitors from Japan, Russia, Canada, and the South Pole were all involved in research at BRW. U.S. Government agencies were represented by NOAA/NOS, the USGS, Army Corps of Engineers, ONR, the Navy, and the Air Force. Personnel from eight universities were involved in research as well. Twenty-five states were represented.

1.2.2. CMDL Programs

Table 1.4 summarizes the 1993 measurement programs at BRW. Operational highlights are as follows:

Aerosols

The TSI CNC continues to measure higher levels of condensation nuclei than the Pollak. The reason for the difference is still under investigation. Because of this difference, independent data sets are maintained for both instruments. Both instruments ran all year with no major problems.

Backscatter, as measured by the nephelometer, continues to show the seasonal trends associated with arctic haze. Springtime highs and summer lows characterize the BRW data. Intermittent problems with the nephelometer were solved during the first quarter of the year by replacing all I.C. chips on board 7.

The aethalometer data acquisition system clock began to lose time early this year and a replacement laptop computer was ordered. Time loss of up to 20 seconds per day was noted. The laptop computer was replaced and a newer version of the software was installed.

A new data logging system was installed for the solar radiation program with aerosols sharing the hardware. For more detail see the Solar Radiation section.

Solar Radiation

The BRW Observatory solar program consists of a downward facing albedo rack approximately 75 m behind the station and 1.75 m above the surface with a quartz pyranometer and a pyrgeometer. An upward facing quartz pyranometer, an RG8 pyranometer, and a tracking NIP are mounted on the Observatory roof. Located in the Dobson dome is a filter wheel NIP with Quartz, OG1, RG2, and RG8 filters. Observations begin in January when the sun returns and cease when the sun sets in November.

TABLE 1.4. Summary of Measurement Programs at BRW in 1993

Program	Instrument	Sampling Frequency
Gases		
CO_2	Siemens Ultramat 5E analyzer	Continuous
	3-L glass flasks	1 pair wk^{-1}
	0.5-L glass flasks, through analyzer	1 pair wk^{-1}
CO_2, CH_4, CO	0.5-L glass flasks, P^3 pump unit	1 pair wk^{-1}
CH_4	Carle automated GC	1 sample $(12\ min)^{-1}$
Surface O_3	Dasibi ozone meter	Continuous
Total O_3	Dobson spectrophotometer no. 91	3 day^{-1}
N_2O, CFC-11, CFC-12, CFC-113, CH_3CCl_3, CCl_4	300-mL stainless steel flasks	1 sample wk^{-1}
N_2O, CFC-11, CFC-12, CFC-113, CH_3CCl_3, CCl_4, HCFC-22, HCFC-141b, HCFC-142b, CH_3Br, CH_3Cl, CH_2Cl_2, $CHCl_3$, C_2HCl_3, C_2Cl_4, H-1301, H-1211	850-mL stainless steel flasks	1 sample mo^{-1}
CFC-11, CFC-12, CFC-113, N_2O CCl_4, CH_3CCl_3	HP5890 automated GC	1 sample h^{-1}
N_2O	Shimadzu automated GC	1 sample h^{-1}
CO	Trace Analytical GC	1 sample $(6\ min)^{-1}$
Aerosols		
Condensation nuclei	Pollak CNC	1 day^{-1}
	T.S.I. CNC	Continuous
Optical properties	Four-wavelength nephelometer	Continuous
Black carbon	Aethalometer	Continuous
Solar Radiation		
Global irradiance	Eppley pyranometers with Q and RG8 filters	Continuous
Direct irradiance	Tracking NIP	Continuous
	Eppley pyrheliometer with Q, OG1 RG2, and RG8 filters	Discrete
Albedo	Eppley pyranometer	Continuous
Terrestrial (IR) Radiation		
Upwelling and downwelling	Eppley pyrgeometers	Continuous
Meteorology		
Air temperature	Thermistor, 2 levels	Continuous
	Max.-min. thermometers	1 day^{-1}
Dewpoint temperature	Dewpoint hygrometer	Continuous
Pressure	Capacitance transducer	Continuous
	Mercurial barometer	Discrete
Wind (speed and direction)	Bendix Aerovane	Continuous
Precipitation	Rain gauge, tipping bucket	
Cooperative Programs		
Total surface particulates (DOE)	High-volume sampler (1 filter wk^{-1})	Continuous
Precipitation gauge (USDA)	Nipher shield, Alter shield, 2 buckets	1 mo^{-1}
Magnetic fields (USGS)	3-Component fluxgate magnetometer and total field proton magnetometer	Continuous
	Declination/inclination magnetometer sample	6 sets mo^{-1}
Various trace gases (OGIST)	Stainless steel flasks	1 set wk^{-1} (3 flasks set^{-1})
CO_2, ^{13}C, N_2O (SIO)	5-L evacuated glass flasks	1 pair wk^{-1}
CH_4 (Univ. of Calif., Irvine)	Various stainless steel flasks	1 set $(3\ mo)^{-1}$
Earthquake detection (Univ. of Alaska)	Seismograph	Continuous, check site 1 wk^{-1}

TABLE 1.4. Summary of Measurement Programs at BRW in 1993—Continued

Program	Instrument	Sampling Frequency
Cooperative Programs - Continued		
$^{13}CH_4$ ($^{13}C/^{12}C$) (Univ. of Washington)	35-L stainless steel flasks	1 (2 wk)$^{-1}$
UV monitor (NSF)	UV spectrometer	1 scan per 0.5 hour
Magnetic fields (NAVSWC)	^3He sensors	Continuous
Sound Source (DOE)	RASS	1 hr^{-1}
Ice Buoys (NOS)	Ice buoys	Continuous
O_2 in air (Univ. of Rhode Island)	3-L glass flasks	1 pair (2 wk)$^{-1}$

The tracking NIP was installed in February and collected data until the end of the solar season with only minor problems. Most of the problems were caused by corrosion in the cable because of the salt air. The clutch in the tracker was repaired when it was found to be loose and causing tracking errors.

The biggest change in the solar program was the installation of a Campbell Scientific Instruments (CSI) data collection system. A comparison between the CSI and the CAMS was performed for a month, with favorable results, and the CAMS was retired. Data from the CSI can be accessed by field personnel and a higher level of data quality can be assured.

Epply blowers were installed on the roof PSPs to assist in keeping snow and ice from collecting on the domes. The new blower system works well and has reduced the maintenance needed to keep the domes ice free.

Carbon Cycle

CO_2 NDIR. CO_2 mixing ratios for the BRW Observatory show the same temporal distribution as in previous years. Winter highs of 360 ppm are seen with summertime lows of 345 ppm. A Siemens Ultramat 5E continues to be the station instrument and responds well to changes in atmospheric CO_2.

During early March a power outage damaged the analyzer, and it was returned to Boulder for repairs. It was returned to BRW and put back into operation by the end of March.

During July the drive assembly for the Linseis recorder began sticking at lower voltage levels. The necessary parts were ordered, but before they arrived the chart recorder failed completely. The recorder unit was repaired and placed back in operation by the end of August.

Methane. For the past few years BRW CH_4 data has shown a decrease in the growth rate. During late 1992 and early 1993 the growth rate actually exhibited a negative trend. This trend continued during 1993. Yearly cycles are seen with mixing ratios of between 1750 ppbv and 1950 ppbv.

During July the Carle GC electrometer board failed and was replaced. The system ran for the rest of the year with no problems.

Carbon Monoxide. A Trace Analytical GC has collected CO data at BRW since the fall of 1991. Like CH_4, the growth for CO has shown a marked decrease. Flask data are available from 1990 on. Annual average mixing ratios of approximately 150 ppbv are measured with data ranging between 250 ppbv and 75 ppbv.

In January the CO program was modified to run with three calibration gases to correct for any non-linearity in the detector. The Hg lamp was replaced in July after it dropped below acceptable output limits.

Flask Samples. The Carbon Cycle Division (CCD) flask samples were collected with few problems during 1993. Data concerning the CCD flasks can be found in section 2.1.6. Whole air collected using the various glass flasks is analyzed for CO, CH_4, and CO_2.

A problem was discovered in the data when MAKS flask data are compared with CMDL 3-L data. The problem was discovered in 1992 and is still under investigation by CMDL personnel in Boulder.

Meteorology

September ushered in an ice storm that coated the streets of Barrow with ice. Temperatures remained cold enough that there was no melting. A storm in October brought enough snow to allow station personnel to ski to work but within 2 days was blown away by the high winds and the ice was uncovered.

Problems were corrected with the TSL hygro-thermometer. The instrument performs an auto-balance, which cleans the mirror, and should return to a zero value. The dewpoint assembly was replaced in May and no further problems occurred.

CAMS

CAMS ran without any significant problems for the entire year. However, plans are being made by most groups in Boulder for the next generation data acquisition system. CAMS is approaching the end of its useful life and alternative collection schemes must be implemented.

Ozone

Surface Ozone. Surface ozone is measured with a Dasibi ozone monitor. The Dasibi measures continuously and ran all year with only routine cleaning of the absorption tubes. Data

continues to show trends of past years; i.e., springtime lows and highs during the dark winter months.

Dobson. Dobson 91 is the instrument in BRW and observations are made from February until October. A semi-automated data acquisition system was added to the Dobson in May and has proven to be quite useful. Station personnel can now see real time ozone amounts as measured by the Dobson in Dobson Units (milli-atmo-centimeters).

N_2O and Halocarbons

Gas Chromatographs. System lock-ups continued to plague the system during 1993. The only cure was to cycle the power. Batteries in the UPS for the DAS were found to be old enough that two of the four would no longer hold sufficient charge to run the system in the event of a power outage. The batteries were replaced. A suspected bad disk drive was replaced in August when several disks were found to be devoid of data. Leaks in the pneumatic lines caused the most problems and occurred on several occasions. The detector for channel B was replaced late in the year.

Flask Samples. Flask samples were collected as available and scheduled. Data concerning the flasks can be found in the Nitrous Oxide and Halocarbons section (5.1.4).

Cooperative Projects

Only programs with problems or unusual occurrences are mentioned in this section.

University of Rhode Island. A series of flask samples were collected during 1993 to test the feasibility of collecting whole air for analysis of O_2/N_2 and CO_2. Data collected by measuring O_2 can yield vital information regarding the fate of fossil fuel CO_2 as well as ocean fertility. The test was successful and a regular schedule of sample collecting has begun.

DOE/EML. Air filters collected at BRW were sent to DOE/EML on a weekly basis for analysis because of an explosion at a nuclear fuel processing plant near Tomsk in the former Soviet Union. A signal was detected in Barrow.

DOE/Sandia National Laboratory. Preliminary site choice was made for the DOE CART/ARM site near Barrow. In cooperation with the North Slope Borough, Department of Wildlife Management, a 12-18 month test of the sound source for the RASS began in July. The test will show if there are any effects on local wildlife because of the high level of sound generated.

USDA/SCS. In July a gust of wind destroyed one of the longest running cooperative programs at the BRW Observatory. The Wyoming rain gage was knocked down when a gust of wind measuring 30 m s^{-1} (66 mph) hit it during July. The warm summer temperatures caused a deeper melt than normal and the anchor bolts gave when the wind hit. There are no plans to fix the gage.

USGS. BRW personnel have assumed the duties of calibration for the USGS Magnetic Observatory. A new MOA with USGS was negotiated (see Section 6.0, page 140). The Barrow Magnetic Observatory is one of thirteen observatories: three in Alaska, seven in the contiguous U.S., and one each in Hawaii, Puerto Rico, and Guam. Six sets of absolute measurements are made once each month to determine the horizontal and vertical intensity and the declination. These numbers are then used to calibrate the continuous measuring instruments at the site.

NOAA/Navy Joint Ice Center. Several ice buoys were installed for a long-term calibration study. There is a question about the long-term-stability of the sensors and BRW was chosen as the most suitable location to test the sensors. Data are collected on a laptop computer and downloaded by personnel from the National Ocean Service in Silver Spring, Maryland.

1.3. SAMOA

M. Winey

1.3.1. OPERATIONS

There was a personnel change at the observatory during the year. The SMO station chief ended a 4-year term and went to a teaching position at the American Samoa Community College. The electronic technician was then installed as station chief and an environmental engineer was hired.

The most exciting and disturbing event of the year was the burglary of the main observatory building. A safe that contained money and paper work was stolen. The perpetrators were caught, but none of the stolen property was recovered. A new safe was cemented into the floor of the office. Some structural changes were also made to the building to improve security.

Two hurricanes made close calls early in the year. Minor damage was incurred and was easily repaired by station personnel. These storms were a reminder of the past few years when two hurricanes did extensive damage.

The two observatory vehicles were a constant source of trouble throughout the year. Both the van and the truck neared 100,000 miles of use. Repairs became more frequent and more complex, greatly inconveniencing the staff. Toward the end of the year the process began to replace the truck.

The backup generator logged many hours during power blackouts. One major breakdown occurred but was successfully repaired by the staff. A modification was made to prevent overheating becaue of water loss in the radiator; when the generator overheated once before, the result was a $12,000 overhaul.

Major remodeling of house T-7 occurred once the environmental engineer and family moved in. They did all the work themselves and greatly improved the appearance of the place. Unfortunately, a few termites were seen. Poison was applied in an effort to kill the termites, but this measure has not always been successful in the past.

1.3.2. PROGRAMS

Table 1.5 summarizes the programs at SMO for 1993. Further descriptions of some of the programs follow.

TABLE 1.5. Summary of Measurement Programs at SMO in 1993

Program	Instrument	Sampling Frequency
Gases		
CO_2	Siemens Ultramat-5E analyzer	Continuous
CO_2, CH_4	0.5-L glass flasks, through analyzer	1 pair wk^{-1}
	2.5-L glass flasks, MAKS pump unit	1 pair wk^{-1}
Surface O_3	Dasibi ozone meter	Continuous
Total O_3	Dobson spectrophotometer no. 42	4 day^{-1}
N_2O, CFC-11, CFC-12, CFC-113, CH_3CCl_3, CCl_4	300-mL stainless steel flasks	1 sample wk^{-1}
N_2O, CFC-11, CFC-12, CFC-113, CH_3CCl_3, CCl_4, HCFC-22, HCFC-141b, HCFC-142b, CH_3Br, CH_3Cl, CH_2Cl_2, $CHCl_3$, C_2HCl_3, C_2Cl_4, H-1301, H-1211	850-mL stainless steel flasks	1 sample mo^{-1}
CFC-11, CFC-12, CFC-113, N_2O, CCl_4, CH_3CCl_3	HP5890 automated GC	1 sample h^{-1}
N_2O	Shimadzu automated GC	1 sample h^{-1}
Aerosols		
Condensation nuclei	Pollak CNC	1 day^{-1}
	G.E. CNC	Continuous
	TSI CNC	Continuous
Solar Radiation		
Global irradiance	Eppley pyranometers with Q and RG8 filters	Continuous
Direct irradiance	Eppley pyrheliometer with Q filter	Continuous
	Eppley pyrheliometer with Q, OG1, RG2, and RG8 filters	Discrete
Meteorology		
Air temperature	Thermistors (2)	Continuous
	Max.-min. thermometers	1 day^{-1}
Dewpoint temperature	Polished mirror	Continuous
Pressure	Capacitance transducer	Continuous
	Mercurial barometer	1 wk^{-1}
Wind (speed and direction)	Bendix Aerovane	Continuous
Precipitation	Rain gauge, tipping bucket	Continuous
	Rain gauge, plastic bulk	1 day^{-1}
Precipitation Chemistry		
Anions (NO_3^-, $SO_4^=$)	Dionex QIC ion chromatograph	1 day^{-1} (CMDL)
Cooperative Programs		
CO_2, ^{13}C, N_2O (SIO)	5-L evacuated glass flasks	1 set wk^{-1} (3 flasks set^{-1})
GAGE project: CFC-11, CFC-12, N_2O, CH_3CCl_3, CCl_4 (SIO)	HP5880 gas chromatograph	1 h^{-1}
Various trace gases (OGIST)	Stainless steel flasks	1 set wk^{-1} (3 flasks set^{-1})
Bulk deposition (EML)	Plastic bucket	Continuous (1 bucket mo^{-1})
Hi-vol sampler (EML)	High-volume sampler	Continuous (1 filter wk^{-1})
Hi-vol sampler (SEASPAN Project)	High-volume sampler	Continuous (1 filter wk^{-1})
CH_4,($^{13}C/^{12}C$ ratio) (Univ. of Wash.)	30-L pressurized cylinder	Biweekly
Light hydrocarbons (UCI)	1-L evacuated stainless steel flasks	3-4 flasks qtr^{-1}
O_2 (URI)	2.5-L glass flasks	2 pair mo^{-1}
O_2 (SIO)	3-L glass flasks	2 sets mo^{-1} (3 flasks set^{-1})

Carbon Dioxide

The continuous CO_2 analyzer ran faithfully through the year with only one short period of downtime. Data quality was very high.

The most difficult task of the year was to replace the sample lines that run up the side of the 18-m mast. The wind-induced vibrations in the Dekoron tubing caused cracks and eventually breakage in several places. With the use of climbing gear, the station chief replaced all four lines that extended to the top of the mast. Further restraint was added to the lines to reduce vibration and hopefully prevent future problems of this sort.

The glass fittings on the through-analyzer flask filling apparatus were replaced with Teflon fittings.

A by-pass valve was added to the no. 2 air line upstream of the analyzer. The valve will be open for about an hour every 2 weeks for filling flasks for two cooperative projects. One set of flasks will come from SIO and the other from URI.

Surface Ozone

The Dasibi ozone monitor was down for several months when it became lost in the mail on its way in for repairs. A replacement Dasibi was installed toward the end of the year and worked well after overcoming a small difficulty. The new monitor had water condensation inside the intake line and in the instrument causing erratic output. To take care of this problem, the intake line was insulated and warmed with heat tape to prevent condensation.

The data recorded by CAMS was frequently interrupted because of the sensitive nature of the signal-receiver board. This problem was due to the lack of reliable power for CAMS. Some improvement was made when a power connection was made to the UPS in the Ekto building.

Total Ozone

The Dobson ran well. The instrument was sent to Hawaii for 2 weeks of intercomparison calibration. When the Dobson was returned, a member of the Aerosols, Radiation, Ozone, and Water Vapor Division installed a digital encoder. The encoder is connected to a computer that records the r-dial numbers and calculates the total ozone. This improved setup has relieved the staff of the tedious process of writing the data on paper forms.

Halocarbons and Nitrous Oxide

When operating properly, the dual GC system produces reliable data. There was one small problem and one big problem to contend with during the year. One of the ECD's went bad and had to be replaced, but the old one had to be sent back first. Once the replacement arrived, a successful installation was made quickly with little difficulty.

Computer hang-ups were a far more perplexing problem. In the beginning of the year the system was running day after day with virtually no down time (this can be credited to the previous installation of a UPS). The computer then started to hang-up for no apparent reason. The suspected cause for the malfunction was replaced but this didn't help much. The hard drive was reformatted and the programs reinstalled, again this didn't help. At year's end, it was almost a daily ritual to reboot the stalled system.

Aerosols

After a period of good side-by-side comparison between the TSI and GE, the GE was retired. The TSI performed well with only a few small problems. The Pollak counter also worked reliably throughout the year.

Water condensed inside the TSI and displaced the alcohol. This was remedied by pouring out the liquid and filling the instrument with pure butanol.

The ammeter connected to the Pollak had to be replaced when the needle began to respond sluggishly. Other than that, the Pollak had a good year as usual.

Solar Radiation

The solar radiation instruments are usually very dependable and this year was no exception. The only problem was a leak in the seal around the dome of the Q-pyranometer. In an attempt to pinpoint the leak, a little air pressure was applied to the instrument; a little too much air pressure was used and the whole dome popped off. Since there was no damage to the dome, it was reattached and put back into service leak free.

Meteorology

Everything went well for the meteorological system during the year. However, two occurrences deserve mention. (1) The wind speed reported by the Aerovane was too low. After verifying the integrity of the electronics, a new Aerovane was installed and tested. From then on, the wind-speed indications were reliable. (2) When the registered dewpoint temperatures indicated below-zero readings, the mirror assembly was replaced and the problem solved.

CAMS

For the most part, CAMS did its job of collecting data. The early part of the year was marked by several interruptions because of power problems that resulted in board failures inside the MO3 and ASR CAMS units. This problem was relieved by upgrading the 182-m (600-ft) extension cord that connected the CAMS units to the UPS in the Ekto building. Even after this improvement, all the CAMS units still experienced occasional auto-restarts but these were few and far apart.

Cooperative Programs

The SIO GC produced consistent data during the year. The ignitor in the FID failed and had to be replaced. This fairly delicate operation was performed successfully with only a very short period of interruption in the data. The UPS kept the system going continuously by protecting the equipment from the unreliable power supplied locally. To ensure continued UPS operation, a fresh set of batteries was installed.

The SEASPAN system is another one of those projects that rarely has a problem, but during this year, the big,

heavy blower had to be swapped out two times. There was a spare on hand the first time so there was very little down time, but the second time the replacement had to be shipped. This resulted in several months of down time.

Two new cooperative flask programs were added during the year. One is for SIO and the other for URI.

1.4. South Pole Observatory

K. McNitt

1.4.1. Operations

SPO is part of a larger U.S. Antarctic presence that works in conjunction with NSF and ASA to conduct research at the Amundsen-Scott South Pole Station. SPO is just one of many projects at the geographic South Pole where the elevation is 2835 m above sea level and the average temperature is -49°C.

Because airplanes can only land at the Pole during the relatively warm months of October through February, the station is physically "closed" for 8 months each year, with the exception of one mid-winter "airdrop" resupply in June. Data are transferred digitally via satellite throughout the year; however, air samples taken during the austral winter cannot be returned for analysis until the following spring. Of the 28 winterovers for the 1992-1993 season, four were NOAA employees. Along with the CMDL programs, ERL Environmental Technology Laboratory studied atmospheric boundary layer interactions and changes in relation to ozone-hole development.

Most of the CMDL projects are housed in the Clean Air Facility (CAF), an elevated building located 90 m grid northeast of the main station's fuel arch. As described in previous CMDL Summary Reports, the CAF is reaching its projected lifetime and is scheduled for replacement. Consequently, many upgrading projects for the CAF were left unresolved. But regardless of this, a concerted effort to improve the safety and efficiency of the current building was made.

Because the wind blows predominantly from the grid north or northeast, a "Clean Air Sector" has been designated into which excursions are prohibited without permission. This Clean Air Sector is marked and includes the area grid north of the CAF from 340° to 110°.

CMDL's meteorological instruments are mounted on the walk-up Met. Tower, less than 100 m from the CAF, and operations for the balloon program take place in three locations: the main station science building, the cargo arch, and the Balloon Inflation Tower (BIT).

Power outages were rare this year, but science demands continued to exceed "clean" power supplied by the CAF UPS. UPS-fed receptacles were identified and labeled to prevent accidental overloads, and the backup batteries were replaced. ASA electricians rewired the fire alarm system and rectified potentially dangerous wiring schemes in the building.

1.4.2. Programs

Table 1.6 is a summary of the measurement programs at SPO during 1993, and Table 1.7 is a discrete measurements summary the 1992-1993 winterover year.

Carbon Cycle Division

The Siemans continuous CO_2 analyzer ran without significant problems, although occasional repair of the chart recorder was necessary when the electronics were damaged by static discharge, and there was a period of several weeks at the beginning of the season when no chart paper was available.

Sample flask pairs were filled through the analyzer once per week and through a portable MAKS unit twice per month. The most significant improvement in the SPO carbon cycle program this year was the switch from the "greased connection" flasks to the flasks with Teflon valve seals. The analyzer manifold was modified to fill the new flasks in series, and the new MAKS unit required no modification.

Aerosols

The MRI four-wavelength nephelometer was off-line for 1 month at the beginning of the season while waiting for a replacement filter wheel motor; otherwise, the nephelometer and the TSI condensation nucleus counter ran continuously without extraordinary problems.

Discrete observations with the Pollak condensation nucleus counter took place twice daily for comparison with the TSI instrument.

Solar and Terrestrial Radiation

During the summer, all Eppley pyranometers, pyrgeometers, and the tracking pyrheliometer ran continuously without significant problems. Discrete observations with the filter wheel NIP took place three times daily. After sunset in March, the short-wave instruments were taken off-line for the winter. One up-facing and one down-facing pyrgeometer remained. The down-facing instrument was off-line for 5 months because of damage received during an apparent power surge.

Ozone and Water Vapor

The Dasibi ultraviolet absorbtion ozone monitor no. 322833 replaced instrument no. 5229 after 2 weeks of intercomparisons. The only remarkable problem with the new analyzer was the self-destruction of its pump that was replaced when small plastic shavings were discovered behind the exhaust outlet and the flow rate dropped below an acceptable level.

Discrete observations with the Dobson ozone spectrophotometer took place during the summer

TABLE 1.6. Summary of Measurement Programs at SPO in 1993

Program	Instrument	Sampling Frequency
Gases		
CO_2	Siemans IR analyzer	Continuous
CO_2, CH_4	2.5-L glass flasks, through analyzer	1 pair twice mo^{-1}
	2.5-L glass flasks, MAKS pump unit	1 pair twice mo^{-1}
Surface O_3	Dasibi ozone meter	Continuous
Total O_3	Dobson spectrophotometer no. 82	3 day^{-1}
Ozone profiles	Balloonborne ECC sonde	1 wk^{-1}, summer, autumn, winter; 1 (3 day)$^{-1}$, spring
Water vapor	Balloonborne sonde	10 times yr^{-1}
N_2O, CFC-11, CFC-12, CFC-113, CH_3CCl_3, CCl_4	300-mL stainless steel flasks	1 sample mo^{-1}
N_2O, CFC-11, CFC-12, CFC-113, CH_3CCl_3, CCl_4, HCFC-22, HCFC-141b, HCFC-142b, CH_3Br, CH_3Cl, CH_2Cl_2, $CHCl_3$, C_2HCl_3, C_2Cl_4, H-1301, H-1211	850-mL stainless steel flasks	1 sample mo^{-1}
CFC-11, CFC-12, CFC-113, N_2O, CH_3CCl_3, CCl_4	Shimadzu automated GCs	1 sample h^{-1}
Aerosols		
Condensation nuclei	Pollack CNC	2 day^{-1}
	TSI CNC	Continuous
Optical properties	Four-wavelength nephelometer	Continuous
Solar Radiation		
Global irradiance	Eppley pyranometers with Q and RG8 filters	Continuous, summer
	Eppley pyranometer with Q filter	Continuous, summer
	Net radiometer	Continuous, summer
Direct irradiance	Eppley pyrheliometer with Q, OG1, RG2, and RG8 filters	2 day^{-1}
	Eppley pyrheliometers with Q and RG8 filters	Continuous, summer
Albedo	Eppley pyranometers with Q and RG8 filters filters, downward facing	Continuous, summer
Terrestrial (IR) Radiation		
Unwelling and downwelling	Eppley pyrgeometers	Continuous
Meteorology		
Air temperature	Platinum resistor, 2- and 20-m heights	Continuous
Pressure	Capacitance transducer	Continuous
	Mercurial barometer	1 time wk^{-1}
Wind (speed and direction)	Bendix Aerovane	Continuous
Frost-point temperature	Hygrometer	Continuous
Cooperative Programs		
CO_2, ^{13}C, N_2O (SIO)	5-L evacuated glass flasks	2 mo^{-1} (3 flasks sample^{-1})
Total surface particulates (DOE)	High-volume sampler	Continuous (4 filters mo^{-1})
Various trace gases (OGIST)	Stainless-steel flasks	1 week^{-1} (2 flasks set $^{-1}$), summer only
Interhemispheric $^{13}C/^{14}C$ (CSIRO)	5-L glass flasks	1 or 2 flasks mo^{-1}
O_2, N_2 (Scripps)	Air sampling pump and flasks	1 mo^{-1} (3 flasks set^{-1})
Isotope production (LLNL)	Pressurized cylinders	N/A; checked once mo^{-1}

TABLE 1.7. South Pole Discrete Measurements Summary for the 1992-1993 Winterover Year

	1992		1993									
	Nov.	Dec.	Jan.	Feb.	March	April	May	June	July	Aug.	Sept.	Oct.
CMDL Programs												
Dobson obs.	451	594	397	225	51	-	90	93	45	72	-	214
Pollak obs.	135	149	149	124	168	162	156	156	156	165	165	162
Filter wheel NIP	42	41	72	46	8							6
Smithsonian model comparison (radiation)	21	26	43	31	19							15
Meteorology obs.	30	31	31	28	31	30	31	30	31	31	30	31
CO_2 flasks T.A.	10	6	8	6	10	8	10	8	8	10	8	8
CO_2 flasks MAKS	4	4	8	2	4	4	4	4	4	4	4	4
NOAH flasks	10		6	8	10	2	2	2	2	2	2	
Balloons O_3	9	3	3	5	5	5	4	4	5	9	11	11
Balloons H_2O			1			1		2	2			1
Cooperative Programs												
CSIRO CO_2 flasks	1	2	2	1	1	2	1	2	1	2	1	1
OGC trace gases	10	6	6									6
Scripps CO_2 flasks	6	6	6	6	6	6	6	6	6	6	6	6
Scripps O_2 and N_2 flasks	3	2	3		2	3	3	2	3	3	3	2
DOE radionuclies filters	4	4	4	4	4	4	4	4	4	4	4	4

months when the sun was sufficiently high above the horizon and then in the darkest winter months during each full moon. Dobson no. 82 replaced no. 80 after extensive intercomparisons. This year marked the first year of observations with the new electronic shaft encoder and computerized data acquisition system that worked wonderfully and also drastically reduced the time required for digital transfer of data to Boulder.

The ozonesonde and water vapor programs had a very successful season despite early troubles with the ozondesonde solutions and faulty connections in the telemetry cables. On October 6, 1993, one of our ozonesondes recorded an all-time low, total ozone value of 90 Dobson units. Data from this flight were supported by Dobson observations performed on the same day.

Rubber balloons were launched from the BIT platform during the summer months. Water vapor flights and winter ozonesonde flights required the larger plastic balloons that were filled in the cargo arch and launched from the cargo yard. Launches usually occured once per week except during the months of stratospheric ozone depletion (August-November) when the schedule was changed to every 3 days.

This year several successful dual launches with the ASA Meteorological Department (MET) were completed. There are many advantages to dual launches: Helium and MET balloons are conserved, the plastic balloons reach higher altitudes than the MET rubber balloons, and flight monitoring is easier with the MET automated tracking system than with the NOAA manual system. The CMDL antenna and the ASA MET antenna coexist in the radome on top of the BIT with very few instances of interference. The only interference that occurred was during the summer months when winds were light and the MET balloon rose straight overhead, causing their antenna to point directly at ours. The two antennas cannot physically bump into each other.

Nitrous Oxides and Halocarbons Division

The two Shimadzu Mini-2 electron capture gas chromatographs were inspected and upgraded during the summer by staff from the Nitrous Oxides and Halocarbons Division, adding "watchdog valves" to the gas standards and running new sample lines up the meteorological tower. For the remainder of the year, the GCs measured one sample from the sampling stack on the CAF roof and one from the middle of the tower.

Sample flask pairs were filled with ambient air once per week during the summer and once per month during the winter.

Meteorology

A faulty power supply was the cause of questionable data during days 93212-93222. Otherwise, continuous temperature, wind, and pressure data were recorded without significant problems. Manual weather observations took place daily at midnight UT and data were compared with those collected by the ASA MET Department.

Data Acquisition

This was the last year of operation for most of the CAMS units that ran continuously without unexpected problems, except for occasional eccentricities when updating the date or time.

Cooperative Programs

CSIRO. Long-term monitoring of the ratio $^{13}C/^{12}C$ in atmospheric CO_2 for use in a 2-D global carbon cycle model. One glass flask was pressurized with ambient air per month, two during even numbered months. A new (portable) pump arrived during the summer and operations were trouble-free.

OGIST. Seasonal trends in the amount of chlorine- and bromine-containing trace gases in the Antarctic. Two flasks per week were filled with ambient air. No extraordinary problems were encountered.

SCRIPPS. Long-term monitoring of CO_2, $^{13}C/^{12}C$ ratio, and N_2O. Twice per month, three evacuated glass flasks were exposed to ambient air. No significant problems occurred.

SCRIPPS. Long-term monitoring of O_2 and N_2. Three glass flasks were pressurized with ambient air once per month. Reduced flowrates and broken stopcocks were a problem at the beginning of the season, but the last several months of sampling went smoothly.

LLNL. Quantification of the production rate of radiocarbon by galactic cosmic rays. Seven air-filled cylinders were placed on platforms approximately 800 m downwind of the main station. The cylinders were inspected and cleared of snow periodically; no other operations were required.

DOE. Long-term monitoring of the spatial and temporal distribution of specific and anthropogenic radionuclides in surface air. The DOE pump ran continuously without significant problems; filters were replaced four times per month.

Miscellaneous

The University of Rome lidar and the U.S. Navy ceilometer are no longer CMDL cooperative projects, but assistance was given to the ASA science technicians with operations and maintenance of both instruments. CMDL staff recovered snow stakes throughout the year to help representatives from U.S. Army Cold Regions Research and Engineering Laboratory determine the amount of snow accumulation around the South Pole Station.

1.5. REFERENCE

Thoning, K.W., P.P. Tans, and W.D. Komhyr, Atmospheric carbon dioxide at Mauna Loa Observatory, 2, Analysis of the NOAA GMCC data, 1974-1985, *J. Geophys. Res., 94(D6)*, 8549-8565, 1989.

2. Carbon Cycle Division

P.S. BAKWIN (EDITOR), T.J. CONWAY, E.J. DLUGOKENCKY, D.W. GUENTHER, D. KITZIS, P.M. LANG, K.A. MASARIE, P.C. NOVELLI, K.W. THONING, P.P. TANS, AND L.S. WATERMAN

2.1. CONTINUING PROGRAMS

2.1.1. IN SITU CARBON DIOXIDE MEASUREMENTS

The mixing ratio of atmospheric CO_2 was measured with continuously operating NDIR analyzers at the four CMDL observatories during 1993 as in previous years. Monthly and annual mean CO_2 concentrations (in the WMO 1985 mole fraction scale (X85)) are given in Table 2.1. These values are provisional, pending final calibration of station standards. Preliminary selected monthly-average CO_2 mixing ratios for the entire record through 1993 are plotted versus time for the four observatories in Figure 2.1.

The CO_2 in situ systems operated during 1993 from a low of 86.2% at BRW to a high of 97.5% of the year at MLO. SMO and SPO were operational 96.5% of the time. This is based on the number of valid hourly-averaged CO_2 mixing ratios that were calculated for the year, taking into account missing data because of reference gas calibrations during the year. The major loss of data at BRW was due to a mechanical failure in the CO_2 NDIR analyzer in February that was corrected in late March.

The growth rates of CO_2 as measured by the in situ observatory systems, returned to more normal values fter showing smaller than average growth rates in 1992. Figure 2.2 shows the instantaneous growth rate at the four CMDL observatories for 1980 through 1993. The BRW growth rate, which typically has greater fluctuations than the other sites, appeared to reach its lowest value in mid-1992, before any of the other sites.

TABLE 2.1. Provisional 1993 Monthly Mean CO_2 Mixing Ratios From Continuous Analyzer Data (ppmv, Relative to Dry Air WO X85 Mole Fraction Scale)

Month	BRW	MLO	SMO	SPO
Jan.	362.45	356.79	355.38	354.04
Feb.	361.81	357.13	355.34	354.22
March	363.43	358.23	355.93	354.06
April	363.03	359.14	355.59	354.17
May	363.22	360.05	354.67	354.31
June	360.51	359.37	355.42	354.58
July	351.55	357.22	355.41	355.05
Aug.	347.69	355.31	356.10	355.50
Sept.	349.14	353.81	355.74	355.72
Oct.	354.12	354.03	355.82	355.72
Nov.	358.41	355.20	356.14	355.75
Dec.	360.17	356.70	356.63	355.55
Year	357.96	356.92	355.68	354.89

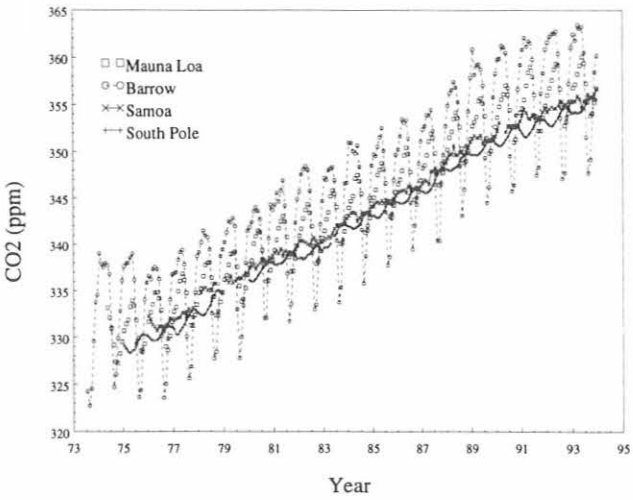

Fig. 2.1. Preliminary selected monthly mean CO_2 mixing ratios at the four CMDL observatories.

The minimum appeared to propagate southward with lesser magnitude, reaching SPO last by the first quarter of 1993.

New data acquisition systems are planned for the eventual replacement of the CAMS units at the four observatories. Five Hewlett Packard UNIX workstations were purchased in 1993 that will take over the task of controlling data acquisition not only for the CO_2 in situ system, but for the CH_4 and CO in situ

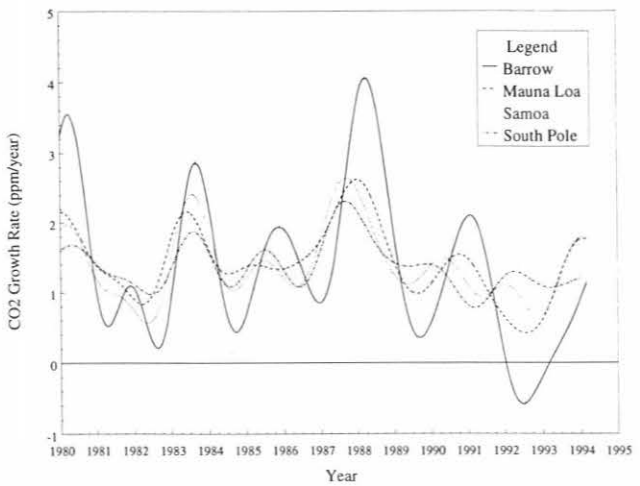

Fig. 2.2. The variation of the CO_2 mixing ratio growth rate for 1980-1993. The curves are the time derivatives of the deseaonalized, smoothed daily mean data for the four CMDL observatories.

chromatograph systems as well. These computers, with associated equipment, are scheduled to be installed at the observatories starting in 1994. These types of systems will be compatible with the computer systems used in the Boulder laboratory for flask sample analysis and reference gas calibrations, so that software will be identical for all analysis systems throughout the Carbon Cycle Division.

2.1.2. Flask Sample Carbon Dioxide Measurements

Carbon dioxide measurements of air samples collected throughout the CMDL cooperative flask sampling network during 1993 continued to provide evidence for recent unexplained variations in the global carbon cycle. Provisional mean CO_2 mixing ratios for 1993, along with revised values for 1991 and 1992, are reported for 32 sites in Table 2.2. This is the first full year of data from the Baltic Sea (BAL) and Vestmanaeyjar, Iceland (ICE). Three new sites were added to the network in 1993: Hegyhatsal, Hungary (HUN); Wendover, Utah (UTA); and Gozo, Malta (GOZ).

TABLE 2.2. Provisional 1991-1993 Annual Mean CO_2 Mixing Ratios From Network Sites

Code	Station	CO_2 (ppm) 1991	1992	1993
ALT	Alert, N.W.T., Canada	357.3	357.5	357.7
ASC	Ascension Island	353.9	355.2	355.8
BAL	Baltic Sea			359.9
BME	Bermuda (east coast)	356.1	357.1	356.8
BMW	Bermuda (west coast)	356.6	356.3	357.3
BRW	Barrow, Alaska	357.6	357.5	358.2
CBA	Cold Bay, Alaska	357.3	357.3	357.8
CGO	Cape Grim, Tasmania	352.8	353.6	354.5
CHR	Christmas Island	355.4	356.5	357.3
CMO	Cape Meares, Oregon	356.7	356.4	358.5
GMI	Guam, Mariana Islands	356.1	356.4	356.6
HBA	Halley Bay, Antarctica	353.2	354.6	355.1
ICE	Vestmanaeyjar, Iceland			357.4
IZO	Izaña Observatory, Tenerife	[ ]	356.2	357.5
KEY	Key Biscayne, Florida	356.5	357.3	358.4
KUM	Cape Kumukahi, Hawaii	355.8	356.3	357.1
MBC	Mould Bay, Canada	357.6	357.4	357.8
MHT	Mace Head, Ireland	[ ]	356.1	356.7
MID	Midway Island	357.0	356.8	357.5
MLO	Mauna Loa, Hawaii	355.6	356.5	356.9
NWR	Niwot Ridge, Colorado	356.1	356.9	357.4
PSA	Palmer Station, Antarctica	353.2	354.2	355.1
QPC	Qinghai Province, China	[ ]	356.6	357.3
RPB	Ragged Point, Barbados	355.9	356.0	356.7
SEY	Mahé Island, Seychelles	353.9	354.9	356.0
SHM	Shemya Island, Alaska	356.7	357.2	357.7
SMO	American Samoa	354.2	354.9	355.6
SPO	South Pole, Antarctica	353.1	354.1	354.8
STM	Ocean Station M	356.5	356.6	357.5
SYO	Syowa Station, Antarctica	353.3	354.2	354.5
TAP	Tae-ahn Peninsula, S. Korea	359.7	360.5	360.4
UUM	Ulaan Uul, Mongolia		356.6	357.1

Square brackets indicate insufficient data to calculate annual mean.

The selection of new network sites continues to be motivated by the need to include measurements from continental regions in global carbon cycle analyses. Three examples of this strategy are shown in Figure 2.3, where the CO_2 data for Ulaan Uul, Mongolia (UUM); Tae-ahn Peninsula, South Korea (TAP); and Qinghai Province, China (QPC) are plotted. The remote desert site at UUM and the high plateau location of QPC appear to be excellent sites for sampling well-mixed continental air, unaffected by local vegetation or pollution sources of CO_2. The coastal site at TAP is more heavily influenced by local anthropogenic sources, as evidenced by the higher variability, but it has already yielded useful information relevant to regional CH_4 emissions [*Dlugokencky et al.*, 1993].

Sampling was temporarily discontinued in the Pacific Ocean from the Blue Star Line ships *Southland Star*, PAC (August) and *Wellington Star*, PAW (July), and in the South China Sea from the Chevron ship *Carla A. Hills*, SCS (February). Pacific Ocean sampling was restarted in October from the Blue Star Line ship *California Star* and given the 3-letter code OPC. Sample collection resumed in the South China Sea from aboard the *Great Promise* in November, retaining the same site code, SCS.

The lower-than-average rate of increase of atmospheric CO_2 observed in 1992 continued in 1993. The CO_2 data for Mould Bay and South Pole are shown as examples in Figures 2.4 and 2.5. An analysis of the flask network data through 1992 yielded a globally-averaged CO_2 growth rate of 0.6 ppm yr^{-1} from 1991 to 1992 [*Conway et al.*, 1994].

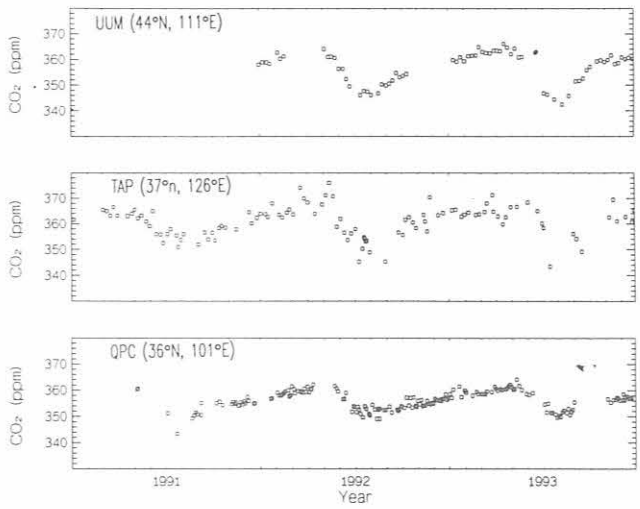

Fig. 2.3. CO_2 mixing ratios determined for flask samples collected at Ulaan Uul, Mongolia (UUM); Tae-ahn Peninsula, South Korea (TAP); and Qinghai Province, China (QPC) from 1991 through 1993. The square symbols represent the average CO_2 mixing ratios for two flasks collected in series.

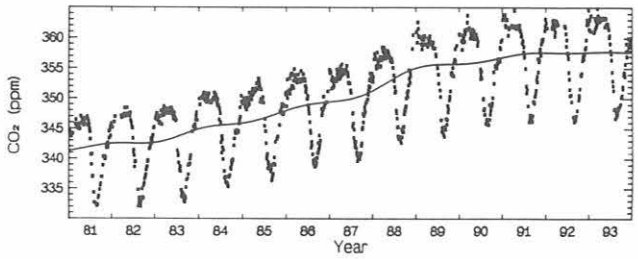

Fig. 2.4. CO_2 mixing ratios measured in flask samples collected at Mould Bay, Canada (MBC). The square symbols represent the average value for two flasks collected in series. The smooth curve represents the deseasonalized long-term trend. Note the near-zero increase in 1992 and the slight increase in 1993.

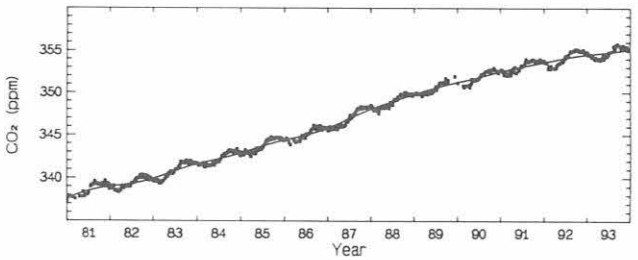

Fig. 2.5. CO_2 data and long-term trend for SPO. Note that the 1992-1993 growth rate decline is not as pronounced as at Mould Bay.

The average growth rate for the latitude band from 30° to 90°N, based on data through the end of 1992, was essentially zero. The global and semihemispheric growth rates through 1993 are given in Table 2.3.

The globally-averaged CO_2 increase from 1992 to 1993 was only ~0.7 ppm, about half the average 1981-1991 annual increase. Most of the change in the 1992-1993 global growth rate compared with 1991-1992, is due to a recovery of the growth rate from 30° to 90°N to 0.7 ppm yr^{-1}. The CO_2 growth rates for the other semihemispheres during 1992-1993 were nearly equal to or slightly less than during 1991-1992. The variation with time of the globally-averaged CO_2 growth rate is shown in Figure 2.6. The uncertainty of this curve is ~0.2 ppm yr^{-1} from 1981 to 1987, and ~0.1 ppm yr^{-1} thereafter. For the last 6 months of 1993, this curve is less certain because the end of the curve is poorly constrained until several months of 1994 data are included. A preliminary look at available 1994 data suggests that the upturn of the CO_2 growth rate at the end of 1993, evident in Figure 2.6, will continue into 1994.

TABLE 2.3. Semihemispheric and Globally Averaged CO_2 Growth Rates (ppm yr^{-1})

Period	30-90°S	0-30°S	0-30°N	30-90°N	Global
1981-1991	1.43	1.48	1.51	1.59	1.50
1991-1992	0.93	0.89	0.62	0.09	0.64
1992-1993	0.87	0.82	0.59	0.67	0.74

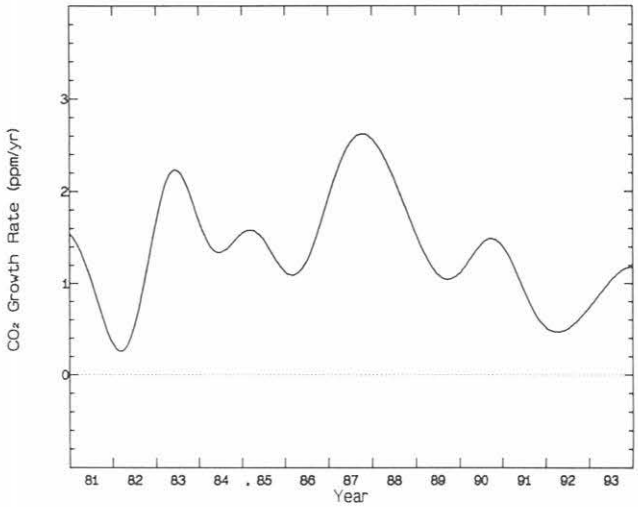

Fig. 2.6. The globally averaged CO_2 growth rate obtained from the flask network data. Because this curve is based on data only through the end of 1993, the last 6 months must be viewed with caution. Preliminary 1994 data suggest that the upturn of the growth rate in 1993 will continue into 1994.

2.1.3. In Situ Methane Measurements

During 1993, in situ measurements of atmospheric CH_4 continued with a frequency of 60 samples per day at MLO and BRW. The precision of the measurements (~0.2%) is limited in part by variations in laboratory temperature that affect the flow rate of the flame ionization detector (FID) fuel, H_2. In Figure 2.7, reference peak heights are plotted for a 2-wk period at MLO. A distinct diurnal cycle is evident. This is observed because the H_2 cylinder is stored in an attached, but unheated portion of the MLO laboratory, where temperature mearly tracks the outside temperature. The low pressure setting of the cylinder regulator determines the H_2 flow rate at the FID, and is sensitive to temperature. Fortunately, the temperature change is slow enough that the measure-ments are not affected too severely. At BRW, variations in reference peak height are even larger than at MLO, but these probably cannot be fully explained by variations in laboratory temperature. A temperature controlled, heated module is being built where high-precision pressure regulators will be housed, and these will determine the gas flow rates without the effects of varying room temperature. The gas sample valve will be moved from the GC oven into the heated module. The benefit of this is that the GC oven can then be used to bake out the silica gel and molecular sieve columns at much higher temperatures than currently achievable with the valve inside the oven since the valve can be

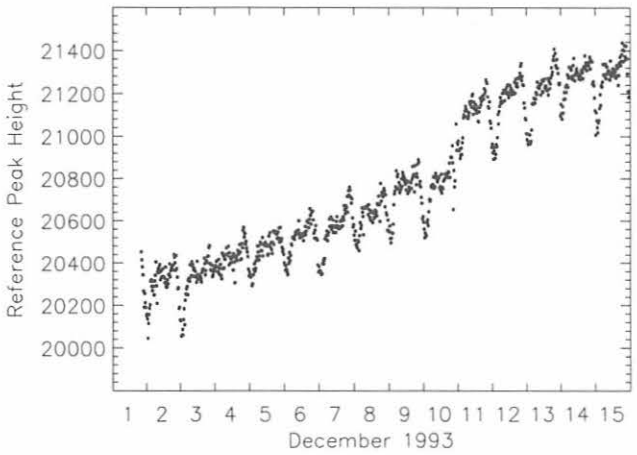

Fig. 2.7. Methane reference gas peak heights, in counts (where 1 count = 0.125 mV), for a 2-wk period at MLO. Peak heights were quantified with an HP3393A integrator.

damaged by heating above 150°C. A GC containing these modifications should be installed at MLO during 1994.

Edited, unconstrained, daily mean CH_4 mixing ratios are shown in Figure 2.8*a* for BRW and 2.8*b* for MLO. Features in the data in 1993 are similar to previous years. At MLO, CH_4 is highly variable on time scales of days to weeks because of variations in atmospheric transport [*Harris et al.*, 1992]. At BRW, most of the highest values are because of local CH_4 emissions. At both observatories, CH_4 is lower during summer than during winter because of chemical destruction by hydroxyl radical. Methane seasonal cycles at MLO and BRW are explored in more detail below.

In Figure 2.9*a*, standard deviations from the daily means are shown for MLO. The maximum frequency

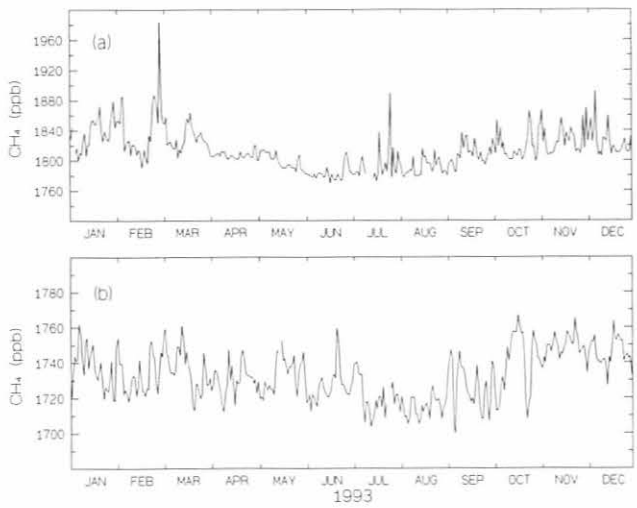

Fig. 2.8. Daily mean CH_4 mixing ratios in ppb for (a) BRW and (b) MLO for 1993. The data are unconstrained, but have undergone a quality control step to ensure that the analytical instrument was working optimally when they were obtained [*Masarie et al.*, 1991].

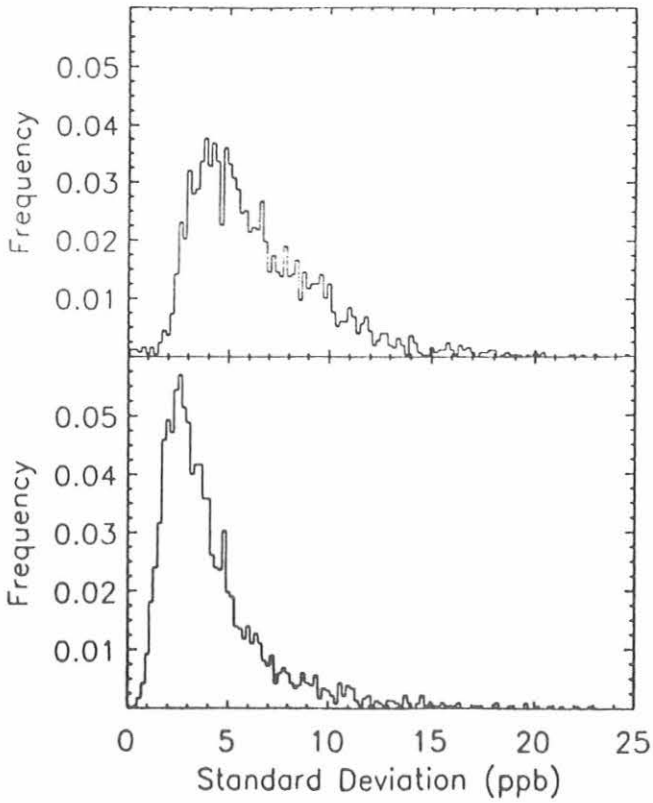

Fig. 2.9. (*a*) Histogram of standard deviations for MLO daily means calculated from hourly averages. (*b*) Same as a, but data were constrained to time periods between 0000 to 0700 LST to capture downslope conditions. In both cases, there is one datum lying outside the range plotted.

occurs at s ~4.5 ppb, and the distribution has a relatively long tail. The shape of the distribution depends on the instrument precision and natural variations in the CH_4 mixing ratio at the sampling site. At MLO a diurnal cycle in the methane mixing ratio sometimes exists with a peak-to-peak amplitude of ~10 ppb because of the upslope and downslope wind regimes [*Peterson and Rosson*, 1993]. Daily means were also calculated for times of predominantly downslope conditions (0000-0700 LST) that represent free tropospheric air. The associated standard deviations are shown in Figure 2.9*b*. Note that the maximum in the distribution shifts to s ~2.5 ppb, close to the instrument precision, and much of the long tail is no longer present. Still, the distribution is not Gaussian. This results because natural variations in CH_4 mixing ratios, due to variations in transport, are still present.

The CH_4 time-series is a combination of three primary factors: (1) a long-term trend because of the small imbalance between CH_4 sources and sinks; (2) an annual cycle because of the seasonality of some CH_4 sources and the CH_4 photochemical sink; and (3) short-term variations occurring on time scales of days to weeks due to variations in atmospheric transport at the

sampling sites. These components were separated for analysis by first fitting a quadratic polynomial to the data to represent the long-term trend and a series of four harmonics to represent the average seasonal cycle.

$$f(t) = a_1 + a_2 t + a_3 t^2 + \sum_{i=1}^{4} [a_{2i+2} \sin(2\pi i t) + a_{2i+3} \cos(2\pi i t)] \quad (1)$$

Digital filtering of the residuals is applied to determine short-term variations (filter cut off = 4.56 cycles yr^{-1}) and interannual variations in the long-term trend (filter cut off = 0.55 cycles yr^{-1}).

The average, detrended seasonal cycles for BRW (*a*) and MLO (*b*) are shown as the solid curves in Figure 2.10. These curves show only the fundamental and harmonic frequencies. The filled circles are detrended monthly means (±1s) determined from a smooth curve fitted to daily means. At MLO, the average position of the seasonal maximum was at the end of November, and the seasonal minimum was during the first week of August. The average peak-to-peak seasonal cycle amplitude was 25.1 ppb. At BRW, the average position of the seasonal maximum was at the beginning of February, and the minimum occurred on average at the end of June. The average seasonal-cycle amplitude at BRW was 47.2 ppb. Minimum values at both sites occurred during the summer when the photochemical sink was most active. The minimum at BRW preceded MLO by about 6 weeks. This is probably due to the seasonality of CH_4 emissions from boreal wetlands that become active during early summer and reach their peak emissions during late summer, somewhat canceling the effect of chemical destruction. Although the emissions from boreal wetlands and rice agriculture also play a part in determining the phase and amplitude of the CH_4 seasonal cycle at MLO, the effect is smaller due to the large distances between MLO and the source regions.

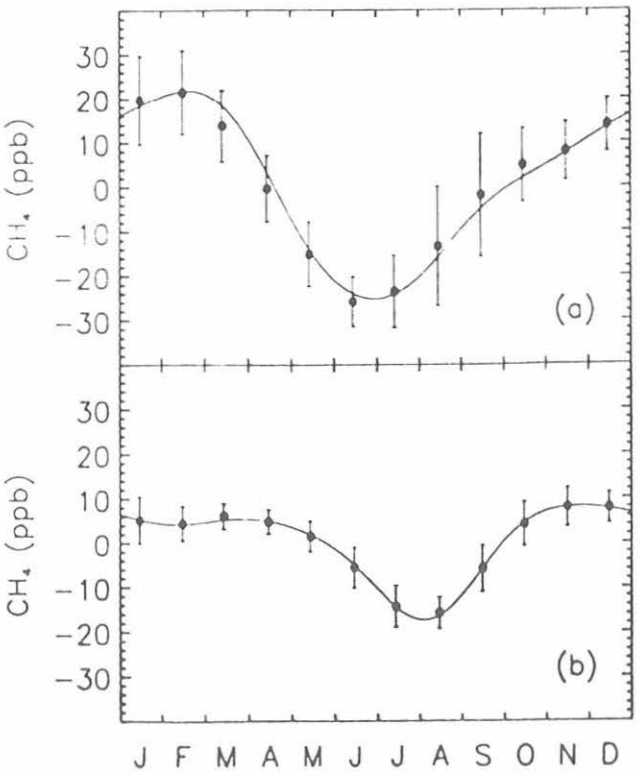

Fig. 2.10. Average seasonal cycles for BRW (*a*) and MLO (*b*) determined from the fundamental and harmonic frequencies in eq. 1. Detrended monthly means are also shown (±1s); these were determined from the smooth curve fits to complete data records for each site.

2.1.4. Flask Measurements of Methane

During 1993, the determination of the global distribution of atmospheric CH_4 continued at 37 sampling sites of the Carbon Cycle Division's cooperative air sampling network. The gaps in the data records (see section 2.1.2) prevent us from including annual means for shipboard samples collected in 1993. Sampling was started at three new sites during the year: Hegyhatsal, Hungary, HUN (March), Wendover, Utah, UTA (May), and Dwejra Point, Gozo, Malta, GOZ (October). Two of the sites are continental (HUN and UTA), and they should provide interesting new data to complement the other sites in the CMDL predominantly ocean-based network. Provisional annual mean values for 1993 are given in Table 2.4.

One of the best known constraints on understanding the global atmospheric CH_4 budget is the rate of growth. Because of the importance of CH_4 as a greenhouse gas, variations in the trend have been newsworthy, especially during 1992 to 1993 when dramatic changes in growth rate were observed [*Steele et al.*, 1992; *Dlugokencky et al.*, 1994*a*, *b*]. The CH_4 growth rates for the northern and southern hemispheres determined from the smoothed CMDL flask sample data are shown in Figure 2.11. In both hemispheres, a long-term decrease in the rate of increase was observed. In addition, significant interannual variations were also present.

In the southern hemisphere, there was a large increase in the growth rate during 1988-1989. Such changes can be explored quantitatively using mass balance equations. For the southern hemisphere, the rate of increase in CH_4 is given by

$$dS/dt = Q_s + f(N-S) - kS \quad (2)$$

where S and N are the burdens for the southern and northern hemispheres, Q_s is the CH_4 source strength in the southern hemisphere, f is the inverse of interhemispheric exchange time (~1 yr^{-1}), and k is the

inverse of the methane lifetime (~0.1 yr^{-1}). The second derivative is:

$$d^2S/dt^2 = df/dt(N-S) + fd(N-S)/dt + dQ_s/dt - kdS/dt - Sdk/dt. \quad (3)$$

Except for the first term on the right-hand side, all of the terms in eq. 3 can be estimated from the measurement data, and d^2S/dt^2 is determined by taking the derivative of the growth rate curve in Figures 2.11 and 2.12. In 1988-1989, it was ~10 ppb yr^{-2} or 14 Tg yr^{-2}. The difference in hemispheric burdens is determined as the difference between the annual means for each hemisphere, which is about 90 ppb or 125 Tg. It was assumed that this difference does not vary with time, although interannual variations in this parameter have been observed [*Steele et al.*, 1992]. The last three terms on the right-hand side of eq. 2 were interpreted as the fall off in the southern hemisphere growth rate, determined as twice the coefficient a_3 from a fit of eq. 1 to the smoothed southern hemisphere data. This gives -0.5 ppb yr^{-2} or -0.7 Tg yr^{-2}. Filling in these values in eq. 3 suggests that an enhancement by about 12% over average interhemispheric transport is necessary to explain the observation. *Steele et al.* [1992] suggested that increased interhemispheric transport occurred in 1988-1989 because of a La Niña event. La Niña events are characterized by relatively cold surface temperatures in the equatorial Pacific and positive westerly wind anomalies at 200 mbar in the central, equatorial Pacific. Such conditions may be conducive to enhanced transport of trace gases between the hemispheres. Since CH_4 mixing ratios are always greater in the northern hemisphere than the southern hemisphere, such increased transport would lead to an apparent increase in the growth rate in the southern hemisphere.

TABLE 2.4. Provisional 1993 Annual Mean CH_4 Mixing Ratios From the Flask Network Sites

Code	Station	CH_4 (ppm)
ALT	Alert, N.W.T., Canada	1799.1
ASC	Ascension Island	1678.2
BAL	Baltic Sea	1810.3
BME	Bermuda (east coast)	1773.6
BMW	Bermuda (west coast)	1772.8
BRW	Barrow, Alaska	1807.0
CBA	Cold Bay, Alaska	1792.9
CGO	Cape Grim, Tasmania	1667.6
CHR	Christmas Island	1693.3
CMO	Cape Meares, Oregon	1782.1
GMI	Guam, Mariana Islands	1723.6
GOZ	Dwejra Point, Gozo, Malta	[]
HUN	Hegyhatsal, Hungary	[]
ICE	Vestmanaeyjar, Iceland	1793.2
ITN	WITN, Grifton, N. Carolina	1810.7
IZO	Izaña Observatory, Tenerife	1754.1
HBA	Halley Bay, Antarctica	[]
KEY	Key Biscayne, Florida	1750.9
KUM	Cape Kumukahi, Hawaii	1745.5
MBC	Mould Bay, Canada	1803.2
MHT	Mace Head, Ireland	1787.3
MID	Midway Island	1760.0
MLO	Mauna Loa, Hawaii	1727.1
NWR	Niwot Ridge, Colorado	1760.6
PSA	Palmer Station, Antarctica	1668.3
QPC	Qinghai Province, China	1764.7
RPB	Ragged Point, Barbados	1733.7
SEY	Mahé Island, Seychelles	1687.2
SGI	South Georgia Island	[]
SHM	Shemya Island, Alaska	1794.6
SMO	American Samoa	1672.5
SPO	South Pole, Antarctica	1666.7
STM	Ocean Station M	1796.6
SYO	Syowa Station, Antarctica	1677.2
TAP	Tae-ahn Peninsula, S. Korea	1833.9
UTA	Wendover, Utah	[]
UUM	Ulaan Uul, Mongolia	1797.0

Square brackets indicate insufficient data to calculate annual mean.

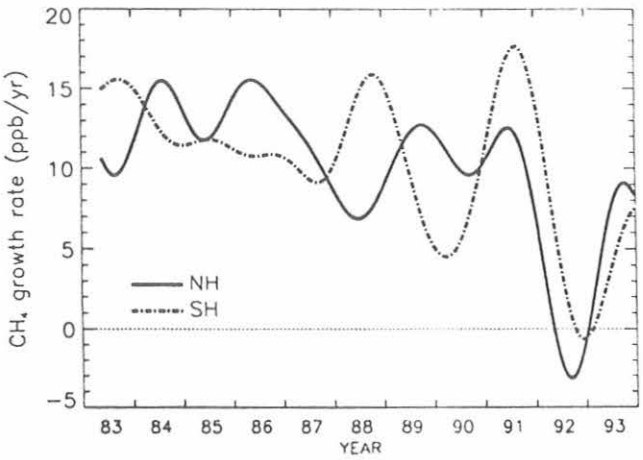

Fig. 2.11. Instantaneous growth rate curves averaged over the northern (solid line) and southern hemispheres (dashed line).

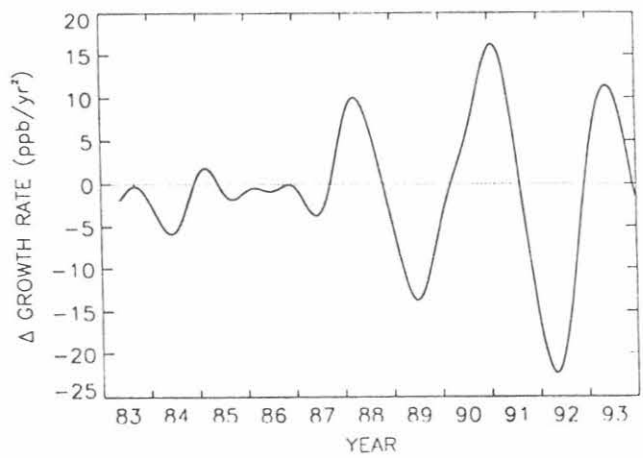

Fig. 2.12. Derivative of the southern hemisphere growth rate curve shown in Figure 2.11 (dashed line). The positive deviations are used to evaluate the left hand side of equation 3 (section 2.1.4).

This hypothesis is supported by an observed simultaneous decrease in the growth rate in the northern hemisphere by a similar amount.

The effects of a change in interhemispheric transport on the hemispheric growth rates were investigated with a 2-box model, with one box for each hemisphere. In the model, sources and sinks were constant, but the interhemispheric exchange term was increased by 10% during 1988 and then returned to normal in 1989. The growth rate for the model result is shown in Figure 2.13. The apparent decrease in growth rate in the year following the increased inter-hemispheric exchange occurs in the model result, and the observation, as the trend, comes back to its average value.

During 1991, another large oscillation in the growth rate was observed, but a La Niña was not. Enhanced interhemispheric transport may have resulted because of the effects of aerosol injected into the atmosphere by the eruption of Mount Pinatubo [*Pitari*, 1993]. The change in f required to explain the measurements was about 18%. A corresponding change in growth rate in the northern hemisphere was not observed, suggesting that if interhemispheric exchange was responsible for the change in southern hemispheric growth rate at that time, there must have been a significant change in northern hemisphere sources or sinks.

During 1992 and 1993, the CH_4 growth rate in the southern hemisphere decreased dramatically. The increase in CH_4 during 1992 was (5.0 ± 0.8) ppb and (3.6 ± 1.0) ppb during 1993. These values compare with a trend of (10.6 ± 0.1) ppb yr^{-1} averaged over the full measurement period (1983-1993). The cause of this decrease is still unknown. In part it is a response to the large increase in growth rate just prior to this, but CH_4 stable isotope data [*Lowe et al.*, 1994] indicate that decreased emissions of fossil CH_4 in the northern hemisphere [*Dlugokencky et al.*, 1994*a*] and decreased biomass burning in the tropics may have played a significant role.

2.1.5. In Situ Carbon Monoxide Measurements

Quasi-continuous in situ measurements of CO were made at BRW during 1993 using the gas chromatograph-mercuric oxide reduction detector previously described [*Peterson and Rosson*, 1993]. The only difference in the analysis procedure in 1993 compared with previous years was to change the calibration approach from a 2-point linear (two standards) to a 2-point piecewise linear calibration (three standards). The standardization procedure and the reference gases were changed on January 16, 1993. The new reference gases had CO mixing ratios of 77.4, 150.9, and 224.2 ppb CO. As before, all standards were referenced to the CMDL CO standard scale [*Novelli et al.*, 1991]. The instrument was operational 98% of the time.

Preliminary CO hourly-average mixing ratios measured in situ during 1993 are compared with those for 1992 (Figure 2.14*a,b*). These data have not been filtered for background conditions (i.e., constrained by wind speed or direction). The time series exhibits periods of low variability punctuated by short-term increases or decreases. These events reflect the influence of local sources and the transport of air parcels from other locations. The seasonal cycle is typical of CO in the high northern latitudes. Both years show maximum CO mixing ratios in late winter and early spring, and a minimum occurs in summer. The annual mean CO mixing ratio determined from the in situ measurements made at BRW during 1993 was 134.6 ppb. In spite of the high frequency variation seen in the in situ record, this annual average agrees well with that

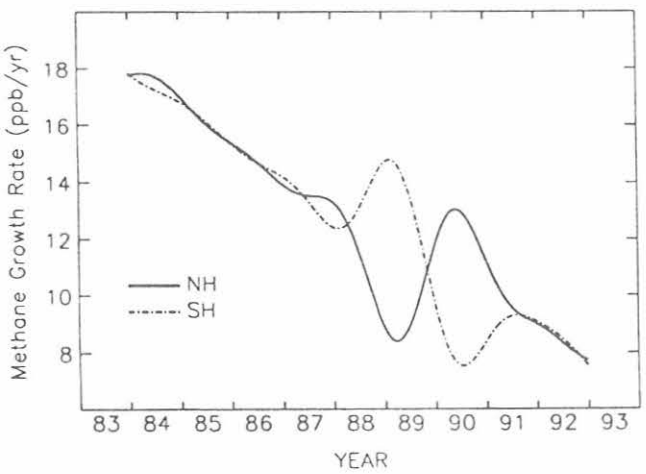

Fig 2.13. Growth rate curves determined from a 2-box model where interhemispheric transport was increased by 10% during 1988 and then returned to normal in 1989. All other source and sink terms in the model remained constant.

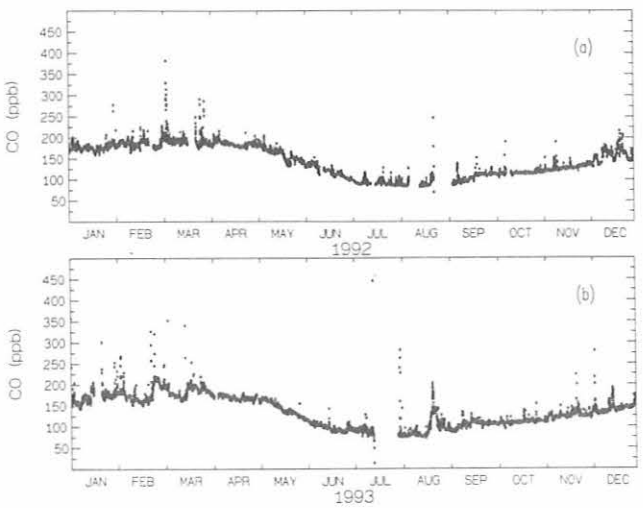

Fig. 2.14. (*a*) Preliminary in situ hourly average CO mixing ratios at BRW in 1992. (*b*) Preliminary in situ hourly average CO mixing ratios at BRW in 1993.

TABLE 2.5. Flask Network Sites for CO Analysis and Preliminary Annual Mean CO Levels (ppb)

Code	Station	Latitude	First Sample*	Annual Mean†
ALT	Alert, N.W.T., Canada	82°N	April 1992	132.8 (3.5)
ASC	Ascension Island	8°S	Feb. 1989	74.1 (3.9)
BAL	Baltic Sea	55°N	Aug. 1992	184.5 (17)
BME	Bermuda (east coast)	32°N	June 1991	128.4 (6.4)
BMW	Bermuda (west coast)	32°N	July 1991	128.0 (5.0)
BRW	Barrow, Alaska	71°N	July 1988	134.2 (3.2)
CBA	Cold Bay, Alaska	55°N	April 1992	133.8 (4.3)
CGO	Cape Grim, Tasmania	41°S	June 1991	50.7 (0.8)
CHR	Christmas Island	2°N	Dec. 1989	72.9 (2.1)
CMO	Cape Meares, Oregon	45°N	Jan. 1992	137.0 (3.6)
GMI	Guam, Mariana Islands	13°N	Oct. 1989	86.0 (3.0)
GOZ	Dwejra Point, Gozo, Malta	36°N	Oct. 1993	
ICE	Heimaey, Iceland	63°N	Oct. 1992	131.5 (2.6)
ITN	WITN, Grifton, N. Carolina	35°N	July 1992	174.1 (14)
IZO	Izaña Observatory, Tenerife	28°N	Nov. 1991	106.7 (3.7)
KEY	Key Biscayne, Florida	25°N	Aug. 1991	100.3 (4.3)
KUM	Cape Kumukahi, Hawaii	20°N	June 1989	101.8 (4.5)
MBC	Mould Bay, Canada	76°N	Feb. 1992	131.1 (3.4)
MHT	Mace Head, Ireland	54°N	June 1991	126.1 (3.4)
MID	Midway Island	28°N	Jan. 1992	113.4 (5.2)
MLO	Mauna Loa, Hawaii	20°N	July 1989	88.5 (4.8)
NWR	Niwot Ridge, Colorado	40°N	Dec. 1988	117.7 (5.4)
QPC	Qinghai Province, China	36°N	July 1991	116.2 (7.6)
RPB	Ragged Point, Barbados	13°N	March 1993	92.5 (2.8)
SEY	Mahé Island, Seychelles	4°S	Sept. 1990	80.5 (2.5)
SMO	American Samoa	14°S	Sept. 1988	55.3 (1.9)
TAP	Tae-ahn Peninsula, S. Korea	36°N	Nov. 1990	233.7 (28)
UTA	Wendover, Utah	40°N	May 1993	
UUM	Ulaan Uul, Mongolia	44°N	Jan. 1992	151.5 (6.7)

*The month and year air samples were first collected in a glass flask fitted with Teflon O-ring stopcocks and analyzed for CO.

†Preliminary 1993 mean mixing ratios and the standard error are taken from a smooth curve fit to the measured CO in flask samples as described in *Novelli et al.*, 1991.

determined from weekly flask samples that are collected to represent background conditions (Table 2.5).

The unfiltered annual mean for in situ measurements made in 1993 was lower than that determined for 1992 (145.4 ppb). This decrease is consistent with the global CO decrease observed in the flask data (see section 2.1.6).

In situ measurements of CO at MLO continued during 1993. The analysis system was similar to that described previously [*Peterson and Rosson*, 1993]. Calibration is conducted using a 2-point piecewise linear calibration scheme. The three standards were changed on December 15, 1993; their CO values were 74.5, 137.4, and 178.6 ppb. The system operated about 94% of the time; some additional data was lost because of problems related to data storage. The annual mean value for 1993 calculated from the in situ data (92.3 ppb) is not significantly different than the value determined from the weekly flask samples (88.5 ± 4.8 ppb).

2.1.6. Flask Measurements of Carbon Monoxide

Carbon monoxide mixing ratios were measured in a subset of flasks collected as part of the cooperative flask sampling program. Measurements were made when glass flasks fitted with Teflon O-ring stopcocks were used to collect the air sample. Table 2.5 lists the land-based sites where CO was measured in 1993, the date of the first CO measurement, and where possible, the 1993 annual mean value for the site. Samples for CO were also collected on trans-Pacific and South China Sea cruises through June 1993 (data not presented). In early 1994 these programs resumed (see section 2.1.2). Analysis of air from flasks for CO and H_2 were made on a semi-automated Trace Analytical RGA. Methane, CO, and H_2 analyses used a common reference gas (AAL-17270, 112.9 ppb CO). The response characteristics of the instrument used for flask analyses were non-linear over the range of atmospheric values. Preliminary CO mixing ratios were calculated using AAL-17270 as an internal reference, final values were determined using a 6-8 point calibration curve [as described in *Peterson and Rosson*, 1993; *Novelli et al.*, 1994*a*]. The precision of the CO method, estimated as the difference of mixing ratios determined for each flask in a simultaneously collected pair of flasks, was typically 2 ppb or better. An automated flagging routine was installed with flagged flask pairs having a difference of greater than 3 ppb. Hydrogen was referenced to an arbitrary scale awaiting the preparation of accurate standards.

Annual mean CO values for 1993 were calculated for stations that had samples collected during the whole the year (Table 2.5). These mean values were calculated from a curve fit to the complete time series, the smoothed curve reduces the effects of any particular sample on the whole data set. The data are smoothed in time using algorithms developed at CMDL [*Thoning et al.*, 1989].

Mixing ratios of CO determined in flask samples were used to determine the distribution of CO from June 1990 to June 1993. Locations were used that had at least 2 years of measurements before June 30, 1993. This included 10 fixed sites and 17 shipboard sites from the *Wellington Star* (a similar shipboard sampling program aboard the *Southland Star* is described by *Lang et al.* [1992]). Each of these 27 sites showed a decrease in CO over the 3-yr period. The data from each site was smoothed in time as described previously, and a meridianal curve was fit to each biweekly period. These curves represent the surface presented in Figure 2.15.

These smoothed data were combined to calculate a quasi-global average CO mixing ratio (inset, Figure 2.15). There was a slow decrease in CO levels during 1990 and 1991, then CO levels dropped sharply in 1992

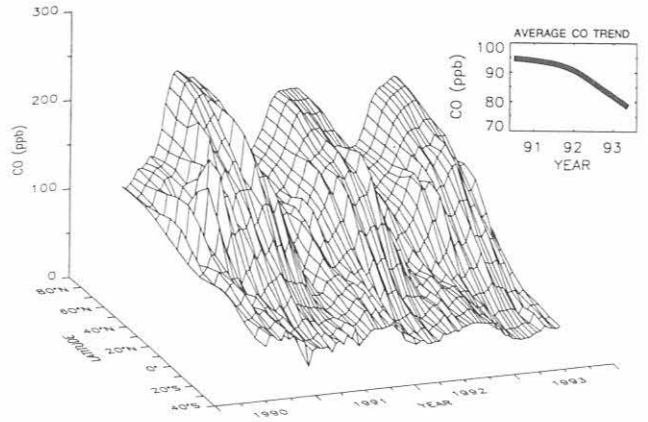

Fig. 2.15. Three-dimensional representation of the distribution of CO in the marine boundary layer. The surface represents data smoothed in time and latitude for the period June 1, 1990, to June 30, 1993. The inset shows the average CO mixing ratio during this period.

and the first half of 1993. Possible reasons for this change include decreases in CO emissions because of decreases in fossil fuel combustion and biomass burning, or an increase in CO oxidation from increased levels of OH [*Bakwin et al.*, 1994; *Novelli et al.*, 1994*b*].

2.1.7. CO Standards

The primary CMDL CO standards were prepared gravimetrically and then propagated to a set of working standards [*Novelli et al.*, 1991]. These working standards were also calibrated against three CO-in-air standards prepared by the CMDL Nitrous Oxide and Halocarbon Division in March 1992 using gravimetric methods. The differences in CO values assigned to the working standards using different reference gases were less than 1% [*Novelli et al.*, 1994*a*].

The CMDL CO standards were compared with standards used by the NASA-Langley, Differential Absorption CO Measurement Group (Hampton, Virginia) and the Fraunhofer Institute (IFU) (Garmisch-Partenkirchen, Germany). The intercalibration of eight standards having CO levels between 100 and 165 ppb indicated agreement between CMDL and NASA of better than 2%. Calibration of six standards by CMDL and IFU having CO mixing ratios between 50 and 200 ppb indicated agreement to better than 4%. The details of the intercalibrations and their results are presented in *Novelli et al.* [1994*a*].

2.1.8. New Air Sampling System

A new system was developed that will assure good measurements of the stable isotopic composition of oxygen in CO_2 ($^{18}O/^{17}O$) in flasks previously compromised by water condensation. The unit, dubbed the Airkit, houses a thermoelectric cooled water condenser with a micro-controlled air sampling system that eliminates most manual operations by the sample taker. Preliminary laboratory tests indicate good $^{18}O/^{17}O$ values from a very wet airstream. This system will be field tested in the coming year at SMO.

2.1.9. Aircraft Project

The aircraft project was started in 1992 to measure CO_2, CH_4, and CO gradients, and seasonal cycles from the boundary layer to the mid-troposphere. By sampling the free troposphere, mid-continent trace gas values can be measured without being affected by localized sources and sinks. These values can then be used to limit the number of regional source-sink scenarios that need to be considered in inverse-modeling studies. In addition, if the CO_2 values are measured often enough, a seasonal cycle can be constructed. The seasonal cycle variation with altitude indicates the rate at which mixing ratio changes propagate upwards. This vertical mixing rate information can also help constrain the models by better defining atmospheric circulation.

In 1993, vertical profiles of CO_2, CH_4, and CO were sampled at least every 2 weeks over Carr, Colorado (40.9°N, 104.8°W), using a previously-developed automated sampling system in a light, single engine aircraft (Cessna T-182). The profiles consist of 20 samples each, generally taken mid-morning between about 2 and 6 km above sea level (which is about 0.5 to 4.5 km above ground level at Carr). Winds below the boundary layer are usually from the south at less than 5 m s^{-1}, and winds above the boundary layer are usually from the north or west at more than 10 m s^{-1}. Figure 2.16 shows the results from a typical flight. Where sample pairs were taken at a given altitude to test pair agreement, the line plots the average of the pair values. All three trace gases show decreasing mixing ratios with increased height since there are anthropogenic sources but few sinks at ground level during the winter. The

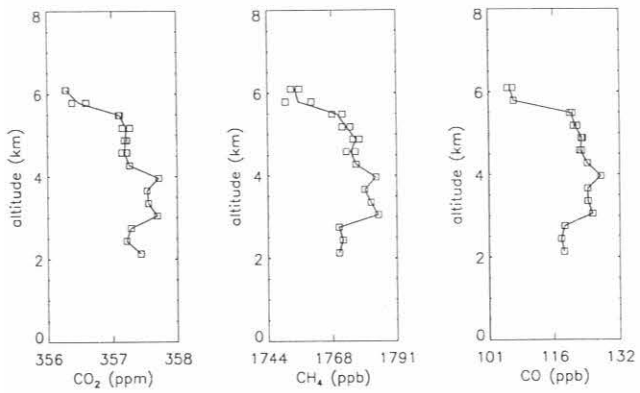

Fig. 2.16. Typical profiles of CO_2, CH_4, and CO versus height (km) over Carr, Colorado, December 14, 1993.

increase in mixing ratios for all three gases between about 3.0 and 5.5 km, and particularly the well-correlated increase at 4 km, may indicate an urban-polluted air mass that has been transported to the sampling site. Trajectory analysis from the previous year during this season suggests that the air aloft is transported from the west and crosses the California coast anywhere between San Francisco and the Mexican border. Although profiles over Carr are often interrupted by these polluted air masses, the gradients and seasonal trends remain consistent over multiple flights.

Sampling at the Carr site began in November 1992, so with over a year of data available at the end of 1993, a seasonal cycle can be estimated for any given altitude range. Figure 2.17 shows the CO_2 data for 1993 in a 1-km wide band centered at 3 km above sea level. The overlaid curve is the sum of the first two harmonics of the fitted seasonal cycle using the same fitting techniques as are used for network flask data.

Figure 2.18 shows seasonal cycle plots for 1-km wide bands centered at 3-, 4-, 5-, and 6-km above sea level. The plot shows two significant features. The first is a decrease in seasonal cycle amplitude of about 0.6 ppm between the 3- and 6-km bands that gives a consistent picture of decreasing source-sink effects with increasing altitude. The second feature is a delay of about 6 weeks in the onset of spring draw-down between the lowest and highest altitudes. This information can be used to help constrain the vertical mixing rate of the troposphere in this region as an additional constraint for global circulation models.

In addition to data collection, work continued on sampling methods in 1993. A new version of the automated sampling system was developed using two-valve flasks that may be flushed with sample air before filling. The previous design had only one valve per flask and relied on evacuating the flask before sampling, a process that was subject to contamination and leaks. Also in 1993, attempts were made to use

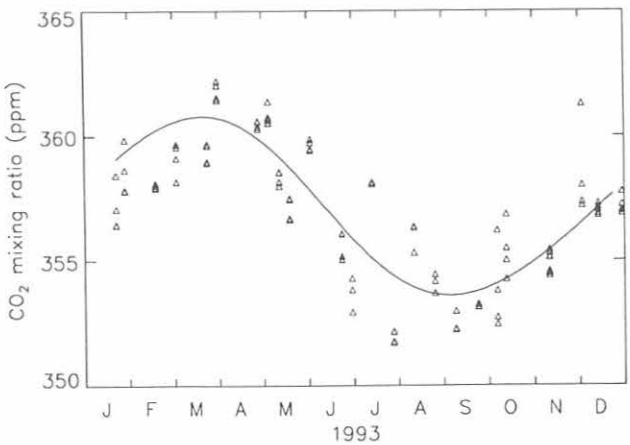

Fig. 2.17. CO_2 seasonal cycle at 3-km height over Carr, Colorado, for 1993.

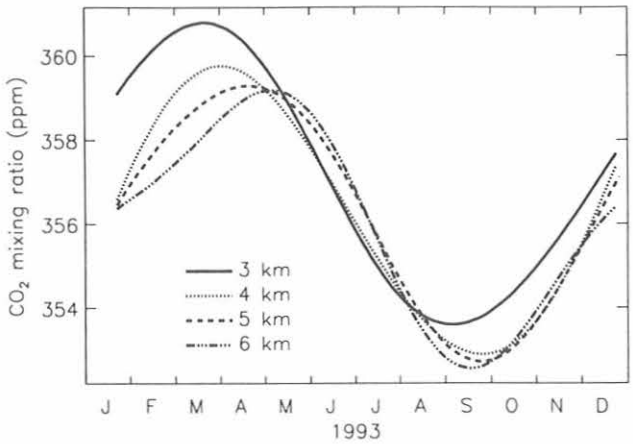

Fig. 2.18. CO_2 seasonal cycle at 3-, 4-, 5-, and 6-km height over Carr, Colorado, for 1993.

different models of light aircraft (Cessna T-210) to reach higher into the troposphere, up to 8.5 km above sea level. Early efforts were plagued by contamination from the plane engine exhaust, but this work will continue. The first version of the sampling system was also flown in a Russian AN26 aircraft over Bennett Island (150°E, 76°N) in an attempt to measure possible local CH_4 emissions. Although the sampling system performed well overall, a leak in the pump head contaminated the results. The visit to Russia was also used to lay the groundwork for a 2-yr biweekly sampling program over Yakutsk (129°E, 62°N) to begin in 1994.

2.1.10. Tall Towers Program

There are 2 full years of continuous CO_2 data from the 610-m tall TV tower in eastern North Carolina (35°21'55"N, 77°23'38"W, 9 m above sea level). For measurements at 496 m above the ground, the rate of data return is about 85%. There are also measurements at 51 and 123 m. Some statistics of the data for June 1993 through May 1994 are given in Table 2.6 (data for June 1992 through May 1993 are given in *Peterson and Rosson* [1993]). In addition, flask samples for CO, CH_4, and isotope ($^{13}C/^{12}C$ and $^{18}O/^{16}O$ in CO_2) analysis are collected from the 496-m level once each week.

In Figure 2.19 the daily afternoon (1500-1700 LST) mean CO_2 mixing ratios at 496-m height on the North Carolina tower are plotted with the flask data from the two Bermuda sites (BME and BMW). The difference between the mixing ratios at these locations gives an approximate measure of the afternoon drawdown or increase in CO_2 within the atmospheric boundary layer at the tower site because of regional surface fluxes. In winter, the afternoon means at 496 m on the tower are generally 2-5 ppm higher than at Bermuda, likely reflecting small net respiration and CO_2 emissions from fossil fuel combustion around the tower site. In summer, afternoon means at the tower

TABLE 2.6. Statistics of Daily Mean and Median CO_2 Mixing Ratios at the 51-, 123-, and 496-m levels on the North Carolina Tower

Month	51 m		123 m		496 m					
	Mean	Median	Mean	Median	Mean	STDV	Median	LQ	UQ	N*
					1993					
June	NA	NA	361.87	361.67	355.35	2.84	355.48	353.46	357.82	22
July	370.11	369.16	361.52	361.47	353.80	3.80	353.85	351.10	356.46	31
Aug.	364.45	364.35	355.90	354.98	350.76	4.38	351.80	347.24	354.56	26
Sept.	370.20	366.24	363.07	361.92	355.83	4.45	354.88	353.50	358.46	29
Oct.	365.79	363.09	362.15	360.94	356.96	4.83	355.81	353.74	359.00	11
Nov.	368.83	368.52	366.59	364.81	362.22	3.78	362.29	359.20	364.59	27
Dec.	369.59	369.73	368.00	367.99	364.83	2.77	364.99	362.43	367.18	29
					1994					
Jan.	369.89	369.68	368.94	368.12	365.99	3.23	365.49	364.42	367.19	20
Feb.	370.80	369.46	369.07	367.27	366.23	4.32	364.89	363.21	367.43	28
March	368.80	369.83	367.17	366.90	365.15	2.15	364.77	363.77	366.14	25
April	369.71	368.83	367.05	366.51	363.42	2.49	363.74	361.67	364.99	29
May	366.28	366.35	363.49	363.38	360.63	2.94	360.99	359.47	362.02	26

LQ and UQ indicate lower and upper quartiles, respectively.
NA indicates data not available.
*Number of days used in the average.

are typically 2-10 ppm lower than at Bermuda, indicating rapid daytime photosynthesis in the vicinity of the tower. Occasionally (i.e., a few times per summer), unusually low CO_2 mixing ratios are observed in the flask samples from Bermuda. For example, air samples taken at BME and BMW on September 3 and 4, 1992, respectively (plotted as triangles in Figure 2.19), show values 5-10 ppm below those obtained for the previous and subsequent weeks. These low values fall within the range of afternoon mixing ratios observed during the same period at the tower, suggesting that the samples may reflect transport of low-CO_2 air from the continental boundary layer to Bermuda. Isobaric back trajectory analysis (J. Harris, personal communication, 1993) shows rapid (1-2 day) transport of air from the southeast United States to Bermuda during this period.

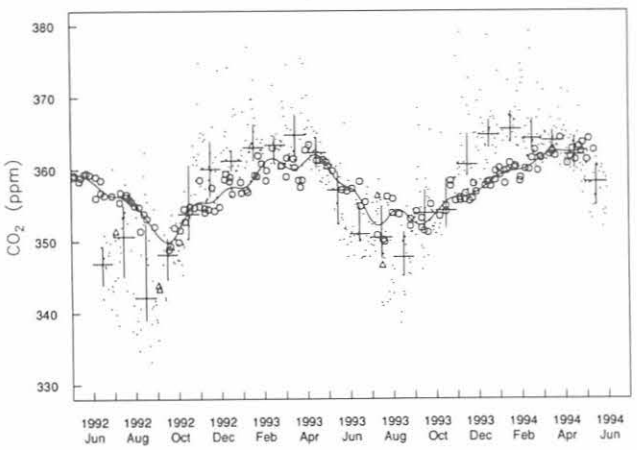

Fig. 2.19. Daily afternoon (1500-1700 LST) CO_2 mixing ratios at 496 m on the North Carolina tower (points) and CMDL flask data from Bermuda (open symbols). The large crosses denote monthly medians (horizontal bars) and inner quartiles (vertical bars) of the tower data, and the solid line is a smoothed fit [*Thoning et al.*, 1989] to the Bermuda data (circles), with points lying more than two standard deviations from the curve plotted as triangles.

The isotopic composition of CO_2 carbon in flask samples collected at 496-m height is shown in Figure 2.20, plotted against the reciprocal of CO_2 mixing ratio. In this plot the intercept ($1/CO_2 = 0$) gives a measure of the isotopic composition of the CO_2 source or sink that causes the observed variations in CO_2 mixing ratio. Cold and warm season data show significantly different relationships. During the cold season the CO_2 source has an isotopic composition of -28.2 (±1.0, 1 standard deviation)‰, close to the value for the global average fossil fuel source of -28.5‰ [*Andres et al.*, 1995]. This result indicates that regional sources are dominated by fossil fuel combustion during the colder half of the year. In the warm season a much heavier (-22.8 (±1.0)‰) CO_2 flux signature is indicated by the isotope measurements, consistent with the increased contribution of biological processes.

The relationship between CO and CO_2 in flask samples taken weekly from the 496-m level are shown in Figure 2.21. Carbon monoxide is a product of incomplete combustion of organic material (fossil fuel and biomass) and is also formed in the atmosphere from the photooxidation of CH_4 and other hydrocarbons. Carbon monoxide is removed from the troposphere

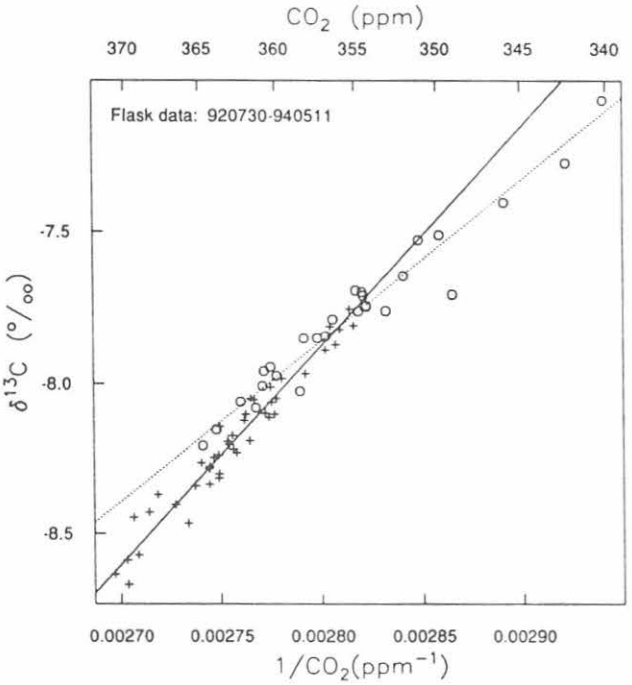

Fig. 2.20. The relationship between $\delta^{13}C$ and CO_2 in flask samples from 496 m on the North Carolina tower. Cold season (November-April, pluses and solid line) and warm season (May-October, circles and dashed line) data are plotted separately. The intercepts of orthogonal distance regression [*Press et al.*, 1992] lines are -28.2 ± 1.0‰ (r^2 = 0.95, n = 43) for the cold season, and -22.8 ± 1.0‰ (r^2 = 0.95, n = 27) for the warm season.

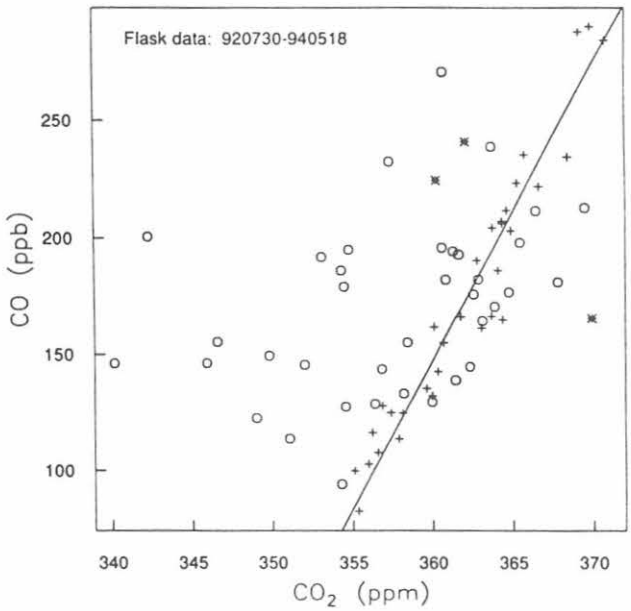

Fig. 2.21. The relationship between CO and CO_2 in flask samples taken weekly from the 496 m level on the North Carolina tower. Winter (November-February, pluses) and non-winter (circles) data are plotted separately, and the slope of an orthogonal distance regression to the wintertime data only (with three outliers (stars) excluded on the basis of examination of the residuals) is 12.7 ± 0.8 ppb/ppm (r^2 = 0.93, n = 32).

mainly by reaction with the hydroxyl radical, and the lifetime of CO in the troposphere at the latitude of the tower ranges from around 1 month in summer (when OH is most abundant) to greater than 12 months in winter [*Novelli et al.*, 1992]. A strong linear relationship exists between CO and CO_2 at the tower in winter (November-March, slope = 12.7 (±0.8) ppb CO/ppm CO_2, r^2 = 0.93, with three outliers removed based on examination of the residuals). The photochemical sources and sinks of CO, and the biogenic sources and sinks of CO_2, are slow in winter and the relationship in Figure 2.21 likely reflects a combustion source for both species. The slope of the relationship is about 60% of that expected from CO and CO_2 emission inventories for fossil fuel combustion in the United States [J. Logan, personal communication, 1993; *Bakwin et al.*, 1994], probably because the source of CO_2 from soil respiration is not zero in winter. In summer, biogenic sources and sinks of CO_2 dominate fossil fuel sources, and no discernible relationship between CO and CO_2 was found.

A significant linear relationship was observed between CO and CH_4 in all seasons (Figure 2.22). The slope for wintertime data only is indistinguishable from the slope for all of the data, but the correlation is somewhat better in winter (r^2 = 0.81 for winter, r^2 = 0.54 for all data). This result probably reflects

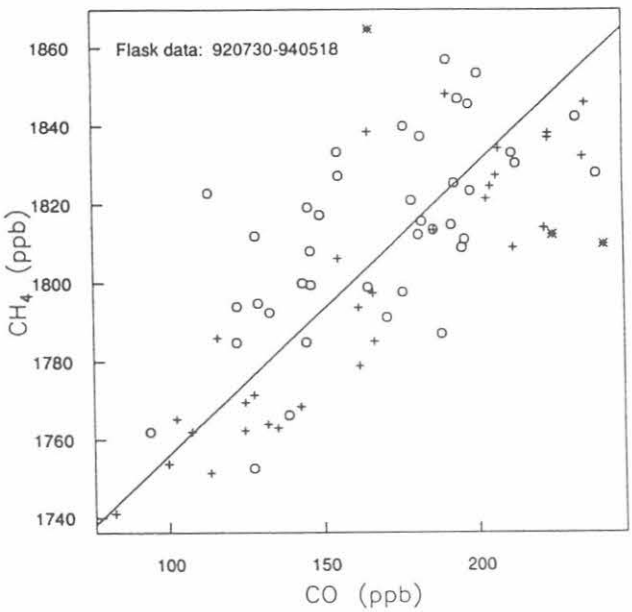

Fig. 2.22. The relationship between CH_4 and CO_2 in flask samples from 496 m above the surface. Winter (November-February, pluses) and non-winter (circles) data are plotted separately. The orthogonal distance regression line is fit to all of the data, and the slope is 0.70 ppb/ppb (r^2 = 0.66, n = 144). Three data points (stars) were excluded from the wintertime data analysis on the basis of the CO versus CO_2 relationship (see Figure 2.21).

colocated industrial sources for CO and CH_4 (e.g., population centers). Apparently, regional biogenic sources and sinks for CH_4 are small relative to urban-industrial sources.

2.2. REFERENCES

Andres, R.J., G. Marland, T. Boden, and S. Bischoff, Carbon dioxide emissions from fossil fuel combustion and cement manufacture 1751-1991 and an estimate of their isotopic composition and latitudinal distribution, in *The Carbon Cycle, Procedings., 1993 Global Change Institute,* Snowmass, CO, July 19-30, 1993, Cambridge Univ. Press, in press, 1995.

Bakwin, P.S., P.P. Tans and P.C. Novelli, Carbon monoxide budget in the northern hemisphere, *Geophys. Res. Lett., 21,* 433-436, 1994.

Conway, T.J., P.P. Tans, L.S. Waterman, K.W. Thoning, D.R. Kitzis, K.A. Masarie, and N. Zhang, Evidence for interannual variability of the carbon cycle from the NOAA/CMDL global air sampling network, *J. Geophys. Res., 99,* 22,831-22,855, 1994.

Dlugokencky, E.J., J.M. Harris, Y.S. Chung, P.P. Tans, and I. Fung, The relationship between the methane seasonal cycle and regional sources and sinks at Tae-ahn Peninsula, Korea, *Atmos. Environ., 27A,* 2115-2120, 1993.

Dlugokencky, E.J., K.A. Masarie, P.M. Lang, P.P. Tans, L.P. Steele, and E.G. Nisbet, A dramatic decrease in the growth rate of atmospheric methane in the northern hemisphere during 1992, *Geophys. Res. Lett., 21,* 45-48, 1994*a*.

Dlugokencky, E.J., L.P. Steele, P.M. Lang, and K.A. Masarie, The growth rate and distribution of atmospheric methane, *J. Geophys. Res., 99,* 17,021-17,043 1994*b*.

Harris, J.M., P.P. Tans, E.J. Dlugokencky, K.A. Masarie, P.M. Lang, S. Whittlestone, and L.P. Steele, Variations in atmospheric methane at Mauna Loa Observatory related to long-range transport, *J. Geophys. Res., 97,* 6003-6010, 1992.

Lang, P.M., L.P. Steele, L.S. Waterman, R.C. Martin, K.A. Masarie, and E.J. Dlugokencky, NOAA/CMDL atmospheric methane data for the period 1983-1990 from shipboard flask sampling, NOAA Tech. Memo. ERL CMDL-4, 88 pp., NOAA Environmental Laboratories, Boulder, CO, 1992.

Lowe, D.C, C.A.M. Brenninkmeijer, G.W. Brailsford, K.R. Lassey, and A.J. Gomez, Concentration and ^{13}C records of atmospheric methane in New Zealand and Antarctica: evidence for changes in methane sources, *J. Geophys. Res., 99,* 16,913-16,925, 1994.

Masarie, K.A., L.P. Steele, and P.M. Lang, A rule-based expert system for evaluating the quality of long-term in situ, gas chromatographic measurements of atmospheric methane, NOAA Tech. Memo. ERL CMDL-3, 37 pp., NOAA Environmental Research Laboratories, Boulder, CO, 1991.

Novelli, P.C., L.P. Steele, and J.W. Elkins, The development and evaluation of a gravimetric reference scale for measurements of atmospheric carbon monoxide, *J. Geophys. Res., 96,* 13,109-13,121, 1991.

Novelli, P.C., L.P. Steele, and P.P. Tans, Mixing ratios of carbon monoxide in the troposphere, *J. Geophys. Res., 97,* 20,731-20,750, 1992.

Novelli, P.C., J.E. Collins, Jr., R.C. Myers, G.W. Sachse, and H.E. Scheel, Re-evaluation of the NOAA/CMDL carbon monoxide reference scale and comparisons to CO reference gases at NASA-Langley and the Fraunhofer Institute, *J. Geophys. Res., 99,* 12,833-12,839, 1994*a*.

Novelli, P.C., K.A. Masarie, P.P. Tans, and P.M. Lang, Recent changes in atmospheric carbon monoxide, *Science, 263,* 1587-1590, 1994*b*.

Peterson, J.T.. and R.M. Rosson, *Climate Monitoring and Diagnostics Laboratory, No. 21, Summary Report 1992,* 131 pp., NOAA Environmental Research Laboratories, Boulder, CO, 1993.

Pitari, G., A numerical study of the possible perturbation of stratospheric dynamics due to Pinatubo aerosols: Implications for tracer transport, *J. Atmos. Sci., 50,* 2443-2461, 1993.

Press, W.H., S.A. Teukolsky, W.T. Vetterling, and B.P. Flannery, *Numerical Recipes in C,* 994 pp., second edition, Cambridge University Press, Cambridge, 1992.

Steele, L.P., E.J. Dlugokencky, P.M. Lang, P.P. Tans, R.C. Martin, and K.A. Masarie, Slowing down of the global accumulation of atmospheric methane during the 1980's, *Nature, 358,* 313-316, 1992.

Thoning, K.W., P.P. Tans, and W.D. Komhyr, Atmospheric carbon dioxide at Mauna Loa Observatory, 2, Analysis of the NOAA GMCC data 1974-1985, *J. Geophys. Res., 94,* 8549-8576, 1989.

3. Aerosol, Radiation, Ozone, and Water Vapor Division

B. BODHAINE, E. DUTTON, R. EVANS, R. GRASS, J. HARRIS, D. HOFMANN, W. KOMHYR, D. NELSON, J. OGREN, AND S. OLTMANS

3.1. CONTINUING PROGRAMS

3.1.1. SURFACE AEROSOLS

3.1.1.1. BASELINE OBSERVATIONS

Operations

The aerosol monitoring program at BRW, MLO, and SPO continued during 1993 as in previous years. CN concentration was measured continuously with TSI (butanol-based) CN counters at BRW, MLO, and SPO. Daily calibration points were provided by Pollak CN counters at all stations. Aerosol scattering extinction coefficient (σ_{sp}) at 450-, 550-, 700-, and 850-nm wavelengths was measured continuously at BRW, MLO, and SPO with four-wavelength nephelometers. Aerosol absorption coefficient has been measured continuously using aethalometers at BRW since April 1988, MLO since April 1990, and at SPO during December 1986-December 1991.

Figure 3.1 shows daily geometric means of CN concentration (lower portion of each plot), σ_{sp} (middle portion of each plot), and Ångström exponent (upper portion of each plot) at the BRW, MLO, and SPO stations for 1993. Two independent values of Ångström exponent (α) were calculated from the 450-, 550-, and 700-nm channels of σ_{sp} data using the relation $\alpha = -\Delta \log \sigma_{sp}/\Delta \log \lambda$, where α is Ångström exponent and λ is wavelength. These averages were calculated only if data for all three wavelengths were available. A graphical presentation of the monthly geometric means of the entire data record for BRW, MLO, and SPO is shown in Figure 3.2. Monthly geometric means of the 1993 aerosol data are listed in Table 3.1.

Discussion

The BRW data in Figure 3.1 show a σ_{sp} maximum of about 3×10^{-5} m^{-1} during spring, typical of the well-known Arctic haze. Minimum values of σ_{sp} below 10^{-6} m^{-1} occurred in July-August. The BRW long-term record shown in Figure 3.2 clearly shows this annual cycle in σ_{sp}, with springtime monthly means of about 10^{-5} m^{-1} and summertime monthly means of about 10^{-6} m^{-1}. The BRW CN record shows a more variable semiannual cycle with a maximum that usually coincides with the maximum in σ_{sp} and a secondary maximum in late summer or early fall. The 1993 annual geometric mean for CN is 195 cm^{-3} (compared with 228 cm^{-3} for 1992) and the annual mean for σ_{sp} (550 nm) is 4.85×10^{-6} m^{-1} (compared with 4.62×10^{-6} m^{-1}) for 1992. Note that the G.E. counter CN record is shown as a solid line and the TSI counter CN record is shown as a dashed line. The individual squares plotted on the CN graph are monthly means of Pollak counter observations. These are shown separately because the TSI and Pollak counter give independent data sets, whereas the G.E. counter was calibrated using the Pollak counter data. Gaps in the data are apparent because of the averaging process that excludes data if local pollution is evident or if wind direction is not from the clean air sector. The BRW aerosol data set was presented by *Bodhaine* [1989] and *Quakenbush and Bodhaine* [1986].

The MLO σ_{sp} data shown in Figure 3.1 are typical of the long-term record, with the highest values in April and May, and lower values in fall and winter. Large events are apparent in the springtime, caused by the long-range transport of Asian desert dust in the upper troposphere to the vicinity of Hawaii. As discussed in the 1988 Summary Report [*Elkins and Rosson*, 1989], σ_{sp} values were generally higher since the installation of the new nephelometer in 1985 and have not reached the low values expected in winter. The MLO CN record shown in Figure 3.1 is typical, giving an annual geometric mean concentration of 381 cm^{-3} (compared with 375 cm^{-3} during 1992); the annual mean of σ_{sp} (550 nm) is 9.20×10^{-7} m^{-1} (compared with 8.58×10^{-7} m^{-1} during 1992). Note that all MLO aerosol data presented here are in the form of geometric means during 0000-0800 HST (1000-1800 UT) in order to include data for nighttime downslope wind conditions only. The MLO data set was presented by *Massey et al.* [1987]. A special study concerning aerosol measurements during the MLOPEX experiment is presented in section 3.2.2.

The SMO 1993 CN data are not presented because of problems associated with the sampling stack during that year. The SMO nephelometer was removed from service in March 1991. Future plans for the SMO aerosol program include a new humidity-controlled, size-controlled sampling system and a new multi-wavelength nephelometer.

The SPO σ_{sp} and CN data are shown in Figure 3.1. These data show a strong annual cycle reaching a maximum in the austral summer and a minimum in the austral winter, similar to previous years. The σ_{sp} data show events due to the transport of seasalt particles in winter but fairly clean values in the fall. Referring to the long-term data set for SPO shown in Figure 3.2, the σ_{sp} data generally show intermediate values in the austral summer and fall, and large events, sometimes exceeding 10^{-6} m^{-1}, in late winter. These large aerosol events are caused by the transport of seasalt in the upper troposphere from stormy regions near the Antarctic coast to the interior of the continent. The

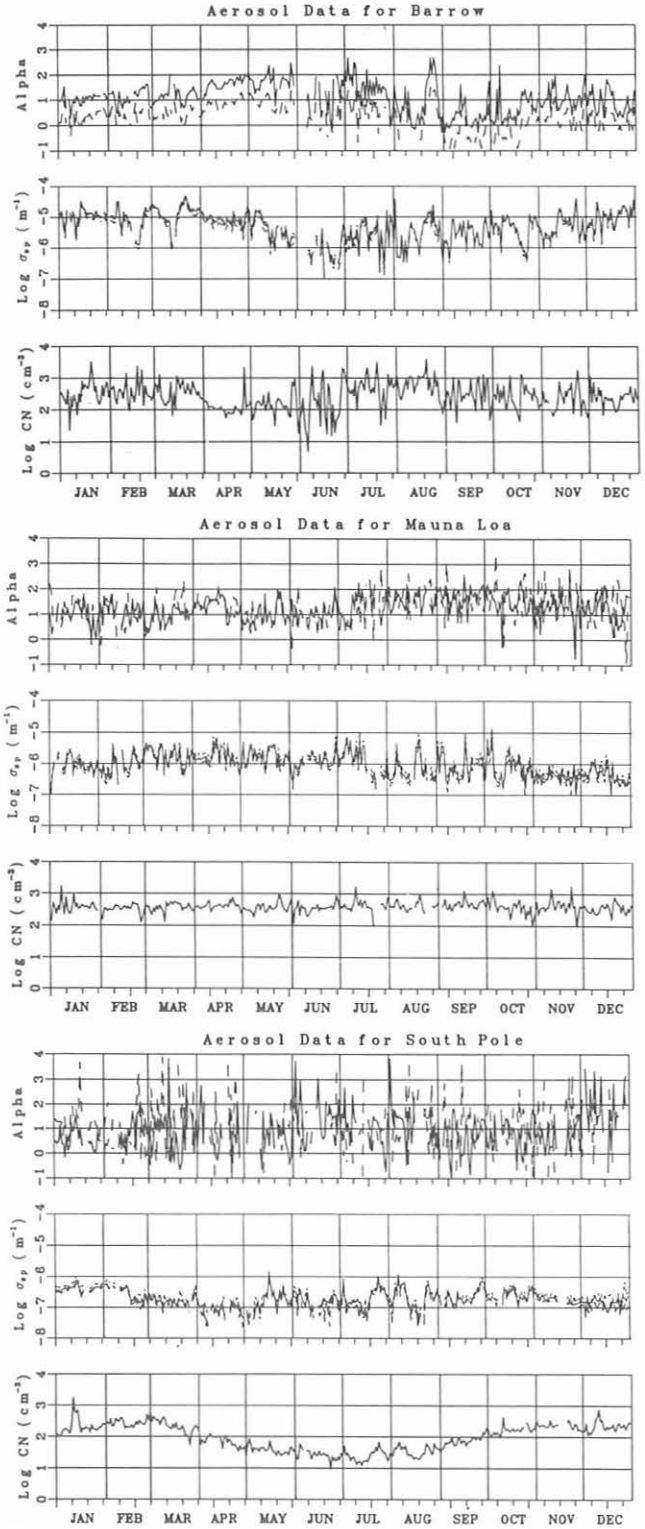

Fig. 3.1. Daily geometric means of σ_{sp} and CN data at BRW, MLO, and SPO for 1993. Data for MLO are included only for 0000-0800 HST. For each station, CN concentration (lower) is shown as a solid line and daily mean Pollak counter data are shown as small squares. σ_{sp} date (middle) are shown for 450 (dotted), 550 (solid), and 700 nm (dashed). Ångstrom exponents (alpha) were calculated from 450 and 550 nm (dotted) and 550 and 700 nm (solid) σ_{sp} data.

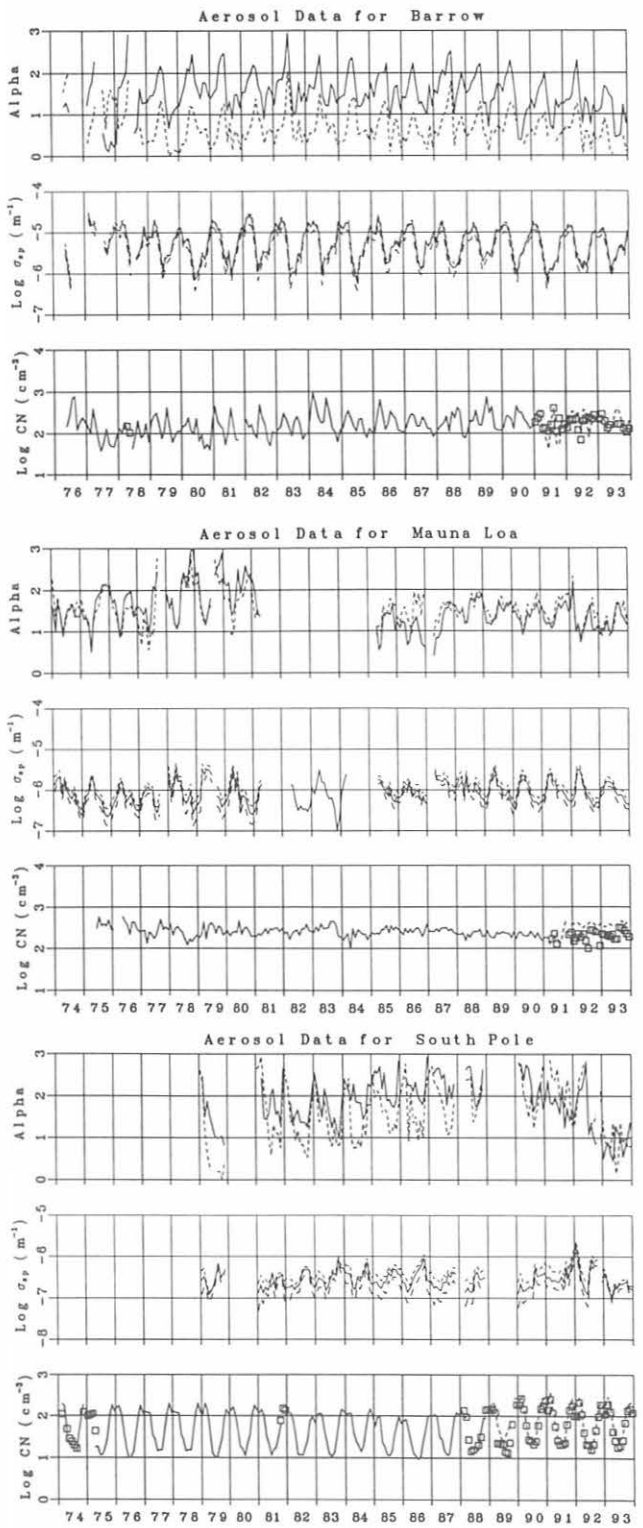

Fig. 3.2. Monthly geometric means of σ_{sp} and CN data for the entire data record at BRW, MLO, and SPO. Data for MLO are included only for 0000-0800 HST. σ_{sp} data (middle) are shown for 450 (dotted), 550 (solid), and 700 nm (dashed). Ångstrom exponents (alpha) were calculated from 450 and 550 nm (dotted) and 550 and 700 nm (solid) σ_{sp} data. Note that G.E. CN counter data are shown as a solid line, TSI CN counter data are shown as a dashed line, and Pollak CN counter data are shown as small squares.

TABLE 3.1. Monthly Geometric Means of CN concentration (cm^{-3}) and σ_{sp} (m^{-1}) at 450, 550, and 700 nm for BRW, MLO, and SPO During 1993

	Jan.	Feb.	March	April	May	June	July	Aug.	Sept.	Oct.	Nov.	Dec.
						BRW						
CN	195	256	239	106	127	122	336	583	209	157	116	210
σ_{sp} (450)	1.22-5	9.62-6	1.59-5	9.86-6	5.03-6	7.09-7	2.33-6	2.51-6	3.28-6	5.70-6	3.57-6	1.10-5
σ_{sp} (550)	1.13-5	8.85-6	1.45-5	8.38-6	4.24-6	7.71-7	2.16-6	2.59-6	3.51-6	5.97-6	3.37-6	1.07-5
σ_{sp} (700)	8.74-6	6.81-6	1.10-5	5.73-6	2.82-6	5.90-7	1.44-6	2.25-6	3.16-6	5.39-6	2.55-6	8.79-6
						MLO						
CN	385	321	364	407	353	347	396	403	473	367	411	363
σ_{sp} (450)	1.08-6	9.88-7	2.21-6	2.26-6	2.11-6	1.38-6	1.62-6	8.20-7	1.16-6	1.09-6	5.35-7	5.75-7
σ_{sp} (550)	8.71-7	8.17-7	1.79-6	1.69-6	1.74-6	1.14-6	1.28-6	5.86-7	8.39-7	7.99-7	3.76-7	4.55-7
σ_{sp} (700)	6.97-7	6.21-7	1.43-6	1.22-6	1.39-6	8.84-7	9.58-7	4.03-7	5.59-7	5.51-7	2.84-7	3.38-7
						SPO						
CN	162	281	216	68	37	26	26	33	73	158	233	197
σ_{sp} (450)	5.01-7	3.26-7	2.03-7	1.06-7	2.03-7	1.85-7	2.31-7	2.88-7	2.67-7	3.03-7	2.32-7	1.87-7
σ_{sp} (550)	3.91-7	2.77-7	1.64-7	9.70-8	1.55-7	1.73-7	2.14-7	2.30-7	2.22-7	2.47-7	1.95-7	1.63-7
σ_{sp} (700)	3.46-7	2.27-7	1.36-7	7.95-8	1.48-7	1.28-7	1.62-7	1.74-7	1.95-7	2.09-7	1.60-7	1.11-7

A compact exponential format is used for σ_{sp} such that $1.22\text{-}5 = 1.22 \times 10^{-5}$.

SPO 1993 annual means were about 90 cm^{-3} (69 cm^{-3} for 1992) for CN and 2.00×10^{-7} m^{-1} (4.41×10^{-7} m^{-1} for 1992) for σ_{sp} (550 nm). The complete SPO data set was presented by *Bodhaine and Shanahan* [1990].

3.1.1.2. Regional Observations

In order to address questions concerning climate forcing by anthropogenic aerosol particles [*Charlson et al.*, 1992; *Penner et al.*, 1994], CMDL is establishing a network of regional aerosol monitoring stations. Two of the stations are located in marine locations and three in continental locations; for each category, one site is relatively free of anthropogenic influences and the others are frequently perturbed by anthropogenic aerosols. Table 3.2 lists the sites, their characteristics, and their status as of December 1993. Each station operates in close collaboration with a local university or government agency that provides onsite support for the measurements.

The scientific questions that define the context of the measurements at these sites include:

- What are the sign, mechanism, magnitude, uncertainty, and spatial distribution of the climate forcing by anthropogenic aerosol particles?
- What are the physical and chemical processes, including their rates and spatial distributions, leading to formation and removal of the particles responsible for the forcing, and how do these processes determine the size- and chemical-composition distributions of the particles?
- What is the sensitivity of the forcing and its spatial distribution to changes in these parameters?
- How has the forcing changed in the past, and how will it change in the future?

Clearly, ground based measurements at a few sites will provide answers to only a few of these questions. Recognizing this, the strategy of the CMDL regional aerosol measurement program is *to determine means, variability, and possible trends of key optical, chemical, and microphysical properties for a number of important aerosol types*. The measurements will provide ground-truth for satellite measurements and global models, as well as key aerosol parameters for global-scale models (e.g., scattering efficiency of sulfate particles, hemispheric backscattering fraction). An important aspect of this strategy is that the chemical measurements are linked to the physical measurements through simultaneous, size-selective sampling and thermal analysis, which allows the observed aerosol properties to be connected to the atmospheric cycles of specific chemical species.

When the sites are fully operational, continuous measurements will include the total particle number concentration (N_{tot}), cloud condensation nucleus number concentration (N_{ccn}), aerosol optical depth (δ), and components of the aerosol extinction coefficient at one or more wavelengths (total scattering σ_{sp},

TABLE 3.2. Regional Aerosol Monitoring Sites

Category	Perturbed Marine	Perturbed Continental	Perturbed Continental	Clean Continental	Clean Marine
Location	Sable Is., Nova Scotia, Canada	Bondville, Illinois	K'puszta, Keszcemet, Hungary	Niwot Ridge, Colorado	Cheeka Peak, Washington
Designator	WSA	BND	KPO	NWR	CPO
Latitude	+43.933	+40.053	+46.967	+40.036	+48.30
Longitude	+060.007	+088.372	-019.550	+105.534	+124.62
Elevation (m)	5	230	180	3020	480
Collaborating Institute	Atmospheric Environment Service, Canada	Univ. of Illinois, Illinois State Water Survey	Univ. of Veszprem, Veszprem, Hungary	Univ. of Colorado, Boulder	Univ. of Washington
Status	Operational Aug. 1992	Expected to be operational July 1994	Expected to be operational Sept. 1994	Site feasibility measurements began Nov. 1993	Operational May 1993
Sample RH	RH <40%	RH<40%	RH<40%	Uncontrolled	RH<40%
Sample size	D_p<1 μm	D_p<1 μm	D_p<1 μm	Uncontrolled	D_p<1 μm
Fractions	1<D_p<10 μm	1<D_p<10 μm			1<D_p<10 μm
Optical measurements	σ_{sp} (3λ), δ(4λ)	σ_{sp} (1λ)	σ_{ap} (1λ), σ_{sp} (1λ), δ(4λ)	σ_{sp} (1λ)	σ_{ap} (1λ), σ_{sp} (1λ), σ_{bsp} (1λ)
Microphysical measurements	N_{tot}	N_{tot}	N_{tot}	N_{tot}	N_{tot}
Chemical measurements	Major ions	Major ions	Major ions	None	Major ions

backwards hemispheric scattering σ_{bsp}, and absorption σ_{ap}). Size resolved impactor and filter samples (submicrometer and supermicrometer size fractions) will be obtained for gravimetric and chemical (ion chromatographic, organic/elemental carbon) analyses. All size-selective sampling, as well as the measurements of the components of the aerosol extinction coefficient, will be performed at a low, controlled relative humidity (40%) to eliminate confounding effects because of changes in ambient relative humidity.

A limited sampling program was conducted from April 1993 to March 1994 to evaluate the suitability for long-term, ground based, aerosol measurements of the proposed monitoring site outside of Laramie, Wyoming. This site was chosen because vertical profiles of aerosol size distribution have regularly been obtained by the University of Wyoming for the last 20 years at this site. However, 12 months of surface measurements of σ_{sp} and N_{tot} revealed that the site is very frequently contaminated by local sources in the Laramie Valley, making it unrepresentative as a clean continental monitoring site. Consequently, measurements of σ_{sp} and N_{tot} were initiated in November 1993 to evaluate the feasibility of using the University of Colorado's facility on Niwot Ridge as a clean continental site. Initial results from this site are promising, although transport of polluted air from metropolitan Denver occurs regularly during afternoon, upslope flow conditions in the summer.

The Cheeka Peak site is operated independently by the University of Washington with major funding from the NOAA Climate and Global Change Program. Although the sampling protocols are essentially identical to those used at the other CMDL sites, all data acquisition and processing is the responsibility of the University of Washington. Eventually, data from this site will be included in the CMDL archive and tabulated in a future CMDL Summary Report.

Summary results for Sable Island for 1992 and 1993 are shown in Figure 3.3 (daily geometric means) and Tables 3.3 and 3.4 (monthly geometric means). Table 3.5 contains statistics on the measured parameters at Sable Island (August 1992-June 1994) for three categories: all cases, and those cases when both N_{tot} and σ_{sp} (550 nm, D<1 μm) are below and above, respectively, one standard deviation of their mean value ("clean" and "dirty," respectively). These criteria correspond to N_{tot} <398 cm^{-3} and σ_{sp} <5.0 Mm^{-1} (clean) and N_{tot} >2089 cm^{-3} and σ_{sp} >22.9 Mm^{-1} (dirty). The Sable Island site was chosen to provide information on the properties of pollution aerosols subsequent to long-range transport from the continent, as well as information on aerosols in the clean marine boundary layer. The initial results reflect the different transport patterns influencing the site, with periods of low aerosol number concentration and light scattering coefficient interspersed with periods of high aerosol loadings. Trajectory analyses of a limited number of cases reveal that transport from the south and southeast

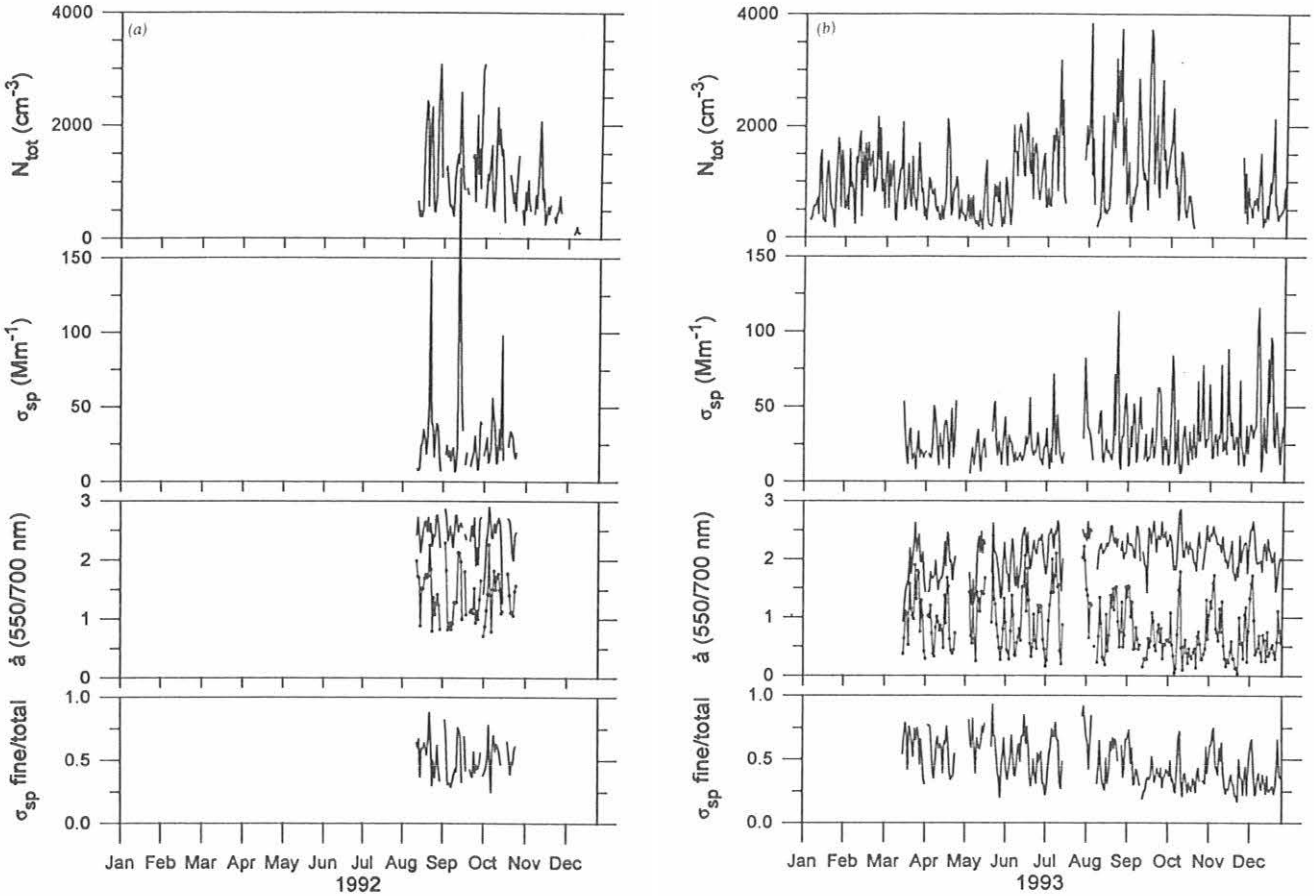

Fig. 3.3. Daily mean aerosol properties at Sable Island (*a*) 1992 and (*b*) 1993. Values of σ_{sp} are measured at 550 nm wavelength.

TABLE 3.3. Sable Island Monthly Means for 1992

Parameter	Maximum Diameter (μm)	Wavelength (nm)	Units	Aug.	Sept.	Oct.	Nov.	Dec.
N_{tot}	All		cm^{-3}	944	1135	1100	591	183
σ_{sp}	10	450	Mm^{-1}	29.7	24.3	26.9	N/A	N/A
σ_{sp}	10	550	Mm^{-1}	26.0	21.8	23.8	N/A	N/A
σ_{sp}	10	700	Mm^{-1}	17.8	15.8	17.1	N/A	N/A
σ_{sp}	1	450	Mm^{-1}	18.8	13.5	16.9	N/A	N/A
σ_{sp}	1	550	Mm^{-1}	14.2	10.0	12.6	N/A	N/A
σ_{sp}	1	700	Mm^{-1}	7.7	5.4	7.1	N/A	N/A

(clean marine) is associated with low aerosol loadings, and that trajectories from the west and southwest (polluted continental) are associated with high aerosol loadings. Monthly mean aerosol loadings are considerably higher than the levels encountered at the CMDL baseline stations because of the proximity of Sable Island to continental pollution sources.

Inclusion of size- and wavelength-dependence of σ_{sp} in the sampling protocol allows identification of systematic shifts in the aerosol size distribution under different conditions (Table 3.5). Fine particles (diameter <1 μm) are responsible for less than half of the aerosol light scattering (550-nm wavelength), and this fraction systematically increases from clean to dirty conditions. Similarly, the Ångström exponent å systematically increases from clean to dirty conditions, for both fine and total size fractions. Together, these two findings indicate that fine particles are systematically smaller, and more abundant, under dirty conditions. Linear regression analysis demonstrates

TABLE 3.4: Sable Island Monthly Means for 1993

Parameter	Maximum Diameter (μm)	Wavelength (nm)	Units	Jan.	Feb.	March	April	May	June	July	Aug.	Sept.	Oct.	Nov.	Dec.
N_{tot}	All		cm^{-3}	693	1064	871	641	425	1050	1188	1167	1265	842	1441	585
σ_{sp}	10	450	Mm^{-1}	N/A	N/A	25.9	27.5	25.0	24.8	25.0	33.5	32.3	25.6	34.4	35.4
σ_{sp}	10	550	Mm^{-1}	N/A	N/A	21.6	24.4	20.7	21.5	20.9	28.3	28.7	23.2	30.9	32.5
σ_{sp}	10	700	Mm^{-1}	N/A	N/A	16.3	20.0	15.8	17.5	16.1	21.9	23.9	20.3	26.3	27.6
σ_{sp}	1	450	Mm^{-1}	N/A	N/A	18.6	16.9	17.7	14.3	14.1	22.1	17.1	11.8	16.4	15.3
σ_{sp}	1	550	Mm^{-1}	N/A	N/A	13.8	12.8	12.9	10.4	9.8	15.4	12.0	8.1	11.5	11.0
σ_{sp}	1	700	Mm^{-1}	N/A	N/A	8.7	8.2	8.0	6.4	5.7	8.7	6.9	4.7	6.8	6.6

TABLE 3.5. Mean Observed Values at Sable Island (August 1992-June 1994)

Parameter	Maximum Diameter (μm)	Wavelength (nm)	Units	Clean Cases	All Cases	Dirty Cases
N_{tot}	All		cm^{-3}	245	912	2884
σ_{sp}	10	450	Mm^{-1}	9.8	28.8	93.3
σ_{sp}	1	450	Mm^{-1}	4.3	15.1	63.1
σ_{sp}	10	550	Mm^{-1}	8.7	25.1	74.1
σ_{sp}	1	550	Mm^{-1}	3.0	10.7	43.7
σ_{sp}	10	700	Mm^{-1}	7.2	20.0	51.3
σ_{sp}	1	700	Mm^{-1}	1.8	6.3	24.0
å	10	450/550	None	0.49	0.69	1.17
å	1	450/550	None	1.76	1.79	1.93
å	10	550/700	None	0.74	0.91	1.49
å	1	550/700	None	2.12	2.19	2.47
σ_{sp} fine/total	1÷10	450	None	0.48	0.56	0.70
σ_{sp} fine/total	1÷10	550	None	0.38	0.46	0.62
σ_{sp} fine/total	1÷10	700	None	0.30	0.36	0.51

Notes: (1) The Ångström exponent is denoted å to avoid confusion in the future with the mass scattering efficiency α. (2) The entries for "σ_{sp} fine/total" are the fraction of the total aerosol light scattering coefficient attributable to submicrometer particles. (3) Geometric means are reported for N_{tot} and σ_{sp}, while arithmetic means are reported for å and σ_{sp} fine/total. (4) Clean and dirty cases are those hours when both N_{tot} and σ_{sp} (550 nm, D<1 μm) are below and above, respectively, one standard deviation of the mean value.

that 75% of the variance in the Ångström exponent (total size fraction) can be explained by variance in the fraction of light scattering caused by fine particles (550 nm wavelength), i.e., the major factor controlling å is the relative abundance of fine and coarse particles (diameter >1 μm).

Information and data from the aerosol group at CMDL is now available on the Internet by FTP and World Wide Web (WWW) servers. Recently processed data, file format specifications, documents summarizing data processing and flow, and clean processed data presented in hourly averaged files for all years of station operation are available by anonymous FTP to ftp.cmdl.noaa.gov, directory "aerosol." In addition to the above, the CMDL WWW server at http://www.cmdl.noaa.gov supplies online plots of recently processed aerosol data and hypertext links to various related documents.

3.1.2. Lidar Observations of Aerosols

(See section 1.1.2. for report on Mauna Loa Lidar data)

3.1.3. Total Ozone Observations

Total ozone observations continued throughout 1993 at 15 of the 16 stations that comprise the U.S. Dobson spectrophotometer network (Table 3.6). Of the 15 stations, 5 were operated by CMDL personnel, 5 by NWS, 2 are domestic cooperative stations, and 3 are foreign cooperative stations.

Early in 1993, the instrument that was at the Poker Flat Research range was installed on the roof of the Geophysical Institute, University of Alaska, Fairbanks. This station is making both total ozone and Umkehr effect observations.

TABLE 3.6. U.S. Dobson Ozone Spectrophotometer Station Network for 1993

Station	Period of Record	Instrument No.	Agency
Bismarck, North Dakota*	Jan. 1, 1963-present	33	NOAA
Caribou, Maine*	Jan. 1, 1963-present	34	NOAA
Wallops Is., Virginia*	July 1, 1967-present	38	NOAA; NASA
SMO*	Dec. 19, 1975-present	42	NOAA
Tallahassee, Florida*	May 2, 1964-Nov. 30, 1989; Nov. 1, 1992-present	58	NOAA; Florida State University
Boulder, Colorado*	Sept. 1, 1966-present	61	NOAA
Fairbankst, Alaska	March 6, 1984-present	63	NOAA; University of Alaska
Lauder, New Zealand	Jan. 29, 1987-present	72	NOAA; DSIR
MLO*	Jan. 2, 1964-present	76	NOAA
Nashville, Tennessee*	Jan. 2, 1963-present	79	NOAA
Perth, Australia	July 30, 1984-present	81	NOAA; Australian Bureau Meteorology
SPO	Nov. 17, 1961-present	82	NOAA
Haute Provence, France	Sept. 2, 1983-present	85	NOAA; CNRS
Huancayo, Peru	Feb. 14, 1964-Dec. 31, 1992	87	NOAA; IGP
BRW	June 6, 1986-present	91	NOAA
Fresno, California*	June 22, 1983-present	94	NOAA

*Stations for which total ozone data are tentatively reevaluated.

The Hauncayo, Peru, station ceased operation at the end of 1992 because of changes in the government structure in Peru. This was not reported to CMDL until after the end of 1993. The WMO is helping to restart the operations at another site in Peru to continue a long record of measurements in a region of the world without many total ozone measurements.

Encoders and computers were added to the Dobson instruments at BRW; SMO; Bismarck, North Dakota; Caribou, Maine; Tallahassee, Florida; Nashville, Tennessee; Fresno, California; and Wallops Island. This change allowed for daily reporting of ozone from these stations to Boulder. The data were relayed to Aristotle University, Thessoloniki, Greece, where nearly real-time maps of total ozone for much of the northern hemisphere were prepared on behalf of the WMO in support of the Second European Stratospheric Arctic and Middle Latitude Experiment.

Provisional daily 1993 total ozone amounts applicable to local apparent noon for the stations listed in Table 3.6 were archived at the World Ozone Data Center (WODC), 4905 Dufferin Street, Ontario M3H 5T4, Canada, in *Ozone Data for the World*. Table 3.7 lists monthly mean total ozone amounts measured at the various stations.

TABLE 3.7. Provisional 1993 Monthly Mean Total Ozone Amounts (m-atm-cm)

Station	Jan.	Feb.	March	April	May	June	July	Aug.	Sept.	Oct.	Nov.	Dec.
Bismarck, North Dakota	316	329	334	346	331	321	320	302	300	272	299	351
Caribou, Maine	309	351	343	341	336	326	315	306	292	298	308	320
Wallops Is., Virginia	266	302	318	312	316	302	299	298	278	273	281	292
SMO	246	245	237	237	238	251	249	247	249	258	252	242
Tallahassee, Florida	-	-	277	291	310	297	301	301	281	267	269	281
Boulder, Colorado	282	296	299	311	303	318	293	286	278	274	279	313
Fairbanks, Alaska*	-	[353]	359	358	347	324	300	292	[275]	[329]	-	-
Lauder, New Zealand	287	268	265	284	290	326	308	347	329	353	330	292
MLO	225	234	249	265	275	262	257	257	256	254	250	243
Nashville, Tennessee	275	298	319	316	314	296	298	297	284	290	284	307
Perth, Australia	275	266	271	261	276	286	281	300	313	319	308	281
SPO	270	266	[278]	-	[269]	[255]	[271]	[270]	-	109	173	277
Haute Provence, France	282	300	319	330	320	320	320	[300]	297	301	290	284
Huancayo, Peru	Station closed											
BRW	-	-	359	377	360	321	285	297	268	260	-	-
Fresno, California	284	296	291	308	306	306	294	294	282	274	263	304

Monthly mean ozone values in square brackets are derived from observations made on fewer than 10 days per month.
*University of Alaska, Fairbanks

Reevaluation of NOAA total ozone data, some of which date back to the early 1960s, continued in 1993. The goal of this effort is to optimize data quality for "ground truth" validation of satellite ozone data, as well as for ozone trend analyses. The data base is comprised of nearly 400 station-years of data. By the end of 1993, data reevaluation was essentially completed for 12 of 25 stations, including those identified by asterisks in Table 3.6. Data for most of the remaining stations listed in the table will be reevaluated in 1994.

As illustrated in Figure 3.4, a tendency toward low ozone values was observed at Dobson stations over the contiguous United States toward the end of 1992 with the values becoming unprecedentedly low in 1993 [*Komhyr et al.*, 1994] (also Figure 3.5). The January through August 1993 ozone amounts were more than 2 standard deviations below normal 72% of the time and more than 3 standard deviations below normal 42% of the time. (Normal values were taken to be average monthly means derived from data obtained at the stations prior to 1982.)

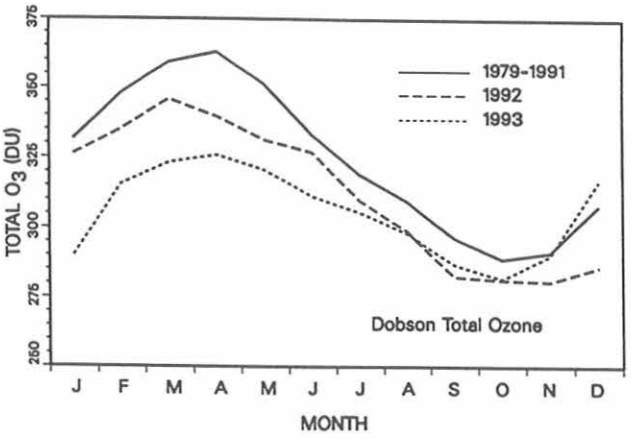

Fig. 3.4. Combined station total ozone monthly means from Bismarck, Caribou, Boulder, Wallops Island, and Nashville for 1992 and 1993 compared with averaged 1979-1991 ozone monthly means at these sites.

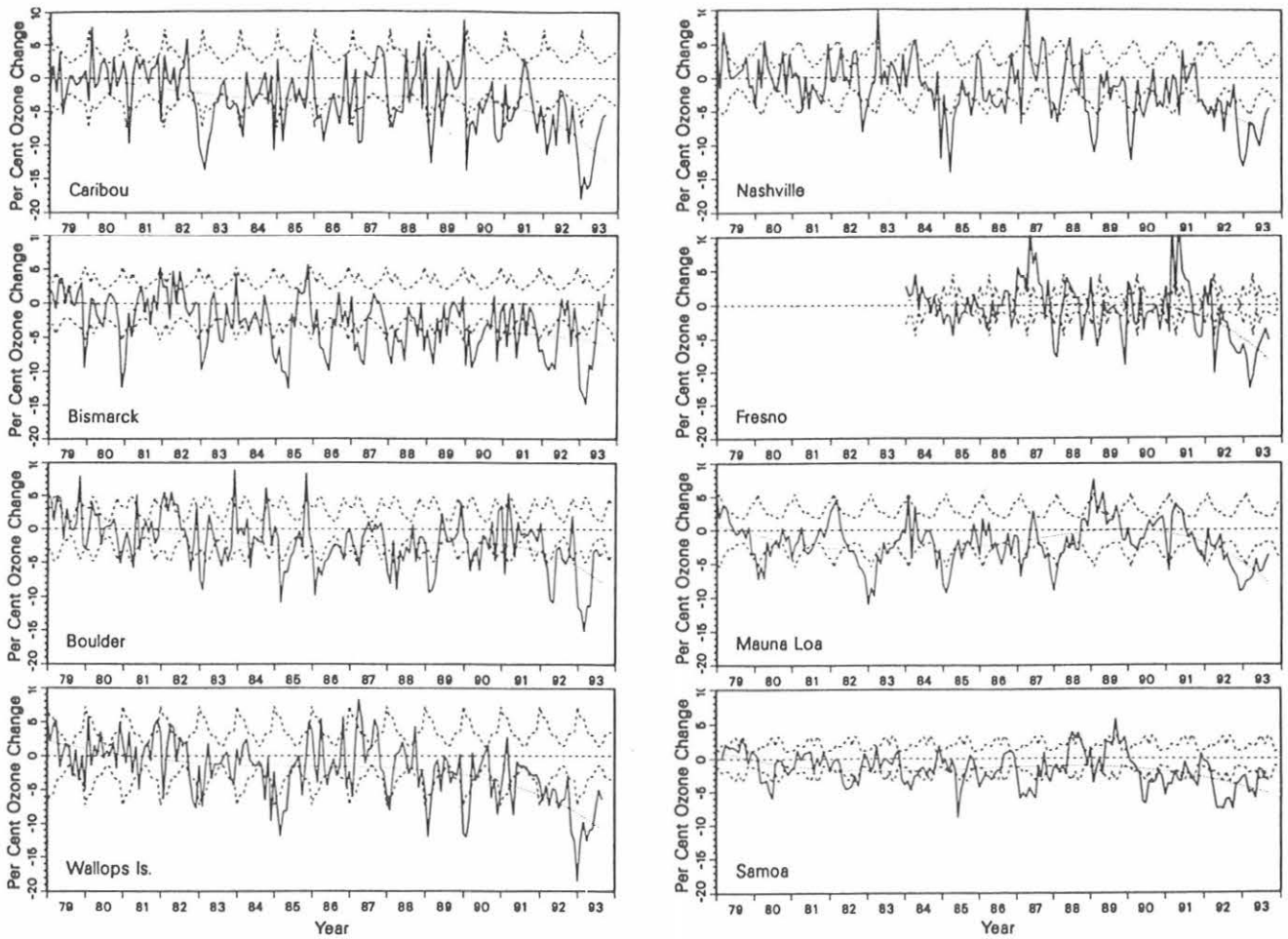

Fig. 3.5. January 1979-September 1993 percent decreases in monthly mean total ozone at six contiguous U.S. stations and in Hawaii and Samoa relative to long-term normal monthly means at the sites. Dashed lines are standard deviations of the normal monthly means expressed in percent. Dotted lines are the 4th degree polynomial fits to the solid line plots and represent the smoothed ozone trends at the stations.

The 1993 monthly mean ozone deviations from monthly normals are quantified in Table 3.8 for six U.S. mainland stations, MLO, and SMO. Fresno data, where observations began in 1983, were referenced to the 1960-1981 normal period from comparison of Boulder and Nashville data for the two time intervals. Note from the table that January-April 1993 ozone values were on average 12.6% below normal, with largest ozone deficits of 18% observed at Caribou and Wallops Island in January 1993. The record low ozone values persisted at four of the six U.S. mainland stations into summer. During May-August, ozone at these stations was on average 8.5% below normal. Ozone recovery toward normal values began in October and proceeded into 1994.

Comparison MLO data in Table 3.8 show a decrease with respect to the long-term normals of 5.5% during May-August 1993. At SMO lower ozone was observed in May-August of 1992 with values, on average, lower than long-term normals by 6.2%.

Figure 3.5 compares 1979-1993 monthly mean ozone data from the eight Dobson stations with long-term normal monthly means measured when atmospheric ozone destruction due to anthropogenic chlorofluorocarbons was minimal. Dashed lines in Figure 3.5 represent standard deviations ($\pm 1\sigma$) of the normal monthly means. The solid lines plot changes in January 1979-September 1993 monthly mean total ozone amounts relative to monthly normals, expressed as a percentage. The dotted line in each plot is a smooth fourth-degree polynomial fit to the solid line plot and represents the smoothed ozone trend for the station and the time interval under consideration.

Three features stand out in the dotted line plots of Figure 3.5. First, except for the short Fresno record, the remaining seven stations' data exhibit zero or near zero ozone trends at times of sunspot maxima (1979-1980 and 1988-1991) and the sunspot minimum (1985-1986). (At MLO and SMO the zero ozone trends corresponding to the 1985-1986 sunspot minimum are displaced toward 1982-1983, the time of the El Chichon volcanic eruption as well as the record 1982-1983 El Niño.) Second, all stations show an overall downward trend in ozone with time, with the downward trends at MLO and SMO being the smallest. Third, all stations show a large increase in the downward ozone trend in 1992-1993.

Annual and seasonal ozone trends were computed, according to the method of *Bojkov et al.* [1990] from deseasonalized CMDL ozone data with solar cycle and equatorial QBO wind effects removed. Resulting trends presumably reflect ozone loss because of: (1) gas-phase photochemistry involving chlorine and bromine species; (2) heterogeneous chemical processes involving chlorofluorocarbons and polar stratospheric cloud and volcanic aerosols; (3) residual QBO effects not adequately accounted for in the model; and (4) dynamic effects induced by ENSO phenomena and stratospheric volcanic aerosols. The trend data for November 1978-September 1993 are compared in Table 3.9. Note (Table 3.9) that at five North American stations (Caribou, Bismarck, Boulder, Wallops Island, and Nashville) having records for the 1978-1993 time interval under consideration, ozone decreased most quickly during spring months at an average rate of -6.0% per decade. The ozone decrease rate was smallest at -1.4% per decade during autumn months. On an annual basis, the average ozone decrease rate at the five stations during November 1978-September 1993 was -4.0% per decade. With the addition of October 1993-December 1993 ozone data (not shown), the average annual seasonal downward ozone trends become smaller by about 1% per decade.

Record low ozone amounts were also observed at SPO during October and November of 1993. Mean monthly total ozone amounts measured during October 15-31 time intervals of 1962-1993 are plotted in Figure 3.6. (Dobson spectrophotometer total ozone observations first became possible at SPO in past years in mid-October following the polar night. With considerably less ozone at the Pole in Octobers of more recent years, fairly reliable data are obtained about a week earlier each year.) The October 1993 mean value of 117 DU was the lowest ever recorded at SPO. (The second

TABLE 3.8. Percent Ozone Decreases at the CMDL Stations in 1993 Relative to Long-Term Normal Ozone Monthly Means

Station	Jan.	Feb.	March	April	Jan.-April O_3 Decreases	May	June	July	Aug.	Sept.	May-Aug. O_3 Decreases
Bismarck, North Dakota	-12.5	-13.4	-14.9	-8.9	-12.4	-9.7	-5.3	+0.5	-1.8	-1.7	-4.1
Caribou, Maine	-18.1	-14.7	-16.5	-15.9	-16.3	-12.7	-9.4	-7.8	-5.8	-5.2	-8.9
Boulder, Colorado	-11.5	-11.9	-15.1	-11.1	-12.4	-11.3	-3.2	-2.9	-3.9	-3.0	-5.3
Wallops Is., Virginia	-18.4	-13.1	-9.7	-12.7	-13.4	-9.9	-10.5	-7.7	-6.6	-6.4	-8.7
Fresno, California*	-8.1	-12.4	-16.4	-10.8	-11.9	-13.2	-7.9	-7.6	-5.8	-5.9	-8.6
Nashville, Tennessee	-13.3	-11.1	-6.6	-6.8	-9.5	-8.8	-10.2	-7.7	-4.9	-4.0	-7.9
MLO	-9.0	-7.7	-7.6	-6.9	-7.8	-4.4	-6.4	-6.2	-4.8	-3.8	-5.5
SMO	-2.7	-2.5	-5.1	-4.6	-3.7	-5.9	-1.4	-1.7	-2.9	-2.8	-3.0

*Values adjusted by-1.9 ± 1.4 (1σ) for reference to the mid-1960s to 1981 normal time interval.

TABLE 3.9. Trends for November 1978-August 1993

Station	Latitude	Annual		Dec.-Feb.		March-May		June-Aug.		Sept.-Nov.	
		Trend	Std. Error	Trend	Std. Error	Trend	Std. Error	Trend	Std. Error	Trend	Std. Error
Caribou, Maine	46.9°N	-4.49	0.86	-5.42	2.11	-6.51	1.28	-2.69	1.00	-2.62	1.57
Bismarck, North Dakota	46.8°N	-3.60	0.70	-3.79	1.63	-6.56	1.11	-2.02	1.14	-1.11	1.17
Boulder, Colorado	40.0°N	-3.50	0.71	-3.33	1.52	-7.21	1.43	-1.45	0.79	-0.92	1.20
Wallops Is., Virginia	37.9°N	-4.73	0.87	-7.03	1.66	-5.53	1.60	-3.99	1.14	-1.83	1.40
Nashville, Tennessee	36.3°N	-3.75	0.80	-5.87	1.50	-4.88	1.59	-3.18	1.02	-0.54	1.46
Fresno, California*	36.8°N	-3.45	2.15	-3.67	2.98	-3.96	3.94	-2.35	2.40	-3.81	2.35
MLO	19.5°N	-.048	0.94	-1.35	1.43	-0.12	1.73	-0.17	1.22	-0.33	0.90
SMO	14.3°S	-1.67	0.80	-0.97	1.16	-2.52	0.97	-1.41	1.38	-1.77	1.04
Average over first five stations		-4.01		-5.09		-6.14		-2.67		-1.40	

*Observations at Fresno began July 1983.

lowest value of 134 DU was observed there in 1987.) Lowest ever ozone values were observed at SPO early in the month. The mean for October 9-14 was 91 DU, and the mean for October 15-18 was 100 DU.

3.1.4. Validation of Satellite Instrument Ozone Data

World primary standard Dobson instrument 83, maintained by CMDL, has been operated during summer months at MLO since 1979. Data obtained have been used to provide "ground truth" for verification of ozone measurements made by the NASA TOMS and SBUV instruments from aboard the Nimbus 7 satellite. The SBUV instrument became inoperable in 1992, followed by failure of the TOMS instrument in early 1993. However, a new TOMS instrument was launched aboard the Russian METEOR satellite in 1992.

Figure 3.7 compares the Dobson instrument 83 data with the original TOMS Version 6 data through 1992 and with the new TOMS data in 1993, showing agreement in results to within about ±0.5%. The long-term ozone measurement precision of Dobson instrument 83 is estimated to be ±1%.

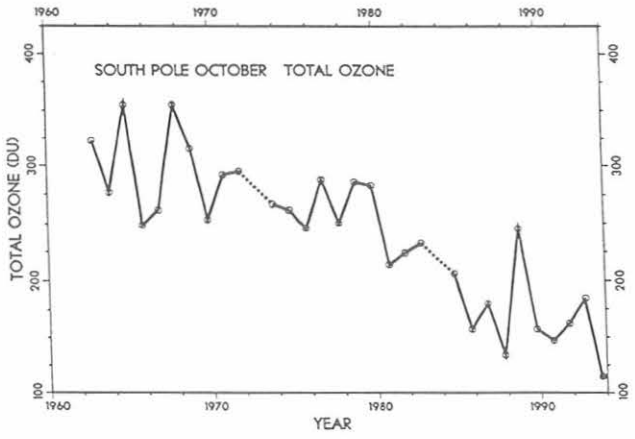

Fig. 3.6. SPO mean total ozone amounts for October 15-31 time intervals of 1962-1993.

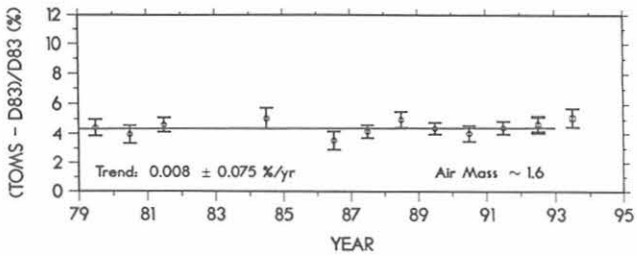

Fig. 3.7. Comparison of TOMS and Dobson data at MLO.

3.1.5. Umkehr Observations

Umkehr observations with automated Dobson ozone spectrophotometers continued during 1993 at Boulder, Haute Provence, France; Lauder, New Zealand; MLO; Perth, Western Australia; and University of Alaska's Geophysical Institute. Umkehr data processing was not performed during 1993 for several reasons, including a change in the computer used to process this data. The change required a rewriting of the suite of computer programs used in the processing.

3.1.6. Calibration of CMDL Dobson Spectrophotometers

Ten Dobson ozone spectrophotometers were calibrated during 1993. Table 3.10 lists all of the instruments calibrated and the resulting calibration difference expressed as a percent difference in ozone. This percent difference is between ozone calculated from the test instrument and the standard instrument measurements with the ADDSGQP observation type at a Mu value of 2, and a total ozone value of 300 DU, before any repair or calibration adjustment is made. The table also lists the place of the calibration and the standard instrument used.

TABLE 3.10. Dobson Ozone Spectrophotometers Calibrated in 1993

Station	Instrument Number	Calibration Date	Calibration Correction (%)	Standard Number	Place
Bologna, Italy	66	May 25	-0.8%	65	Hradec Kralove
Aswan, Egypt	69	May 25	-0.6%	65	Hradec Kralove
Hradec Kralove, Cêska	74	May 25	-0.3%	65	Hradec Kralove
Irene, S. Africa	89	May 25	-1.0%	65	Hradec Kralove
St. Petersberg, Russia	102	May 25	0.0%	65	Hradec Kralove
MLO	76	Aug. 18	-1.3%	83	MLO
SMO	42	June 14	-0.1%	83	MLO
Tamanrasset, Algeria	11	N/A	N/A	65	Boulder
Tehran, Iran	109	N/A	N/A	83	Boulder
Bismarck, N. Dakota	33	Sept. 29	-0.5%	83	Bismarck

CMDL participated in an international Dobson spectrophotometer calibration at Hradec Kralove, Czech Republic, May 20-30, 1993, as part of its role as the world center for Dobson calibrations. Five instruments were calibrated with respect to secondary standard Dobson instrument 65. Four of the instruments had the optical wedge calibration performed.

The SMO Dobson instrument 42 was sent to MLO in June and the calibration level checked against world standard Dobson spectrophotometer 83. The instrument was returned to SPO and an encoder installed for semi-automated operation.

In 1992 it was noticed that the daily ozone values reported for the MLO Dobson instrument 76 were higher than the daily average ozone values calculated from the "absolute calibration" of world standard Dobson spectrophotometer 83 operated at the same station. This difference appeared after July 25, 1992. Dobson instrument 76 was formally intercompared with standard Dobson instrument 83 in the manual mode in June and in the automated mode in August. The average difference in the August intercomparison was 1.3% higher for the Dobson 76 with even higher values closer to noon. A new calibration scale was defined for the Dobson 76, based on the August intercomparison, to be used from July 25, 1992, onward. There is no known explanation for the calibration shift on July 25, 1992.

The CMDL Dobson instrument 33, operated by the Bismarck NWS site, was intercompared with the standard Dobson spectrophotometer 83 in late September. Dobson instrument 33 had the wedge calibration performed and the encoder installed for semiautomated operation.

Two Dobson instruments of the WMO GAW program were rebuilt and calibrated in Boulder as part of CMDL's function as the world center for Dobson calibrations. Dobson instrument 11 operated in Toulouse, France, before it was donated to the WMO and had been modified with an encoder and special electronics. Unfortunately, the original circuit diagrams and part of the electronics were missing. The instrument was stripped and rebuilt as a normal instrument. This instrument was sent to Tamanrasset, Algeria, for use at the newly opened WMO Global Environmental Fund/Global Atmosphere Watch (GEF/GAW) baseline station. A representative of the WMO and of the Czech Republic Hydrometeorological Institute aided in this project. The Tehran, Iran, Dobson instrument 109 was optically realigned, and the electronics were replaced with a solid-state version. It was returned to its station in 1994.

3.1.7. Tropospheric Ozone

Surface ozone measurements continued at nine monitoring sites that include the four CMDL observatories, Niwot Ridge, and four sites in the North Atlantic. Many of the significant characteristics of the ozone distribution at these sites are discussed in *Oltmans and Levy* [1994].

At SPO the 20-year record of surface observations has shown significant ozone concentration decreases [*Schnell et al.*, 1991; *Oltmans and Levy*, 1994]. The largest and most significant declines occurred in the summer (DEC-JAN-FEB) and autumn (MAR-APR-MAY). In recent years, however, the decline has slowed in the summer but has become more pronounced during the rest of the year, particularly the autumn. The summer declines reported earlier were linked to the expected increase in ultraviolet radiation associated with the dramatic decline in stratospheric ozone over Antarctica and the consequent enhancement in tropospheric ozone loss [*Schnell et al.*, 1991]. Coupled with greater photochemical destruction of ozone was an increased transport from the coast of Antarctica to the interior of the continent bringing air with less ozone to the Pole. There are indications that transport patterns may have returned to those seen prior to 1980 [*Peterson and Rosson*, 1993]. Surface ozone values have not, however, recovered.

A plot of the smoothed, monthly mixing ratios (Figure 3.8) shows surface ozone beginning to decline in 1986 and then more dramatically after 1989 remaining relatively low in recent years. During the

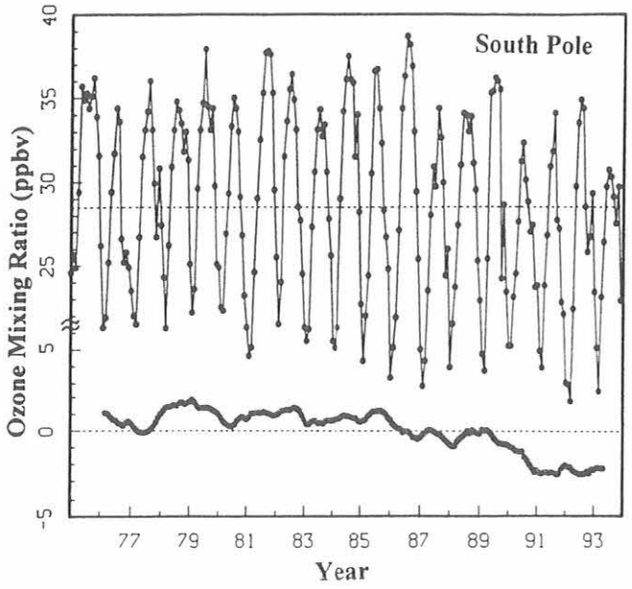

Fig. 3.8. Monthly means and smoothed monthly departures from the long-term monthly mean surface ozone mixing ratios at South Pole. The smoothing is a 24-month running mean.

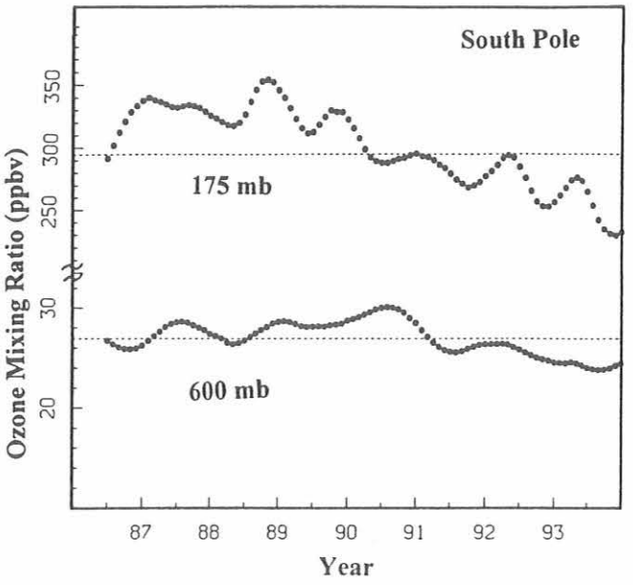

Fig. 3.9. Smoothed monthly departures from the long-term monthly mean ozone mixing ratios for the lower troposphere (600 mb) and lower stratosphere (175 mb). The data are from weekly ozonesonde observations.

springs of 1991-1993, the lower stratosphere (below 14 km) has had particularly low ozone amounts [*Hofmann et al.*, 1994*a*]. This represents a significant downward extension in altitude of the ozone depletion region as a result of the presence of greatly enhanced sulfate aerosol from Mt. Hudson (1991) and Mt. Pinatubo (1992 and 1993) and the resulting heterogeneous destruction of ozone. The lowest seasonal minimum values in surface ozone were recorded in the late summer following each of these years.

Although differing a bit in detail, the ozonesonde record that began in 1986 shows a remarkably similar result for measurements obtained near the surface (600 mb). The ozonesonde data (Figure 3.9) also show that the recent (1991-1993) low values at the surface appear throughout the troposphere and into the lower stratosphere. This suggests that the additional decline seen in recent years at SPO is related to the large spring and early summer deficit in the lower stratospheric reservoir that feeds ozone into the upper stratosphere by cross-tropopause flux processes and thus reduces the contribution from the stratosphere to the tropospheric burden. Since the ozonesonde record does not encompass the period of more gradual decline seen at the surface prior to 1987, it is not possible to determine whether a portion of that earlier decrease was a result of a diminishment of the lower stratospheric reservoir. There is some evidence that in 1986-1991 the ozone in the lowest part of the stratosphere was lower than during 1967-1971 when there is a set of ozone vertical profile measurements at SPO (*Oltmans et al.*, 1994).

Table 3.11 gives the monthly mean ozone mixing ratios for the sites where data is available through 1993.

3.1.8. Ozonesonde Observations

Ozone vertical profile measurements using ozonesondes were continued at SPO, MLO, and Boulder. A continuing goal of the measurements was an assessment of the effect of the Mt. Pinatubo eruption on the ozone distribution in the stratosphere. At SPO the continued presence of significantly elevated H_2SO_4/H_2O aerosol in the lower stratosphere led to unprecedentedly low column ozone amounts during austral spring 1993 [*Hofmann et al.*, 1994*a*]. During September 25 to October 18, there were eight consecutive profile measurements with integrated ozone amounts (total column ozone) less than or equal to 100 DU. These were the lowest column ozone amounts ever recorded. In the region of 17-19 km, essentially all of the ozone was destroyed (Figure 3.10). This represented a vertical extension of the region of ozone loss. In the lower portion of the depletion region (below 16 km) the additional depletion is associated with the presence of Mt. Pinatubo aerosol and the efficient destruction of ozone at temperatures warm enough that polar stratospheric clouds (PSCs) do not form, but where the sulfate aerosol is an effective medium for heterogeneous chemical processing. At altitudes above 20 km, the additional depletion appears to be the result of colder temperatures that enhance the formation of PSCs [*Hofmann et al.*, 1994*a*].

TABLE 3.11. Monthly Mean Surface Ozone Mixing Ratios (ppbv) During 1992 and 1993

Station	Year	Jan.	Feb.	March	April	May	June	July	Aug.	Sept.	Oct.	Nov.	Dec.
Westman Is., Ireland	1993	39.7	41.4	45.1	45.4	44.3	34.7	27.3	28.8	33.0	37.4	38.0	34.2
Mace Head, Ireland	1993	37.2	33.5	38.8	40.6	39.3	30.4	28.3	29.0	30.3	24.2	28.9	36.5
NWR	1993	37.7	40.6	42.7	46.7	43.3	44.0	43.6	39.0	37.2	36.6	43.6	41.9
Bermuda	1993	36.4	38.6	38.7	42.8	36.6	32.2	25.2	22.5		32.4	32.6	34.6
Barbados	1992	23.3	23.3	21.5	19.5	16.4	16.3	17.1		18.4		21.6	24.4
	1993	26.3	22.3	24.7	19.7	18.6	21.6	20.4		14.5	17.8	23.5	26.3

In late 1993 and early 1994 Boulder saw the recovery of ozone in the lower stratosphere to levels seen prior to the eruption of Mt. Pinatubo (Figure 3.11). This was consistent with the significant drop in the particle surface area of the stratospheric aerosol in the mid-latitudes beginning in the middle of 1993 [*Hofmann et al.*, 1994*b*]. The timing of the ozone recovery with the drop-off in particle surface area lends credence to the argument that the low ozone anomaly seen following the eruption of Mt. Pinatubo was a result of the processing of human-produced chlorine on sulfate aerosol in the lower stratosphere.

At MLO ozonesonde measurements began in September 1982 but were discontinued in January 1984 and not resumed until December 1984. Profiles were obtained on about a three-per-month schedule since then. Figure 3.12 shows the trend for the 12-year period beginning in 1982 for levels from the surface to 7 mb. The largest changes are decreases in the lowest part of the stratosphere and upper troposphere, although these trends are not generally significant. Above 30 km at the highest levels routinely attained by the ozonesonde, there are significant increases. The trends in the lower stratosphere are similar in magnitude to those seen at midlatitude northern hemisphere sites during this period [*Logan*, 1994]. It is not clear whether the declines in the upper troposphere are related to those in the lower stratosphere. The extensive Canadian ozonesonde network also shows significant decreases in the troposphere as well as the lower stratosphere [*Tarasick et al.*, 1995].

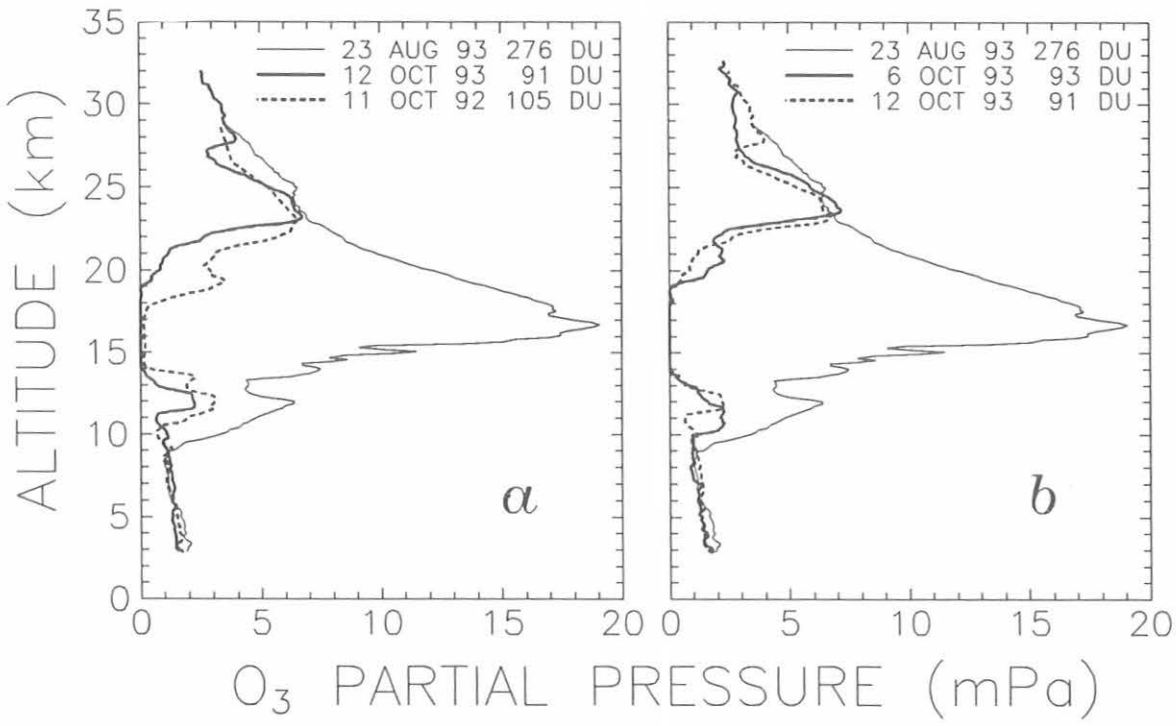

Fig. 3.10. (*a*) Comparison of the pre-depletion ozone profile at South Pole in 1993 with profiles when total ozone reached a minimum in 1992 and 1993. (*b*) Comparison of the pre-depletion profile with two profiles which showed total ozone destruction in the 14-19-km region.

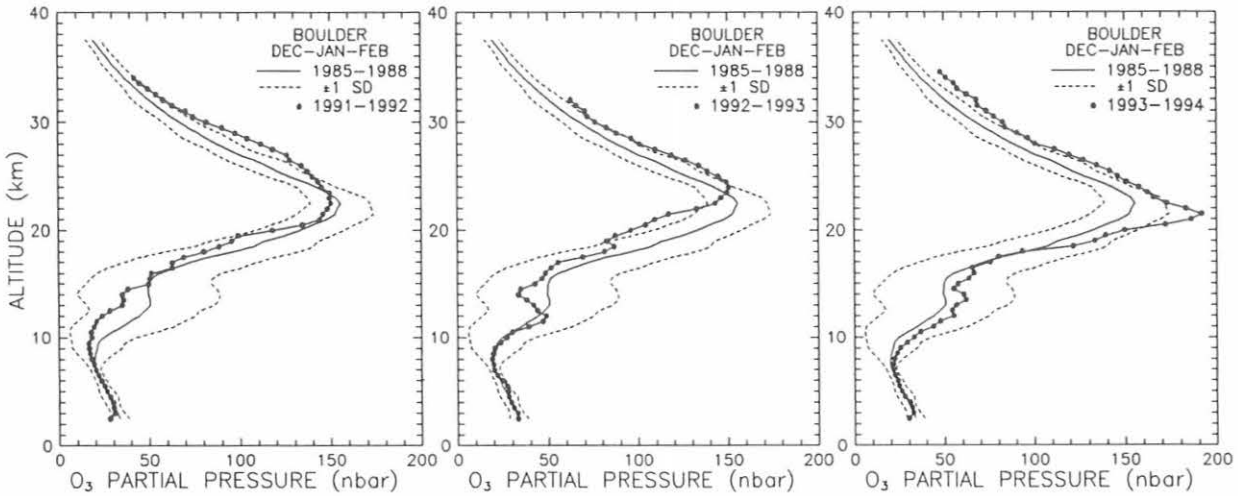

Fig. 3.11. Winter average ozone partial pressure profiles at Boulder, Colorado, after the eruption of Mt. Pinatubo (points connected by heavy solid lines). The thin-solid and dashed profiles represent the 1985-1988 seasonal averages plus and minus one standard deviation.

3.1.9. Stratospheric Water Vapor

In addition to the ongoing monthly water vapor profile measurements at Boulder, the program of winter soundings at SPO was augmented to give a better picture of the strong dehydration that develops in the Antarctic stratosphere.

As temperatures in the stratosphere drop dramatically in May, they become low enough (-80°C) to begin the process of Type I (nitric acid trihydrate) polar stratospheric cloud (PSC) formation. Temperatures do not reach the local water frost point (approximately -90°C), however, until June when Type II PSCs begin to form and dehydration proceeds rapidly. PSCs play a key role by processing chlorine in the winter stratosphere and by removing nitrogen in its chemically active forms. Figure 3.13 shows two stratospheric water vapor profiles obtained at SPO in 1993. In May

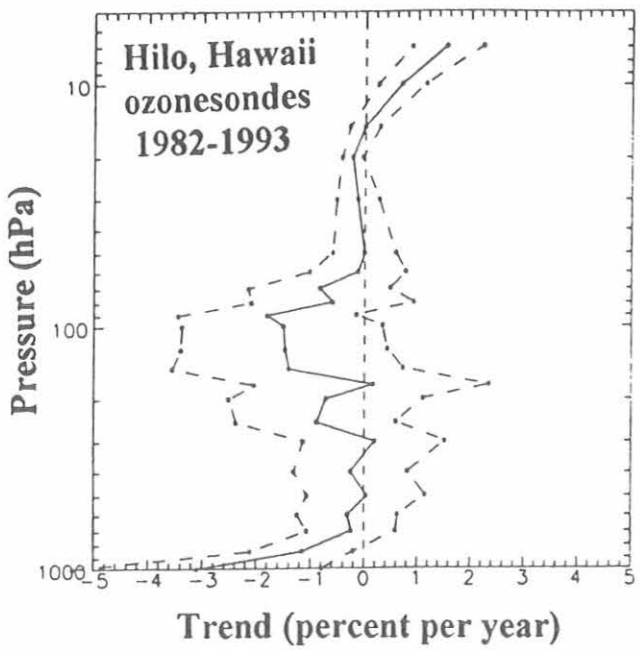

Fig. 3.12. The linear trend (solid line) and 95% confidence interval (dashed line) of the ozone monthly departures as a function of altitude at Hilo, Hawaii, for the period 1982-1993.

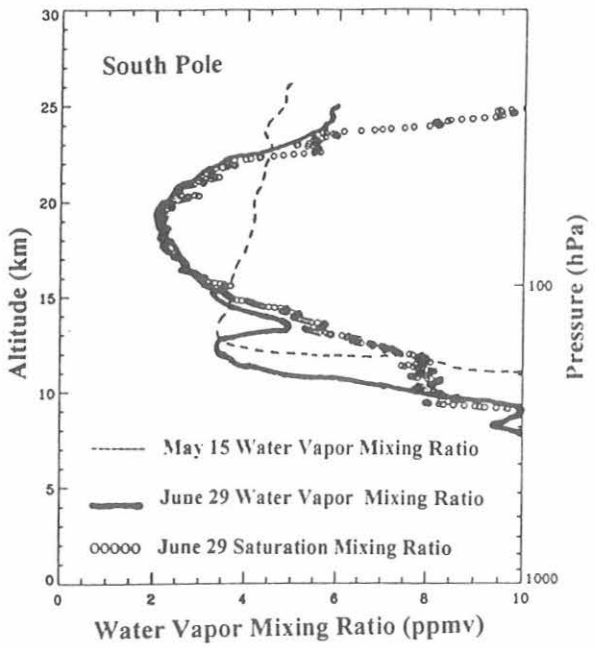

Fig. 3.13. Stratospheric water vapor mixing ratio profiles at SPO on May 15, 1993, and June 29, 1993.

there is no sign of dehydration with stratospheric mixing ratios gradually increasing from 3.5 ppmv at about 12 km to 5 ppmv at the top of the sounding at 27 km. In this region, frost-point temperatures are 7-10 degrees lower than the saturation temperature. By the end of June, a broad region from 15-25 km shows dehydration, and the entire region has saturated conditions. The relative maximum in mixing ratio just below 14 km is a result of ice crystal reevaporation where the falling crystals encounter somewhat warmer conditions.

Lidar profiles from the University of Rome lidar (Figure 3.14) show that by June 29 there is a broad region of PSCs that encompasses the dehydrated region below 20 km. Above 20 km, ice particles have probably already settled to somewhat lower altitudes. Even in the region near 16 km, where some crystals have evaporated, there are still sufficient numbers to keep this region near saturation.

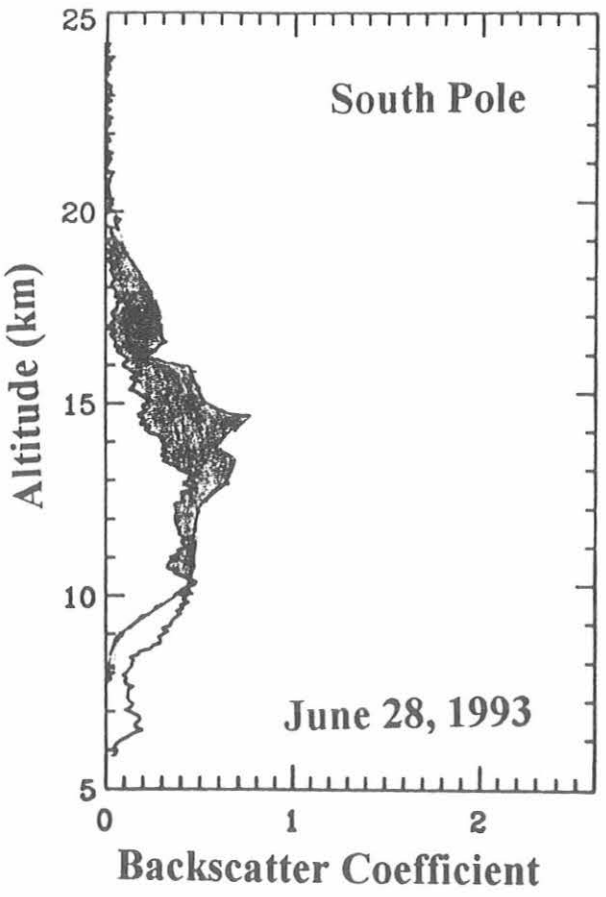

Fig. 3.14. Two lidar profiles of the non-Rayleigh backscatter observed over SPO during 1993. The inner line is the backscatter resulting primarily from the presence of Mt. Pinatubo aerosol and is from a profile in May before PSCs formed. The shaded area shows the enhanced signal due to the presence of PSCs on June 28, 1993.

Data from McMurdo, on the coast of Antarctica, on September 4 show the extent of dehydration achieved by the end of the winter with mixing ratios below 2 ppmv over an altitude range of nearly 10 km. The McMurdo data also show that the dehydration is present throughout the area within the polar vortex not just in the interior of Antarctica. By summer, though air temperatures have warmed dramatically, there is still a large dehydrated region giving strong evidence that the polar vortex is still intact below 20 km. If air from outside the vortex were mixing rapidly into the interior of Antarctica, the stratosphere would be quickly rehydrated since water vapor could no longer be removed.

During the winter above 25 km, the stratosphere stays rather moist with mixing ratios in the 5-6 ppmv range. This probably reflects the descent within the vortex as the air continues to cool and sink.

3.1.10. Surface Radiation

Solar and Terrestrial Atmospheric Radiation

The surface radiation budget (SRB) is a basic and critically important climate variable that has long been inadequately observed because of insufficient global coverage and inherent instrumental limitations. Surface-based radiation monitoring projects are being carried out by CMDL at eight locations: BRW, Erie and Boulder, Colorado (BAO and BLD), Bermuda (BRM), MLO, Kwajalein, Marshall Islands (KWJ), SMO, and SPO. The long-term continuous measurements at these sites include broadband downward solar irradiances and several sites, BRW, BAO, BRM, KWJ, and SPO, also measure downward thermal infrared irradiances. At sites where the measurements were determined to have a representative surface (BRW, BAO, and SPO) upward solar and infrared irradiance measurement projects are also maintained. The more extensive observations are made at CMDL sites where the measurements are more areally representative especially with respect to land surface and cloudiness. Irradiances observed at the more areally representative sites, BRW, BAO, KWJ, BRM, and SPO are being incorporated into an international data base sponsored by the WMO and NASA under the Baseline Surface Radiation Network (BSRN). All data from CMDL sites are also maintained as part of the long-term CMDL surface radiation record that exists for the past 15 years at BRW, MLO, SMO, and SPO. Previous CMDL (and GMCC) Summary Reports have discussed the wide ranging and useful applications of these data to scientific questions.

Recently completed and ongoing projects utilizing the radiation observational results from the CMDL field sites include the detection of a long-term decrease in Arctic haze [*Bodhaine and Dutton,* 1993]; comparison of satellite and BAO-derived SRB under clear and cloudy conditions [*Cess et al.*, 1991, 1993, 1995]; the effects of snow surfaces on atmospheric absorption

[*Nemesure et al.*, 1993]; detection of intermediate-term trends in cloudiness related to radiation perturbations [*Dutton et al.*, 1991; *Schnell et al.*, 1991]; a technique for monitoring long-term climate variability using surface albedo records [*Dutton and Endres*, 1991; *Foster et al.*, 1992]; identification of a strong statistical coherence between the QBO and the MLO long-term transmission record [*Dutton*, 1992*a*]; a surprisingly good agreement between modeled and observed thermal infrared irradiances over the range of globally extreme conditions [*Dutton*, 1992*b*], and a determination of the radiative effects of the Mt Pinatubo volcanic eruption [*Dutton and Christy*, 1992; *Russell et al.*, 1993, and *Dutton et al.*, 1994]. Dramatically new information on cloud absorption is being revealed in an ongoing investigation using CMDL surface and satellite top-of-the-atmosphere solar data, *Cess et al.* [1994]. Numerous additional requests were made and fulfilled for CMDL radiation data for a variety of research applications.

Updated results on the late summer cloudiness and irradiance trends at SPO reported by *Dutton et al.* [1991] are shown in Figure 3.15. As suggested by *Dutton et al.* [1991], the previously observed trends during January and February until 1988, did not project into the future. The current SPO irradiance level shows an autocorrelated return to previous levels. The potential for a >20-year oscillation in these data now exists.

The MLO atmospheric transmission record, updated through 1993, is shown in Figure 3.16. The effects of the eruptions of Mt. Pinatubo and El Chichon are most obvious and are enlarged and compared in the inset of the figure. This record is now continuous for the past 37 years and may provide the best available information

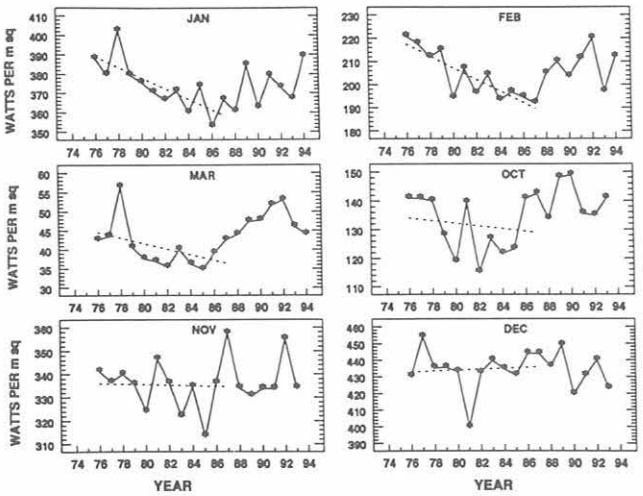

Fig. 3.15. Monthly mean total (direct plus diffuse) solar irradiance at the South Pole. The plotted lines are for linear least-squares fits for 1976 through 1987.

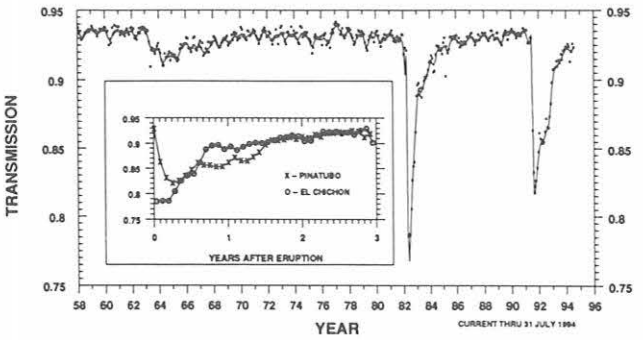

Fig. 3.16. Monthly mean "apparent" atmospheric transmission as determined from broadband direct solar beam observations at Mauna Loa.

on the lack of any significant secular trends in the global background atmospheric transmission of solar radiation over this time. Two to three more years without a major volcanic eruption will be required for the record to once again reach its background level.

Snowmelt date at Barrow, Alaska, was defined as the last date each year that any significant snow remains on the ground (first day each year that <1 inch of snow is reported in visual observations or the daily average surface albedo falls below 30%). Considerable differences between the NWS observations within the village of Barrow and on the tundra near the CMDL site were noted in Figure 3.17. When compared with other tundra albedo data for the late 1960s and early 1970s and the earliest NWS data, the CMDL data [*Dutton and Endres*, 1991] continue to suggest that there was no significant change in the annual date of spring snowmelt near Barrow since the 1940s. The NWS data [*Foster*, 1989] alone suggest an advancing date of snowmelt that can be interpreted erroneously as being due to a general warming, but is instead most likely because of urbanization of the Barrow village.

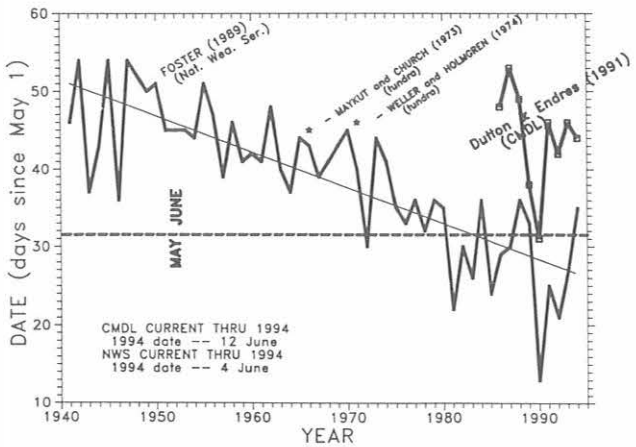

Fig. 3.17. Date of annual spring snowmelt as determined by various researchers at different locations in and around Barrow, Alaska. The downward trend indicated by the Foster (NWS) curve is believed to be due to "urbanization" in Barrow.

The CMDL radiation project accepted the responsibility of working with the WMO GEF/GAW program for the intent of establishing a surface-based solar radiation measurement and research program at each of four global baseline sites located in developing countries. CMDL will acquire the necessary equipment, train onsite observers, and assist in the establishment of programs in Algeria, China, Argentina, and Indonesia over the next 2 years.

Operations

There were only a few significant changes in observatory operations during the year, which is an important attribute of a long-term measurement effort. Blowers were added to the upward facing pyranometer and pyrgeometer at SPO. The new units are very effective in keeping frozen precipitation and condensation off the filter domes. Additional blower units are being acquired as funds allow for implementation at other sites. A critical requirement of the radiation project is to make stable and accurate micro-volt level measurements to ensure that the potential voltage measurement error is small compared with other sources of error. Current data loggers have integrating A/D converters with auto zeroing and achieve 2 microvolt accuracy. Continuous data logging at all eight sites now has 3-minute or better resolution recorded and permanently stored. Data sampling times range from 1 to 2 seconds.

Incoming data are currently received daily in Boulder for all sites except SMO, are processed within 2 days, and reviewed for quality-control purposes. Data editing, processing, and final storage have been moved to medium-sized and personal computers all directly under the control of CMDL, thereby eliminating the dependence of outside computer expertise and resources. Final processing is completed about 1 calendar year after the data are first available for processing. Assignment of final calibration information is ongoing as updated radiometer calibration data are made available. Final data values depend on careful review and application of sensor calibration information that is provided by the CMDL Solar Radiation Facility.

Remote Sensing of Aerosol Optical Properties and Water Vapor

Other than clouds, aerosols and water vapor are the main contributors to thermal-infrared and solar radiation variations and subsequent radiative climate forcing. The potential climate variations resulting from such variations are extensive and varied. The observed and potential radiative variations may be due to either anthropogenic causes such as increased industrial production of aerosols and water vapor feedback resulting from increasing greenhouse gases or from natural causes such as volcanic, biogenic, or surface wind-generated aerosols and inherently varying water vapor. CMDL has a long history of exploratory and operational projects relating to the remote sensing of aerosols and water vapor as related to climate variations. Since 1977 wide-band spectral observations of direct solar irradiance using a filter wheel NIP at BRW, MLO, SMO, and SPO were used to infer aerosol optical depth and column water vapor amounts. These measurements have proven to be durable and stable over time thereby excelling in a monitoring effort even though their accuracy is less than can be obtained by more sophisticated but less robust instrumentation. Additional and exceptional effort has been put into high-precision narrow spectral band optical depth measurements at MLO. At MLO several narrowband (0.005 μm) sunphotometers are routinely operated and, because of the nearly ideal atmospheric conditions and the existence of automated observing platforms, have produced reliably consistent long-term data sets. Results from the MLO aerosol optical depth measurement project are reported by *Dutton et al.* [1994] and *Russell et al.* [1993] and in previous CMDL Summary Reports. One year of narrowband sunphotometer data were collected from Sable Island, Nova Scotia, as part of a comprehensive surface-based aerosol sampling project described in section 3.1.1.2.

3.1.11. Solar Radiation Facility (SRF)

Support for the CMDL solar radiation measurement programs at seven field sites continued during 1993. Sensor procurement, maintenance, and repairs were part of the ongoing activities of the SRF in addition to providing calibrations and characterization information. The seven sites include the four CMDL baseline observatories plus KWJ, BRM, and BAO. Also, a suite of continuous broadband measurements was maintained at the SRF facility in Boulder as part of a historical record dating back to 1977. Instrument characterization methodologies were investigated as part of the ongoing activity of the SRF.

The SRF supported and participated in an intercomparison of automated cavity radiometer systems held at the National Renewable Energy Laboratory (NREL) September 27-October 4, 1993. Four cavity radiometers and other CMDL equipment contributed to the success of the comparison. Post-comparison data analyses and data entry tasks were also performed by CMDL personnel in support of the event. An ongoing collaboration with NREL involving cavity comparisons is part of the SRF means of maintaining the integrity of the calibrations used by CMDL monitoring activities at its sites.

A project was started during 1993 by the SRF as a result of a proposal to the WMO for implementing broadband solar radiation measurements at GEF/GAW sites. Each site will be equipped with pyranometers, pyrheliometers, automated solar trackers, shadowband systems for diffuse-sky radiation measurements, and an automated absolute cavity system for use as a primary

calibration standard. Data acquisition systems identical to those used at the CMDL baseline observatories will be constructed and used at the GEF/GAW sites as well. The instruments, data acquisition components, computers, and cavity radiometer systems destined for each GEF/GAW site will be assembled and put into operation at the SRF in Boulder. Each country will send its representative to Boulder for training in the collection of solar data and calibration techniques using the equipment that will ultimately be shipped to each respective country. The procurement of equipment began in late 1993, and the first trainee is expected during the second quarter of 1994.

3.2. Special Projects

3.2.1. An Analysis of 10-Day Isentropic Flow Patterns for Barrow, Alaska: 1985-1992

Atmospheric transport patterns to BRW were investigated using a newly developed isentropic model described in CMDL Summary Report No. 21 [*Peterson and Rosson*, 1993]. The new model features a layer-averaged mode that is activated whenever an air parcel traveling isentropically approaches the earth's surface and a dynamic preprocessing program that ensures trajectories always arrive at a constant, predetermined altitude. Some highlights of this study [*Harris and Kahl*, 1994] are described below.

Ten-day back trajectories arriving above BRW at 500 m, 1500 m, and 3000 m asl were calculated for the 8-year study period. Cluster analysis was used to summarize trajectories for the entire 8 years, for each year individually, and for each month (e.g., eight January's, eight February's, etc.) The focus of this report is only on some of these results, particularly those relating to transport of Arctic haze to BRW.

Figure 3.18 shows the means of each of the six transport clusters determined for the middle arrival elevation (1500 m asl) where flow is near and usually above the inversion level. Two cluster means in Figure 3.18 indicate transport from south of BRW. Both of these, clusters 1 and 3, have cyclonic curvature, consistent with transport from the area of the Aleutian Low. On average, southerly transport occurs one third of the time. Approximately one quarter (26%) of trajectories to BRW fall into cluster 4, which depicts very light northerly and northwesterly flow, with 10-day origins south of 80°N in the East Siberian Sea. The flow pattern with the next highest frequency (15%) is represented by the mean for cluster 6. It shows moderate northwesterly flow and an origin for trajectories in the central polar basin. Cluster 2, representing 14% of flow to Barrow, has a stronger westerly component than that for cluster 6 and a 10-day origin over north-central Russia near the Taymyr Peninsula. Finally, the mean for cluster 5 indicates northeasterly flow from the Canadian Archipelago with

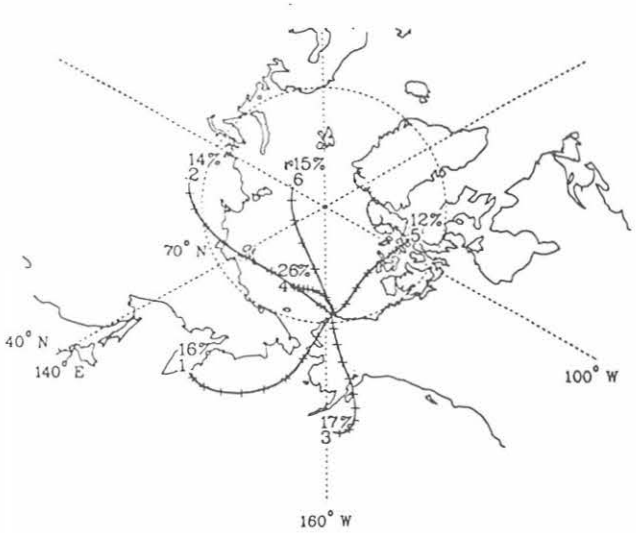

Fig. 3.18. Atmospheric flow patterns for the period 1985-1992 depicted by cluster-mean back trajectories arriving at Barrow at 1500 m asl. Plus signs indicate 1-day upwind intervals. The numbers 10-days upwind of Barrow show (top) the percentage of trajectories occurring in that cluster and (bottom) the cluster number (1-6) used for identification.

a frequency of 12%. Notably absent at this level are any cluster means showing transport within 10 days from either Europe or the contiguous United States.

To more precisely quantify transport from three source regions of particular interest, trajectories were counted that intersected the source boxes shown in Figure 3.19. Although no cluster means originate over Europe for the 1500-m arrival elevation, this region was investigated because it is often cited as a significant source of Arctic haze. Trajectories were counted over the Taymyr region because the cluster means indicated this as a consistent source at all three levels. The north Pacific region is of interest as the most direct source of heat transported to Barrow. Table 3.12 presents the results tabulated according to arrival elevation. The percent frequency of transport from each region is shown, followed in parentheses by the average transport time in days.

March and April trajectories were analyzed in this way (not shown) because recent studies have found decreasing trends in aerosol concentration [*Bodhaine and Dutton*, 1993] and sea-ice extent, and an increasing trend in surface temperature [*Chapman and Walsh*, 1993] during spring. The source region analysis presented no evidence of a significant change in transport that may have been linked to these trends. It is quite likely that our 8-year study period is too short to reveal a true climate change. It could also be that the spring warming seen by *Chapman and Walsh* [1993] is primarily a radiative effect, without an identifiable transport component. *Bodhaine and Dutton* [1993] hypothesize that the decreasing aerosol trend they saw resulted from decreased anthropogenic emissions.

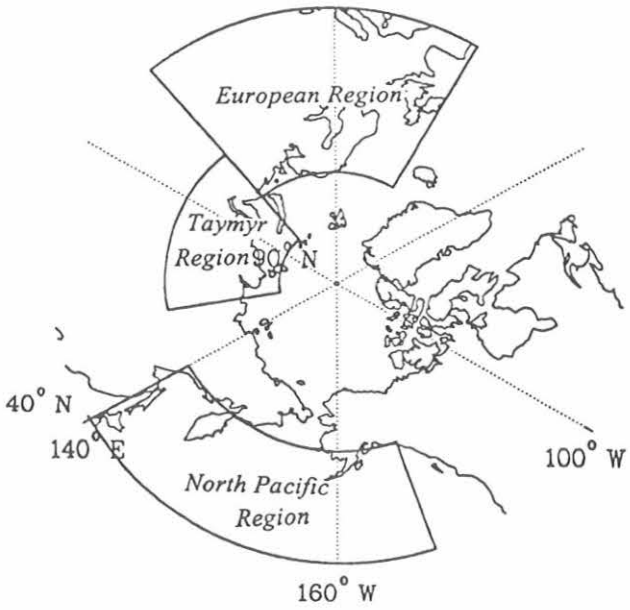

Fig. 3.19. Three potential source regions in which trajectories were tabulated: Europe, north-central Russia near the Taymyr Peninsula, and the north Pacific.

Figure 3.20 shows contour elevation plots of the average modeled transport surfaces for January 1992 for the (*a*) 500-m asl arrival elevation; (*b*) 1500-m asl arrival elevation; and (*c*) 3000-m asl arrival elevation. The surfaces shown in Figure 3.20 are intended to convey a sense of the vertical motion that an air parcel may experience on its journey to Barrow. The contour levels are not intended to imply preferred transport from any particular area. Rather, they are intended to answer the question: If an air parcel transported isentropically to the specified arrival elevation at Barrow were to pass over a certain area, at what altitude would the transport likely take place? Aside from the prominent topography of the Tibetan Plateau, the Rocky Mountains, and the Greenland Ice sheet, the isentropic features of the extratropical northern hemisphere are evident. Isentropic surfaces on individual days during the haze season will vary at times from the January means shown here. Inspection of other winter-spring months proved the surfaces in Figure 3.20 to be representative of the season.

TABLE 3.12. Percent Frequency of Origin and (Average Transport Time in Days) According to Arrival Elevation

Arrival Elevation (m asl)	Europe	Taymyr	North Pacific
500	1.3 (8.0)	21.1 (6.3)	19.8 (4.2)
1500	4.4 (7.6)	24.1 (5.9)	36.3 (4.1)
3000	11.0 (7.0)	23.6 (5.2)	50.1 (3.6)

The lowest transport level, shown in Figure 3.20*a*, is quite flat, indicating travel mostly in the near-surface layer. The higher isentropic surfaces (Figures 3.20*b* and 3.20*c*) are more peaked over the polar basin. In addition, the higher surfaces extend downward from Barrow to the south, whereas the lowest surface is limited in downward extent from Barrow. The result is that upper-level trajectories will encounter more vertical motion than lower ones.

The shape of the isentropic surfaces may have relevance to pollution transport to Barrow, if pollution is assumed to be confined to the lower levels at its source. Table 3.12 shows that transport occurs from the Taymyr region at a frequency greater than 20% at all three levels. However, the pollution assumption implies that direct transport from the Taymyr region must be close to the ground, following a surface similar to that shown in Figure 3.20*a*. Europe is only an occasional origin for 10-day back trajectories at the lower levels, but trajectories arriving at 3000-m asl originate from Europe 11% of the time. Cluster means (not shown) and the average transport surface (Figure 3.20*c*) favor Scandinavia as opposed to midlatitude eastern European sources at this level.

Because of the shape of the isentropic surfaces, trajectories generally ascend from the south and descend from the polar region to BRW. The effect of the isentropic vertical parameterization is not significant for near-surface trajectories, but higher level trajectories could be markedly different than their isobaric counterparts, depending on the degree of wind shear and temperature differences encountered during transport. It appears that isentropic transport to BRW can be slower than horizontal transport because wind speeds are often less along the lower periphery of the isentropic surfaces compared with those on isobaric surfaces.

3.2.2. Aerosol Measurements at MLO During MLOPEX

Introduction

The routine aerosol monitoring program was initiated at MLO in 1974 with the installation of instrumentation for the continuous measurements of CN concentration and aerosol scattering extinction coefficient (σ_{sp}), although apparently the earliest aerosol measurements were made by *Nakaya et al.* [1957]. A brief history of MLO aerosol measurements was given by *Bodhaine* [1983].

The Mauna Loa Observatory Photochemistry Experiment (MLOPEX) was a multi-agency cooperative experiment designed to study the chemistry of the free troposphere near 3.4-km altitude. The experiment consisted of four intensives that were designed to obtain data representative of four different seasons at MLO. The periods chosen were September 16-October

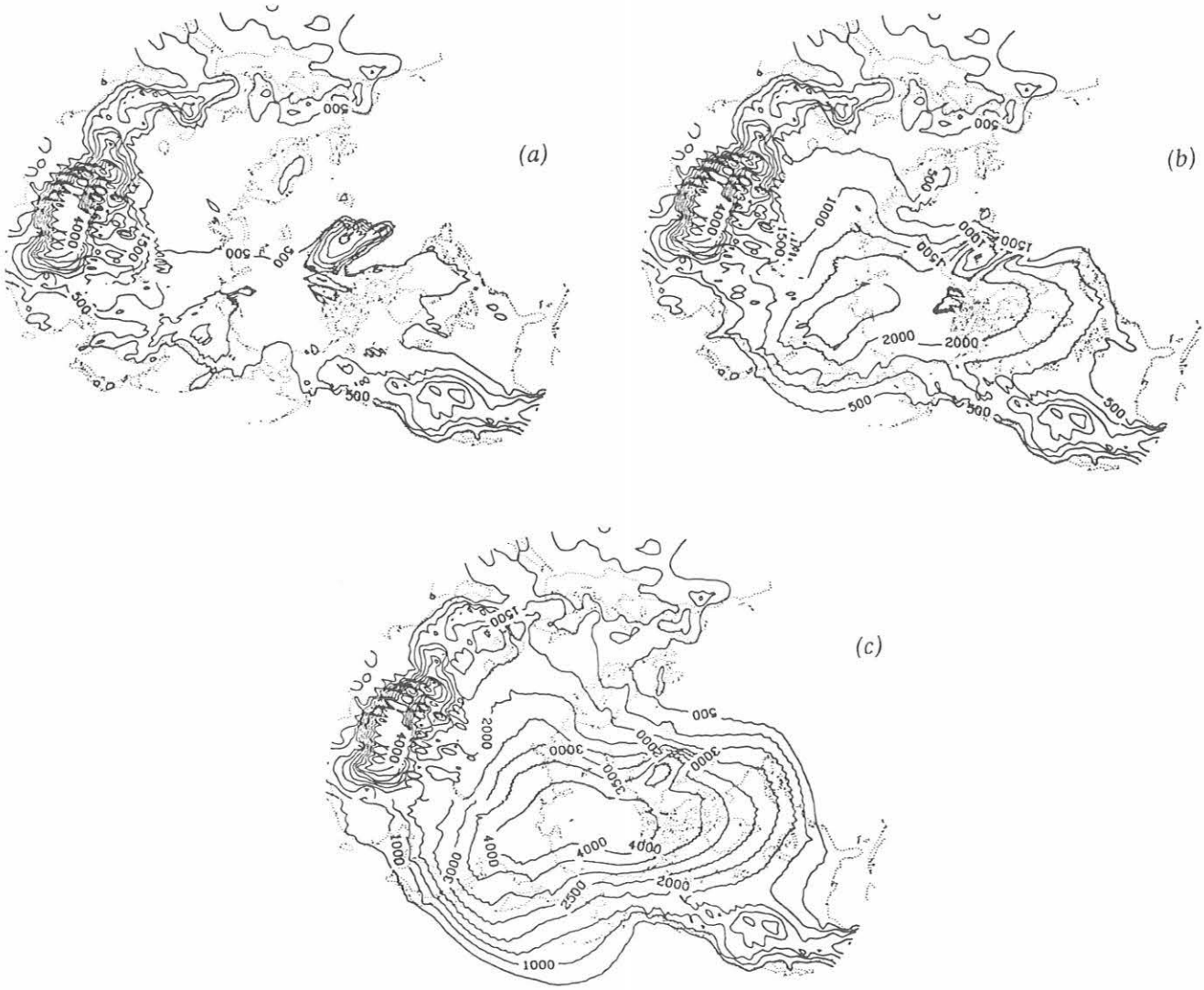

Fig. 3.20. Contour elevation plots (m asl) of the average transport surfaces for January 1992 at the (*a*) 500 m asl arrival elevation, (*b*) 1500-m asl arrival elevation, and (*c*) 3000 m asl arrival elevation. The contour interval is 500 m.

23, 1991; January 15-February 15, 1992; April 12-May 15, 1992; and July 15-August 14, 1992. An important part of this experiment was to investigate the diurnal cycles of the parameters measured, both the effects of the upslope-downslope windflow, and the diurnal photochemical cycles in free tropospheric air. All dates and times are presented here as Julian day-of-year (DOY) and Hawaii Standard Time (HST). For comparison with Universal Time (UT), UT = HST + 10 hours at MLO.

Instrumentation

CN measurements were initiated in 1974 using a G.E. automatic CN counter (1974-1989) and a TSI 3760 CN counter (1989-present). A Pollak CN counter [*Metnieks and Pollak*, 1959] has been operated daily since 1974 to provide comparison points for the automatic CN counters. Aerosol scattering extinction coefficient (σ_{sp}) measurements were initiated in 1974 using a four-wavelength nephelometer similar to the design of *Ahlquist and Charlson* [1969]. Aerosol absorption (σ_{ap}) has been measured at MLO since 1990 using an aethalometer [*Hansen et al.*, 1982]. The instrument and data for 1990-1991 were described by *Bodhaine et al.* [1992]. The SO_2 data shown here were provided by Gerd Hübler (personal communication, 1994).

Data Analysis

Diurnal cycles. Data from intensives 3 and 4 were used to study the character of the diurnal cycle at MLO. Figure 3.21 shows means by hour of the day for the entire periods of intensives 3 and 4. The primary data

set used to form these means was the hourly data produced by the MLO data acquisition system. An hourly data point was deemed acceptable for inclusion in the mean if the 450-, 550-, and 700-nm nephelometer data were all present and if no local pollution was detected during that hour. Next, the Ångström exponent (α) was calculated from the σ_{sp} data. Finally, if CN, wind direction (WD), or wind speed (WS) data were present for that hour, they were included in their means for that hour of the day. Thus the tallies of σ_{sp}, CN, WD, and WS, could all be different for a given hour. However, this procedure was necessary to avoid problems caused by missing data when several data sets are merged.

Referring to Figure 3.21*a*, the average diurnal range in CN concentration was about 300-1000 cm^{-3} between night and day, with the beginning of background sampling conditions at about 2100 HST and the onset of the upslope wind at about 1000 HST. The σ_{sp} data show somewhat narrower background sampling conditions between about 0200 and 0800. Historically, 0000-0800 was the time interval chosen to sample background values of σ_{sp} at MLO [*Bodhaine*, 1978]. The WD data in Figure 3.21*a* show clearly that WD changes from northerly to southerly at about 1800, and back to northerly at about 0900. Clearly, a time lag exists between when WD changes and when stable sampling conditions exist at the site. WS averaged about 5 m s^{-1} during both night and day.

The α data in Figure 3.21*a* show that the particle size tended to be larger during downslope conditions than during upslope conditions during this intensive. Particle sizes are generally larger at this time of year because of Asian dust transport. The interpretation of α data has been discussed by *Bodhaine and DeLuisi* [1985]; however, qualitatively speaking, larger α's imply smaller particles and vice versa.

Figure 3.21*b* shows a similar presentation of the average MLO diurnal cycle during intensive 4. Aerosol scattering extinction coefficient values are about a factor of five lower than in intensive 3. A diurnal cycle of σ_{sp} is apparent with background conditions occurring during about 2200-0800. WD shows an upslope-downslope effect with a change to southerlies at 1800 and the onset of the upslope at 0800. In the summer (Figure 3.21*b*) the winds had an easterly component whereas in the spring (Figure 3.21*a*) the winds had a westerly component. Also, note that the winds were weaker during the upslope-downslope transition periods.

A classic example of an upslope-downslope event with clean background conditions during downslope flow, is shown in Figure 3.22 for DOY 118-119 (April 27-28) 1992. Here the CN concentration shows clean conditions from 1700 on DOY 118 to 1000 on DOY 119, and WD is clearly in the southerly band during that time. The σ_{sp} data are interesting because they apparently settle to background values by about 2000 on DOY 118, but assume a new, lower value during about 0800-1100 on DOY 119 before the upslope event appears. This behavior may be explained by a decrease in aerosol concentration at about 0800 on DOY 119

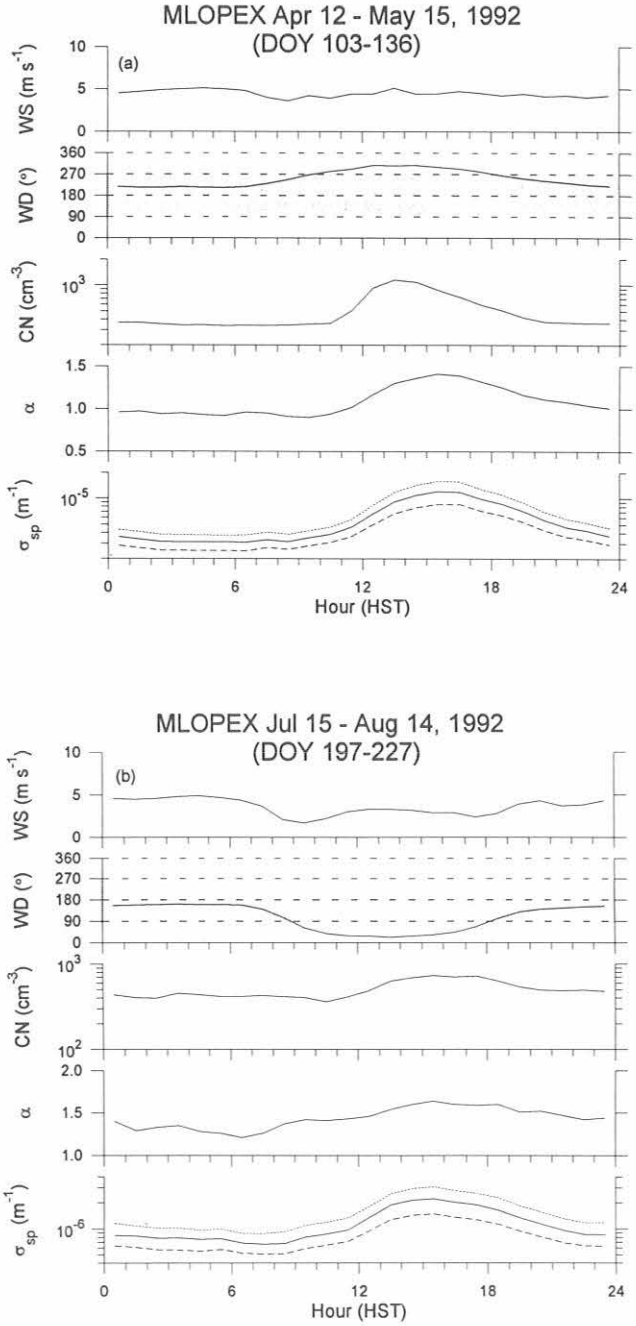

Fig. 3.21. Data for MLOPEX (*a*) intensive 3 and (*b*) intensive 4. Means by hour are shown for wind speed (WS); wind direction (WD); CN concentration; α; and σ_{sp} for 450 (dotted), 550 (solid), and 700 nm (dashed). α values were calculated suing equation (1). The shaded areas on the WD graphs denote winds with a southerly (downslope) component. Hour of the day is shown as HST.

(possibly by a few large dust particles), which gave an obvious decrease in σ_{sp} and an increase in α, but a negligible effect on the CN concentration. Note the fairly high WS on these two days. The SO_2 data superimposed here in Figure 3.22 follow the CN data quite closely, indicating an island source for SO_2. These local sources of SO_2 could be either anthropogenic (e.g., fuel combustion) or natural (e.g., fuming from Kilauea caldera). The black carbon (BC) data in Figure 3.22 show a diurnal cycle that follows the CN and SO_2 data quite closely, suggesting similar sources. Since BC can be produced locally by both natural and anthropogenic sources, it can be a good indicator of a local pollution event.

Asian desert dust event. Examples of Asian dust events are shown in Figure 3.23. Episodes of closely-spaced three-wavelength σ_{sp} data (low values of α) strongly suggest a relatively larger aerosol size, most likely Asian dust [*Bodhaine et al.*, 1981]. The σ_{sp} data in Figure 3.23, at the beginning of DOY 126, show the end of a downslope event dominated by large particles at about 0800 and smaller upslope particles at about 1200. The large particle peak was about 2×10^{-5} m^{-1} with an α near 0. By about 0000 on DOY 127 the data show a small-particle downslope regime, illustrating the patchy nature of the Asian dust. Large particles dominated the upslope-downslope cycle that began at about 0800 on DOY 127 and continued through about 1000 on DOY 128. Similar effects occurred over the next several days and the Asian dust was gone by about DOY 134.

At about 1000 on DOY 128, 129, and 130 three obvious small-particle upslope events broke through the Asian dust cloud. Note the clean downslope event on DOY 135 that gave σ_{sp} values of about 5×10^{-7} and CN concentrations of about 300 cm^{-3}, even though WD did not indicate strong downslope conditions. The multi-wavelength σ_{sp} data clearly identify the presence of

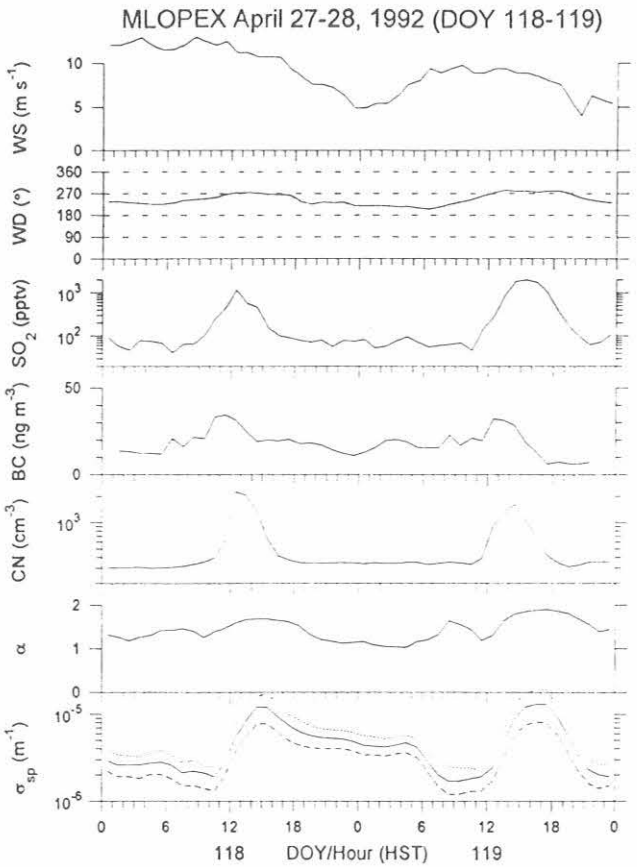

Fig. 3.22. Hourly values of wind speed (WS); wind direction (WD); SO_2 concentration; BC concentration; CN concentration; α; and σ_{sp} for 450 (dotted), 550 (solid), and 700 nm (dashed), on DOY 118-119, 1992. α values were calculated using equation (1). The shaded area on the WD graph denotes winds with a southerly (downslope) component. Hour of the day is shown as HST.

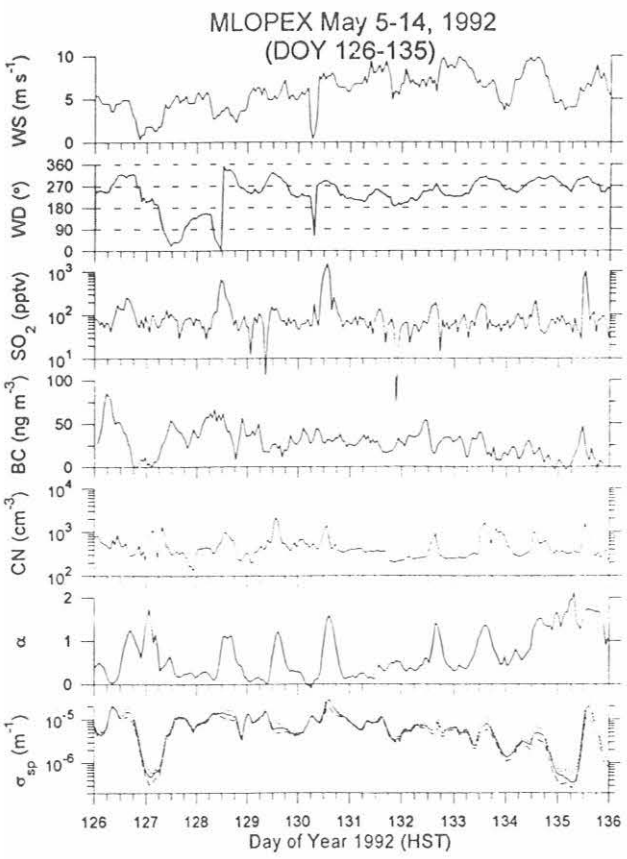

Fig. 3.23. Hourly values of wind speed (WS); wind direction (WD); SO_2 concentration; BC concentration; CN concentration; α; and σ_{sp} for 450 (dotted), 550 (solid), and 700 nm (dashed), on DOY 126-135, 1992, during which an Asian desert dust event occurred. α values were calculated using equation (1). A 3-hour running mean was applied to the BC data. The shaded area on the WD graph denotes winds with a southerly (downslope) component. Hour of the day is shown as HST.

large Asian dust particles as opposed to smaller background-tropospheric or locally-produced particles. Note that Asian dust can dominate the aerosol measurements during upslope as well as downslope flow.

The SO_2 data for this period appear to correlate best with the CN data, and the α data show that SO_2 events tend to be correlated with small-particle events. Of particular interest is the fact that SO_2 events occur during the Asian dust events, raising the possibility that SO_2 may be transported from Asia. The BC data shown in Figure 3.23 tend to follow the σ_{sp} data during the beginning of the record and the CN and SO_2 data during the latter part of the record. This suggests that the BC may have been transported over long distances when it is associated with the desert dust as determined from the σ_{sp} data [*Bodhaine et al.*, 1992].

Mixed regime. Data for DOY 219-228 are presented in Figure 3.24. This 10-day period was chosen to illustrate the difficulty of just classifying MLO data as upslope or downslope. This was a period of generally light and somewhat uncertain winds (with the exception of DOY 220). The particle size distribution, as suggested by the σ_{sp} and α data, was dominated by small particles during both upslope and downslope conditions throughout the entire period. The α data here tend to be somewhat noisier than those during the Asian dust period because the σ_{sp} data are much lower. The cleanest background conditions exhibit σ_{sp} values of about 2×10^{-7} m^{-1} and CN concentrations of about 300 cm^{-3} on DOY 222 and during the clean period of 226-227.

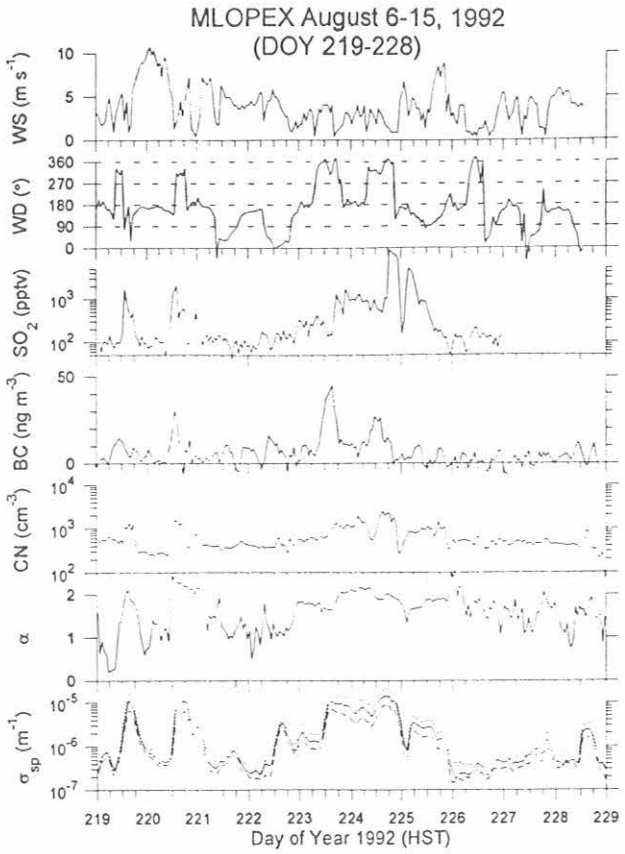

Fig. 3.24. Hourly values of wind speed (WS); wind direction (WD); SO_2 concentration; BC concentration; CN concentration; α; and σ_{sp} for 450 (dotted), 550 (solid), and 700 nm (dashed), on DOY 219-228, 1992, during which rather uncertain conditions existed. α values were calculated using equation (1). A 3-hour running mean was applied to the BC data. The shaded area on the WD graph denotes winds with a southerly (downslope) component. Hour of the day is shown as HST.

The upslope event at about 1200 on DOY 219 is quite obvious in the σ_{sp}, α, CN, and SO_2 data. However, it is not so easy to predict based on WD and WS data. The next upslope event at about 1200 on DOY 220 again shows up clearly in all data records and does have a northerly WD. The secondary peak at about 2300 on DOY 220 appears during southerly winds but seems to be associated with a minimum in WS. Then a strong downslope at 0200 on DOY 221 gave clean conditions before the next upslope event in σ_{sp} at about 1200 on DOY 221.

The downslope event at about 1800 on DOY 221 produced very clean background conditions in both σ_{sp} and CN data, followed by classic upslope wind flow at about 0800 on DOY 222. The secondary event in σ_{sp} (but not in CN) at about 0000 on DOY 223 is unexpected and not easily explained on the basis of these data alone. Likewise, the obvious upslope events at about 1200 on DOY's 223 and 224 are expected, but the polluted values during 0000-1200 on DOY 224 or the peak beginning at about 0200 on DOY 225 are not expected. A clean period begins at about 0000 on DOY 226 and continues until the upslope event begins at about 0800 on DOY 228. Note, however, the slight upslope event at about 0800 on DOY 226 and the spurious event at about 2000 on DOY 227, apparently associated with light winds.

Referring to the SO_2 data in Figure 3.24, it is possible to explain the unexpected features discussed previously. These data show peaks of about 2 ppbv that coincide with the upslope events at about 1200 on DOY 219 and 220. However, a peak during downslope conditions at about 2300 on DOY 220 coincides with those in CN and σ_{sp}. SO_2 events at 0000 on DOY 223, 0000 on DOY 224, 1800 on DOY 224, and 0200 on DOY 225 all occur during downslope conditions and are most likely caused by venting from the Mauna Loa caldera.

The BC data shown in Figure 3.24 tend to follow upslope events, although not always. The three largest events in the BC data coincide with upslope events; however, the volcanic events discussed previously show low BC concentrations. Note the extremely low BC concentrations during DOY 226-227, probably representative of clean background tropospheric conditions.

Data screening. Clearly it would be difficult to

design a computer algorithm for routinely screening data that could cope with the data shown in Figures 3.23 and 3.24. Historically, MLO aerosol data were screened on the basis of time of day and WD. The time window 1000-1800 UT for accepting background σ_{sp} data was used by *Bodhaine* [1978], based on 3 years of nephelometer data. This time window allows for the slow time response of the nephelometer. Wind criteria for accepting MLO aerosol data require WD with a southerly component (90° < WD < 270°) and WS > 0.5 m s^{-1} [*Bodhaine et al.*, 1980]. Currently, routine MLO aerosol data editing also includes the manual identification of suspicious hours that may have been influenced by some unknown short-term local activity. These hours are labeled with "P" flags [*Massey et al.*, 1987]. It is apparent from the previous examples that MLO data should be edited on a day-by-day basis, using as many different data sets as possible, including SO_2 and BC concentration. Continuous SO_2 measurements at MLO would be extremely desirable.

3.2.3. Water Vapor and Ozone Profiles Over the Tropical Pacific During CEPEX

Introduction

The Central Equatorial Pacific Experiment (CEPEX) took place during March 1993. The broad objective of this experiment was to obtain the measurements necessary to establish the roles of cirrus radiative effects and surface evaporation in limiting maximum surface temperature in the equatorial Pacific. In addition to playing a key role in climate in the western and central Pacific region because of the strong convection, it is also the major area where material from the troposphere can be injected into the stratosphere. Because of the cold tropopause temperatures seen in this region during the boreal winter and spring, air passing through the tropopause is dried as it enters the stratosphere. Understanding of the mechanism for this drying is an active area of research and a major focus of this effort. In addition, the horizontal circulation induced by the convection (Walker circulation) was also investigated.

Measurements

Water vapor and ozone profiles were obtained from the research vessel *John Vickers* as it sailed northeast from Honiara, Guadacanal (9.5°S, 160°E), to Nauru (0.3°S, 166.5°), then east to Christmas Island (2°N, 157.5°W). Soundings were made from Christmas Island (Kirimati) for a week (March 20-26) at the end of the ship cruise (March 7-18). During the experiment there were at least 13 partially successful water vapor soundings and 26 ozone soundings. On 12 of the flights, the ozone and water vapor were measured simultaneously. The water vapor profiles were obtained using a balloonborne frost-point hygrometer. For many years such instruments were used to make stratospheric water vapor measurements in Boulder. The uncertainty in the mixing ratio is about ±10%. Ozone was measured with a digital version of the ECC ozone sensor that also has a long history of ozone profile measurements. The estimated uncertainty in the ozone partial pressure is ±5% in the stratosphere and ±7-10% in the troposphere.

Both the water vapor and ozone profiles could be classified into three groups with rather distinct features based on the longitude (and time) of the observations. In the most westerly group of soundings (west of 174°W) done between March 7-13, there was a very low minimum water vapor mixing ratio (<1.5 ppmv) that corresponded in altitude to the local tropopause (Figure 3.25*a*). Ozone was very low (<30 ppbv) throughout the troposphere with a sharp increase in the mixing ratio at the tropopause. Although the only successful water vapor sounding when active convection was nearby was on the first day, the satellite imagery showed strong convection in this region throughout the period of observations. The very low water vapor mixing ratios at the tropopause indicate air is being dried as it passes through this cold trap. The observations of water vapor at the tropopause never showed saturation, but minimum temperature measured during the four-times daily radiosonde ascents were very close to the measured frost-point temperature. Minimum radiosonde tropopause temperatures in this region usually occurred at night or early morning, while the water vapor soundings were done later in the morning. It also may be that the saturation at the tropopause occurs only during the deep convective events when no successful balloon ascents were made.

In the second group of soundings that were done between 173°W and Christmas Island close to the equator, mixing ratios increase a bit at the tropopause but are still low (1-2 ppmv). Above the tropopause amounts are higher by about 1 ppmv. The shape of the profiles in these two groups is also generally the same. In this region convection was not intense and the tropopause was further from saturation even though frost-point temperatures were warmer. The main characteristics of the upper troposphere and stratosphere in this region appear to reflect the processes taking place further to the west.

For the final group of soundings done at Christmas Island at the tropopause (Figure 3.25*b*), the minimum water vapor mixing ratio was between 2.5 and 3.5 ppmv. There is an absence of a sharp step in ozone at the tropopause, and ozone values were much higher in the upper troposphere. Convection, although present over Christmas Island, was not deep and hence neither the ozone nor water vapor profiles show characteristics seen in the more convective region.

Discussion and Conclusion

The water vapor and ozone profiles obtained during CEPEX show that deep convection in the western Pacific dries air passing through the tropopause to very

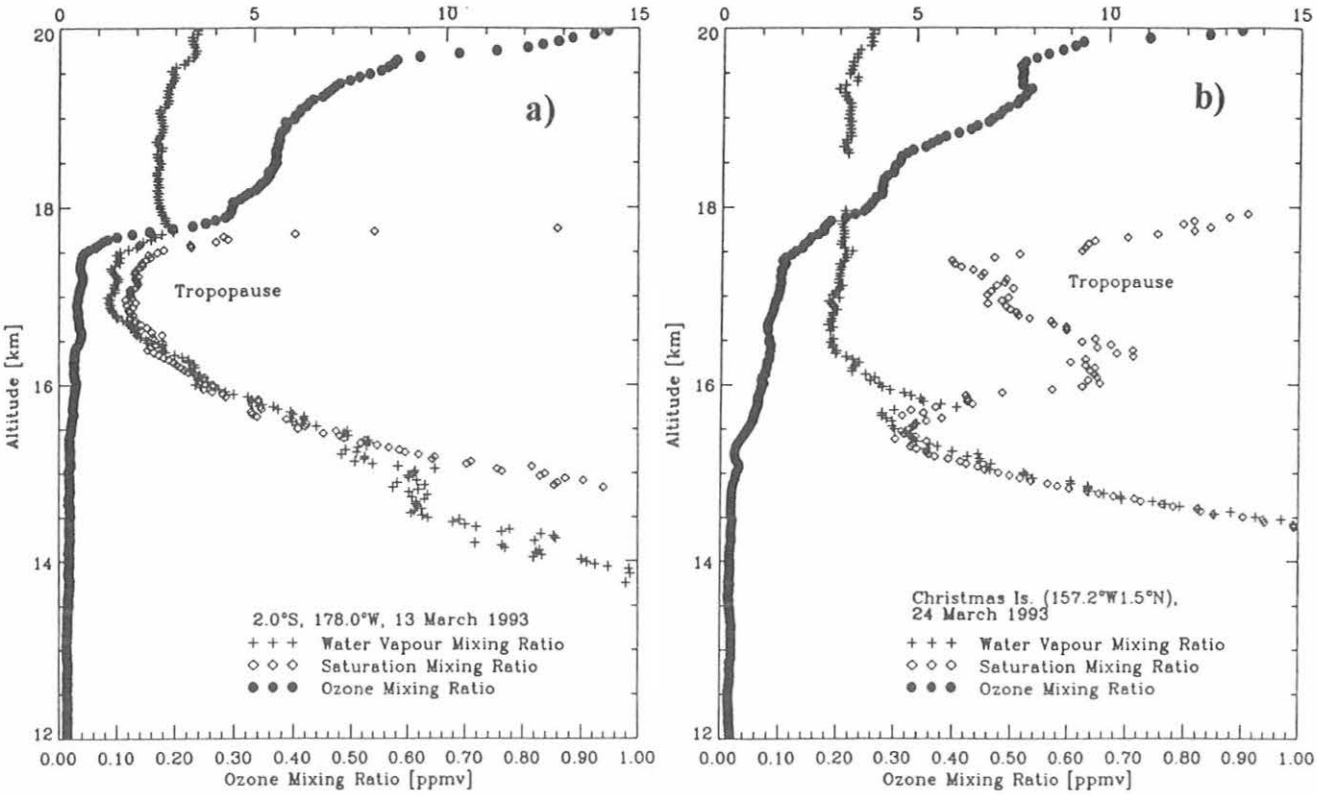

Fig. 3.25. Water vapor and ozone mixing ratio profiles from the upper troposphere and lower stratosphere during CEPEX. In (*a*) the profiles were obtained near the equator at the dateline and show the affects of deep convection. In (*b*) the profiles done on Christmas Island do not show convection penetrating to such high altitudes.

low values (~1 ppmv), which is the primary factor in establishing the dryness of the stratosphere. This drying takes place over a broad region as evidenced by the large horizontal extent over which dehydration was observed. The single, sharp minimum in temperature at the tropopause supports a mechanism for dehydration associated with deep convection in tropical disturbances [*Danielsen*, 1993].

The changes in the stratospheric water vapor profiles seen at Christmas Island not only represent conditions further to the east out of the deep convective region but they also reflect a change in flow pattern in the lower stratosphere. The relatively high ozone values seen in the upper troposphere indicate transport from the stratosphere into the troposphere consistent with downward motion in the eastern branch of the Walker circulation.

3.3. References

Ahlquist, N.C., and R.J. Charlson, Measurement of the wavelength dependence of atmospheric extinction due to scatter, *Atmos. Environ.*, *3*, 551-564, 1969.

Bodhaine, B.A., The Mauna Loa four wavelength nephelometer: Instrument details and three years of observations, *NOAA Tech. Rep. ERL 396-ARL 5*, NOAA Environmental Research Laboratories, Boulder, CO, 1978.

Bodhaine, B.A., Aerosol measurements at four background sites, *J. Geophys. Res.*, *88*, 10,753-10,768, 1983.

Bodhaine, B.A., Barrow surface aerosol: 1976-1986, *Atmos. Environ.*, *11*, 2357-2369, 1989.

Bodhaine, B.A., and J.J. DeLuisi, An aerosol climatology of Samoa, *J. Atmos. Chem.*, *3*, 107-122, 1985.

Bodhaine, B.A., and E.G. Dutton, A long-term decrease in Arctic haze at Barrow, Alaska. *Geophys. Res. Lett.*, *20*, 947-950,1993.

Bodhaine, B.A., and M.K. Shanahan, Condensation nucleus and aerosol scattering extinction measurements at the South Pole Observatory: 1979-1988, *NOAA Data Rep. ERL CMDL-1*, NOAA Environmental Research Laboratories, Boulder, CO, 1990.

Bodhaine, B.A., J.M. Harris, G.A. Herbert, and W.D. Komhyr, Identification of volcanic episodes in aerosol data at Mauna Loa Observatory, *J. Geophys. Res.*, *85*, 1600-1604, 1980.

Bodhaine, B.A., B.G. Mendonca, J.M. Harris, and J.M. Miller, Seasonal variations in aerosols and atmospheric transmission at Mauna Loa Observatory, *J. Geophys. Res.*, *86*, 7395-7398, 1981.

Bodhaine, B.A., J.M. Harris, J.A. Ogren, and D.J. Hofmann, Aerosol optical properties at Mauna Loa Observatory: Long-range transport from Kuwait? *Geophys. Res. Lett.*, *19*, 581-584, 1992.

Bojkov, R.L., L. Bishop, W.J. Hill, G.C. Reinsel, and G.C. Tiao, A statistical trend analysis of revised Dobson total ozone data over the Northern Hemisphere, *J. Geophys. Res.*, *95(9)*, 9785-9807, 1990.

Cess, R.D., E.G. Dutton, J.J DeLuisi, and F. Jiang, Determining surface solar absorption from broadband satellite measurements for clear skies: Comparison with surface measurements, *J. Clim., 4*, 236-247, 1991.

Cess, R.D., S. Nemesure, E.G. Dutton, J.J. Deluisi, G.L. Potter, and J.-J. Morcrette, The impact of clouds on the shortwave radiation budget of the surface-atmosphere system: Interfacing measurements and models, *J. Clim., 6*, 308-316, 1993.

Cess, R.D., M. Zhang, P. Minnis, L. Corsetti, and E.G. Dutton, Absorption of solar radiation by clouds: Observations versus models, *Science*, in press, 1995.

Chapman, W.L. and J.E. Walsh, Recent variations of sea ice and air temperature in high latitudes, *Bulletin Am. Meteorol. Soc., 74*, 33-47, 1993.

Charlson, R.J., S.E. Schwartz, J.M. Hales, R.D. Cess, J.A. Coakley, Jr., J.E. Hansen, and D.J. Hofmann, Climate forcing by anthropogenic aerosols, *Science, 255*, 423-430, 1992.

Danielsen, E.F., In situ evidence of rapid, vertical, irreversible transport of lower tropospheric air into the lower tropical stratosphere by convective cloud turrets and by larger-scale upwelling in tropical cyclones, *J. Geophys. Res., 98*, 8,665-8,681, 1993.

Dutton, E.G., A coherence between the QBO and the amplitude of the Mauna Loa atmospheric transmission annual cycle, *Int. J. Clim., 12*, 383-396, 1992*a*.

Dutton, E.G., An extended comparison between LOWTRAN7-computed and observed broadband thermal irradiance: Global extreme and intermediate surface conditions, *J. Atmos. Oceanic Tech., 10*, 326-336, 1992*b*.

Dutton, E.G., and J.R. Christy, Solar radiative forcing at selected locations and evidence for global lower tropospheric cooling following the eruptions of El Chichon and Pinatubo, *Geophys. Res. Lett., 19*, 2313-2316, 1992.

Dutton, E.G., and D.J. Endres, Date of snowmelt a Barrow, Alaska, U.S.A., *Arc. Alp. Res., 23*, 115-119, 1991.

Dutton, E.G., P. Reddy, S. Ryan, and J. DeLuisi, Aerosol optical depth at Mauna Loa, 1982-1992, *J. Geophys. Res., 99*, 8295-8396, 1994.

Dutton, E.G., R.S. Stone, D.W. Nelson, and B.G. Mendonca, Recent interannual variations in solar radiation cloudiness, and surface temprature at the South Pole, *J. Climate, 4(8)*, 848-858, 1991.

Elkins, J.W., and R.M. Rosson (Eds.), *Geophysical Monitoring for Climatic Change, No. 17: Summary Report 1988*, 142 pp., NOAA Environmental Research Laboratories, Boulder, CO, 1989.

Foster, J.L., The significance of the date of snow disappearance on the Arctic tundra as a possible indicator of climate change, *Arc. Alp. Res., 21*, 60-70, 1989.

Foster, J.L., J.W. Winchester, and E.G. Dutton, The date of snow disappearance on the Arctic tundra as determined from satellite, meteorological station and radiometric in-situ observations, *IEEE Trans. Geosci. Remot. Sens., 30*, 793-798, 1992.

Hansen, A.D.A., H. Rosen, and T. Novakov, Real-time measurement of the absorption coefficient of aerosol particles, *Appl. Opt., 21*, 3060-3062, 1982.

Harris, J.M., and J.D.W. Kahl, An analysis of 10-day isentropic flow patterns for Barrow, Alaska: 1985-1992, *J. Geophys. Res., 99(D12)*, 25,845-25,854, 1994.

Hofmann, D.J., S.J. Oltmans, J.A. Lathrop, J.M. Harris, and H. Vömel, Record low ozone at the South Pole in the spring of 1993, *Geophys. Res. Lett., 21*, 421-424, 1994*a*.

Hofmann, D.J., S.J. Oltmans, J.M. Harris, J.A. Lathrop, G.L. Koenig, W.D. Komhyr, R.D. Evans, D.M. Quincy, T. Deshler, and B.J. Johnson, Recovery of stratospheric ozone over the United States in the winter of 1993-1994, *Geophys. Res. Lett., 21*, 1,779-1,782, 1994*b*.

Komhyr, W.D., R.D. Grass, R.D. Evans, R.K. Leonard, D.M. Quincy, D.J. Hofmann and G.L. Koenig, Unprecedented 1993 ozone decrease over the United States from Dobson spectrophotometer observations, *Geophys. Res. Lett., 21(3)*, 201-204, 1994.

Logan, J.A., Trends in the vertical distribution of ozone: An analysis of ozonesonde data, *J. Geophys. Res., 99*, 25,553-25,585, 1994.

Massey, D.M., T.K. Quakenbush, and B.A. Bodhaine, Condensation nuclei and aerosol scattering extinction measurements at Mauna Loa Observatory: 1974-1985, *NOAA Data Rep. ERL ARL-14*, Air Resources Laboratory, Silver Spring, MD, 1987.

Metnieks, A.L., and L.W. Pollak, Instruction for use of photo-electric condensation nucleus counters, *Geophys. Bull., 16*, 1-18, 1959.

Nakaya, U., J. Sugaya, and M. Shoda, Report of the Mauna Loa expedition in the winter of 1956-57, *J. Faculty Sci.*, 5, 1-36, Hokkaido Univ., Japan, 1957.

Nemesure, S., R.D. Cess, E.G. Dutton, J.J. DeLuisi, Z. Li, and H.G. Leighton, Impact of clouds on the shortwave radiation budget of the surface-atmosphere system for snow-covered surfaces, *J. Clim., 7*, 581-585, 1993.

Oltmans, S.J., and H. Levy II, Surface ozone measurements from a global network, *Atmos. Environ., 28*, 9-24, 1994.

Oltmans, S.J., D.J. Hofmann, W.D. Komhyr, and J.A. Lathrop, Ozone vertical profile changes over South Pole, in *Ozone in the Troposphere and Stratosphere, Part 2, NASA Conf. Pub. 3266*, edited by R.D. Hudson, pp. 578-581, National Aeronautics and Space Administration, Greenbelt, MD, 1994.

Penner, J.E., R.J. Charlson, J.M. Hales, N. Laulainen, R. Leifer, T. Novakov, J. Ogren, L.F. Radke, S.E. Schwartz, and L. Travis, Quantifying and minimizing uncertainty of climate forcing by anthropogenic aerosols, *Bull. Amer. Meteor. Soc. 75*, 375-400, 1994.

Peterson, J.P., and R.M. Rosson (Eds.), *Climate Monitoring and Diagnostic Laboratory, No. 21, Summary Report 1992*, 131 pp., NOAA Environmental Research Laboratories, Boulder, CO, 1993.

Quakenbush, T.K., and B.A. Bodhaine, Surface aerosols at the Barrow GMCC Observatory: Data from 1976 through 1985, *NOAA Data Rep. ERL ARL-10*, Air Resources Laboratory, Silver Spring, MD, 1986.

Russell, P.B., E.G. Dutton, R.F. Pueschel, J.M. Livingston, T. DeFoor, D. Allen, P. Pilewskie, M.A. Box, J.A. Reagan, B.M. Herman, S.A. Kinne, and D.J. Hofmann, Pinatubo and pre-Pinatubo optical depth spectra: Mauna Loa measurements, comparison, inferred particle size distributions, radiative effects, and relationship to lidar, *J. Geopyhs. Res., 98*, 22,969-22,985, 1993.

Schnell, R.C., S.C. Liu, S.J. Oltmans, R.S. Stone, D.J. Hofmann, E.G. Dutton, T. Deshler, W.T. Sturges, J.W. Harder, S.D. Sewell, M. Trainer, and J.M. Harris, Decrease of summer tropospheric ozone concentrations in Antarctica, *Science, 351*, 726-729, 1991.

Tarasick, D.W., D.I. Wardle, J.B. Kerr, J.J. Bellefleur, and J. Davies, Tropospheric ozone trends over Canada: 1980-1993, *Geophys. Res. Lett.*, in press, 1995.

4. Acquisition and Data Management Division

G. HERBERT (EDITOR), M. BIENIULIS, T. MEFFORD, AND K. THAUT

4.1. CONTINUING PROGRAMS

4.1.1. STATION CLIMATOLOGY

The climatology of surface weather observations at the CMDL observatories is based on hourly-average measurements of the wind direction and speed, atmospheric pressure, air and dewpoint temperatures, and the precipitation amount. The 17-year station climatologies are an important record for the interpretation of measured values of aerosols, trace gases, and for long-term changes in the records themselves. Such measurements also serve to delineate periods of local contamination. The sensors currently in use were selected not only for high accuracy, but also for ruggedness, to minimize failure in the extreme conditions of the polar region. Since 1-minute average values are also recorded to determine the variability within the hourly-average values, the sensors must also have a minimum response time of less than 1 minute. To the extent that it is practical, WMO siting standards [*WMO*, 1969] are followed; i.e., winds are measured at 10 m and temperatures at 1.25 to 2 m heights (Table 4.1). Thermometers are also positioned at the top of the local sampling tower to measure the temperature gradient to determine the stability of the surface boundary layer.

On DOY 302 the first of a new set of sensors was installed at MLO and the sensors described in Table 4.1 were decommissioned, with the sole exception of the Aerovane model 120 on the 8.3-m mast. (The Aerovane was retained because it ties the changes in the near-surface wind flow, due to continued building at MLO, to the climatology for the past 25-30 years.) A detailed discussion of the new meteorological sensors follows the observatory climatologies. If Table 4.1 is compared with the previous CMDL Summary Reports [e.g. *Peterson and Rosson*, 1993], small changes in the heights of sensors will be noted. The values in Table 4.1 reflect the results of a detailed audit of all sensors conducted at the time the older sensors were decommissioned for BRW (April 1994), SMO (June 1994), and SPO (January 1994). There were no changes in the instrumentation at BRW, SMO, or SPO in 1993.

Barrow

Descriptions of the BRW station and its climate are given in previous CMDL Summary Reports [e.g., *DeLuisi*, 1981]. Wind roses of hourly average resultant wind directions and speed are presented in 16 direction classes and 4 speed classes (Figure 4.1). Winds from the "clean-air" sector, north-northeast to southeast occurred 57.0% of the time as compared with 62.3% for the 16-year climatology. Wind speeds greater than 10 ms^{-1} occurred 18.8% of the time as compared with 11.7% of the 16-year climatology. The average speed of 6.9 ms^{-1} (Table 4.2) for the year is the highest average in the 17 years at this location. For September and December the maximum are new records as well.

TABLE 4.1. CMDL CAMS Meteorological Sensor Deployment December 31, 1993*

	BRW		MLO		SMO		SPO	
Sensor	Serial No.	Elevation, m	Serial No.	Elevation, m	Serial No.	Elevation, m	Serial No.	Elevation, m
Primary anemometer†	576	16.5	1829	8.3	070	14.3	826	10.9
Secondary anemometer†	782	40.5						
Pressure transducer‡	2366	9.5	225	3398.4	752	78.5	28	2838
Mercurial barometer	641	9.5	278	3398.4	961	78.5	215	2838
Air temperature A§	8801	2.5	8805	1.7	8803	9.1	293	1.8
Air temperature B§¶	8802	14.7	8809	37.8	8806	2.3	291	20.7
Air temperature C**	G008	3.2	G046	2.0	GO50	10.7	G001	2.4
Dewpoint	G008	3.2	G046	2.0	GO50	10.7	G001	2.4
Rain gauge		~4		0.8		~4		

See Table 4.6 for upgraded specifications.

*Except at MLO where the values refer to conditions as of October 29, 1993.

†Aerovane, model no. 120, Bendix, Inc., Baltimore, Maryland.

‡Pressure transducer, model no. 1201F1b, Rosemount, Inc., Minneapolis, Minnesota. Heights of all pressure sensors are given with respect to MSL.

§Linearized thermistors, Yellow Springs Inst. Co., model no. 44212, Yellow Springs, Ohio, except at SPO where platinum resistor thermometers, Yellow Springs Inst. Co., model no. RTD-358, Yellow Springs, Ohio, are used.

¶Thermometer, positioned at the top of the local sampling tower to facilitate an estimation of boundary layer stability.

**Hygrothermometer, Technical Services Laboratory model no. 1063, Fort Walton Beach, Florida.

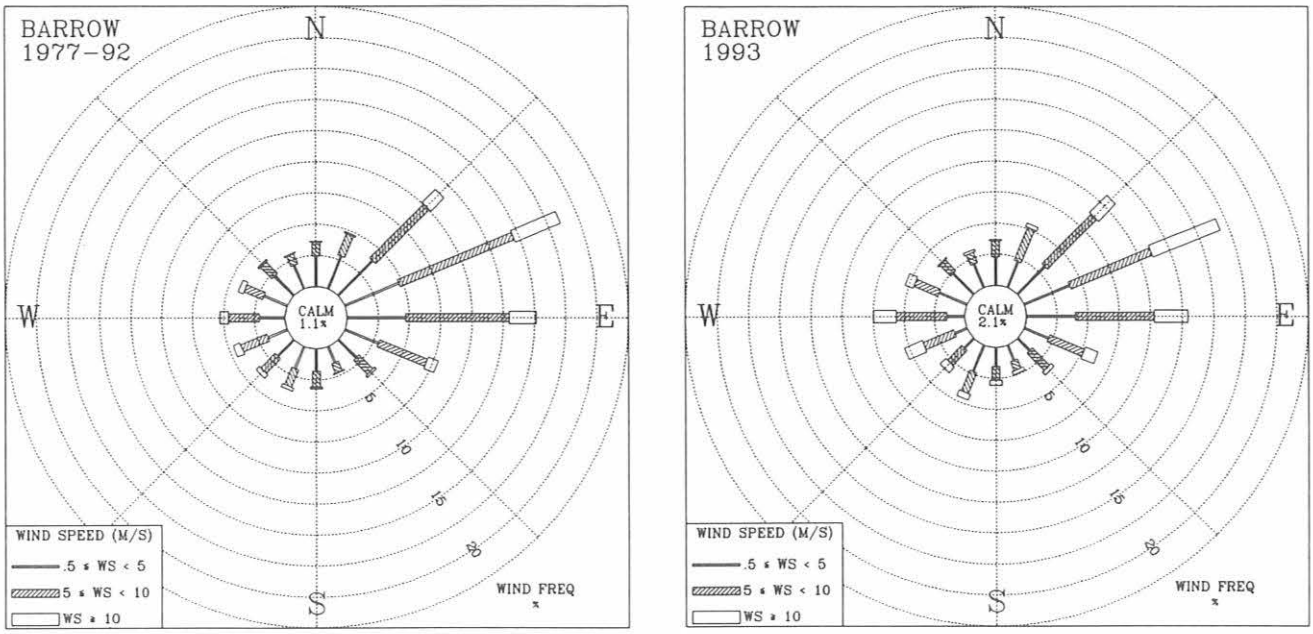

Fig. 4.1. Wind rose of surface winds for BRW for 1993 (left) and 1977-1992 (right). The distribution of resultant wind direction and speed are given in units of percent occurrence for the 16-year period. Wind speed is displayed as a function of direction in three speed classes.

TABLE 4.2. BRW 1993 Monthly Climate Summary

	Jan.	Feb.	March	April	May	June	July	Aug.	Sept.	Oct.	Nov.	Dec.	1993
Prevailing wind direction	WSW	NE	ENE	NE	ENE	E	E	W	WNW	ENE	SSW	ENE	ENE
Average wind speed (m s^{-1})	7.3	6.9	5.8	6.3	7.0	5.0	5.9	6.0	8.6	8.9	5.8	8.7	6.9
Maximum wind speed* (m s^{-1})	18	18	13	14	14	14	21	14	19	22	17	21	22
Direction of max. wind* (deg.)	105	57	69	54	104	54	253	228	333	270	203	87	270
Average station pressure (hPa)	1006.3	1018.6	1015.3	1019.0	1020.8	1015.2	1015.6	1012.3	1008.1	1007.8	1007.9	1012.7	1013.3
Maximum pressure* (hPa)	1024	1044	1045	1028	1033	1028	1027	1026	1021	1023	1021	1035	1045
Minimum pressure* (hPa)	981	993	990	1009	1009	998	992	997	991	991	981	983	981
Average air temperature (°C)	-26.1	-24.9	-24.9	-15.0	-5.7	0.9	5.3	1.6	-0.1	-5.0	-14.6	-22.3	-10.8
Maximum temperature* (°C)	-3	-3	-16	-6	2	17	21	8	9	2	-2	-12	21
Minimum temperature* (°C)	-47	-48	-37	-27	-20	-5	-1	-2	-7	-22	-36	-34	-48
Average dewpoint temperature (°C)	-28.4	-27.3	-27.5	-17.0	-7.4	-0.9	2.3	0.1	-2.5	-7.1	-16.8	-24.8	-13.1
Maximum dewpoint temperature (°C)	-4	- 3	-17	-8	1	5	13	8	6	0	-3	-14	13
Minimum dewpoint temperature (°C)	-51	-53	-40	-29	-22	-6	-4	-5	-13	-25	-39	-37	-53
Precipitation (mm)	0	0	0	0	0	0	9	22	19	5	0	0	54

Instrument heights: wind, 16.5 m; pressure, 9.5 m (MSL); air temperature, 2.5 m; dewpoint temperature, 3.2 m. Wind and temperature instruments are on a tower 25 m northeast of the main building.

*Maximum and minimum values are hourly averages.

The annual-average temperature of -10.8°C (Table 4.2) is the second highest on record. Monthly-average temperatures for July, October, and November were also the second highest for the 16-year record. The annual-average pressure was not significantly different from the long-term mean, but a new record low monthly pressure occurred for January. The summertime precipitation total for the year measured 54 mm, which is below the 16-year average of 66 mm.

Mauna Loa

The climatological summary of MLO is better understood when it is considered in two distinct regimes, the night (downslope) period (1700-0600 HST) and the day (upslope) period (0700-1800 HST). The 16-year night and day wind roses illustrate the two distinct wind patterns (Figures 4.2 and 4.3).

Night Regime. The 16-year wind rose (Figure 4.2), shows that 91.3% of all winds observed had a southerly component. In 1993, the percent occurrence of nocturnal winds was 90.3%. Pressure gradient controlled winds ($WS \geq 10$ ms^{-1}), from predominately westerly and south-easterly directions, occurred 8.4% of the time in 1993, while the 16-year record shows a 7.0% occurrence. The annual-average wind speed is not significantly different from the long-term mean (Table 4.3). The monthly average wind speed for January set a new maximum record while the value for November is a new minimum value. The upslope or northerly component winds (north-northwest through east-northeast) 4.7% of the time are primarily the result of daytime, upslope flow extending into the early evening hours.

Day Regime. The 1993 daytime wind rose (Figure 4.3) indicates that winds from the west-northwest through east-northeast occurred 56.9% of the time compared with the expected occurrence of 58.8% based on the 16-year record. Pressure gradient controlled winds ($WS \geq 10$ ms^{-1}) occurred 8.5% of the time in 1993, while the 16-year record shows an expected occurrence of 5.5%. While the percentage of occurrence of pressure-gradient determined winds, generally associated with storms, is the same for both time-regimes for 1993, the expected value is less in the daytime case. The day wind rose is more uniformly distributed in the light wind classes than the night wind rose. This is due to the occurrence of variable wind directions during the transition periods at dawn and dusk, most of which are included in this regime.

The average air temperature for 1993 (Table 4.3), combining both day and night records, was 7.1°C, 0.1°C above the long-term average while the average pressure, 680.5 mb, equals the 16-year average.. Monthly mean wind speeds for January set a new maximum for that month, and November set a new minimum for that month. The monthly mean pressure for January and October set new record minimum values for those months. The monthly mean temperature for June set a new maximum and September set a new minimum. The precipitation total for the year measured 299 mm which is significantly below the 16-year average of 520 mm. This is the second lowest precipitation amount reported in the past 7 years.

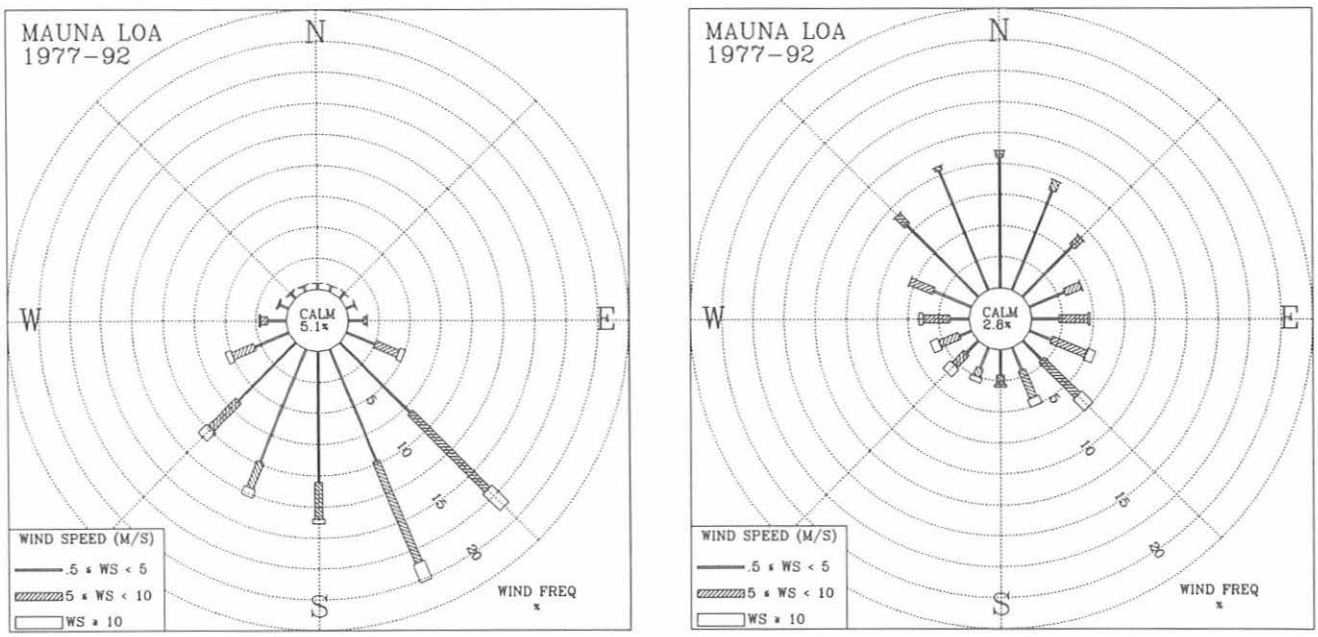

Fig. 4.2. Wind roses of the surface winds for MLO for 1977-1992 night (left) and day(right). The distribution of resultant wind direction and speed are given in units of percent occurrence for the 16-year period. Wind speed is displayed as a function of direction in three speed classes.

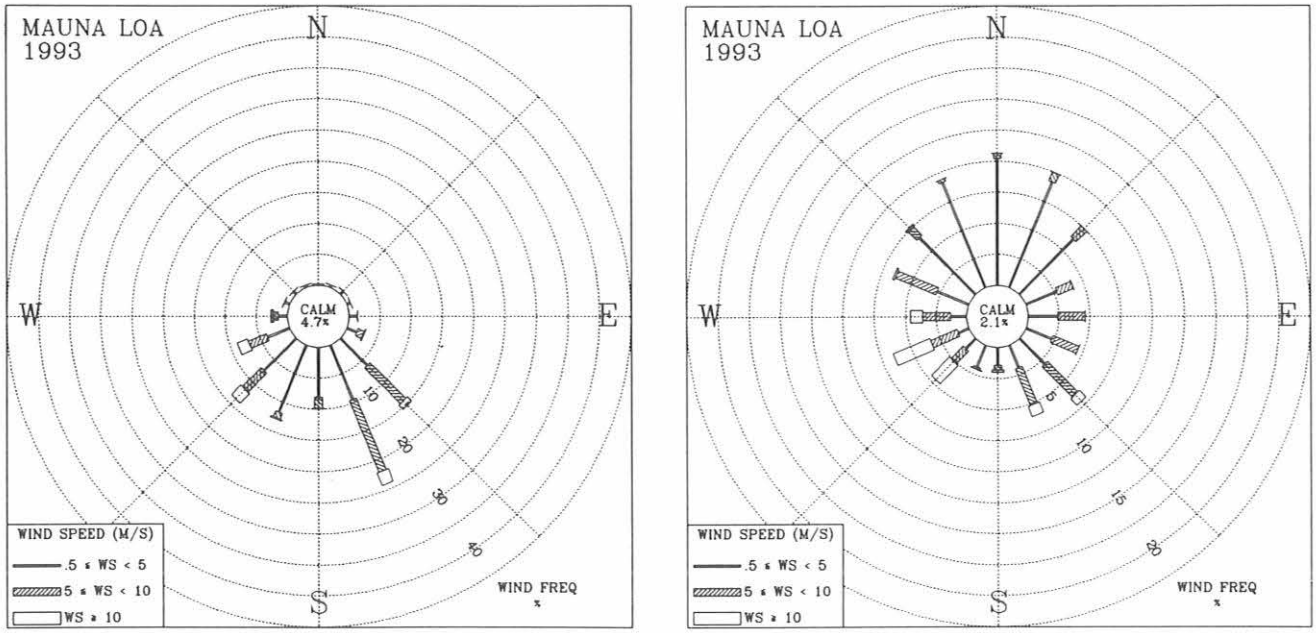

Fig. 4.3. Wind roses of the surface winds for MLO for 1993 night (left) and day (right). The distribution of resultant wind direction and speed are given in units of percent occurrence for the year. Wind speed is displayed as a function of direction in three speed classes.

Samoa

A comparison of SMO's 1993 wind rose (Figure 4.4) with that of the 16-year period shows a higher percentage (68.8%) of "clean air" sector winds (north-northwest through southeast) in 1993 than in the 16-year record (59.3%). Yet the 1993 value is less than the 75.8% observed in 1992. The occurrence of winds in the 10 ms^{-1} or greater class is 7.0% in 1993 while the expected occurrence based on the 16-year record is 4.8%. The average wind speed for the year, 5.3 ms^{-1} (Table 4.4) is near normal. Monthly average wind speed for May was a new record high, while the monthly average wind speeds for January and February were new minimum values.

Average station pressures for the months of January and February were also in the lowest 10% compared with the 16-year record (Table 4.4). The average station pressure for the year was 1000.6 mb, a large 1.3 mb above the long-term average at Cape Matatula. The average air temperature, 27.6°C, is 0.5°C above the 16-year average. The precipitation total for the year measured 1934 mm which is below the 16-year average of 2095 mm.

South Pole

The distribution of the surface wind direction in 1993 (Figure 4.5) shows a lower percentage of winds (92.6%) from the "clean air" sector (grid north-northwest through east-southeast) than the 16-year average (93.9%). A higher percentage of winds in the >10 ms^{-1} class (3.2%) was observed in 1993 than the long-term average (4.0 %). While the average wind speed of 5.4 ms^{-1} is equal to the long-term average, the average value for March is a new maximum for that month.

The 1993 annual-average station pressure was 677.0 mb, 2.1 mb below the 16-year average (Table 4.5). The 1993 value is the third lowest annual-average pressure recorded in the 17-year history. The annual-average temperature was -49.3°C, 0.3°C below the long-term annual average. While the monthly-average temperatures for August and December were in the lowest 10 percentile of the record, no other monthly means were records. The minimum temperature of the year was observed to be -76°C in August.

Meteorological Measurement System Upgrade

The last major upgrade in the meteorological sensors at the CMDL stations occurred 6 years ago when the Technical Service Laboratory (TSL) model number 1063 hygrothermometer was selected as the preferred instrument for measuring humidity. This is the same instrument used by the National Weather Service to measure temperature and humidity at airport locations. While individual instruments have been replaced, the basic complement of instruments has not changed in the past 20 years. Recently it has become increasingly difficult to purchase replacement instruments and reliable parts. For the same reasons it has been more difficult to keep the Control and Monitoring System (CAMS) operational as well. Thus it was decided to

TABLE 4.3. MLO 1993 Monthly Climate Summary

	Jan.	Feb.	March	April	May	June	July	Aug.	Sept.	Oct.	Nov.	Dec.	1993
							Night						
Prevailing wind direction	SW	WSW	SSE	SSE	SSE	SSE	SSE	SE	SSE	SSE	SE	SE	SSE
Average wind speed (m s^{-1})	7.7	6.0	5.2	4.6	5.1	5.2	3.7	3.5	3.2	4.4	4.0	5.4	4.9
Maximum wind speed* (m s^{-1})	20	15	15	12	14	14	12	9	10	15	11	15	20
Direction of max. wind* (deg.)	263	269	227	161	161	151	149	141	159	226	154	123	263
Average station pressure (hPa)	676.8	678.5	679.7	680.9	680.1	681.1	680.8	681.5	681.0	679.7	679.2	679.6	679.9
Maximum pressure* (hPa)	682	682	686	684	684	684	684	685	684	683	682	683	686
Minimum pressure* (hPa)	666	674	669	678	676	679	678	679	677	675	677	676	666
Average air temperature (°C)	2.4	3.3	3.0	5.5	5.0	8.3	6.5	5.2	5.2	5.2	4.7	4.7	4.9
Maximum temperature* (°C)	10	9	10	13	10	15	13	10	10	10	9	10	15
Minimum temperature* (°C)	-4	-3	-3	1	1	5	3	3	2	2	0	1	-4
Average dewpoint temperature (°C)	-16.4	-20.9	-15.9	-19.4	-18.3	-20.1	-9.9	-6.2	-3.6	-10.0	-22.3	-18.1	-15.7
Maximum dewpoint temperature (°C)	4	0	7	7	4	7	7	6	8	8	2	3	8
Minimum dewpoint temperature (°C)	-35	-35	-37	-36	-34	-33	-26	-20	-20	-27	-35	-35	-37
Precipitation (mm)	77	0	0	0	1	0	14	0	3	4	0	0	98
							Day						
Prevailing wind direction	WSW	W	N	N	NW	NE	SE	NE	N	WNW	NNW	ESE	NNW
Average wind speed (m s^{-1})	7.8	6.1	5.2	4.4	5.0	5.1	3.9	3.5	3.5	4.6	3.2	4.9	4.8
Maximum wind speed* (m s^{-1})	19	17	16	10	13	15	13	9	8	17	11	16	19
Direction of max. wind* (deg.)	244	245	235	161	151	150	137	89	156	181	164	130	244
Average station pressure (hPa)	676.7	678.5	679.7	681.0	680.2	681.3	681.0	681.6	681.1	679.7	679.2	679.6	680.0
Maximum pressure* (hPa)	682	682	686	684	684	684	684	684	684	684	682	683	686
Minimum pressure* (hPa)	666	674	670	678	676	679	679	679	678	674	676	675	666
Average air temperature (°C)	6.0	7.8	7.8	10.9	10.3	13.4	10.5	9.9	9.5	9.2	9.2	8.4	9.3
Maximum temperature* (°C)	13	14	16	17	16	19	18	15	16	15	14	15	19
Minimum temperature* (°C)	-3	-2	-3	1	2	6	4	3	3	2	2	1	-3
Average dewpoint temperature (°C)	-11.0	-15.0	-8.7	-11.6	-9.6	-10.3	-1.5	0.9	0.3	-3.7	-13.5	-14.4	-8.9
Maximum dewpoint temperature (°C)	6	5	11	11	6	9	10	8	9	8	7	6	11
Minimum dewpoint temperature (°C)	-36	-32	-37	-35	-32	-32	-26	-19	-23	-25	-33	-33	-37
Precipitation (mm)	64	0	0	0	0	0	41	0	39	39	4	13	201

Instrument heights: wind, 8.3 m; pressure, 3398.4 m (MSL); air temperature, 1.7 m; dewpoint temperature, 2.0 m. Wind and temperature instruments are on a tower 15 m southwest of the main building.

*Maximum and minimum values are hourly averages.

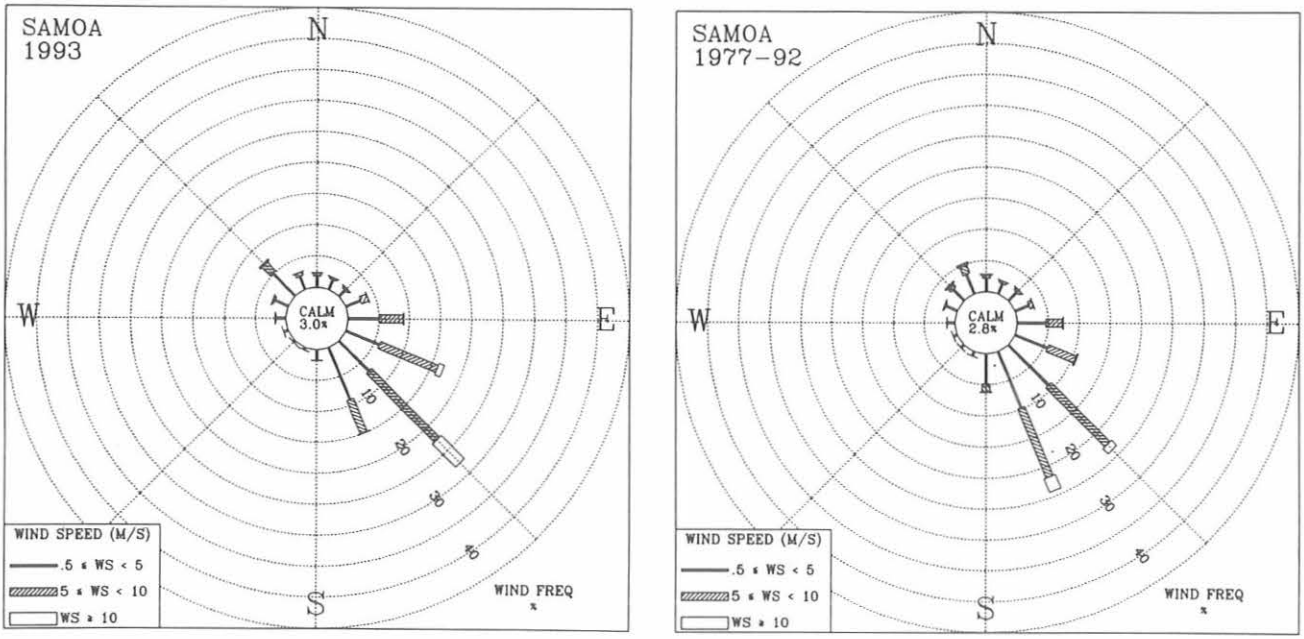

Fig. 4.4. Wind roses of the surface winds for SMO for 1993 (left) and 1977-1992 (right). The distribution of resultant wind direction and speed are given in units of percent occurrence for the year and 16-year period, respectively. Wind speed is displayed as a function of direction in three speed classes.

TABLE 4.4. SMO 1993 Monthly Climate Summary

	Jan.	Feb.	March	April	May	June	July	Aug.	Sept.	Oct.	Nov.	Dec.	1993
Prevailing wind direction	SE	NW	NW	SE	SE	SE	SE	ESE	SE	SE	SE	SE	SE
Average wind speed (m s^{-1})	2.5	2.3	4.0	3.9	8.0	6.6	7.4	5.2	6.3	6.1	6.1	4.4	5.3
Maximum wind speed* (m s^{-1})	14	10	12	13	15	14	13	10	13	12	14	15	15
Direction of max. wind* (deg.)	306	305	318	310	139	99	139	124	137	149	123	33	139
Average station pressure (hPa)	997.9	997.7	1000.4	999.7	1001.8	1001.9	1001.8	1002.6	1002.7	1001.7	1000.5	998.7	1000.6
Maximum pressure* (hPa)	1004	1003	1004	1003	1006	1006	1006	1006	1007	1006	1005	1002	1007
Minimum pressure* (hPa)	998	989	996	996	997	998	998	998	998	998	997	994	988
Average air temperature (°C)	28.7	28.8	28.0	28.4	27.5	26.9	25.9	27.0	27.0	27.0	27.8	28.6	27.6
Maximum temperature* (°C)	37	36	35	35	32	32	33	33	35	35	36	35	37
Minimum temperature* (°C)	22	23	23	24	24	22	21	22	23	22	24	23	21
Average dewpoint temperature (°C)	23.3	22.9	23.5	24.0	22.7	22.1	21.1	22.1	21.9	21.5	22.7	23.8	22.6
Maximum dewpoint temperature (°C)	26	25	25	25	25	24	24	25	24	24	25	26	26
Minimum dewpoint temperature (°C)	19	20	19	22	19	19	18	17	19	18	20	22	17
Precipitation (mm)	202	144	290	179	86	63	94	86	198	277	112	202	1934

Instrument heights: wind, 14.3 m; pressure, 78.5 m (MSL); air temperature, 9 m. Wind and temperature instruments are on Lauagae Ridge, 110 m northeast of the main building. Pressure sensors are in the main building.

*Maximum and minimum values are hourly averages.

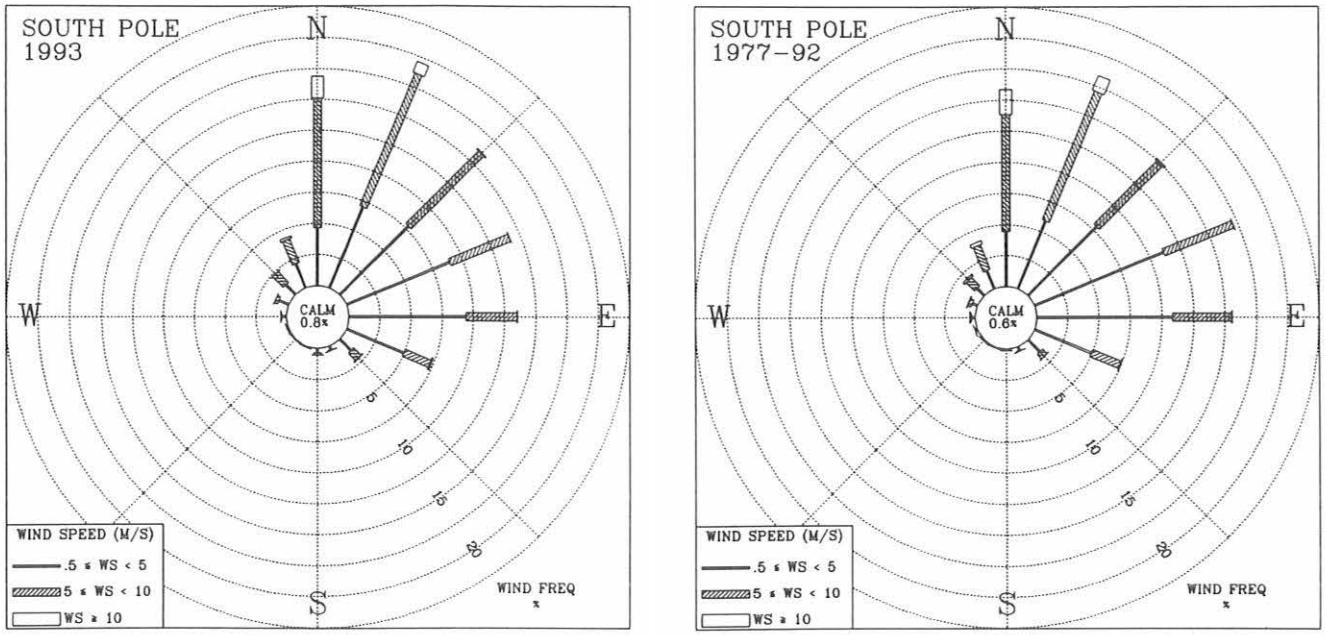

Fig. 4.5. Wind roses of the surface winds for SPO for 1993 (left) and 1977-1992 (right). The distribution of resultant wind direction and speed are given in units of percent occurrence for the year. Wind speed is displayed as a function of direction in three speed classes.

TABLE 4.5. SPO 1993 Monthly Climate Summary

	Jan.	Feb.	March	April	May	June	July	Aug.	Sept.	Oct.	Nov.	Dec.	1993
Prevailing wind direction	ENE	N	NE	NNE	NNE	ENE	N	E	NNE	NNE	NNE	N	NNE
Average wind speed ($m\ s^{-1}$)	4.7	5.1	6.6	5.4	6.0	5.4	4.3	5.3	5.8	6.6	4.9	4.6	5.4
Maximum wind speed* ($m\ s^{-1}$)	10	10	13	11	14	12	12	11	13	15	11	12	15
Direction of max. wind* (deg.)	2	347	19	9	6	7	353	348	9	351	24	357	351
Average station pressure (hPa)	693.0	680.1	680.2	677.5	673.8	673.7	670.9	667.4	672.1	672.1	682.6	681.1	677.0
Maximum pressure* (hPa)	706	693	696	690	690	694	690	687	687	685	694	690	706
Minimum pressure* (hPa)	683	665	670	667	661	660	656	650	655	660	674	674	650
Average air temperature (°C)	-27.4	-41.5	-52.4	-57.6	-56.4	-60.4	-56.4	-63.8	-59.0	-50.4	-38.4	-28.8	-49.3
Maximum temperature* (°C)	-18	-26	-35	-46	-34	-30	-40	-47	-44	-33	-29	-20	-18
Minimum temperature* (°C)	-36	-55	-62	-68	-71	-74	-73	-76	-74	-61	-48	-37	-76
Average dewpoint temperature (°C)	-28.4	-41.7	-52.0	-58.1	-56.6	-60.4	-57.1	-63.0	-57.8	-50.1	-39.2	-30.1	-49.5
Maximum dewpoint temperature (°C)	-19	-27	-36	-47	-35	-31	-41	-46	-43	-33	-29	-23	-19
Minimum dewpoint temperature (°C)	-37	-56	-63	-68	-69	-70	-71	-72	-71	-61	-49	-40	-72
Precipitation (mm)	0	0	0	0	0	0	0	0	0	0	0	0	0

Instrument heights: wind, 10.9 m; pressure, 2938 (MSL); air temperature, 1.8 m. The anemometer and thermometer are on a tower 100 m grid east-southeast of CAF. Pressure measurements are made inside CAF.

*Maximum and minimum values are hourly averages.

reconsider the specific instruments used to measure the station pressure, temperature gradient and wind speed and direction, along with a dedicated data acquisition system, in designing a replacement weather measuring system.

Due to the recent, mostly favorable, experience with the TSL 1063 hygrothermometer (Technical Services Laboratory, 630 Lovejoy Road, Fort Walton Beach, Florida 32549) it was decided to continue to use this instrument for dry air and dewpoint temperature measurements at ground level at the observatories. A good reason could not be found for changing to another precipitation gauge so the tipping bucket rain gauge used from the 1976-1977 period (Belford Instrument Company, 1600 South Clinton St. Baltimore, Maryland 21224) was incorporated into the design of the replacement system.

After limited testing and review, a variable-capacitance ceramic sensor, similar to the old Rosemount transducer (Rosemount Inc., 12001 W. 78th St., Eden Prairie, Minnesota 55344) was selected. The new sensor is a Setra model 270 barometer (Setra Systems, 45 Nagog Park, Acton, Massachusetts 01727). When the five pressure transducers purchased for the stations and Boulder were compared with the mercury barometer in Boulder, the average daily difference was less than 0.1 mb with a standard deviation of 0.2 mb. These values are consistent with the specified accuracy of the sensor (Table 4.6).

To eliminate the need for semi-annual calibration of the thermometers used to measure the temperature gradient, standard RTD (Resistor Temperature Device) sensors were selected for which matching electronics could be purchased. The sensor is a Logan 4150 series platinum resistance probe in a steel sleeve that was machined to reduce the thermal mass and inherent thermal transfer in a ventilated flow (Logan Enterprises, 8844 US North West, Liberty, Ohio 43357). For the range of air temperatures at the CMDL stations, an accuracy of 0.1°C can be realized (Table 4.6). Linearized thermisters, YSI part number 44212 (Yellow Springs Instrument Co., Yellow Springs, Ohio 45387) were previously used to measure the air temperature. (Radiation shielding was accomplished using the Gill aspirated temperature-dewpoint radiation shield model number 43406 (R.M. Young Company, 2801 Aero-Park Drive, Traverse City, Michigan 49684). Due to small non-linearity in the calibration, a "warm" and "cold" season calibration had to be used to guarantee 0.1°C accuracy over the specified range of -50° to +50°C. Since 1976, platinum resistance probes have been used at SPO to obtain accurate temperatures below -50°C. Cambridge System Inc., model number 137-MI-TC (Cambridge System Inc., Newton, Massachusetts) temperature-dewpoint measuring system aspirated radiation shields were used to shield the thermometers. Measurements indicate that the thermometer is aspirated at an average rate of about 1 ms^{-1}.

After a careful review of the anemometers used at SPO, it was decided that the R.M. Young (RMY) model number 05105 (R.M. Young Company) propeller anemometer would withstand the severe antarctic conditions. (RMY model number 05305, a high performance anemometer designed for air quality measurements, was used at MLO where there is a higher percentage of light winds during the upslope-downslope transitions.) Unlike the Bendix Friez aerovane model number 120 (Bendix Corp., Baltimore, Maryland 21204), which was used for wind speed and direction measurements since the initial installations in 1973-1975 and that uses a magneto and is subject to magnet strength changes and line loss errors, the RMY sensor produces a pulse for unit run-of-wind. Wind tunnel testing indicated that the aerovane had a threshold wind speed of 1-1.3 ms^{-1}, while similar tests showed the RMY sensors to reach threshold speeds at about 0.4-0.7 ms^{-1}.

The design of the revised electronics for the meteorological sensors has focused on distributing the signal acquisition electronics so that only serial digital signals are transmitted over long distances and thus eliminate the need for on-site calibrations whenever

TABLE 4.6. CMDL Upgraded Meteorological Sensor Specifications*

Sensor	Range	Resolution	Accuracy	Threshold Sensitivity
RMY wind speed	0 to 60 ms^{-1}	0.01 ms^{-1}		1 ms^{-1}
RMY wind direction	0 to 355 degrees	0.1 degree		1 ms^{-1}
Setra station pressure	600 to 1100 mb	0.005%	±0.03% FS	
RTD temperatures	-200 to +600°C	0.1 C	±0.3 C FS ±0.1 C (-85 to +50 C)	
TSL hygrothermometer	-60 to +60 C	0.1 C	0.5% RMS, 1% MAX (>0 C) 2% MAX (<0 C)	

RMY, R.M. Young Company, Traverse City, Michigan; RTD, resistor temperature device; TSL, Technical Services Laboratory, Fort Walton Beach, Florida.

*Values refer to conditions at MLO as of October 30, 1993.

possible. Individual analog-to-digital converter modules MetraByte (MB) module numbers 1000/2000 (Kiethley MetraByte Co., 440 Myles Standish Blvd., Taunton, Massachusetts 02780) interface the sensors to the computer interface by a RS-485 interface. Non-volatile memory is used to store sensor identification and calibration information. It is also possible to invoke digital filtering of the signals. The measurements from each sensor-module pair are, therefore, filtered and calibrated to give values scaled in physical units. A computer requests data from the individual sensors at intervals determined by the filtering that is employed.

A rack mounted computer is used to acquire and store all of the data. The primary data file is initialized daily after the system does a survey of the active sensors. One-minute average values from each sensor are stored in the data file. To the maximum extent possible, these values are fully calibrated. The system also provides features to allow the operator to enter supplementary observations and calibration information such as weather and mercury barometer observations. The system also provides a simple text editor for metadata entries. In all cases these observations and entries are stored with the data files since they pertain to the data and determine, in part, its quality. Multitasking of the data acquisition program and data display-input program is accomplished under the Microsoft Windows environment.

4.1.2. Data Management

During 1993, the CAMS operated 98.15% of the time. CAMS gathers data from sensors that operate continuously at each of the four CMDL observatories. The CAMS performance was monitored by comparing the number of data files recorded against those expected for the year. In CAMS, there are data files regularly recorded 12 or 24 times a day. In Tables 4.7*a* and 4.7*b*, the hourly solar radiation file was used to monitor the ASR CAMS. The hourly CO_2 data files were used for the CO_2 CAMS. The hourly-average meteorological data file was used for the MO3 CAMS.

Due to the remoteness of the observatories, power outages are common and are the main reason for data loss. Hardware failure is another reason for data loss. During 1993, BRW had two boards fail plus the CO_2 analyzer went down, MLO had three boards and two power supplies fail, SMO had two boards fail, and SPO had one board and one power supply fail.

4.2. Special Project: Boundary Wind and Temperature Study at MLO, 1992-1993

Introduction

Perched on the north flank of the Hawaiian Mauna Loa volcano at an elevation of 3.4 km, MLO has been an important source of background atmospheric-aerosol and chemistry measurements for more than 35 years. The Mauna Loa volcano rises to an elevation of 4.17 km and stands as a major obstacle to the midPacific subtropical flow creating widely varying local wind regimes. At this latitude (19°N) the dominant climatological feature is the midNorth Pacific subtropical anticyclone centered to the southeast of Hawaii in winter and to the northeast in the summer months [*Blumenstock and Price*, 1974]. In the winter and spring period the synoptic scale wind field is predominately westerly at this latitude. During the summer months the flow is easterly on the southern side of the anticyclone. Superimposed on the large-scale synoptic flow is the diurnal up-down slope wind produced by diurnal heating and cooling of Mauna Loa. In the transition months the synoptic scale winds are significantly less important, and the local winds at MLO are determined in large measure by the regional scale thermal "breathing" of Mauna Loa. The resulting circulation, pressure, temperature, and moisture distributions are described in a series of studies and reports [*Price and Pales*, 1963; *Chin et al.*, 1971; *Mendonca*, 1969].

In 1984 an eruption and subsequent lava flow from fissures along the Mauna Loa east rift zone produced a lava flow to a point 2 km east of the observatory. This put a sense of urgency in efforts to construct a recently-approved lava barrier to the south of MLO to deflect

TABLE 4.7*a*. CMDL CAMS Operations Summary, 1993

Individual CAMS	Expected No. of Blocks 1993	Percent Data Capture and [Blocks Missing] BRW	MLO	SMO	SPO
ASR	8760*	99.49% [45]	98.04% [172]	99.94% [5]	99.40% [46]
CO2	8396	87.49% [1050]	99.83% [14]	99.65% [29]	98.75% [105]
MO3	4380†	99.45% [24]	98.56% [53]	99.38% [27]	99.75% [11]
Total	21536‡	94.80% [1119]	98.85% [239]	99.72% [61]	99.21% [162]

*The expected number of ASR blocks from SPO is 7680.

†The expected number of MO3 blocks from MLO is 3672.

‡The expected total number of blocks from MLO is 20828; the expected total number of blocks from SPO is 20456.

TABLE 4.7*b*. Number of Blocks of CAMS Data Expected and Blocks Recorded in 1993

Block Type	Description	BRW		MLO		SMO		SPO	
		Expected	Recorded	Expected	Recorded	Expected	Recorded	Expected	Recorded
A	Hourly aerosol data	2190	2181	2190	2148	2190	2187	2190	1907
B	Secondary aerosol data*	Variable	0	Variable	1344	Variable	2189	Variable	0
C	Hourly CO_2 data†	8396	7346	8396	8382	8396	8367	8396	8291
D	Daily CO_2 data	365	325	365	365	365	370	365	369
E	Hourly CO_2 calibration data	364	374	364	361	364	366	364	386
F	CO_2 calibration report	52	53	52	52	52	53	52	58
H	Daily aerosol data	365	366	365	361	365	364	365	345
I	Meteorological calibration	365	360	305	303	365	364	365	365
M	Hourly meteorological data	4380	4356	3672	3619	4380	4353	4380	4369
N	Surface ozone calibration	52	56	45	34	52	5	0	0
O	Daily surface ozone data	365	365	305	300	365	365	365	368
S	Hourly solar radiation data	8760	8715	8760	8588	8760	8755	7680	7634
T	Daily solar radiation data	365	363	365	358	365	365	320	317
W	Daily meteorological data	365	364	305	301	365	365	365	368

*Nominal block count equal to total hours in year less 52 7-hour calibration periods.
†Nominal block count equal to 52 7-hour calibration periods.

any future flows that may originate above the observatory. From a micro-meteorological perspective, the concern at the time was that the lava barrier would selectively deflect the downslope winds or possibly create a separation of the low-level winds isolating MLO from the prevailing winds aloft. A stair-accessible tower was proposed to facilitate sampling above the influence of the lava barrier.

The lava barrier was constructed in January 1986, and in December the 40-m tower was erected. For the first time it was possible to install and maintain instrumentation well above the influence of the cluster of buildings that make up the observatory. Its predecessor, a 27-m tall antenna mast, was judged by most to be unsafe to climb due to its telescoping-type construction and age. In February 1987 an anemometer was installed on top of the 40-m tower. This was the second of two anemometers at the observatory, the first being at a height of 8.5 m, from which the station's wind climatology was derived [for the latest update, see *Peterson and Rosson*, 1993]. Some months later when the measurements from both anemometers were compared, it was discovered that during periods of southerly winds, a distinct flow separation occurred in which the wind direction at the top of the tower was significantly different than that at the 8.5-m level. In some cases the difference was in excess of 90°. At such times the depth of the downslope flow is very shallow, less than 40-m deep. Using a captive balloon to obtain wind profiles in the lowest 0.5 km, *Mendonca* [1969] found the top of the nocturnal downslope flow to be at about 50 m in three soundings in September-November 1966. It is, therefore, reasonable to expect that a layer depth of less than 40 m could occur at other times of the year. Other than Mendonca's balloon study, there are few relevant observations of the temporal changes of the MLO boundary layer as a function of height.

The Bendix aerovane model no. 120 was used at MLO for the past 2 decades because of its durability, but at the price of a relatively high starting speed of 1-2 ms^{-1} and a long distance constant (63% recovery) of about 5 m [*Mazzarella*, 1972]. Starting thresholds in excess of 1 ms^{-1} and longer distance constants limited the response of the anemometer such that it was not a reliable sensor of wind fluctuations at heights less than 10 m where wind speeds were more often less than 3 ms^{-1}. A more sensitive anemometer was needed to depict changes that occur during the light wind characteristic of upslope-downslope transitions.

The objective of this report is to define the instruments, the installation process, and the procedure used to obtain a data set describing the first 40 m of the MLO boundary layer as a function of height and time. In addition, the wind and temperature profiles for the MLO Photochemical Experiment II (MLOPEX II) intensives from January 15, 1992, to February 15, 1992, April. 15, 1992, to May 15, 1992, and from July 15, 1992 to August. 15, 1992, are available from Internet by anonymous FTP @ftp.cmdl.noaa.gov. MLOPEX II is a continuation to an earlier field study and modeling of the photochemistry of the remote troposphere conducted at MLO in 1988 [*Ridley and Robinson,* 1993].

Instrumentation

During 1991 a large number of meteorological sensors were obtained from government surplus. Among these were sensitive cup anemometers (Climate model 011-4), wind vanes (Climate model 012-1), and aspirated air and dewpoint temperature sensors (Cambridge System model 137-MI-TC). The cup

anemometers and air and dewpoint-temperature sensors needed modification before they could be used in the field. The anemometers were of a 1960s design in which the light from a small lamp was interrupted by a rotating chopper producing one pulse per revolution. A 16-slot chopper was installed yielding an event for approximately every 10 cm of wind as compared with an event for every 148 cm of wind with the single chopper setup. A frequency measurement with a resolution of 1 Hz yields a wind speed measurement to a resolution of about 0.25 ms^{-1}. The circuitry was removed from the air and dewpoint-temperature sensor, and the aspirated sun shield was used for a thermometer housing. Precision RTD platinum resistance thermometers (Logan model 4150) were used.

The anemometers were calibrated in the NCAR wind tunnel. The standard deviation of the calculated wind speed at 5 ms^{-1} was 0.18 ms^{-1} for the six anemometers. The accuracy of the wind tunnel was about 0.2 ms^{-1}. The wind vanes were mechanically aligned to an accuracy of $\pm 1°$. Additional uncertainty on the order of ± 2-$3°$ was added when the vanes were installed on the tower. All six thermometers were compared against a standard instrument and found to agree to within $\pm 0.1°C$.

Anemometers and thermometers were installed on the 40-m tower at approximately 3, 6, 10, 20, 29, and 38 m heights. A 1.2-m long arm was used to extend the anemometer and wind vane from the south side of the tower. Wind directions from 20 to 320° were relatively unaffected by the tower structure. The thermometers were also attached to this arm approximately 0.3 m from the tower. At each level, electronic modules were used to translate the signals from the sensors to a computer-compatible serial protocol (RS-485). A frequency-to-serial converter (MetraByte model M2602) was used to measure wind speed, and a bridge module (MetraByte model M2532) was used to measure the resistance changes that indicated wind direction. A RTD type 392 module (MetraByte model M1422) was used to interface the temperature probes. All modules were interrogated once a minute by a personal computer. Individual values were displayed on the computer monitor for quality assessment purposes. The observations were also stored on disk and sent to Boulder for further analysis. During the first 9 months that included MLOPEX II, January, April, and August intensifies, a telephone linkup between Boulder and MLO was used to transfer data on a daily schedule.

Discussion of Measurements

Case study April 23-29, 1992. Figure 4.6. displays the hourly-average wind profile in the first 40 m for the 7-day period April 23-29, 1992. The height is shown in meters on a logarithmic scale; time is in Hawaiian Standard Time (HST). This was a period of unusually steady winds from the west during which the MLOPEX observers noted considerable haze. Such windy periods are usually associated with migrating cyclones from higher latitudes and can represent periods of long-range transport from as far as the Asian continent. The large-scale pressure gradient will tend to overpower the local, thermally-driven upslope flow during such times. On April 23, a well-defined northerly upslope developed, but as the westerlies increased in intensity on subsequent days, the upslope consisted of a very slight veering of the wind during the daytime hours. As the strength of the westerly winds decreased on April 28-29, the winds shifted to a more northerly direction during the daytime hours.

The temperature profiles in Figures 4.7 and 4.8 show the temperature change as a function of height for April 23 and 25, respectively. The temperatures are hourly averages. On April 23 during the downslope flow (0000-0700 HST), the west-southwesterly winds were less than 10 ms^{-1} (Figure 4.6) and the temperature profiles showed very small changes in temperature until 0700 HST. Such temperature profiles are typical of the stable, nocturnal boundary layer. Note that the transition from westerly to northerly winds takes less than an hour (0900-1000 HST), and the temperature decreases by 3°C or more at all levels. This is due to the arrival of the cool, moist air from the Saddle region below MLO. With the return to a westerly flow at 1400 HST the sounding warms by about 2°C. After sunset the temperatures cool below 10 m and warm above that level to become nearly isothermal for the remainder of the day.

The situation is considerably different on April 25, when the effect of the thermally-driven upslope is masked by the dominant westerly flow from the west with no significant decrease in wind speed observed. The temperature profile (Figure 4.8) reflects the effect of a well-mixed boundary layer, as one would expect with winds greater than 10 ms^{-1}. The nocturnal sounding (0000-0600 HST) is isothermal with little change. Due to the mixing, all levels warm and cool adiabatically during the daytime, returning to a steady isothermal temperature between 8-9°C after sunset. (The 0.2-0.3°C warming at 30 m on all soundings indicates that this thermometer is biased to that degree.) In the steady nocturnal wind conditions of 0400 HST, April 25 (Figure 4.6) the Richardson number ($Ri = (g/\theta)(d\theta/dz)/dU/dz)^2$, $g = 9.8\ ms^{-2}$) is calculated to be 0.0004. Thus with a logarithmic wind profile, $u^*(10\ m) = 0.83\ ms^{-1}$ ($u^* = kzdu/dz$, $k = 0.4$), and the z_o ($u(z) = u^*\ln(z/zo)/k$) is about 1 cm [*Kaimal and Finnigan*, 1994]. At 1200 HST the Richardson number is -0.003, $z_o = 0.02$ cm, and $u^* = 0.56\ ms^{-1}$.

Climatology. The distribution of wind speed in four classes as a function of wind direction in 16 classes for the 10 and 38-m levels is shown in Figure 4.9. The wind roses include all of the hourly observations for the 2-year period in two classes, daytime and nighttime, since the diurnal forcing of the flow at MLO dominates the seasonal forcing. The times used to separate the

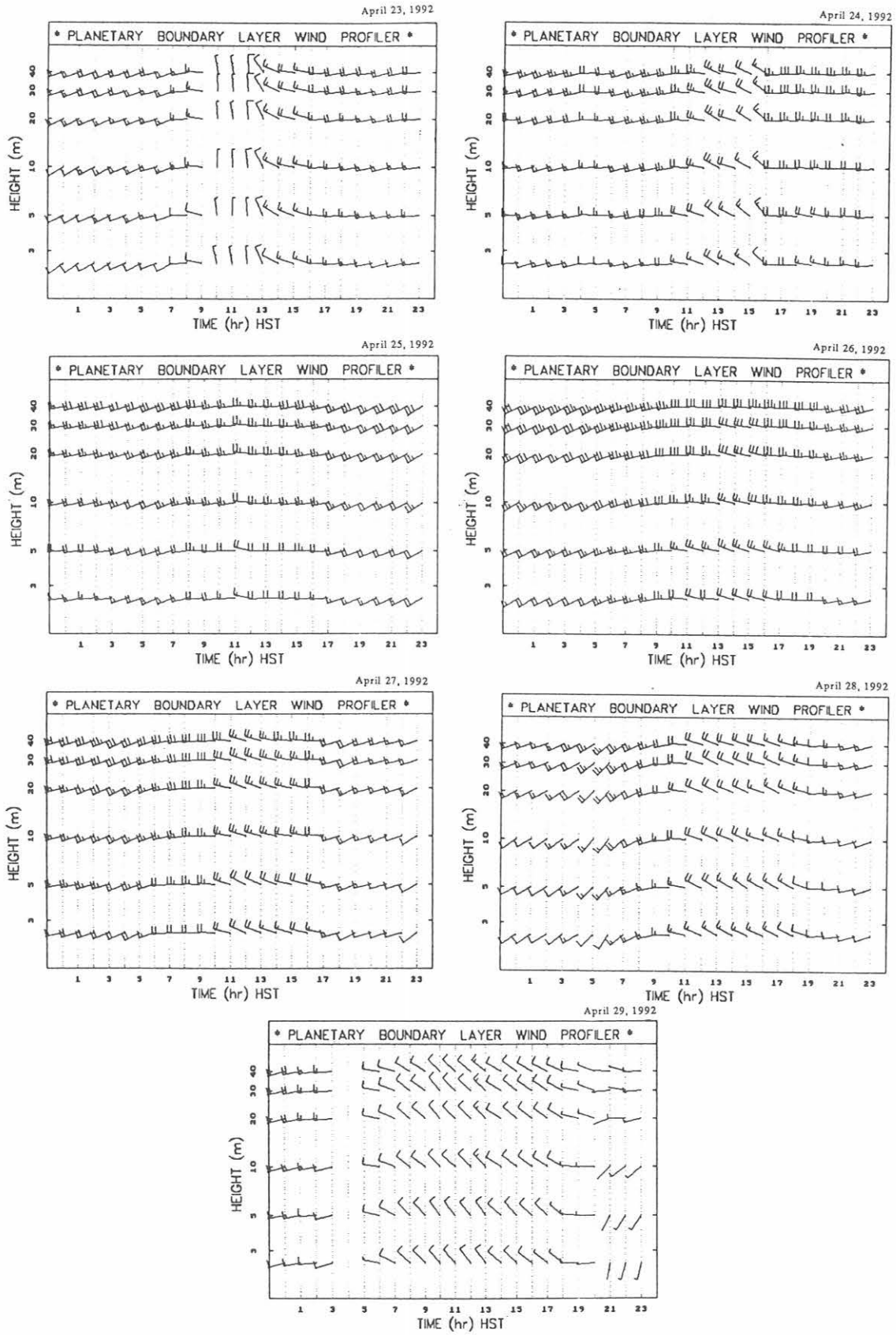

Fig. 4.6. Profiles of hourly average winds at MLO for April 23 through April 29, 1992. Individual wind barbs equal 10 knots.

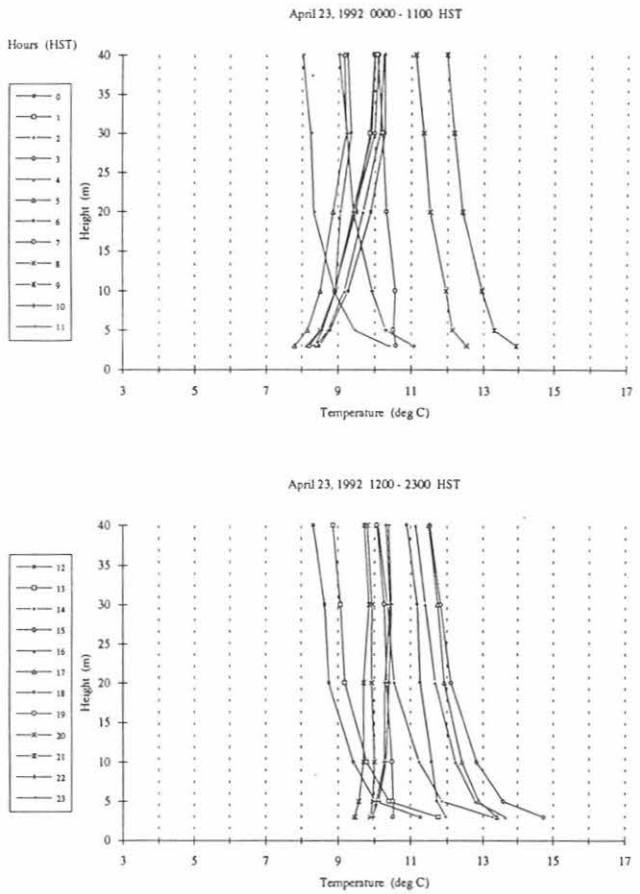

Fig. 4.7. Profiles of hourly average temperatures at MLO for April 23, 1992.

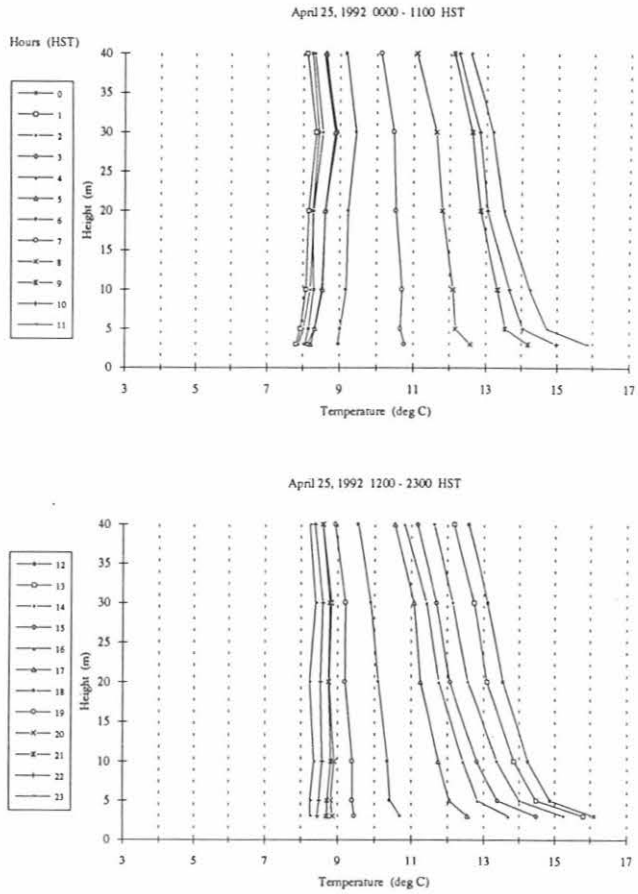

Fig. 4.8. Profiles of hourly average temperatures at MLO for April 25, 1992.

daytime-nighttime regimes (0900 to 2000 HST, and 2100 to 0800 HST) were based on the most common time of transition from upslope to downslope. The northerly, upslope flow is clearly the dominant feature during the daytime at both levels while southerly, downslope winds are most predominant at night. During the daytime, the secondary maximum of stronger winds from the southeast and west directions are associated with periods when the large-scale pressure gradient dominates the upslope-downslope regime. The pressure gradient wind signature is also evident in the nighttime wind roses. The small percentage of northerly winds in the nighttime roses is due, in most part, to periods when the upslope flow persists for more than 12 hours, which usually occurs during the summer months. It is noteworthy that while there is clearly a higher percentage of stronger winds at the 38-m level than at 10 m as would be expected, there is also a higher percentage of calm winds (WS<0.5 ms^{-1}) at the top of the tower as well.

As in Figure 4.9, the frequency of occurrence of wind speeds as a function of direction was calculated at the intervening four levels, and the results for all directions for both daytime and nighttime periods are shown in Table 4.8. The daytime flow is predominately upslope driven by the thermal heating of the mountain. Due to a well-mixed boundary layer, changes of the distribution of winds with height are small above the 3-m level. While there is a decrease in the percentage frequency in the three higher speed classes in the lowest 10 m, the changes are small above that level. The changes in the percent occurrence of winds less than 0.5 ms^{-1} (calm) decreases with height, except for a small increase at 38 m.

Reflecting the increase in stability in the boundary layer at night, the distribution of the wind speed with height takes on a different character from the daytime situation. While the percentage frequency of occurrence of calm conditions and of winds greater than 5 ms^{-1} increase with height, the most common wind (0.5 to 5 ms^{-1} range) percentage of occurrence decreases with height. Considering winds from the south-southwest to west directions at speeds greater than 5 ms^{-1}, indication of the large-scale significant winds, there is a general increase in the percentage of

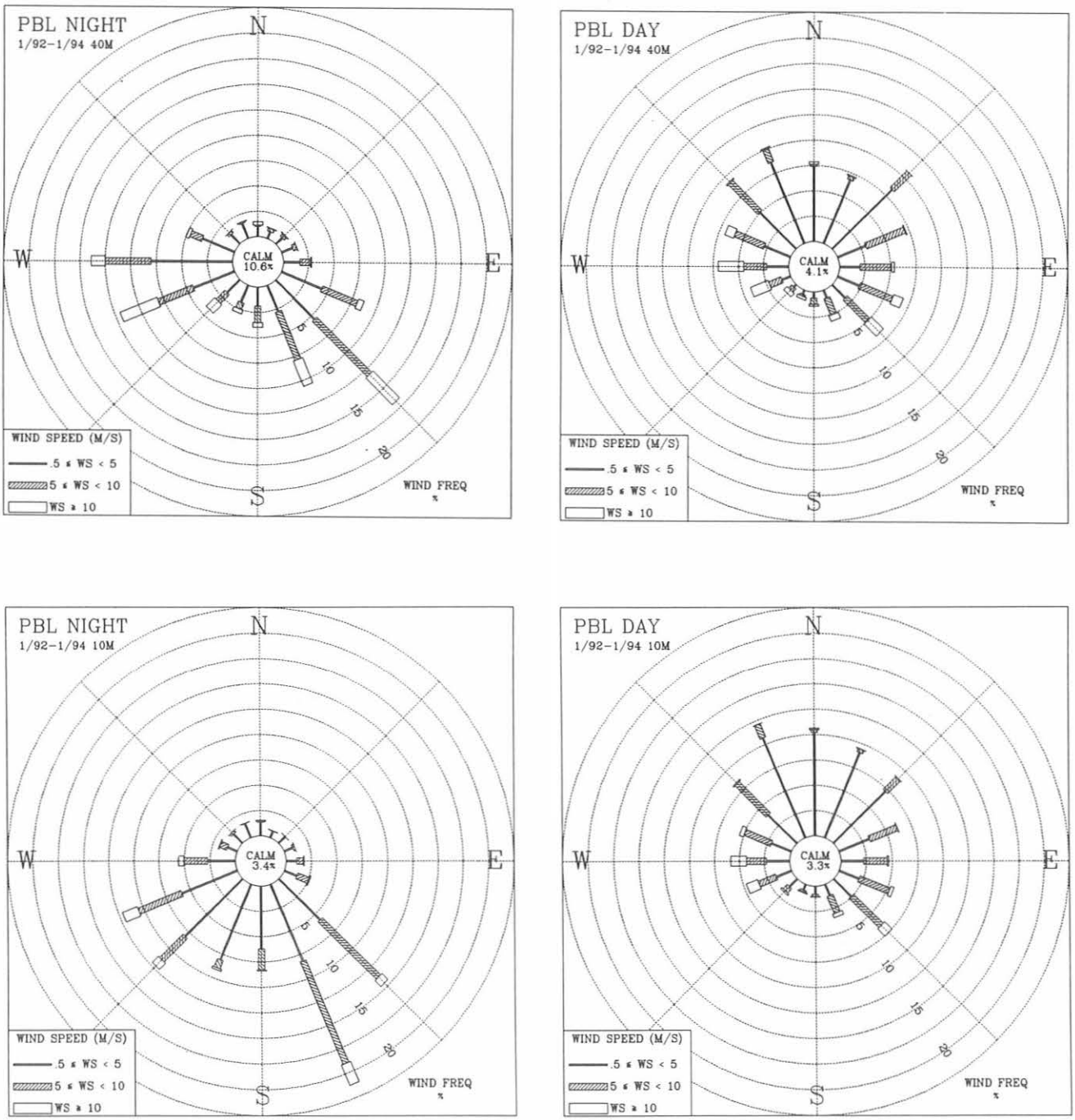

Fig. 4.9. Wind roses of the 10 m and 40 m level winds at MLO for night (left) and day (right) regimes. The distribution of resultant wind directions and speed are given in units of percent occurrence for the period January 1992 through January 1994. Wind speed is displayed as a function of direction in three classes.

TABLE 4.8. Percent Frequency of Occurrence of Wind Speed at Six Height Levels

Winds	Wind Height					
Speed ($m\ s^{-1}$)	3 m	6 m	10 m	20 m	29 m	38 m
Daytime conditions (0900 to 2000 HST)						
Calm	4.8	3.9	3.3	3.1	3.1	4.1
.5 to 5	73.8	67.1	60.8	54.6	53.5	53.6
5 to 10	19.4	24.8	30.1	33.5	33.5	32.1
10	2.0	4.1	5.8	8.8	9.9	10.3
Nighttime conditions (2100 to 0800 HST)						
Calm	4.1	3.1	3.4	4.8	7.5	10.6
.5 to 5	70.5	62.8	54.9	47.9	44.3	42.1
5 to 10	23.2	29.8	35.2	36.4	34.2	32.1
10	2.2	4.3	6.5	10.8	14.0	15.2
5*	5.2	7.9	9.0	13.0	13.9	13.5

*Direction limited to west through west southwest.

occurrence with height. Interestingly, above 10 m the percentage occurrence at all wind speeds is relatively constant with height.

Summary

Based on this analysis, the measured gradients of temperature and wind are generally uniform above 10 m. Thus measurements at 10 m and near the top of the tower will describe the temperature and wind structure of the boundary layer over this range of heights. The 10-m level was selected as the reference level to remain consistent with WMO observational recommendations. A thermometer and anemometer are positioned at 38 m to characterize the flow on the upper half of the tower. Due to terrain irregularities it would be difficult to characterize the flow in any useful way with wind measurements below 3-5 m. However, temperature measurements at 2 m are important to depict the stability of the surface layer (Figure 4.8).

4.3. REFERENCES

Blumenstock, D.L., and S. Price, The climate of Hawaii, in *Climates of the States*, vol. 2., pp. 614-639, NOAA, USDC, Water Information Center, Inc., Port Washington, NY, 1974.

Chin, J.F.S., H.T. Ellis, B.G. Mendonca, R.F. Pueschel, and H.J. Simpson, Geophysical monitoring at Mauna Loa Observatory, *NOAA TM ERL APCL-13*, 36 pp., 1971.

DeLuisi, J. (ed.), *Geophysical Monitoring for Climatic Change No. 9 Summary Report 1980*, 163 pp., NOAA Environmental Research Laboratories, Boulder, CO, 1981.

Kaimal., J.C., and J.J. Finnigan, *Atmospheric Boundary Layer Flows, Their Structure and Measurement*, 289 pp., Oxford Univ. Press, NY, 1994.

Mazzarella, D.A., An inventory of specifications for wind measuring instruments, *Bull. Amer. Meteor. Soc. 53*, 860-871, 1972.

Mendonca, B., Local wind circulation on the slopes of Mauna Loa, *J. Appl. Meteorol., 8*, 533-541, 1969.

Peterson, J.T., and R.M. Rosson (eds.), *Climate Monitoring and Diagnostics Laboratory No. 21 Summary Report 1992*, 132 pp., NOAA Environmental Research Laboratories, Boulder, CO, 1993.

Price, S., and C.J. Pales, Mauna Loa Observatory: The first five years, *Mon. Weather Rev., 91*, 665-680, 1963.

Ridley, B.A., and E. Robinson, The Mauna Loa Observatory photochemistry experiment, *J. Geophys. Res. 97*, 10,285-10,290, 1992.

World Meteorological Organization (WMO), *Guide to Meteorological Instrumentation and Observing Practices, No. 8, Tech. Paper 3*, 347 pp., World Meteorological Organization, Geneva, 1969.

5. Nitrous Oxide and Halocarbon Division

T.M. THOMPSON (EDITOR), J.W. ELKINS, J.H. BUTLER, S.A. MONTZKA, R.C. MYERS, T.J. BARING, S.O. CUMMINGS, G.S. DUTTON, J.M. GILLIGAN, A.H. HAYDEN, J.M. LOBERT, T.H. SWANSON, D.F. HURST, AND C.M. VOLK

5.1. CONTINUING PROGRAMS

5.1.1. FLASK SAMPLES

Air samples were collected in pairs and analyzed as in the past with one change. In mid-June, flasks started being humidified by filling them with air flowing through a bubbler prior to their being returned to the field sites. This conditioning step is an attempt to passivate the flask walls and minimize surface chemistry for compounds like carbon tetrachloride (CCl_4). Filling instructions were revised and, therefore, flasks are purged 50% longer. The efficacy of these changes is currently being assessed.

Other minor program changes also instituted in June included: (1) using flow meters with the larger flasks during filling so that flushing rates are equal, (2) conducting field site pump performance tests periodically, and (3) checking flask pressures after filling and before analysis on each instrument. More 0.85 and 2.5 L flasks were added; therefore, instruments such as the gas chromatograph-mass spectrometer (GC-MS) were guaranteed sufficient air for analyses.

A maintenance trip was made to Alert, Northwest Territories, Canada, in May to install an air sampling inlet system [*Montzka et al.*, 1992]. The air inlets are at 10 m and 5 m on the north tower. Flasks are currently filled only from the highest inlet. SPO is the other field site where flasks are filled through this type of inlet system.

A year of analyzing the flask air samples on the original electron capture-gas chromatograph (EC-GC) and the Autoflask system is complete. The Autoflask system is patterned after the Radiatively Important Trace Species (RITS) GC in situ system [*Montzka et al.*, 1992]. This comparison showed some weaknesses in the Autoflask flask inlet plumbing and system control software. Necessary changes were made, and an additional period of overlapping analyses will be done before the old GC is retired from service.

Chlorofluorocarbon (CFC) -11 and -12 concentration growth rates continue to decrease as their expected usage diminished [*Elkins et al.*, 1993]. In 1993 the CFC-11 growth rate was about 1 ppt yr^{-1} with CFC-12 being 10 ppt yr^{-1} (Figure 5.1).

The growth rate of nitrous oxide (N_2O) has decreased since 1991 from about 1 ppb yr^{-1} to 0.5 ppb yr^{-1}. The yearly global means of measurements from flasks collected at seven sites show that mixing ratios of N_2O appear to have leveled off in 1993 (Figure 5.2). The cause of this decrease in the growth rate is unknown and may be the result of many mitigating factors. Worldwide use of fertilizer has decreased by over 10% which will lessen its source of N_2O. Since the eruption of Mt. Pinatubo in June 1991, northern hemispheric temperatures have decreased by 0.5°C; this could reduce the N_2O amount produced by bacteria that are strongly influenced by temperature change. Since the summer of 1990 through the end of 1993, the SOI was consistently negative. A large negative anomaly (<-1) indicates a warming event in the tropical ocean that usually means less equatorial upwelling and less flux of deep water N_2O into the atmosphere. Two such events were recorded in the summer of 1991 and summer of 1992 through the spring of 1993.

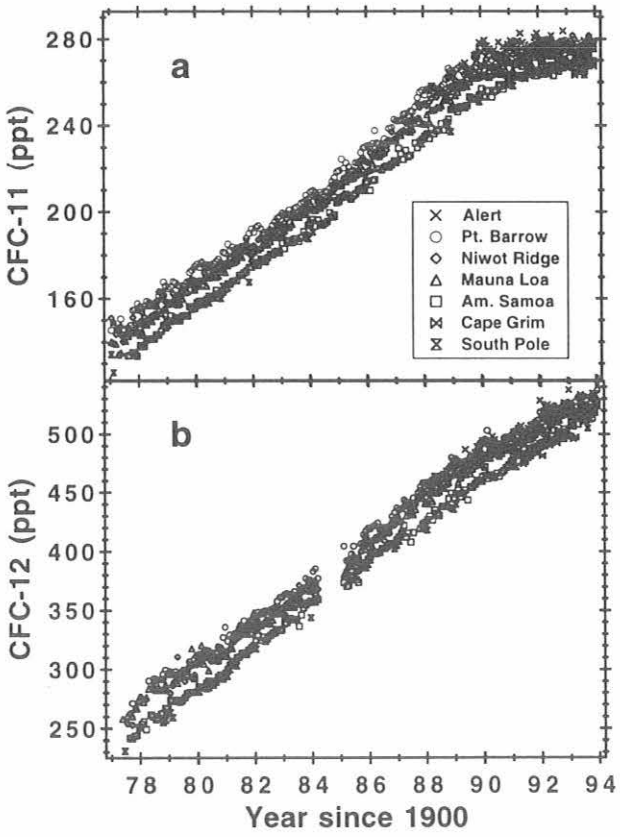

Fig. 5.1. Monthly means of atmospheric mixing ratios measured from flasks collected at the seven NOAH flask network sites for (*a*) CFC-11 and (*b*) CFC-12. Values are reported as dry mole fractions [*Elkins et al.*, 1993] in parts-per-trillion (ppt). A color figure is available from the authors.

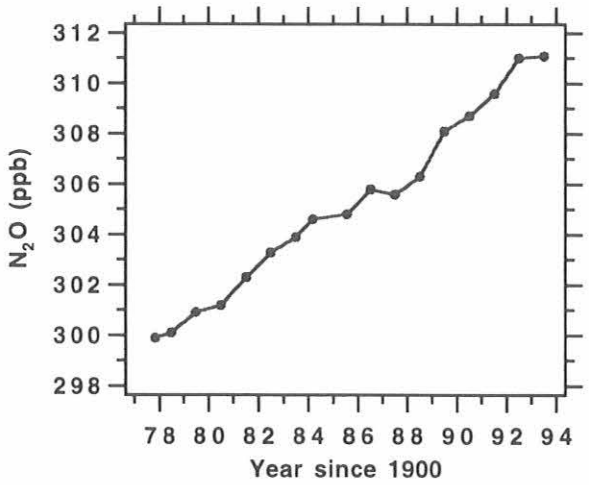

Fig. 5.2. Yearly global means of atmospheric N_2O mixing ratios collected at the seven NOAH flask network sites. Values are reported as dry mole fractions in parts-per-billion (ppb).

5.1.2. RITS Continuous Gas Chromatograph Systems

During scheduled maintenance trips to the field sites, calibration tank regulator heaters and automatic shut-off solenoid valves were installed. The regulator heaters operate at 60°C and reduce contamination buildup. The solenoid valves are in-line between the two calibration tank regulators and the stream select valve. If a power outage occurs, the solenoid valves close preventing the possible loss of valuable calibration gases.

Electron capture detectors (ECDs) at BRW, NWR, and SMO had to be replaced during 1993. In all cases the channel that measures CFC-11, CFC-113, CH_3CCl_3, and CCl_4 was the one that had baseline frequency gradually increase from a nominal 100 Hz to well over 1000 Hz. The method of cleaning a detector by flowing H_2 through it at normal operating temperature for 24 hours or more did not improve the background frequency.

Calibration cylinder gases at the field sites typically last about 1.5 years. The ratios of the chromatogram areas for all components in the two calibration tanks are monitored for possible drift. When a calibration cylinder's pressure falls below 1.3 MPa it is replaced. The new tank components' mixing ratios were determined with a precision better than 0.5%. For a chemical like N_2O, whose growth rate in the atmosphere is small being similar to the calibration precision, step jumps can occur in the data when calibration gases are changed. A technique to counteract this problem and also attempt to detect drift in the working standards was instituted in 1993. Two well-calibrated gas standards (round robins), one at ambient and the other at ~10% below ambient mixing ratios, were taken to the field sites over a period of a month and analyzed in place of outside air for 2 days. This intercalibration documented working standard mixing ratios over a span of a few weeks at all of the sites except SPO. GC linearity and precision were also determined. By continuing this procedure quarterly, problems associated with standards' drift and instrument vagaries should be minimized. Some adjustments in the data base will probably be required as this method becomes routine and attempts are made to back correct the data based on better defined instrument calibration curves.

Monthly mean data for CFC-11 are pictured in Figure 5.3. The marked decrease in growth rate is obvious and comparable to that determined from the longer flask record. Likewise, CFC-12 data are shown in Figure 5.4 and correlate well with the flask mixing ratios. The data for N_2O (Figure 5.5) were adjusted because of the round robin intercalibrations. These data are preliminary and may require further adjustment as the

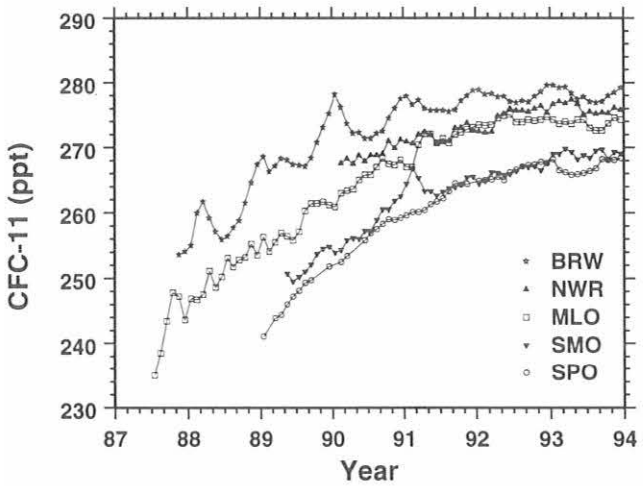

Fig. 5.3. Monthly average CFC-11 mixing ratios in ppt from the in situ GCs.

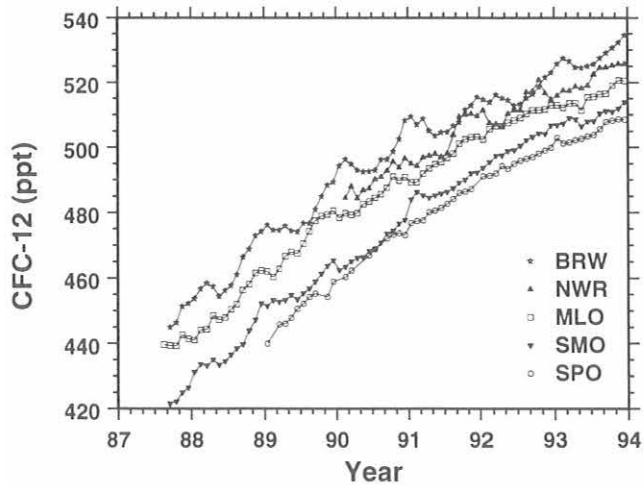

Fig. 5.4. Monthly average CFC-12 mixing ratios in ppt from the in situ GCs.

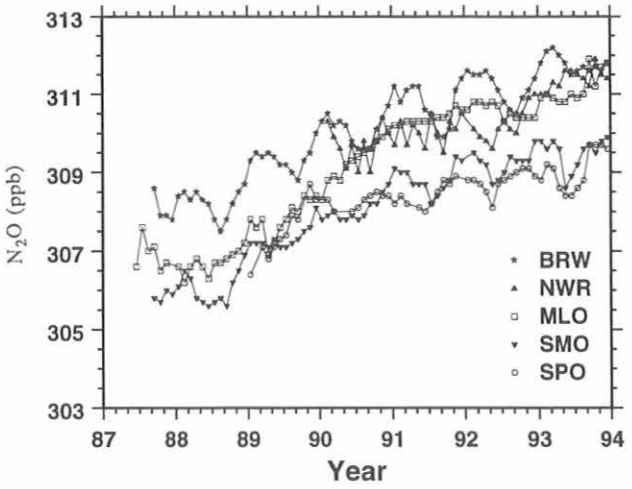

Fig. 5.5. Monthly average N_2O mixing ratios in ppb from the in situ GCs. New calibration and water vapor corrections were applied.

intercalibrations continue. NWR data were corrected for the period when the Nafion drier was not installed. This removed or reduced the annual cycle seen in previously published results.

5.1.3. Low Electron Attachment Potential Species (LEAPS)

Measurements of halons H-1301 and H-1211, CFC-113, CH_3Br, and CH_3Cl continued with the new LEAPS GC system throughout 1993. Except for H-1301, these compounds were also measured by GC-MS throughout the year. Halon data from the EC-GC installed in April 1992 are extremely precise (within 0.01-0.03 ppt on average), although the response for H-1211 is still non-linear on the new system. By mid-1992, the data suggested a substantial slowdown in the growth of the two halons in the atmosphere [*Butler et al.*, 1992]. However, the recent values, which are more frequent and more precise and that extend the data set from 5 to 7 years, indicate that the slowdown may not be as substantial as previously reported. During 1993, atmospheric H-1211 increased at 0.1-0.2 ppt yr^{-1} (3-7% yr^{-1}), and H-1301 increased at about 0.2 ppt yr^{-1} (10% yr^{-1}). At the end of 1993, the latitudinally weighted, mean mole fractions of H-1301 and H-1211 are 2.1 and 3.1 ppt, representing 25-35% of organic bromine in the remote atmosphere (Figure 5.6).

Because of a numerical error in the calculation routines, previously reported values for H-1211 should be adjusted upward by 15%. Reanalyses of cylinder SRL-K-009288, an Aculife-treated steel cylinder that has served as the principal secondary standard for all reported halon values, have agreed within ±0.2 ppt for each of the halons over 3-5 years. Earlier calibrations, however, were not as precise as those done since early 1992, therefore it is difficult at this time to determine

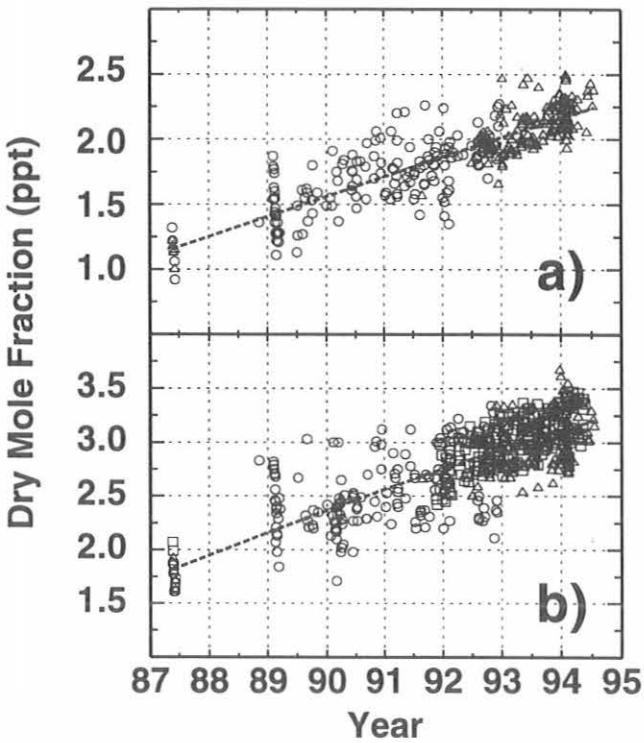

Fig. 5.6. Composite plots of all CMDL halon data (a) H-1301 (b) H-1211. Circles represent analyses with the old EC-GC, triangles represent analyses with the new EC-GC, squares are for data obtained by GC-MS (H-1211 only).

drift within this range. Data from the GC-MS and EC-GC systems agree within ±0.1 ppt overall.

One indicator of potential sampling error or storage effects is a comparison of agreement for flask pairs versus that for individual measurements of the same flask. From purely statistical considerations, one would expect flask-pair agreement to be better than the precision for individual measurements if there is no flask or sampling effect. This is because the value obtained for each flask is a mean and, consequently, a closer estimate of the true mean than is an individual measurement. From EC-GC measurements, it is clear that agreement for H-1301 within pairs of simultaneously collected flasks is similar to the analytical precision for repeat measurement of individual flasks (Figure 5.7*a*). Because surface effects in all flasks are not expected to be identical, this indicates that there is little chance of storage having affected H-1301. The median standard deviations for replicate analyses and for flask-pair agreement are both around ±0.01 ppt (±0.5%). However, for H-1211, agreement between flasks is somewhat poorer than for replicate analyses (Figure 5.7*b*). The median standard deviation for replicate analyses is ±0.02 ppt (±0.7%), but for flask pairs is ±0.04 ppt (±1.3%). This is not a large effect and it may be symptomatic of some problem occurring within a flask after it has been sampled.

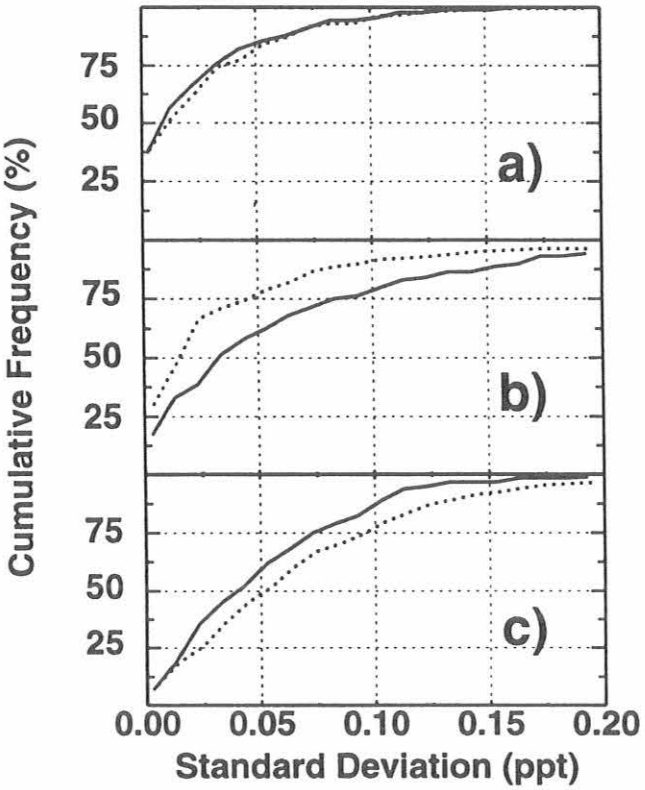

Fig. 5.7. Cumulative error plots for repeat analysis of individual flasks (dotted line) and analysis of flask pairs (solid line): (a) H-1301 by EC-GC, (b) H-1211 by EC-GC, (c) H-1211 by GC-MS.

Whether this effect involves H-1211 directly or some other compound affecting the analysis is uncertain at this time. It does not appear related to sampling site, sampling dates, or time between sampling and analysis. The possibility that it may be something other than H-1211 is underscored by a similar evaluation for GC-MS data. In this case, the agreement for H-1211 between flasks is actually slightly better than that for replicate analyses, as one would expect from purely statistical considerations (Figure 5.7*c*). Because the GC-MS is specific for the m/z = +85 ion from H-1211 and the ECD is less specific, it is more probable that the larger differences between flask pairs, as observed by EC-GC, may be some matrix effect, such as that caused by a co-eluting compound. It is also possible, however, that the effect is just beyond the detection ability of the GC-MS.

5.1.4. Alternative Halocarbon Measurements

Hydrochlorofluorocarbons (HCFCs) are important substitutes for CFCs in industrial applications. Their use will significantly shorten the time required for complete elimination of CFCs in industry [*UNEP*, 1991]. Although HCFCs contain chlorine, models indicate that they have a much reduced potential to deplete stratospheric ozone compared with CFCs. Ozone destruction capacity for HCFCs, as predicted by semi-empirical steady state ozone depletion potentials, ranges between 1 and 12% that of CFC-11 [*WMO*, 1991; *Solomon et al.*, 1992]. However, the ozone depletion potential for HCFCs over short periods, such as the next 5-10 years when chlorine is expected to reach a maximum in the stratosphere, is more accurately estimated with time-dependent ozone depletion potentials [*Solomon and Albritton*, 1992]. Because HCFCs have shorter atmospheric lifetimes than CFC-11, time-dependent depletion potentials can be as much as five times higher than steady-state ozone depletion potentials. For these reasons, and because of uncertainties concerning the chemistry and dynamics of the atmosphere, there is increasing concern over extensive use of HCFCs as replacements for CFCs. Some nations have accelerated the timetable for eliminating HCFCs earlier than recommended by the Copenhagen Amendments to the Montreal Protocol [*UNEP*, 1993]. Monitoring the global spatial and temporal variability of HCFCs is necessary for maintaining an accurate atmospheric chlorine inventory as replacements gain acceptance in the marketplace and for validating model predictions concerning the fate of these compounds in the atmosphere [*Prather and Spivakovsky*, 1990].

Paired sample flasks filled at the four CMDL stations and three cooperative flask sampling locations during 1993 were analyzed in the Boulder laboratory using gas chromatography with mass spectrometric detection for HCFC-22, HCFC-142b, and HCFC-141b [*Montzka et al.*, 1993; 1994*a*, *b*]. Results for both HCFC-22 and HCFC-142b represent a continuation of measurements made in previous years. Before 1993, however, only preliminary mixing ratios were reported for HCFC-142b [*Swanson et al.*, 1993]. In addition to finalizing standardization for HCFC-142b, a consistent set of calibration standards was also prepared for HCFC-141b in 1993.

Chlorodifluoromethane (HCFC-22)

Measurements of the most abundant atmospheric HCFC continued in 1993 (Figure 5.8; Table 5.1). The latitudinally-weighted global mean mixing ratio for HCFC-22 in mid-1993 was 106 ppt (Table 5.2). This is an increase of 4 ppt over the global mean determined for mid-1992 [*Montzka et al.*, 1993]. The growth rate for HCFC-22 from November 1991 through December 1993 is estimated at 4.9 (±1.0) ppt yr^{-1}. The average difference between the northern and southern hemisphere during 1993 was 13 ± 1 ppt.

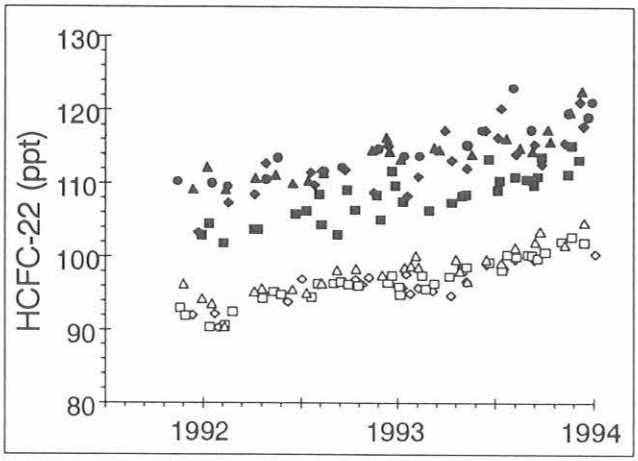

Fig. 5.8. Mixing ratios determined for HCFC-22 from air collected in flasks from seven different remote sampling locations: Alert, (•); BRW, (▲); Niwot Ridge, (♦); MLO, (■); SMO, (Δ); CGO, (□); and SPO, (◊).

1-chloro-1,1-difluoroethane (HCFC-142b)

Hydrochlorofluorocarbon-142b is used predominantly as a substitute for CFC-12 in the fabrication of closed-cell foam [*AFEAS*, 1994]. It was also used to a lesser extent as an aerosol propellant and in refrigeration applications. The shift to HCFC-142b and away from CFC-12 for blowing foam began in 1988, and industry predicted that complete conversion would occur before the end of 1993 [*UNEP*, 1991].

The latitudinally-weighted global mean mixing ratio for HCFC-142b in mid-1993 was 4.3 (±0.1) ppt (Figure 5.9; Table 5.1 and 5.2). This is an increase of 1.0 ppt over the global mean determined for mid-1992. The growth rate for HCFC-142b over the entire sampling period (December 1991 through December 1993) is estimated at 1.1 ppt yr^{-1}.

Mixing ratios determined for HCFC-142b during early 1992 in the northern hemisphere (Figure 5.9) are in reasonable agreement with those reported by *Schauffler et al.* [1993] from air collected in the upper troposphere

TABLE 5.1. CMDL Measurements of HCFCs from Flasks (1991-1993)

Station	Date	HCFC-22 (ppt)	HCFC-142b (ppt)	HCFC-141b (ppt)	Station	Date	HCFC-22 (ppt)	HCFC-142b (ppt)	HCFC-141b (ppt)
ALT	1991.871	110.2			BRW	1993.767	117.4	5.8	1.29
ALT	1992.052	110.0	3.6		BRW	1993.781	115.8	6.0	1.48
ALT	1992.128	109.5	3.8		BRW	1993.882	119.8	5.9	1.86
ALT	1992.328	110.5	4.3		BRW	1993.943	122.6	6.4	1.97
ALT	1992.385	113.4	4.1						
ALT	1992.620	111.5	4.1		CGO	1991.885	93.0		
ALT	1992.713	112.1	4.1		CGO	1991.910	91.9		
ALT	1992.907	114.7	5.0	0.55	CGO	1992.036	90.3	2.3	
ALT	1993.038	113.6	5.0	0.65	CGO	1992.115	90.6	2.4	
ALT	1993.112	113.7	5.4	0.70	CGO	1992.153	92.4	2.6	
ALT	1993.362	115.2	5.5	0.93	CGO	1992.306	94.2	2.2	
ALT	1993.438	117.2	5.7	0.87	CGO	1992.363	95.1	2.7	
ALT	1993.595	122.9		1.05	CGO	1992.402	94.8		
ALT	1993.688	117.2	5.6	1.51	CGO	1992.555	94.5	2.6	
ALT	1993.880	119.5	6.4	1.64	CGO	1992.587	96.2	2.7	
ALT	1993.975	119.0	6.8	1.99	CGO	1992.669	96.3	2.2	
ALT	1993.995	121.0	7.6	1.87	CGO	1992.705	96.6	2.4	
					CGO	1992.746	96.2	3.0	
BRW	1991.951	109.2			CGO	1992.798	96.0	2.9	
BRW	1992.022	112.2			CGO	1992.951	96.4*	3.3	0.23
BRW	1992.120	109.1	3.3		CGO	1992.970	97.4*	2.7	0.19
BRW	1992.268	110.7	3.8		CGO	1993.008	95.8	3.0	0.24
BRW	1992.372	111.2	3.3		CGO	1993.014	94.8	3.7	0.20
BRW	1992.459	110.0	4.1		CGO	1993.126	97.4	2.9	0.20
BRW	1992.538	110.4	3.5		CGO	1993.145	95.6	3.6	0.14
BRW	1992.618	111.4	4.2		CGO	1993.186	96.3	3.1	0.26
BRW	1992.866	114.5	4.8		CGO	1993.266	97.3	3.3	0.35
BRW	1992.940	116.3	5.3		CGO	1993.334	98.2	3.6	0.33
BRW	1992.959	114.3*	4.9	0.55	CGO	1993.356	98.6	3.4	0.35
BRW	1993.016	113.2	5.1	0.58	CGO	1993.471	99.2	3.7	0.34
BRW	1993.186	114.9	5.5	0.69	CGO	1993.537	98.2	3.6	0.34
BRW	1993.214	114.6	4.5	0.91	CGO	1993.564	100.3	4.0	0.43
BRW	1993.381	114.0	5.1	0.85	CGO	1993.608	99.9	3.7	0.46
BRW	1993.556	116.2	5.0	1.04	CGO	1993.669	100.2	3.3	0.45
BRW	1993.627	114.9	5.7	1.24	CGO	1993.688	100.2	3.5	0.45
BRW	1993.688	114.5	5.3	1.34	CGO	1993.718	99.8	3.8	0.42

TABLE 5.1. CMDL Measurements of HCFCs from Flasks (1991-1993)—Continued

Station	Date	HCFC-22 (ppt)	HCFC-142b (ppt)	HCFC-141b (ppt)	Station	Date	HCFC-22 (ppt)	HCFC-142b (ppt)	HCFC-141b (ppt)
CGO	1993.756	100.6	3.5	0.53	NWR	1993.606	114.1	5.2	1.35
CGO	1993.841	102.0	4.2	0.45	NWR	1993.701	115.4	5.5	1.63
CGO	1993.890	102.7	3.9	0.52	NWR	1993.740	112.6	5.3	1.29
CGO	1993.953	101.9	4.1	0.59	NWR	1993.855	115.5	5.9	1.69
					NWR	1993.932	121.1	6.1	1.98
MLO	1991.995	102.9			NWR	1993.951	117.8	5.9	1.88
MLO	1992.033	104.4	2.9						
MLO	1992.109	101.8	3.1		SMO	1991.901	96.2		
MLO	1992.262	103.6	2.9		SMO	1991.995	94.2		
MLO	1992.281	103.6	3.2		SMO	1992.046	93.6	2.4	
MLO	1992.473	105.7	3.5		SMO	1992.112	90.4	2.4	
MLO	1992.530	106.1	3.6		SMO	1992.262	95.2	2.5	
MLO	1992.596	108.5	3.3		SMO	1992.301	95.7	2.9	
MLO	1992.607	104.3	3.0		SMO	1992.456	95.5	2.8	
MLO	1992.691	103.0	3.3		SMO	1992.530	95.0	2.7	
MLO	1992.740	109.1	5.0		SMO	1992.607	96.3	3.3	
MLO	1992.779	106.3	3.9		SMO	1992.686	98.2	2.9	
MLO	1992.893	108.4	4.0		SMO	1992.784	98.3	3.8	
MLO	1992.913	105.0	3.6		SMO	1992.921	97.5		
MLO	1992.970	111.6	4.6		SMO	1993.036	98.6	2.6	0.25
MLO	1992.989	109.7*	4.6	0.41	SMO	1993.069	98.8	2.9	0.28
MLO	1993.027	107.5	3.8	0.41	SMO	1993.093	100.2	3.3	0.40
MLO	1993.162	106.3	3.9	0.53	SMO	1993.107	98.6	3.6	0.29
MLO	1993.280	107.4	4.2	0.66	SMO	1993.299	99.6	3.4	0.39
MLO	1993.334	108.2	4.8	0.71	SMO	1993.321	98.1	3.7	0.32
MLO	1993.353	108.4	4.2	0.70	SMO	1993.359	96.7	3.3	0.33
MLO	1993.469	113.3	4.9	0.91	SMO	1993.455	99.6	3.6	0.46
MLO	1993.515	109.1	4.5	0.87	SMO	1993.532	99.2	3.4	0.36
MLO	1993.526	110.4	4.8	0.71	SMO	1993.603	101.3	3.9	0.50
MLO	1993.603	110.9	5.6	1.02	SMO	1993.704	102.0	4.0	0.61
MLO	1993.660	110.6	4.9	1.17	SMO	1993.729	103.5	3.7	0.61
MLO	1993.699	109.8	4.7	1.13	SMO	1993.855	101.7	3.8	0.63
MLO	1993.718	111.0	4.8	1.20	SMO	1993.953	104.7	4.4	
MLO	1993.737	113.6	5.1	1.10					
MLO	1993.871	111.3	4.7	1.43	SPO	1991.948	92	2.1	
MLO	1993.890	115.2	5.3	1.39	SPO	1992.063	92.1	2.1	
MLO	1993.929	113.2	5.1	1.39	SPO	1992.079	90.3	2.1	
					SPO	1992.434	93.8	3.1	
NWR	1991.978	103.3			SPO	1992.506	96.9	2.7	
NWR	1992.131	107.3	3.5		SPO	1992.590	96.2	2.8	
NWR	1992.265	108.4	3.4		SPO	1992.694	96.4	2.8	
NWR	1992.322	112.7	3.5		SPO	1992.781	96.8	2.7	
NWR	1992.552	111.5	4.0		SPO	1992.817	96.2	2.5	
NWR	1992.571	109.7	3.9		SPO	1992.853	97.1	3.0	
NWR	1992.609	111.7	3.6		SPO	1993.022	95.7	3.0	0.24
NWR	1992.727	111.8	4.0		SPO	1993.044	97.6	3.1	0.25
NWR	1992.877	108.7	3.6		SPO	1993.066	94.9	2.9	0.28
NWR	1992.954	115.1	4.5	0.57	SPO	1993.104	95.7	3.6	0.20
NWR	1993.049	108.3	5.8	0.47	SPO	1993.181	95.4	2.9	
NWR	1993.104	110.9	4.4	0.69	SPO	1993.274	94.7	2.7	
NWR	1993.244	117.2	6.0	1.00	SPO	1993.353	96.6	3.3	0.36
NWR	1993.280	113.1	4.6	0.84	SPO	1993.458	98.9	3.2	0.30
NWR	1993.356	112.1	4.9	0.89	SPO	1993.545	98.4	3.5	0.38
NWR	1993.452	117.2	5.3	1.08	SPO	1993.603	99.7	3.0	0.37
NWR	1993.515	116.3	5.3	1.33	SPO	1993.701	99.6	3.6	0.31
NWR	1993.529	120.3	5.7						

*Revised from that reported in *Swanson et al.* [1993]

TABLE 5.2. Estimates for Mid-Year Global Mean Mixing Ratios and Globally-Averaged Growth Rates

	1992 Mixing Ratios (ppt)	1993 Mixing Ratios(ppt)	All Data Growth Rates
HCFC-22	102	106	4.9 ppt yr^{-1}
HCFC-142b	3.3	4.3	1.1 ppt yr^{-1}
HCFC-141b	—	0.7	>100% yr^{-1}

of the northern hemisphere (2.9-3.9 ppt, CMDL versus 2.1-3.4 ppt, NCAR) [*Montzka et al.*, 1994*a*]. Informal comparisons of gas standards prepared independently at these two laboratories were performed at CMDL and indicate that the standards agree to within 5%.

When compared with levels calculated from emission estimates [*AFEAS*, 1994] and a finite-increment model, the results from both laboratories are 1.5-1.8 times (or 1.3-1.5 ppt) greater than expected [*Montzka et al.*, 1994*a*]. Although the reasons for this discrepancy are unclear at present, it is not likely that this difference results from inaccurate estimates of atmospheric lifetime for HCFC-142b. HCFC-142b has been emitted into the atmosphere for only a short period of time relative to its predicted atmospheric lifetime and, therefore, model calculations performed with a much longer lifetime than 20 years (100-1000 years) do not remove the discrepancy between observations and model results based on available emission estimates.

1,1-dichloro-1-fluoroethane (HCFC-141b)

HCFC-141b is currently used as a CFC-11 substitute for blowing closed-cell foams and as a substitute for CFC-113 as a solvent and cleansing agent. Unlike HCFC-142b, HCFC-141b was not commercially available until the beginning of 1993 when toxicological studies were scheduled to be completed [*UNEP*, 1991]. Before 1993, many companies in the foam sector stated their intention to eliminate CFC-11 for this use during that year [*UNEP*, 1993; *EPA*, 1993]. While substitution of CFC-113 with HCFC-141b is also likely to occur rapidly, industry experts estimate that only ~5% of past demand for CFC-113 will be satisfied with HCFCs owing to the many alternative processes and approaches that were developed by industry to reduce the amount of CFC-113 needed in these applications [*UNEP*, 1991].

The latitudinally-weighted global mean mixing ratio for HCFC-141b in mid-1993 was 0.7 (±0.1) ppt (Figure 5.10; Table 5.1 and 5.2) [*Montzka et al.*, 1994*a*]. The global mean mixing ratio increased exponentially during 1993, at greater than 100% yr^{-1}. The rapid increase in ambient mixing ratio during 1993 is likely the result of a dramatic shift towards use of HCFC-141b in industrial applications after toxicological studies were completed.

Recently, *Schauffler et al.* [1995] reported mixing ratios for HCFC-141b from samples collected during a number of cruises in the Pacific, Southern, and Arctic Oceans over the past 2 years. A comparison of mixing ratios determined from samples collected at similar times and at similar latitudes, reveals that results from the two independent laboratories agree to within 0.1 ppt [*Schauffler et al.*, 1995].

Stability of HCFCs in Flasks

Because measurements are based on the analysis of air contained within flasks that were filled at an earlier date, it is necessary to ensure that these compounds are stable within these containers over time before reliable and accurate mixing ratios can be reported. The potential for production and/or loss of HCFC-22, -142b, and -141b within sample flasks is investigated here by: (1) reanalyzing air within a flask after a period of time

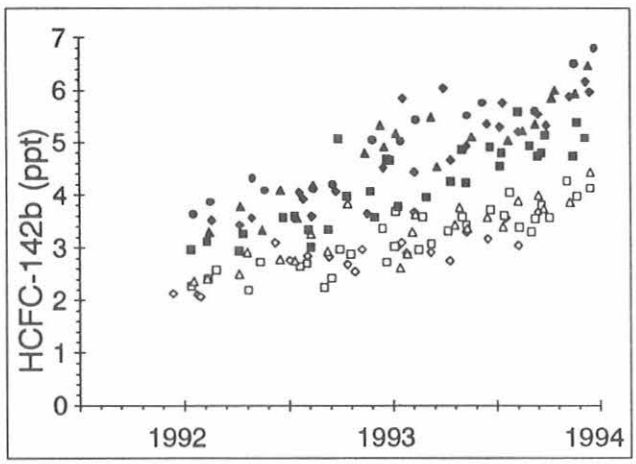

Fig. 5.9. Mixing ratios determined for HCFC-142b from air collected in flasks from seven different remote sampling locations: Alert, (•); BRW, (▲); Niwot Ridge, (♦); MLO, (■); SMO, (Δ); CGO, (□); and SPO, (◊).

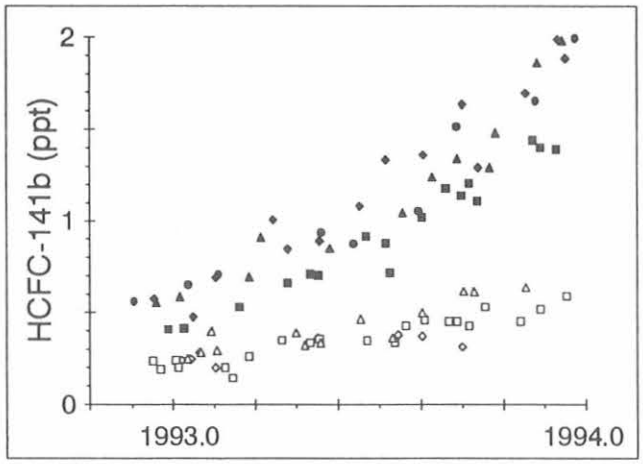

Fig. 5.10. Mixing ratios determined for HCFC-141b from air collected in flasks from seven different remote sampling locations: Alert, (•); BRW, (Δ); Niwot Ridge, (♦); MLO, (■); SMO, (Δ); CGO, (□); and SPO, (◊).

has elapsed to see if consistent results are obtained; (2) determining if relationships between the amount of time the air is stored in a flask and reported mixing ratios are apparent; (3) determining if differences attributable to humidity levels within a flask are apparent in results from SPO and CGO; and (4) determining if disagreements in HCFC mixing ratios within simultaneously filled flasks are significant relative to the precision of the analysis.

After they were received in Boulder, selected flasks were analyzed two or more times to study the effects of storage time on different compounds within flasks (Figure 5.11). Results from the two analyses are compared with the variability observed for duplicate injections of air from flasks that were collected in 1992 and 1993. For more than 90% of the flasks that were reanalyzed, the results obtained for all three HCFCs were within the 95% confidence interval for variability observed for duplicate injections of air from flasks. The larger differences observed for HCFC-141b and -142b upon reanalysis are associated with the initial stages of the measurement program when mixing ratios and signal-to-noise ratios were exceptionally low.

Although the second analysis was usually performed under identical instrumental conditions, a more polar, chromatographic column was sometimes used (Figure 5.11). In the chromatographic analysis of complex environmental samples, it is useful to compare results obtained under different instrumental conditions to ensure that these results are independent of the conditions chosen. Analysis of air samples with capillary columns having different polarity allows for an estimate of the importance of coeluting compounds on the results obtained for atmospheric HCFCs using this chromatographic instrument. For all three HCFCs, results obtained during reanalysis with the more polar column were not significantly different from the initial analysis. Because it is unlikely that a compound would interfere consistently under different instrumental conditions, these results suggest that measurements of these HCFCs are free of these types of interferences.

Flask samples sent from the stations in 1991, 1992, and 1993 (excluding SPO) were analyzed at the CMDL Boulder laboratories anywhere from 2 to 76 days after they were collected (mean = 24 days; median = 22 days). These delays result from shipping and instrument availability. Longer delays are associated with samples collected at SPO because no shipments leave this site during the southern hemisphere winter. To ascertain if these delays adversely affect HCFC measurements, residuals from loess fits to the data obtained at each station are compared with the time elapsed between sampling and analysis of each flask (Figure 5.12). A loess smoothing fraction of 0.3 was used to generate the residuals plotted in this figure to remove variability associated with seasonality and nonlinear growth rates but retain short-term variability. No

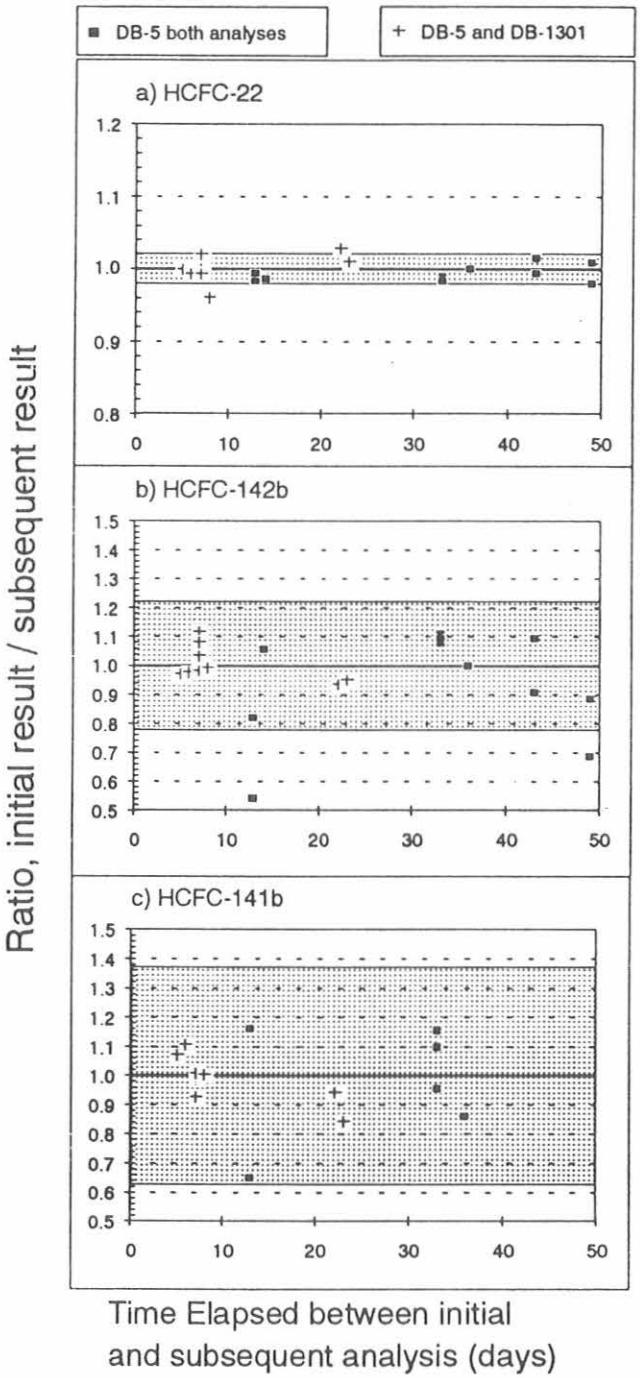

Fig. 5.11. Results obtained when air within samples flasks was re-analyzed after a period of time had elapsed for (*a*) HCFC-22, (*b*) HCFC-142b, and (*c*) HCFC-141b. Squares represent re-analyses that were performed under identical instrumental conditions. Plus symbols (+) represent results from re-analyses that were performed with a more polar analytical column (DB-1301 versus DB-5). The shaded area represents 2 times 95% of the range of variability observed for duplicate injections of air from all flasks collected in 1992 and 1993.

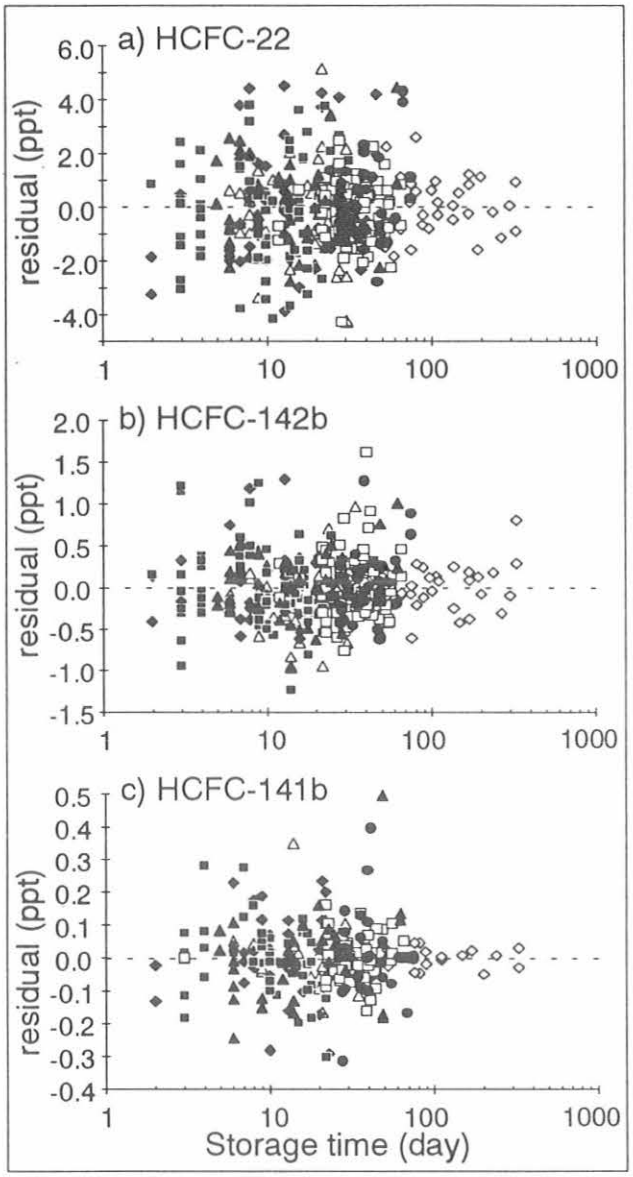

Fig. 5.12. Residuals from loess fits to flask data obtained over time are plotted against elapsed time between flask collection and analysis for (*a*) HCFC-22, (*b*) HCFC-142b, and (*c*) HCFC-141b. Symbols represent the different sampling stations (see Figure 5.8). The loess fits are performed for each compound at each sampling station with a smoothing fraction of 0.3.

significant relationship between storage time and residual is observed, and scatter in the residual does not increase at longer storage times. Although the scatter observed in Figure 5.12 represents an upper limit for the magnitude of problems associated with sample storage in these flasks under a wide range of sample humidities, it also encompasses variability associated with the atmosphere and instrumental analysis.

The effect of humidity on mixing ratios for HCFCs within flasks can be investigated by comparing data from SPO with the results obtained at CGO. For compounds emitted predominantly in the northern hemisphere, and for which atmospheric growth and loss rates are small when compared with intrahemispheric mixing rates, similar mixing ratios are observed at SPO and CGO [*Steele et al.*, 1987; *Elkins et al.*, 1993]. Ambient conditions at these two locations, however, are significantly different; while air collected at SPO can be extremely dry, air is sampled from within the marine boundary layer at CGO and ambient temperatures are, on average, ~60°C higher. Losses of certain compounds such as CCl_4 within electropolished stainless-steel flasks are known to be dependent upon the amount of water in a flask [*Schauffler et al.*, 1993; *Montzka et al.*, 1994*b*]. Despite large losses of CCl_4 within a number of flasks filled at SPO, ambient mixing ratios for HCFC-22 and HCFC-142b are very similar at both of these stations (Figure 5.13). These results suggest that within the range of humidities encountered at these two stations, mixing ratios determined for these HCFCs are independent of the amount of water present within these flasks [*Montzka et al.*, 1994*b*].

Based on the majority of measurements made for HCFC-141b in flasks collected at SPO, a similar conclusion can be drawn for this HCFC. However, in three flasks it appears as if mixing ratios from SPO are low relative to the measurements made concurrently at CGO. While this suggests that HCFC-141b may undergo losses within extremely dry flasks, rather large uncertainties are associated with these measurements owing to the extremely low mixing ratios of this compound in the southern hemisphere during early 1993. Furthermore, observed differences between mixing ratios determined for HCFC-141b within flasks collected at SPO and CGO are not correlated with carbon tetrachloride losses in these flasks, suggesting that the characteristics of a flask that cause losses of carbon tetrachloride do not affect mixing ratios determined for HCFC-141b.

Results from the flask measurement program are based on flask pairs collected simultaneously and in a parallel flow arrangement. During analysis, each flask is treated independently, and the results obtained are averaged to arrive at a best estimate for ambient air mixing ratios at the time the flask was filled. Results obtained for compounds within simultaneously filled flasks should agree to within the analytical precision of the instrument. Disagreements between mixing ratios determined within flasks that are filled in parallel can indicate problems associated with filling flasks, flask cleanliness, and compound integrity within flasks.

For all three HCFCs, the median difference observed between simultaneously filled flasks is similar to the median uncertainty associated with repetitive injections of air from a single flask (Figure 5.14). Furthermore, the entire distribution of flask-pair differences are

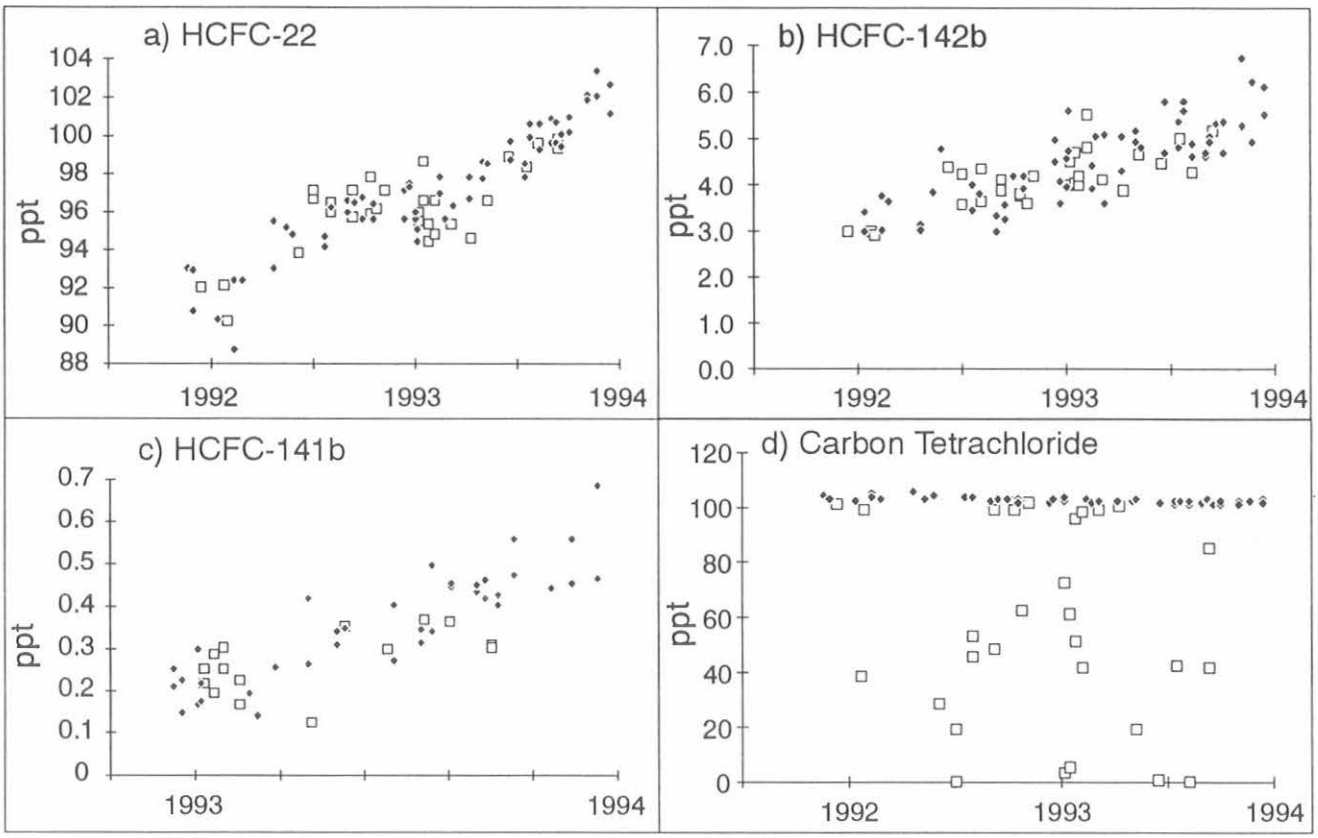

Fig. 5.13. Mixing ratios observed within individual flasks for different HCFCs at both CGO (♦) and SPO (□) for (*a*) HCFC-22, (*b*) HCFC-142b, (*c*) HCFC-141b, and (*d*) CCl_4.

similar to, if not lower than, observed analysis standard deviations for all three HCFCs, and this suggests that no measurable differences are observed in flasks filled simultaneously at the sampling stations. For HCFC-22, however, there are instances where values obtained from simultaneously filled flasks disagree significantly (≤5% occurrence for disagreements greater than 3 ppt). Sample pairs with such large differences are not used when calculating atmospheric growth rates or global background mixing ratios [*Montzka et al.*, 1993]. In the discussion above, it was concluded that HCFC-22 is stable within flask canisters for extended periods under widely differing ambient water mixing ratios and, therefore, it is difficult to explain these larger differences based on the instability of HCFC-22 within flasks. A more likely cause for these larger differences rests with problems associated with filling flasks or flask cleanliness. Separate analyses have shown that levels of HCFC-22 are typically 100-1000 times higher in laboratory air than in ambient air at remote sampling locations (S. Montzka, unpublished data). Occasional problems with small leaks or insufficient purging of flasks either during filling or analysis could generate the type of result observed.

Measurement of Additional Chlorinated Compounds with GC-MS Instrumentation

The versatility of the GC-MS technique allows for the detection of many different compounds within a single chromatogram. In addition to the compounds already quantified with GC-MS during a single analysis of air from flasks (HCFCs, CFCs, halons, methyl halides, methyl chloroform, and carbon tetrachloride), monitoring of several more chlorinated compounds began in 1993. Mixing ratios for methyl chloride (CH_3Cl), dichloromethane (CH_2Cl_2), chloroform ($CHCl_3$), and tetrachloroethylene (C_2Cl_4) were determined for air contained within flasks. Measurements of these additional compounds are performed by monitoring ions unique to these chlorinated hydrocarbons at predetermined elution times. No additional changes to the experimental technique are required. Preliminary results for these compounds are presented in Figure 5.15.

5.1.5. Gravimetric Standards

New Blending Manifold

An ultraclean gas blending manifold was designed and built for the preparation of gravimetric standards.

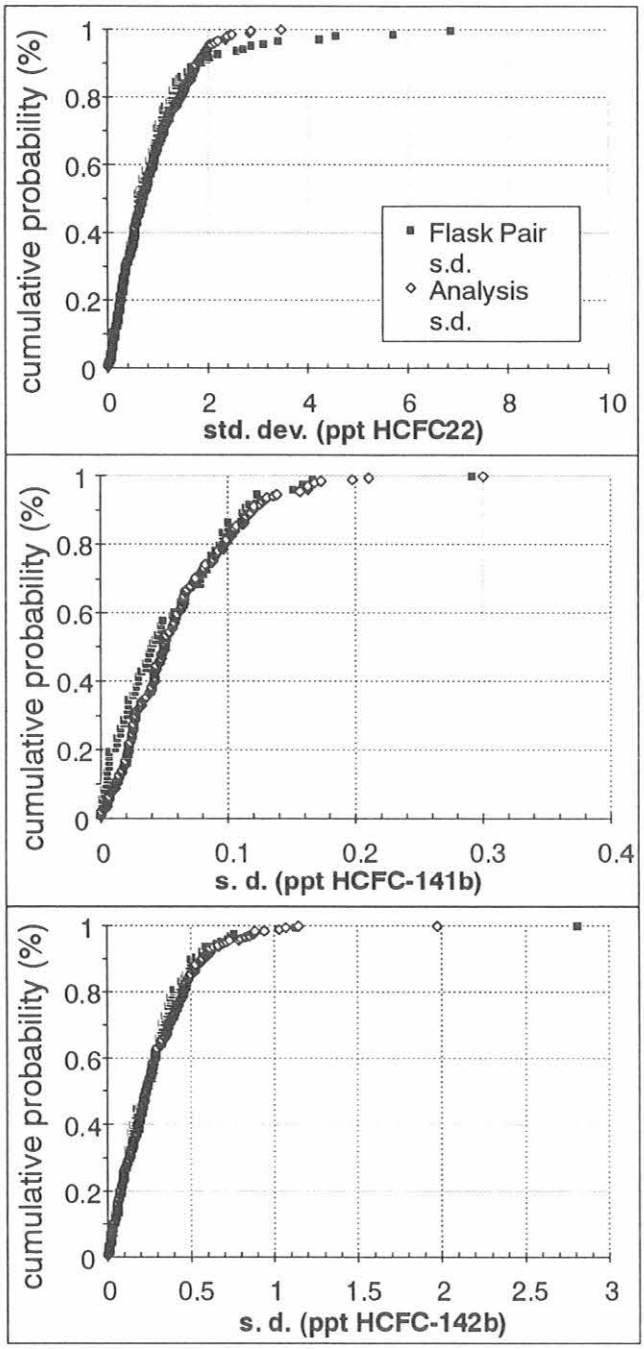

Fig. 5.14. Standard deviations obtained for duplicate injections of air from individual flasks (analysis s.d.) plotted on a cumulative probability scale. Also shown are the differences measured in simultaneously filled flasks (pair standard deviations). The data presented are for all samples collected and analyzed through the end of 1993.

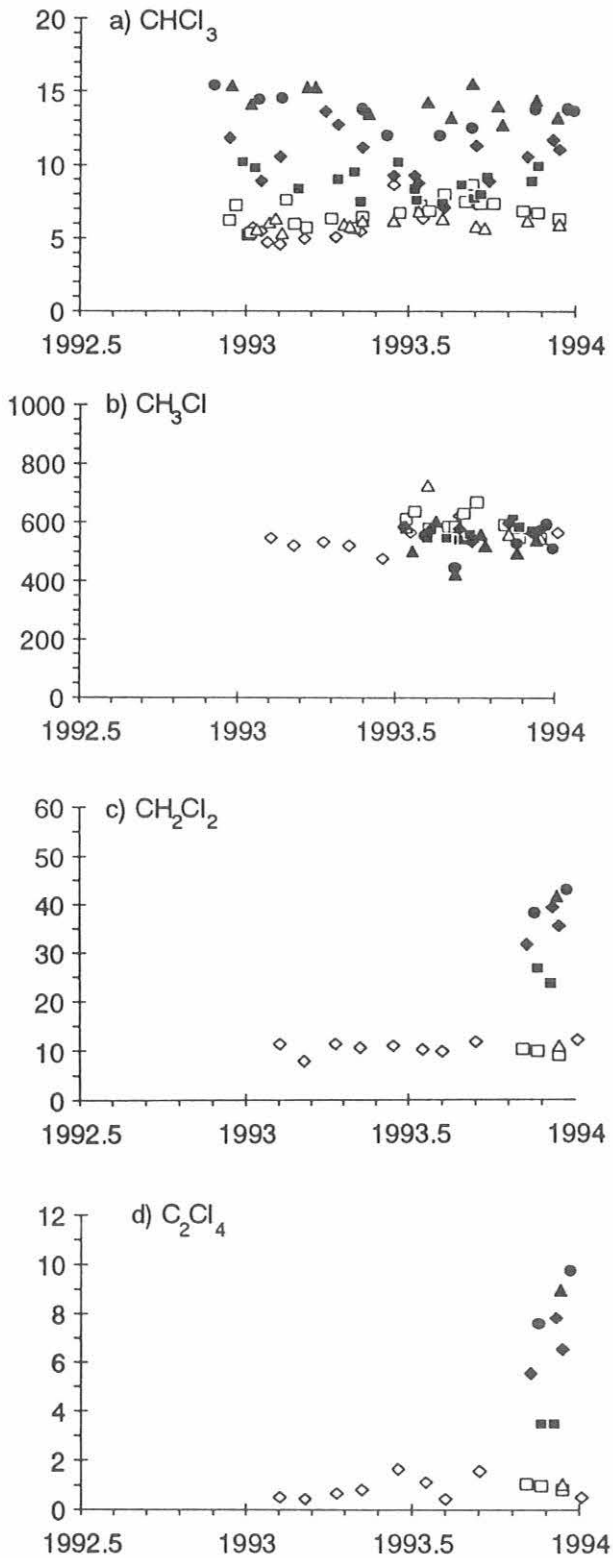

Fig. 5.15. Mixing ratios determined for different chlorinated compounds from air collected in flasks at seven different remote sampling stations. Symbols are identical to those in Figure 5.8. Mixing ratios for compounds other than CH_3Cl are reported relative to a preliminary calibration scale.

The main manifold system (Figure 5.16) was made using electropolished stainless steel tubing (6.35 mm o.d.) that was connected together using an automatic tube welder providing relatively smooth weld joints on

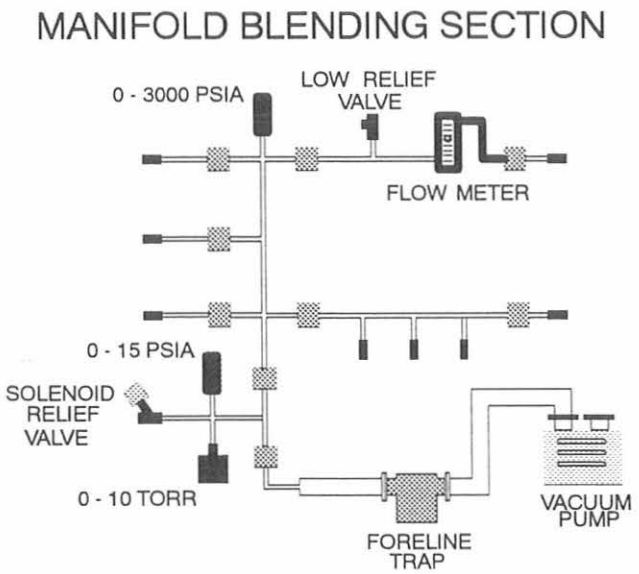

Fig. 5.16. Main section of gas blending manifold.

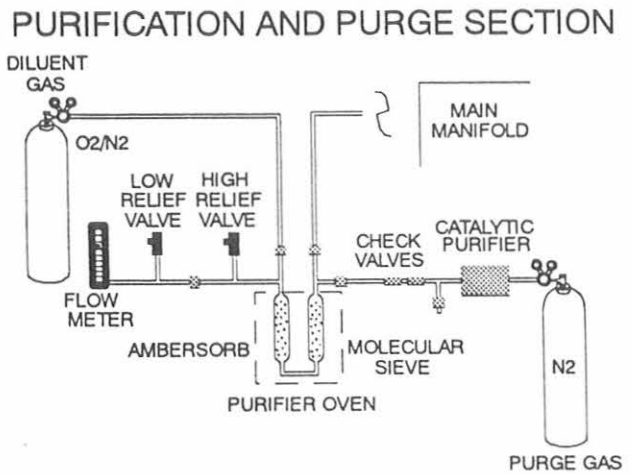

Fig. 5.17. Purification section of gas blending manifold.

the interior surface of the tubing. Welded, metal-gasket face-seal fittings were also used to connect the subsections of the manifold together and at the cylinder connection ports. Packless all-metal diaphragm valves with welded, metal-gasket face-seal fittings were used at all valve locations. Three strain gauges were installed on the manifold system for pressure measurements. A 0-20.7 MPa gauge is used for measuring pressure in the main part of the manifold. Two additional gauges measure pressures from vacuum to 103.4 kPa and from vacuum to 1.33 kPa. These low pressure gauges are isolated from the main part of the manifold by a valve in the vacuum segment of the manifold. The low pressure gauges are protected from high pressures by using a high-vacuum solenoid valve wired to a pressure-readout meter. Vacuum is achieved using a high flow rate vacuum pump. A foreline trap containing molecular sieve prevents oil vapors from entering the manifold. The manifold can be evacuated to approximately 4 Pa. A gas purification section of the manifold (Figure 5.17) is used for further purification of diluent gases such as air or N_2 supplied by commercial gas suppliers. Two traps containing Ambersorb and Molecular Sieve 13X can be heated to 250°C while they are purged with high-purity N_2. The traps are then cooled to room temperature prior to use. The N_2 used to purge the traps can also be used to purge the manifold of residual gases.

Standards

A suite of calibration standards containing N_2O and CO_2 in air were prepared this year for the CSIRO Division of Atmospheric Research. The standards were gravimetrically prepared at nominal mixing ratios ranging from 265 ppb to 345 ppb of N_2O. Carbon dioxide was added to the parent N_2O mixture that was used to prepare the ppb level N_2O mixtures at nominal mixing ratios ranging from 330 ppm to 430 ppm.

Standards containing methyl bromide (CH_3Br) and methyl chloride (CH_3Cl) in air were prepared this year. In the past, both methyl halides were used as refrigerants, solvents, and in organic synthesis [*Braker and Mossman*, 1980]. Methyl bromide is mostly used as a pesticide. Small aliquots of each compound were added to individual Aculife-treated aluminum compressed-gas cylinders providing ppb level mixtures. The Aculife treatment provides an internally inert surface that prevents both methyl halides from reacting with the aluminum. The mixtures were then blended together into one cylinder. Gravimetric standards containing from 5 to 25 ppt of CH_3Br and 400 to 1000 ppt of CH_3Cl were then prepared. The response factors (GC-MS response per mole injected) for both ppb and ppt level CH_3Br and CH_3Cl standards were consistent to within 5%.

Standards containing HCFC-141b and HCFC-142b were also prepared using the same gravimetric techniques used to prepare the methyl halide standards. Single component standards containing each HCFC were prepared at ppb levels. The standards at ppb levels were combined together, and the mixture containing both compounds was used to prepare standards at 5, 25, 50, and 500 ppt with a ratio of approximately 1:1 for HCFC-141b and HCFC-142b. Response factors determined by GC-MS analysis of each HCFC within the suite of standards (ppt to ppb levels) were consistent to within 5%.

5.2. Special Projects

5.2.1. Aircraft Project: Stratospheric Photochemistry, Aerosols, and Dynamics Expedition (SPADE)

Compact correlations between long-lived tracer molecules (e.g., CFCs, N_2O, CH_4, and H_2O) in the

stratosphere are used to calculate the average age of air samples [*Pollock et al.*, 1992], the chlorine budget of the atmosphere [*Kawa et al.*, 1992; *Woodbridge et al.*, 1995], the ozone depletion potentials of substitute CFCs [*Pollock et al.*, 1992], and lifetimes of long-lived trace gases [*Plumb and Ko*, 1992]. The results of tracer correlations of CFC-11, CFC-113, CH_4, and N_2O in the midlatitudes during SPADE in November 1992 and through April and May 1993, are compared to an earlier mission, the Airborne Arctic Stratospheric Expedition (AASE-II), from August 1991 through March 1992. Trace gases whose local lifetime are longer than quasi-horizontal transport time are in climatological slope equilibrium. A scatter plot of the mixing ratio of one versus the other collapses to a compact curve because they share surfaces of constant mixing ratio [*Plumb and Ko*, 1992]. In general, the long-lived tracers such as N_2O, CH_4, CFC-11, and CFC-113 reach slope equilibrium throughout the stratosphere, hence define a compact correlation when plotted against each other.

Exceptions to this general rule can occur when mixing across exchange surfaces is faster than diffusion along mixing ratio isopleths. One such exception occurred in Stratospheric Photochemistry Dynamics and Aerosols Expedition (SPADE) during the flight of May 7, 1993. Using the tracer correlations during slope equilibrium allows the calculation of lifetimes of the tracers in the stratosphere, and in some cases in the absence of tropospheric sinks, the total atmospheric lifetime of the specie.

For the first time, CH_4 measurements from an in situ GC are compared against an in situ tunable diode laser (TDL) spectrometer and three different water vapor techniques conducted during SPADE.

Experimental Methods

The Airborne Chromatograph for Atmospheric Trace Species (ACATS), was a cooperative development between CMDL and the NOAA Aeronomy Laboratory (AL). The first ACATS instrument was a single-channel GC capable of measuring CFC-11 and CFC-113 once every 120 seconds aboard the NASA ER-2 aircraft during AASE-II. The instrument remained unchanged in the November 1992 deployment of SPADE. A second GC channel was added for CH_4 measurements during the second deployment of SPADE in April and May 1993. Because of longer times required for separation of CH_4 and CO from the air peak, both channels sampled every 180 seconds. ACATS occupies a rectangular space (45.7 cm wide × 86.4 cm long × 20.3 cm tall) inside the AL reactive nitrogen package and mounted together inside the equipment bay (Q-bay) of the ER-2 aircraft. The two instruments shared gases on a common cylinder rack, pump motor, and data acquisition system to reduce space and weight. The GC's sample air inlet, forward facing, L-shaped, stainless steel tubing, 6.4 mm diameter was located on the lower Q-bay hatch extending 20 cm away from the fuselage in order to sample outside the aircraft (Figure 5.18).

Typical ER-2 flight speeds of 200 m s^{-1} (0.8 mach) required faster sampling rates than commercial GCs provide to gain adequate data spacial resolution. The sampling rates are made possible by a 12-port, 2-position gas sample valve from Valco Instruments, Inc. (Houston, Texas). The gas sample valve diverts or heart-cuts the large oxygen peak away from the ECD to improve the resolution of the smaller trace species. In addition to the gas sample valve, each channel contains two gas chromatographic separation columns, a pre-column and a main column, and an ECD from Shimadzu Corp. (Tokyo, Japan). Upon injection of the sample into the GC, the gas sample valve position is switched and the carrier gas sweeps the sample 5 cm^3 for CFC channel and 15 cm^3 for CH_4 channel into the pre-column and subsequently through the main analytical separation column. Both channels share a clean supply of ultra-high purity N_2 carrier gas

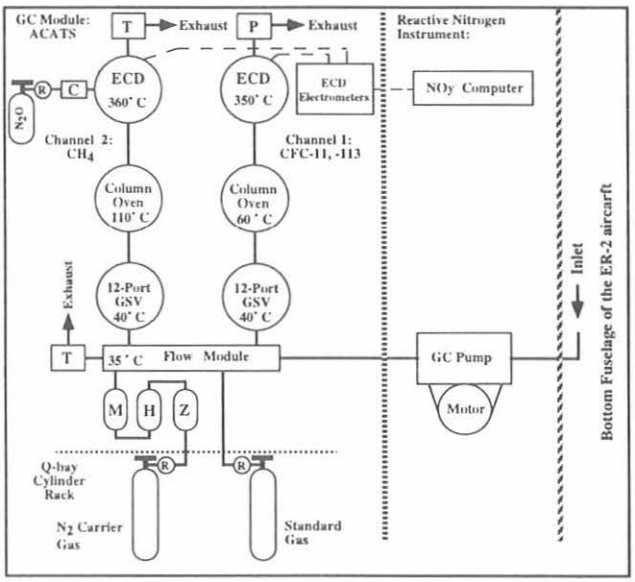

Fig. 5.18. Schematic of the ACATS. The instrument contained two separate GC channels that were used to measure CFC-11, CFC-113, and CH_4 with 180-seconds resolution. The nitrogen carrier gas was scrubbed in series through a hot zirconium (labeled Z) column (9.5 cc at 350°C) to remove CFCs, a Hopcalite (H) trap (manganese dioxide and copper oxide mixture, 40 cc at ambient temperature) to oxidize possible CO contamination of CO_2, and finally a molecular sieve (M) 13X trap (40 cc at ambient temperature). The crimped (C) tubing located after the regulator (R) of the pure (N_2O tank that delivers 20 ppm of N_2O into the ECD of channel 2. A proportional-integral-differential (PID, MKS Instruments, Massachusetts) controller (P) maintain the pressure to about 93.0 ± 0.1 kPa on the ECD of channel 1, while two pressure relief valves (T. Tavco, California) maintain separately the ECD pressure of channel 2 and the pressure of the sample loop to about 93.0 ± 0.1 kPa.

(99.999%, General Air, Colorado) and a stream selection array of solenoids that can supply either sample air or calibration gas while maintaining continuous flow throughout the flight.

The measurement technique for CH_4 was adapted from the work of *Goldan et. al.* [1982]. The advantage of this technique is that a flame, a problem for some high-altitude applications, is not required as in the flame ionization detector for detection of CH_4. An ECD can be "sensitized" to CH_4 and CO by doping the carrier gas into the detector with mixing ratios about 15-50 ppm of nitrous oxide. Pure N_2O was delivered to the CH_4 ECD through a small piece of crimped tubing into the ECD make-up flow of ~10^{-3} cm^3 min^{-1}, yielding a mixing ratio of approximately 20 ppm of N_2O in N_2 inside the ECD.

The halocarbon channel used a 1 m pre-column and a 2 m analytical column of 10% OV-101 (Analabs, Massachusetts) preconditioned at 170°C and temperature controlled at 55°C. During the course of the SPADE mission, two different column packing combinations were used on the CH_4 channel. In the first, a pre-column with a 3.2-mm o.d. and 3-m long was packed with Porapak Q (a porous polymer) was used. It was pre-conditioned at 230°C with 20-30 cm^3 min^{-1} N_2 flow for about 8 hours. The main column of 3.2-mm o.d. by 3-m was packed with molecular sieve, conditioned always to 350°C. Unfortunately, Porapak Q produced CO at temperatures above 50°C. At 100°C, mixing ratios in excess of 500 ppb of CO were found. In the second combination, a pre-column (3.2-mm o.d. by 3-m long) packed with silica gel and was preconditioned at 350°C with 20-30 cm^3 min^{-1} N_2 flow did not produce any detectable CO (>26 ppb). This pre-column was temperature controlled at 50°C with a backflush flow of 100 cm^3 min^{-1} maintained by a differential pressure flow controller (Model VCD-1000, Porter Instruments, Pennsylvania). The main column was increased to 4.8 mm o.d., with a flow controlled at 60 cm^3 min^{-1} by a mass flow controller (Model FC-260, Tylan Corp., California), and a constant temperature of 105°C. To maintain constant detector sensitivity, the ECD housing was purged with a 3 cm^3 min^{-1} flow rate of pure N_2, operated at a constant current of 1 nA, and were pressure controlled at 93 kPa. The temperatures of the ECDs on the halocarbon and CH_4/CO channels were controlled with an Omega (Stamford, Connecticut) temperature controller (Model CN9000A) at 350°C and 360°C, respectively.

Every fifth sample injection was a multi-component standard with 600 ppb of CH_4, 57 ppt of CFC-113, and 130 ppt of CFC-11. This yielded a single-point calibration every 15 minutes during a flight. Using calibrated secondary standards from the Carbon Cycle Division of CMDL in ground based checks [*Dlugokencky et al.*, 1994], showed that the calibration curve was linear for CH_4 but had a large positive intercept of ~400 ppb as a result of interference from the oxygen peak of the sample. Thus the single-point calibration standard of 600 ppb was not sufficient to establish the calibration curve for CH_4. Values of CH_4 measured by ACATS in the troposphere were calibrated by using a correlation of CH_4 versus CFC-11 measurements [*Elkins et al.*, 1993; *Dlugokencky et al.*, 1994] from the CMDL cooperative flask station at Niwot Ridge, Colorado (40.05°N, 105.59°W, altitude 3472 m). The station resides in the midtroposphere at nearly the same latitude as Moffett Field, California (37°N, altitude 30 m). The calibration scales for CFC-11 and CFC-113 were established by comparing the instrumental response to the gravimetric standards prepared by similar techniques described in *Novelli et al.*, [1991]. The stability of the CFC-11 scale is described in *Elkins et al.*, [1993].

The other measurements used here are described in the following: from the ATLAS tunable diode laser (TDL) spectrometer [*Lowenstein et al.*, 1990, 1993] from the ALIAS TDL spectrometer [*Webster et al.*, 1994]; from the Harvard Lyman α/OH fluorescnce instrument [*Hinsta et al.*, 1994]; from balloonborne frost-point hygrometers [*Oltmans*, 1985]; and H_2O from the AL Lyman α/OH fluoroescene instrument [*Kelly et al.*, 1989]. The sampling of these instruments is typically 1 Hz. For use here, the data were averaged for 20 seconds before each ACATS sample, except for ATLAS N_2O that was averaged for 10 seconds. As a comparison, the AASE-II measurements CFC-11 and -113 from ACATS are included here. The AASE-II measurements and their correlation are discussed in *Woodbridge et al.*, [1995]. Measurements of CH_4 collected from flask samples using the Whole Air Sampler during AASE-II are also included [*Schauffler et al.*, 1993].

Results

During SPADE, ACATS provided measurements of CFC-11 on ten flights (November 9 and 12, 1992; April 30, May 1, 3, 6, 7, 12, 14, and 18, 1993, 1215 data points) of CFC-113 on nine flights (November 12, 1992; April 30, May 1, 3, 6, 7, 12, 14, and 18, 1993, 1117 points), and CH_4 on eight flights (April 30, May 1, 3, 6, 7, 12, 14, and 18, 1993, 970 points).

Perhaps the most interesting individual flight during the SPADE campaign was that of May 7, 1993 (see Figure 5.19). The ER-2 ascended to a cruising altitude of about 20 km (7.5 kPa) and operated in racetrack patterns such that the plane sampled the same locations several times. Three distinct levels of mixing ratios can be seen in the ACATS data. Ambient tropospheric levels of CH_4 and CFC-11 are observed during the ascent and descent. During the ascent the high CH_4 measurements (CH_4 > 1.80 ppm) were attributed to polluted air above the San Francisco Bay area. Midlatitude and polar stratospheric vortex mixing ratios were measured during the main portion of the flight. The higher mixing ratios (CH_4 ~1.40 ppm and CFC-11 ~140 ppt), immediately following the ascent and

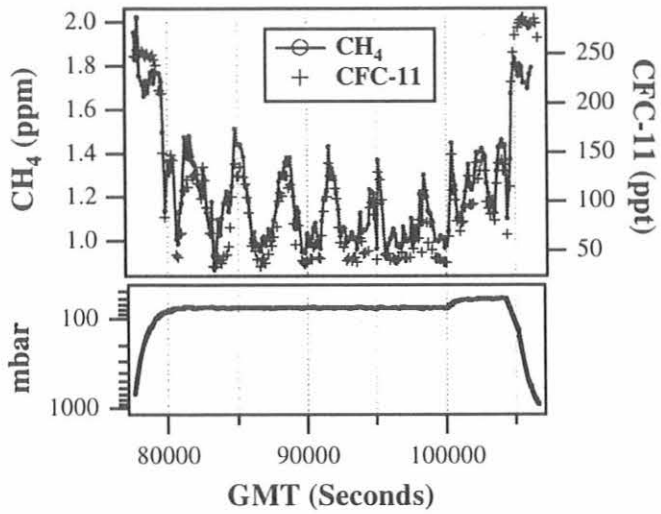

Fig. 5.19. ACATS CH_4 and CFC-11 mixing ratios measured during the flight of May 7, 1993, with accompanying pressure profile. Tropospheric measurements were observed on the ascent and descent. Two distinct air pacels with constant mixing between the air parcels were encountered in the lower stratosphere (20 km, about 7.5 kPa) as the plane repeatedly circled through the same location.

throughout the constant altitude portion of the flight, are typical of midlatitude lower stratospheric air. Similar mixing ratios were measured throughout the SPADE campaign (see Figure 5.20 for complete ACATS SPADE data) and AASE-II. The low mixing ratios (CH_4 < 1.00 ppm and CFC-11 < 50 ppt) are levels consistent with polar vortex air measurements made during AASE-II. The polar air parcel was located near the Pacific coast (north of 37°N and west of 123.75°W) and was encountered eight separate times.

Comparison of the ACATS tracers measured during AASE-II and SPADE shows that the May 7 flight does not obey the same correlations as the remaining data, especially the CFC-11 data (Figure 5.20). This flight exhibits a breakdown in slope equilibrium where mixing between the two air parcels has not had enough time to mix along global mixing ratio isopleths. Since there is mixing between two distinctly different air parcels, a linear fit intersects the original correlation at two points, namely the initial midlatitude and polar air mixing ratios.

Figure 5.20 shows the various SPADE correlations between the long-lived tracers and the May 7 flight displayed with a plus (+) symbol. The thick, solid lines are least-square fits to the combined data sets from AASE II and SPADE: the fit spans only the range of measured mixing ratios. The two missions can be usefully combined since there was only a short time span between the missions, growth rates of the species in the stratosphere have not changed significantly, and the missions were conducted at comparable latitudes. Drawing a linear fit through this flight (excluding the tropospheric values), the initial polar vortex CFC-11 mixing ratio can be inferred as 11 ± 5 ppt, CFC-113 as 8 ± 8 ppt, CH_4 as 870 ± 50 ppb, and N_2O as 90 ± 10 ppb. These mixing ratios are indicative of higher stratospheric air that has gone through vertical descent over the polar region, typical of values seen during AASE-II.

The correlations of CFC-11 versus N_2O and CH_4 are the most affected and may be related to the relative lifetimes of the tracers. The linear portion of the correlation plots in Figure 5.20, excluding data from May 7, can be used to calculate the stratospheric lifetime of the species, if slope equilibrium is obeyed and the ratio of the gradients of the species are nearly constant (a necessary condition for linearity) [*Plumb and Ko*, 1992]. Potential temperature (θ) values below 430 K were excluded to filter tropospheric values from the data. Using the arguments of *Plumb and Ko* [1992] for calculating steady-state lifetimes the linear relationship between two tracers can be expressed as:

$$\tau_1/\tau_2 = (\sigma_1/\sigma_2)(d\sigma_2/d\sigma_1) \qquad (1)$$

where τ_1 and τ_2 are the stratospheric lifetimes as defined as the mass of the compound in the total atmosphere divided by the stratospheric loss, σ_1 and σ_2 are mixing ratios of specie 1 and 2, and $d\sigma_2/d\sigma_1$ is the the slope of the linear correlation between the species. Since the growth rates of CFC-11 [*Elkins et al.*, 1993] and CH_4 [*Dlugokenesky et al.*, 1994] have decreased to near zero, and the growth rate of N_2O is small (0.2-0.3% yr^{-1}), steady state can be assumed.

The fit through the CH_4 and CFC-11 correlation (containing 1013 points) is σ_{CH_4} (ppm) =(0.0029 ± 0.0001)*$\sigma_{CFC\text{-}11}$(ppt) + (1.02 ± 0.01), where σ_{CH_4} and $\sigma_{CFC\text{-}11}$ are the mixing ratios of each tracer. CFC-11 has no significant tropospheric sink. The stratospheric lifetime is equivalent to the atmospheric lifetime estimated to be 55 ± 8 years [*Elkins et. al.*, 1993]. The CFC-11 lifetime is the best known of all tracers measured during SPADE, because the industrial emissions are known to better than ±5% and because an extensive set of worldwide measurements exists for CFC-11. The calculated stratospheric CH_4 lifetime is then 129 ± 20 years and compares well with the lifetime of 147 years estimated by *WMO* [1991]. The large uncertainty in the calculations is proportionally divided between the uncertainty in the CFC-11 lifetime, mass of the atmosphere, the uncertainty in the mixing ratios, and a small contribution from the error in the slope.

Nitrous oxide was used as a stratospheric tracer because of its long lifetime and relatively small growth rate. The most reliable and consistent N_2O data from the AASE-II and SPADE campaigns was provided by the ATLAS instrument [*Loewenstein et al.*, 1993]. Using CFC-11 as a lifetime standard in eq. 1 and the asymptotic linear slope near the tropopause, [σ_{N_2O} (ppb) = 0.662 ± 0.006) $\sigma_{CFC\text{-}11}$ + (143.7 ± 0.7) 2100 points] a stratospheric lifetime of 106 ± 16 years was calculated.

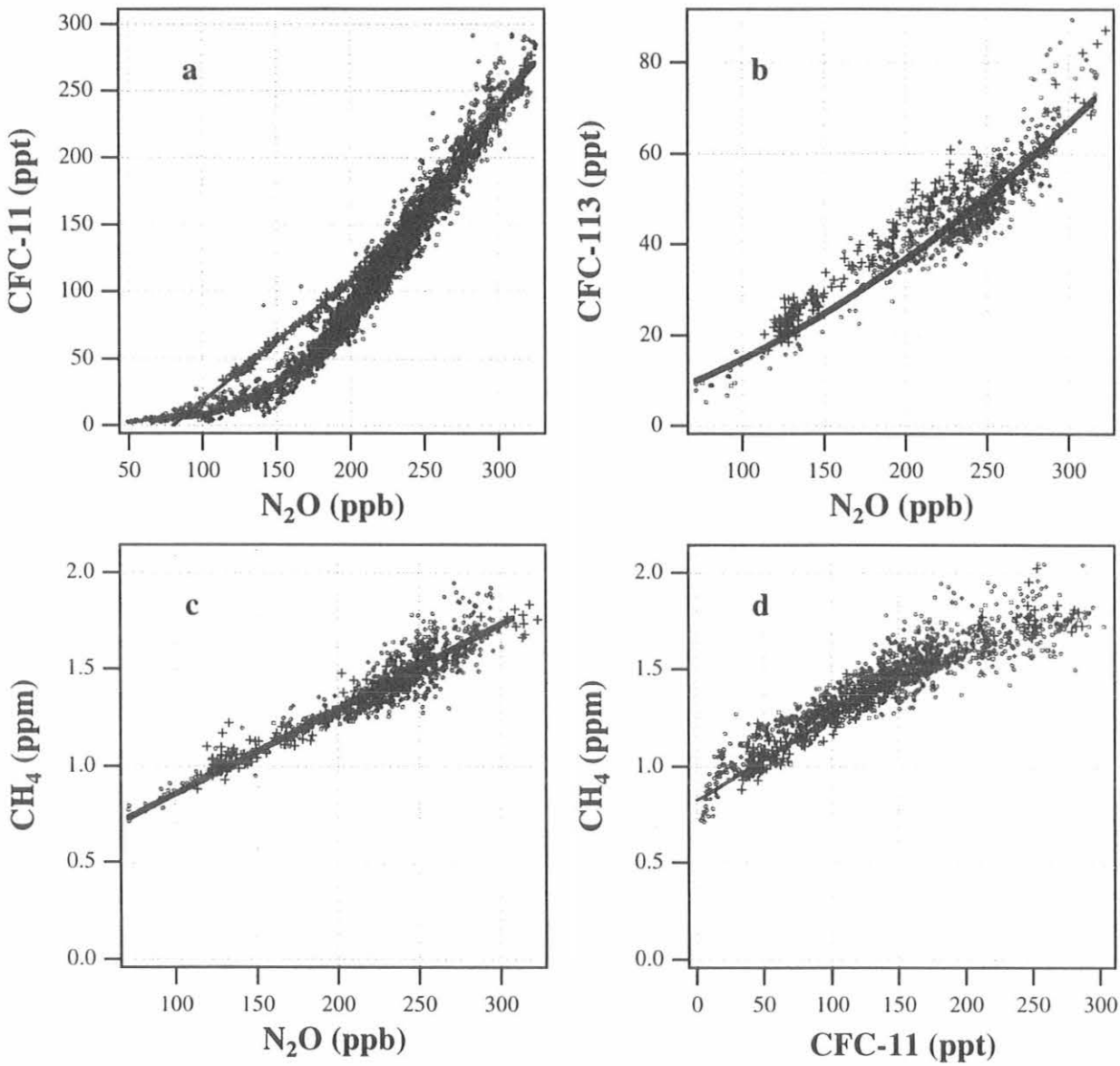

Fig. 5.20. Correlations between ACATS species for (*a*) CFC-11, (*b*) CFC-113, (*c*) CH_4 versus ATLAS N_2O, and (*d*) ACATS CH_4 versus ACATS CFC-11. The squares (□) are data for all of the ACATS SPADE flights excluding May 7, 1993, which are shown as the pluses (+). The solid lines are least squares fits through the same species by combining data from the AASE-II and SPADE missions. Both Figures 5.20*a* and *d* show considerable deviation, with respect to the flight on May 7, from the combined mission fit. This is probably the result of rapid mixing between two distinct air parcels originating from the midlatitudes and the polar regions.

Since there are no significant tropospheric sinks for N_2O, this value is also equal to the atmospheric lifetime. In contrast, higher estimates are reported yielding 132 years and 170 years by *WMO* [1991] and by *Prinn et al.*, [1990] respectively, where the latter use inverse method calculations and global tropospheric data from N_2O. Based on new absorption cross sections for O_2 in the Schumann-Runge band, *Ko et al.*, [1991] calculate an atmospheric lifetime of 110 years using vertical profiles of N_2O from satellites and *Minschwaner et al.*, [1993] calculate a lifetime of 123 ± 20 years from balloon measure-ments. These results are in support of the more recent, shorter lifetime estimates.

During the SPADE campaign, both ACATS and the TDL spectrometer, ALIAS [*Webster et al.*, 1994], were measuring CH_4. A comparison between the two measurements for θ>430 K, gives a fit ALIAS σ_{CH_4} (ppm) = (0.86 ± 0.04) * ACATS σ_{CH_4} + (0.03 ± 0.03)(ppm) (r^2 = 0.8516), where the average residual standard deviation of the fit is 0.1 ppm. This discrepancy is not within the stated experimental error limits of the ALIAS (5-10%) and ACATS (7%)

instruments, and is surprising since a comparison of laboratory standards is within the errors [*Webster et al.*, 1994]. The comparison between ACATS CH_4 and CFC-11 shows tropospheric mixing ratios of the two species agree with those from the CMDL network (σ_{CH_4} = 1.75 ppm and $\sigma_{CFC\text{-}11}$ = 270 ppt). The ALIAS data would give a considerably lower value of 1.52 ppm for tropospheric CH_4. Since ALIAS relies on spectroscopic parameters for calibration and not in-flight calibration, an error in either the line strength or air-broadening coefficients could be responsible for this difference. Therefore, the ACATS values were used for CH_4 for this work.

The dominant sink for stratospheric CH_4 is from oxidation by the hydroxyl radical (OH) [see *Le Texier et al.*, [1988]). As CH_4 is oxidized, both H_2O and H_2 are produced. Molecular hydrogen is subsequently oxidized to H_2O. The rate and efficiency at which CH_4 oxidizes and the rate the remaining H_2 is oxidized lends to the production efficiency of H_2O from CH_4. In the midlatitude lower stratosphere, H_2 is produced more rapidly than H_2O and the rate at which H_2 oxidizes is slower than the CH_4 rate. Thus, the H_2 oxidation is not concurrent with CH_4 oxidation, leading to a local H_2O production expressed as dH_2O/dCH_4 of less than 2.0. Mixing with dehydrated air (occurs more often in the southern hemisphere) and mixing with low water vapor air parcels can also yield a lower production. Figure 5.21 shows three different H_2O measurements: Harvard H_2O measurements on the ER-2 aircraft, AL measurements on the ER-2 aircraft, and CMDL measurements on balloons at a nearby location, Crow's Landing, California, plotted against ACATS CH_4 conducted during SPADE. The slope of each line gives the production that ranges from -0.8 ± 0.4 for the CMDL H_2O measurements, -1.34 ± 0.04 for AL H_2O measurements, and -1.77 ± 0.04 for the Harvard H_2O measurements. The difference between the production of H_2O cannot be the result of the CH_4 measurements since ACATS agrees well with previous CH_4 measurements of Whole Air Sampler [*Schauffler et al.*, 1993] versus AL H_2O during AASE-II (Figure 5.21). Correlation of ALIAS CH_4 with Harvard H_2O yields a slight increase in the production of H_2O (-2.28 ± 0.04) that is higher than the theoretical value at this altitude [*Le Texier et al.*, 1988]. While arguments were made by *Dessler et al.* [1994] that the production should be near 2, the absolute value of Harvard H_2O is also higher than the two other H_2O measurements.

Conclusions

Slope equilibrium is generally obeyed in the polar regions and midlatitudes at the altitudes (0-21 km) covered by the ER-2 aircraft. An exception occurs after the breakup of the polar vortex and its subsequent mixing with the midlatitudes when quasi-horizontal mixing is not fast enough to establish the original slope equilibrium. If the lifetime of one tracer is much less than the lifetime of the second tracer, a new slope on the cross-plot is established that is maintained by conservative mixing between the two air parcels. If the application of CFC-11 as a stratospheric lifetime standard is valid and slope equilibrium is obeyed, then based on the measurements presented here, the calculated lifetime of N_2O is shorter (106 ± 16 years) than previously estimated (150-170 years) by examining tropospheric N_2O budgets. Unless an unknown tropospheric sink exists, there could be large missing sources as high as 50% of the total N_2O source that remain unaccounted for in the inventory of sources.

5.2.2. Automated Four-Channel Field Gas Chromatographs

The NOAH Division continued to build and test the newest generation of four-channel GCs. These instruments are designed to make frequent, automated measurements of radiatively important and halogenated trace gases. The deployment of four-channel GCs at existing CMDL observatories (BRW, MLO, SMO, and SPO), the NWR cooperative site, and new field sites at WITN tower (North Carolina), Harvard Forest (Massachusetts), and Alert, Canada, will expand both the geographical coverage of trace gas monitoring and the number of species measured.

Features

Much of the technology found in the new generation of field GCs has evolved through the development of compact, lightweight, automated GCs for in situ trace gas analysis aboard the ER-2 aircraft. Thus, the field GCs are very compact and modular with each channel having its own 12-port gas sampling valve, chromatographic column pair, ECD, and electrometer. If a component requires maintenance or repair, it can effectively be removed and replaced without disrupting measurements on the other channels.

The control and acquisition software for the instrument runs on a conventional IBM-compatible personal computer with a 80486 CPU. The control and data acquisition hardware within the GC consists of a 96-channel analog-to-digital (A/D) board, a digital I/O board, and a dedicated four-channel A/D board for logging ECD signal data. The run program includes on-screen display of chromatograms and pertinent engineering data such as component and zone temperatures, sample loop flow rate and pressure, carrier gas flow rates, carrier gas and calibration gas tank pressures, and the relative humidity of the sample stream. A new and extremely useful feature of the run program is the real-time integration of peaks, which permits a "quick look" at data and aids in troubleshooting.

Using an eight-port stream selection valve, several ambient air streams and calibration gas flows can be sampled and analyzed in a user-defined sequence. Ambient air streams are dried through Nafion tubing to

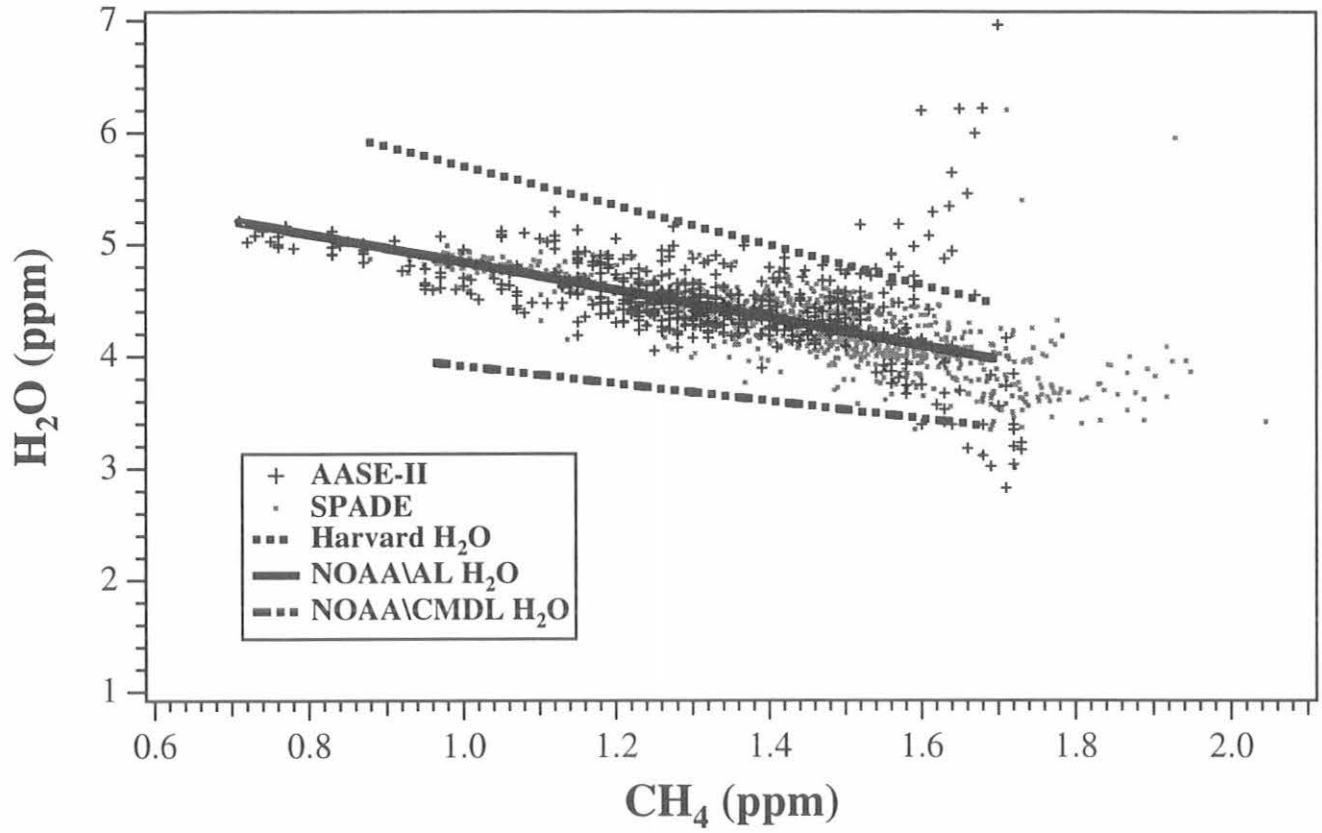

Fig. 5.21. Methane and water vapor correlations can be used to estimate the production efficiency at which CH_4 is oxidized to H_2O. The solid line is a linear fit (y = -1.24*x + 6.08) through the combined AASE-II (+) and the SPADE (•) missions over the range CH_4 <1.7 ppm. The absolute value of the slope is the production efficiency. The top dashed line is a similar fit (y = -1.77*x + 7.45) using the SPADE Harvard H_2O. The bottom dashed line is y = -0.8x + 4.7 for ACATS CH_4 versus CMDL H_2O.

a dewpoint of -25°C before analysis. The four sample loops are pressure-controlled using a pressure sensor and valve feedback system.

Each column pair, ECD, mass flow controller and sample loop is isothermally maintained by proportional, integral, derivative algorithm temperature controllers. Temperature data are logged to disk by an RS-485 loop between the temperature controllers and the computer, and controller setpoints can be changed from the keyboard. Column pairs and ECDs are encapsulated in well-insulated, cylindrical ovens 13 cm in diameter and 18 cm high that provide excellent temperature stability (1 s.d., ± 0.1°C).

There are currently five possible channels for implementation in these four-channel automated gas chromatographs. The more pertinent chromatography parameters for each channel are listed in Table 5.3. These include column dimensions (o.d. × length) and packing materials, sample loop sizes, special detection methods employed (if any), species measured, and the precision of measurement of each specie at its mixing ratio in high-pressure tanks of Niwot Ridge air.

Work will begin in 1994 to utilize the sample loop pressure control for "pressure-calibrations," the injection of different pressures of a calibration gas to generate calibration curves. Pressure-calibration curves show little nonlinearity over a pressure range of 15% (90% to 105% of a given setpoint). If satisfactory results can be obtained through this method, the need for having several calibration tanks at a given site will be eliminated.

TABLE 5.3. Pertinent Chromatography Parameters for Each Channel of New Automated Field GC, Species Measured, and Precision of Measurements

Parameter	Description
	Channel 1
Precolumn	3.175 mm × 2.0 m unibeads 1S
Main column	3.175 mm × 4.0 m molecular sieve 5A
Sample size	5 cm^3
Detector	N_2O-doped ECD
Species measured:	*Precision:*
H_2	0.6%
CH_4	0.4%
CO	1.0%
	Channel 2
Precolumn	3.175 mm × 1.5 m unibeads 2S
Main column	3.175 mm × 2.5 m unibeads 2S
Sample size	2.5 cm^3
Detector	ECD
Species measured:	*Precision:*
CFC-12	0.2%
CFC-11	0.2%
CFC-113	2.8%
	Channel 3
Precolumn	3.175 mm × 2.0 m OV-101 (20%)
Main Column	3.175 mm × 5.0 m OV-101 (20%)
Sample size	5.0 cm^3
Detector	ECD
Species measured:	*Precision:*
CFC-11	0.2%
CFC-113	0.5%
Chloroform	5%
Methyl chloroform	0.5%
Carbon tetrachloride	0.5%
Trichloroethylene	Unknown
Perchloroethylene	1.5%
	Channel 4
Precolumn	4.7625 mm × 2.0 m Porapak Q
Main Column	4.7625 mm × 3.0 m Porapak Q
Sample size	15.0 cm^3
Detector	ECD
Species measured:	*Precision:*
N_2O	0.2%
SF_6	1.2%
	*Channel 5**
Trap no. 1	3.175 mm × 0.040 m unibeads 1S
Trap no. 2	3.175 mm × 0.024 m Porapak Q
Precolumn	3.175 mm × 0.5 m unibeads 2S
Main column	3.175 mm × 1.0 m unibeads 2S
Sample size	40.0 cm^3
Detector	O_2-doped ECD
Species measured:	*Precision:*
HCFC-22	2.8%

*Samples are first pre-concentrated on trap no. 1 cooled to -50°C. Species of interest are desorbed from this trap by heating to 110°C, then are focused on trap no. 2 cooled to -50°C. Trap no. 2 is rapidly heated to 110°C just prior to injection.

5.3. REFERENCES

AFEAS (Alternative Fluorocarbons Environmental Acceptability Study), *Historic production, sales and atmospheric release of HCFC-142b*, Washington, D.C., USA, 1994.

Braker, W., and A.L. Mossman, *Matheson Gas Data Book*, Sixth Edition, 711 pp., Matheson Gas Products, Secaucus, NJ, 1980.

Butler, J.H., J.W. Elkins, B.D. Hall, S.O. Cummings, and S.A. Montzka, A decrease in the growth rates of atmospheric halon concentrations, *Nature, 359*,403-405,1992.

Collins, J.E., Jr., G.W. Sachse, B.E. Anderson, A.J. Weinheimer, J.G. Walega, and B.A. Ridley, AASE-II in situ tracer correlations of methane, nitrous oxide, and ozone as observed aboard the DC-8, *Geophys. Res. Lett., 20(22)*, 2543-2546, 1993.

Dessler, A.E., E.M. Weinstock, E.J. Hintsa, J.G. Anderson, C.R. Webster, R.D. May, J.W. Elkins, and G.S. Dutton, An examination of the total hydrogen budget of the lower stratosphere, *Geophys. Res. Lett., 21(23)* 2563-2566, 1994.

Dlugokencky, E.J., K.A. Masarie, P.M. Lang, P.P. Tans, L.P. Steele, and E.G. Nisbet, A dramatic decrease in the growth rate of atmospheric methane in the northern hemisphere during 1992, *Geophys. Res. Lett., 21(1)*, 45-48, 1994.

Elkins, J.W., T.M. Thompson, T.H. Swanson, J.H. Butler, B.D. Hall, S.O. Cummings, D.A. Fisher, and A.G. Raffo, Decrease in the growth rates of atmospheric chlorofluorocarbons 11 and 12, *Nature, 364*, 780-783, 1993.

EPA (Environmental Protection Agency), Protection of stratospheric ozone, *Federal Register, 58*, 15,014-15,048, 1993.

Goldan, P.D., F.C. Fehsenfeld, and J.P. Phillips, Detection of carbon monoxide at ambient levels with an N_2O-sensitized electron-capture detector, *J. Chromatogr., 239*, 115-126, 1982.

Hintsa, E. J., E.M. Weinstock, A.E. Dessler, and J.G. Anderson, SPADE H_2O measurements and the seasonal cycle of stratospheric water vapor, *Geophys. Res. Lett., 21(23)*, 2559-2562, 1994.

Kawa, S.R., D.W. Fahey, L.E. Heidt, W.H. Pollock, S. Solomon, D.E. Anderson, M. Loewenstein, M.H. Proffitt, J.J. Margitan, and K.R. Chan, Photochemical partitioning of the reactive nitrogen and chlorine reservoirs in the high-latitude stratosphere, *J. Geophys. Res., 97(D8)*, 7905-7923, 1992.

Kelly, K.K., A.F. Tuck, D.M. Murphy, M.H. Proffitt, D.W. Fahey, R.L. Jones, D.S. McKenna, M. Loewenstein, J.R. Podolske, S.E. Strahan, G.V. Ferry, K.R. Chan, J.F. Vedder, G.L. Gregory, W.D. Hypes, M.P. McCormick, E.V. Browell, and L.E. Heidt, Dehydration in the lower Antarctic stratosphere during late winter and early spring, 1987, *J. Geophys. Res., 94*, 11,317-11,357, 1989.

Ko, M.K.W., N.D. Sze, and D.K. Weisenstein, Use of satellite data to constrain the model-calculated atmospheric lifetime for N_2O: Implications for other trace gases, *J. Geophys. Res., 96(D4)*, 7547-7552, 1991.

Le Texier, H., S. Solomon, and R.R. Garcia, The role of molecular hydrogen and methane oxidation in the water vapor budget of the stratosphere, *Q.J.R. Meteorol. Soc., 114*, 281-295, 1988.

Loewenstein, M., J.R. Podolske, and S.E. Strahan, ATLAS instrument characterization: Accuracy of the AASE and AAOE nitrous oxide data sets, *Geophys. Res. Lett., 17*, 481-484, 1990.

Loewenstein, M., J.R. Podolske, D.W. Fahey, E.L. Woodbridge, P. Tin, A. Weaver, P.A. Newman, S.E. Strahan, S.R. Kawa, M.R. Schoeberl, and L.R. Lait, New observations of the NO_y/N_2O correlation in the lower stratosphere, *Geophys. Res. Lett., 20(22)*, 2531-2534, 1993.

Minschwaner, K., R.J. Salawitch, and M.B. McElroy, Absorption of solar radiation by O_2: Implications for O_3 and lifetimes of N_2O, $CFCl_3$, and CF_2Cl_2, *J. Geophys. Res., 98(D6)*, 10,543-10,561, 1993.

Montzka, S.A., J.W. Elkins, J.H. Butler, T.M. Thompson, W.T. Sturges, T.H. Swanson, R.C. Myers, T.M. Gilpin, T.J. Baring, S.O. Cummings, G.A. Holcomb, J.M. Lobert, and B.D. Hall, in *Climate Monitoring and Diagnostics Laboratory No. 20: Summary report 1991*, pp. 60-81, edited by E.E. Ferguson and R.M. Rosson, NOAA Environmental Research Laboratories, Boulder, CO, 1992.

Montzka, S.A., R.C. Myers, J.H. Butler, J.W. Elkins, and S.O. Cummings, Global tropospheric distribution and calibration scale of HCFC-22, *Geophys. Res. Lett., 20*, 703-706, 1993.

Montzka, S.A., R.C. Myers, J.H. Butler, and J.W. Elkins, Early trends in the global tropospheric abundance of hydrochlorofluorocarbon-141b and -142b, *Geophy. Res. Lett., 21(23)*, 2483-2486, 1994*a*.

Montzka, S.A., R.C. Myers, J.H. Butler, J.W. Elkins, and S.O. Cummings, Atmospheric measurements of HCFC-22 at the South Pole, *Ant. J. U. S., 28(5)*, 267-269, 1994*b*.

Novelli, P.C., J.W. Elkins, and L.P. Steele, The development and evaluation of a gravimetric reference scale for measurements of atmospheric carbon monoxide, *J. Geophys. Res., 96(D7)*, 13,109-13,121, 1991.

Oltmans, S.J., Measurements of water vapor in the stratosphere with a frostpoint hygrometer, *Proceedings of 1985 International Symposium on Moisture and Humidity*, pp. 251-258, Instrument Society of America, Washington, DC, 1985.

Plumb, R.A., and M.K.W. Ko, Interrelationships between mixing ratios of long-lived stratospheric constituents, *J. Geophys. Res., 97*, 10,145-10,156, 1992.

Pollock, W.H., L.E. Heidt, R.A. Lueb, J.F. Vedder, M.J. Mills, and S. Solomon, On the age of stratospheric air and ozone depletion potentials in polar regions, *J. Geophys. Res., 97(D12)*, 12,993-12,999, 1992.

Prather M., and C.M. Spivakovsky, Tropospheric OH and the lifetimes of hydrochlorofluorocarbons, *J. Geophys. Res., 95(D11)*, 18,723-18,729, 1990.

Prinn, R., D. Cunnold, R. Rasmussen, P. Simmonds, F. Alyea, A. Crawford, P. Fraser, and R. Rosen, Atmospheric emissions and trends of nitrous oxide deduced from 10 years of ALE-GAGE data, *J. Geophys. Res., 95(D11)*, 18,369-18,385, 1990.

Schauffler, S.M., L.E. Heidt, W.H. Pollock, T.M. Gilpin, J.F. Vedder, S. Solomon, R.A. Lueb, and E.L. Atlas, Measurements of halogenated organic compounds near the tropical tropopause, *Geophys. Res. Lett., 20(22)*, 2567-2570, 1993.

Schauffler, S.M., W.H. Pollock, E. L. Atlas, L.E. Heidt, and J.S. Daniel, Atmospheric distributions of HCFC-141b, *Geophys. Res. Lett.*, in press, 1995.

Solomon, S., and D. Albritton, Time-dependent ozone depletion potentials for short- and long-term forecasts, *Nature, 357*, 33-37, 1992.

Solomon, S., M. Mills, L.E. Heidt, W.H. Pollock, and A.F. Tuck, On the evaluation of ozone depletion potentials, *J. Geophys. Res. 97(D1)*, 825-842, 1992.

Steele, L.P., P.J. Fraser, R.A. Rasmussen, M.A.K. Khalil, T.J. Conway, A.J. Crawford, R.H. Gammon, K.A. Masarie, and K.W. Thoning, The global distribution of methane in the troposphere, *J. Atmos. Chem., 5*, 125-171, 1987.

Swanson, T.H., J.W. Elkins, J.H. Butler, S.A. Montzka, R.C. Myers, T.M. Thompson, T.J. Baring, S.O. Cummings, G.S. Dutton, A.H. Hayden, J.M. Lobert, G.A. Holcomb, W.T. Sturges, and T.M. Gilpin, in *Climate Monitoring and Diagnostics Laboratory No. 21: Summary report 1992*, 59-75, edited by J.T. Peterson and R.M. Rosson, NOAA Environmental Research Laboratories, Boulder, CO, 1993.

UNEP (United Nations Environment Programme), *Montreal Protocol 1991 Assessment: Report of the Technology and Economic Assessment Panel*, December, 1991.

UNEP (United Nations Environment Programme), *Montreal Protocol 1993 Report of the Technology and Economic Assessment Panel*, July 1993.

Webster, C.R., R.D. May, C.A. Trimble, R.G. Chave, and J. Kendall, Aircraft laser infrared absorption spectrometer (ALIAS) for in situ stratospheric measurements of HCl, N_2O, CH_4, NO_2, and HNO_3, *Appl. Opt., 33(3)*, 454-472, 1994.

Woodbridge, E.L., J.W. Elkins, D.W. Fahey, L.E. Heidt, S. Solomon, T.J. Baring, T.M. Gilpin, W.H. Pollock, S.M. Schauffler, E.L. Atlas, M. Loewenstein, J.R. Podolske, C.R. Webster, R.D. May, J.M. Gilligan, S.A. Montzka, K.A. Boering, and R.J. Salawitch, Estimates of total organic and inorganic chlorine in the lower stratosphere from in situ and flask measurements during AASE II, *J. Geophys. Res.*, in press, 1995.

WMO (World Meteorological Organization), Scientific assessment of ozone depletion: 1991, *WMO Global Ozone Res. and Monitoring Proj. Rep. 25*, WMO Global Ozone Research and Monitoring Project, Geneva, Switzerland, 1991.

6. Cooperative Programs

Evaluation of Arctic Meteorological Buoys

GERALD F. APPELL
NOAA National Ocean Service, Ocean Systems Development Group, Silver Spring, Maryland 20910

INTRODUCTION

The United States Interagency Arctic Buoy Program (USIABP) was formed in 1991 to establish and maintain a network of drifting meteorological buoys in the Arctic. The USIABP is a collaborative program funded by nine government agencies/ programs and managed by the National Ice Center in Suitland, Maryland. The USIABP supports the International Arctic Buoy Program (IABP) which consists of numerous countries participating in the collection of meteorological data from Arctic drifting buoys.

The buoys are located to define surface synoptic scale atmospheric pressure, air temperature, and sea-ice drift fields. The data are available in real time, via ARGOS satellite transmissions, to operational weather fore-casting centers as well as research into climate change. At the inception of the program, 25 buoys gathered temperature and pressure data in the Arctic with 72% reported on the Global Telecommunications System (GTS). In early 1994, 47 buoys were in operation with 96% reported on the GTS.

There are many different buoys used by the IABP with different sensors, configurations and sampling schemes. Many of the temperature measurements reported by the buoys were suspect when compared to atmospheric model predictions. In 1993 it was decided by the USIABP to halt deployment of new buoys until the sources of temperature measurement errors were investigated. A program was established to evaluate the available "off-the-shelf" Arctic buoy systems being used by the IABP. As part of this evaluation, a long-term test site was established at the CMDL facility in Barrow, Alaska.

THE FIELD TEST SITE

In August 1993, a Coastal Climate buoy and a DSI-TAD buoy were placed at the Barrow facility. A data acquisition system was placed at the site consisting of a Telonics ARGOS uplink receiver and a Compaq notebook computer. Buoy transmissions are received and logged on the computer. Weekly interrogations of the computer are performed from Silver Spring, Maryland, and data files are downloaded. In December 1993, a Canadian MetOcean CALIB buoy was added to the array, and in March 1994 a Norwegian ICEX buoy was placed at the site.

DATA ACQUISITION AND ANALYSIS

All buoys in the test program undergo temperature sensor calibration at the National Weather Service Test Facility in Sterling, Virginia, prior to shipment to Barrow.

Each buoy has its own measurement scheme, sampling interval, data format, and data transmission interval. Data collected in Silver Spring are processed and reduced into a standard 1-hr averaged data format. CMDL meteorological data are sent monthly for comparison with buoy data. Solar radiation data from CMDL is collected weekly via a recently established link to Internet.

Measurements are analyzed and compared to CMDL standards. Temperature differences between sensors and/or standards are analyzed to determine the effects of sensor height differences, solar radiation, and wind. Preliminary results indicate significant differences attributed to the measurement height of the sensors above the surface and to solar radiation effects.

CMDL measurements at BRW are on a tower located approximately 20 m from the buoy array. The CMDL temperature sensors are 2.5 m (BRW 2.5 m) and 15 m (BRW 15 m) above the ground. They are aspirated and kept clean of ice and snow by the staff at CMDL. Figure 1 shows temperature data from three buoys compared to the CMDL temperature standards during February 16-18, 1994. This period had winds below 5 m s^{-1} and insignificant solar radiation. The Coastal Climate buoy measures temperature at approximately the same height above the ground as the BRW 2.5-m sensor. The DSI-TAD buoy has an internal temperature sensor in a spherical hull approximately 1 m in diameter that sits on the surface. The CALIB buoy is a cylindrical buoy with an external temperature sensor that is measuring at a height of 1 m off the surface. The Coastal Climate buoy generally tracks the BRW 2.5 m sensor to within 1°C. The DSI-TAD buoy shows a strong time lag to the falling temperatures because of its internal sensor. The CALIB sensor shows lower temperatures at times when there is a vertical temperature gradient indicated by the BRW 2.5 m and

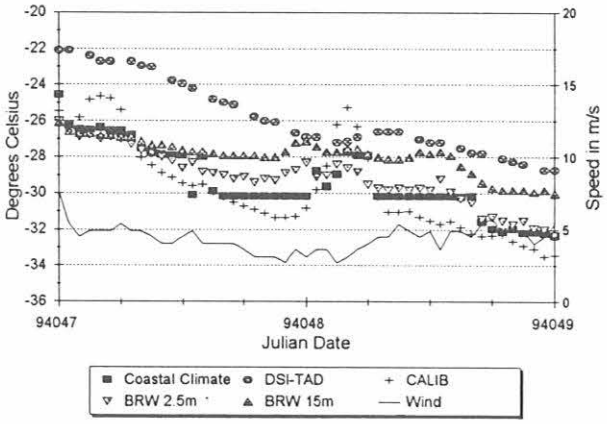

Fig. 1. Hourly-averaged temperature measurements for three buoys and the BRW standards. The BRW sensors are identified by their height, BRW 2.5 m is the sensor at 2.5 m above the ground, BRW 15 m is 15 m above the ground

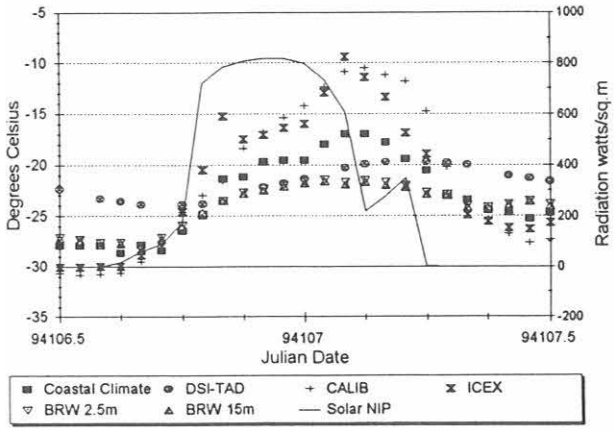

Fig. 2. Hourly-averaged temperature readings for four buoys and the BRW standards. Direct solar radiation is shown by measurements from the Normal Incidence Pyrgeometer (NIP). The effects of solar heating are depicted.

BRW 15 m sensors, showing the gradient continues to ground level.

Figure 2 shows a 24-hr period on April 17, 1994. This period shows a typical day of strong solar radiation with low temperatures and light winds. The aspirated BRW sensors show no vertical temperature gradients. The additional ICEX buoy is a spherical type buoy that sits on the surface and has an external temperature sensor at approximately 1 m above the ground. All sensors have some form of radiation shielding. The ICEX and the CALIB buoys show strong effects from solar heating while the Coastal Climate buoy does not due to a larger radiation shield. The DSI-TAD shows moderate effects with long response times.

FUTURE PLANS

It is planned to introduce one more buoy to the site in August 1994. We will also place a 3-m Rohn tower with aspirated temperature sensors at the 1-m and 2.5-m level, a solar radiation sensor, and an anemometer. These sensors will complement information on the vertical and horizontal spatial effects of the temperature field when compared to the CMDL Barrow standards. The tower will be located in the buoy array area. The site will remain until sufficient long-term data has been acquired to assess the performance of each buoy.

Global Precipitation Chemistry Program Measurements at Mauna Loa Observatory

R.S. ARTZ
NOAA Air Resources Laboratory, Silver Spring, Maryland 20910

W.C. KEENE AND J.N. GALLOWAY
University of Virginia, Charlottesville, Virginia 22903

INTRODUCTION

The Global Precipitation Chemistry Program (GPCP) was initiated in 1979 to address questions regarding the composition of precipitation chemistry prior to the advent of fossil-fuel combustion and to study the influence of sulfur and nitrogen species transported over long distances on the remote troposphere. This program was funded by the NOAA Air Resources Laboratory and was conducted in collaboration with the University of Virginia Department of Environmental Sciences and Cary Arboretum, New York. Published reports summarize progress to date [e.g., *Galloway et al.*, 1984,1992, 1994; *Keene et al.*, 1986.

METHODS

The GPCP has analyzed samples of precipitation collected at 14 land-based sites and during 12 oceanic cruises. Samples of precipitation were collected by event in scrupulously washed polyethylene containers. Immediately after collection, pH was measured, samples were treated with $CHCl_3$ to prevent biological activity, and aliquots were subsequently sent to the University of Virginia for analyses for all major organic and inorganic chemical constituents.

One of the stations of the GPCP was located at the Mauna Loa Observatory (MLO). Beginning in August of 1983, 305 event precipitation chemistry samples were collected through a cooperative venture involving CMDL MLO. The MLO data set was collected to provide complete event chemistry suitable for process-oriented studies on Hawaii. All samples were collected on an event basis using a wet-only sampling device and were discarded if they remained in the collector more than 24 hours following the cessation of precipitation. No attempt was made to collect small volume events or samples over weekends and holidays.

DISCUSSION

The high data quality coupled with complete major ion analysis and short measurement periods will allow us to address a number of questions regarding the chemical climatology of MLO. In particular, we will investigate sources for nitrogen at MLO through rigorous trajectory studies using the daily chemistry data and the ARL HY-SPLIT [*Draxler*, 1992] model. The effect of the volcano on SO_4^{-2} can be addressed with this data set. We will also assess volcanic contributions to H_2SO_4 acidity in precipitation at the site. This analysis will contribute substantially to the understanding of nitrogen and sulfur cycling in the remote marine troposphere.

The data set is currently being analyzed in conjunction with transport models and we anticipate publishing the results in a peer-reviewed journal article. Unfortunately, due to reductions in Air Resources Laboratory funding, collection and analysis of precipitation at MLO ceased in February 1994.

REFERENCES

Draxler, R.R., Hybrid Single-Particle Lagrangian Integrated Trajectories (HY-SPLIT): Version 3.0—User's Guide and Model Description, NOAA Tech. Memo., *ERL ARL-195*, Air Resources Laboratory, Silver Spring, MD, 1992.

Galloway, J.N., G.E. Likens, and M.E. Hawley, Acid precipitation: natural versus anthropogenic components, *Science, 236*, 829-830, 1984.

Galloway, J.N., H.Levy II, and P.S. Kasibhatla, Year 2020: Consequences of population growth and development on deposition of oxidized nitrogen, *Ambio, 23(2)*, 1994.

Galloway, J.N., J.E. Penner, C.S. Atherton, J.M. Prospero, H. Rodhe, R.S. Artz, Y.J. Balkanski, H.G. Bingemer, R.A. Brost, S. Burgermeister, G.R. Carmichael, J.S. Chang, R.J. Charlson, S. Cober, W.G. Ellis, C.J. FIscher, J.M. Hales, D.R. Hastie, T. Iversen, D.J. Jacob, K. John, J.E. Johnson, P.S. Kasibhatla, J. Langner, J. Lelieveld, H. Levy, II, F. Lipschultz, J.T. Merrill, A.F. Michaels, J.M. Miller, J.M. Moody, J. Pinto, A.A. Pszenny, P.A. Spiro, L. Tarrason, S.M. Turner, and D.M. Whelpdale, Sulfur and nitrogen levels in the North Atlantic Ocean's Atmosphere: A systhesis of field and modeling results, *Global Biogeochem. Cycles, 6*, 77-100, 1992.

Keene, W.C., A.A. P. Pszenny, J.N. Galloway, and M.E. Hawley, Sea-salt corrections and interpretation of constitutent ratios in marine precipitation, *J. Geophys. Res., 91*, 6647-6658, 1986.

Global Atmospheric O_2/N_2 Measurements from Isotope Ratio Mass Spectrometer Analysis

MICHAEL L. BENDER, JOHN T. ELLIS, AND MARK O. BATTLE
Graduate School of Oceanography, University of Rhode Island, Narragansett, Rhode Island 02882

INTRODUCTION

Measurement of atmospheric oxygen can provide important constraints on the global carbon cycle. When O_2 is monitored with sufficient accuracy, the monitoring is complemented with measurements of CO_2, and the observations are augmented with an atmospheric circulation model, it is possible to gain understanding about new production of organic matter in ocean surface water, the distribution of terrestrial sources and sinks of carbon, and the oceanic storage of anthropogenic CO_2 [*Keeling et al.*, 1993; *Keeling and Shertz*, 1992].

To this end, air sample collection began at BRW in December of 1992. Working in conjunction with SIO, we have also started collecting samples in SMO and from the top of the light tower at Cape Kumukahi, Hawaii (via the MLO station). Sampling at these two stations began in June of 1993. The samples collected at these CMDL stations supplement our ongoing acquisitions at Cape Grim, Tasmania; Baring Head, New Zealand; Sable Island, Canada; and Syowa, the Japanese coastal Antarctic station. The CMDL Carbon Cycle Division in Boulder, Colorado, performs the complementary measurements of carbon dioxide for all of these samples.

SAMPLING AND ANALYTIC TECHNIQUE

Samples are collected in 2-L glass flasks equipped with a pair of shaft-seal valves fitted with Viton o-rings. A small pump draws ambient air through a cold trap, drying the sample. The flask is flushed with at least 40 liters of dry air before being filled to a pressure of one atmosphere. Duplicate pairs of these flasks are collected biweekly at each site.

The O_2/N_2 ratio of air is measured using a conventional isotope ratio mass spectrometer. As with all such devices, the O_2/N_2 ratio is measured relative to some arbitrary reference. In our case, we use air collected by the CMDL Carbon Cycle Division at Niwot Ridge, Colorado, and stored in high-pressure aluminum cylinders. For use on the mass spectrometer, these cylinders are used to fill 70-L glass flasks that we refer to as working standards.

For analysis, gas from samples and standards is admitted into evacuated glass inlet lines. Each inlet is connected to the mass spectrometer by a 1-m length of fused silica tubing with an inside diameter of 25 microns. The volume of each inlet is adjustable with a manually controlled piston, allowing us to equalize the flow rates from the inlets by compensating for variation in collection pressure of the samples or depletion of the standard. The analysis of a flask consists of at least four expansions of each sample-standard comparison. Two of the expansions are carried out with one inlet-sample/inlet-standard pairing. The relationship is then reversed for the two remaining expansions. The spectrometer is configured to simultaneously measure masses 29 ($^{15}N^{14}N$) and 32 ($^{16}O_2$). This coincident measurement of the two species, along with repeated switching between the sample and working standard, and long integration times, provides a high level of analytic precision.

We have chosen to express the relative changes in the O_2/N_2 in units of "per meg." This is similar to a percent change and is mathematically defined as

$$\delta(O_2/N_2) = \left(\frac{(O_2/N_2)_{\text{sample}}}{(O_2/N_2)_{\text{standard}}} - 1 \right) \times 10^6 \quad .$$

In these units, 4.8 per meg (1/0.2095) is equivalent to 1 ppm V since O_2 is 20.95% of air by volume. The procedure outlined above gives an analytic precision of approximately 4 per meg.

RESULTS

To date, we have collected roughly 1 year of data at BRW. The values of the O_2/N_2 measurements are presented in Figure 1, where the seasonal cycle is clearly visible with an amplitude of ~170 per meg. Preliminary results from Cape Kumukahi and SMO show seasonal cycles of smaller amplitude, but with less than a full year of data available, the size is hard to quantify. Our more extended records from Tasmania and New Zealand show a seasonal amplitude of ~90 per meg. Since the seasonal cycle comes from the combined effects of the ocean biosphere, thermal

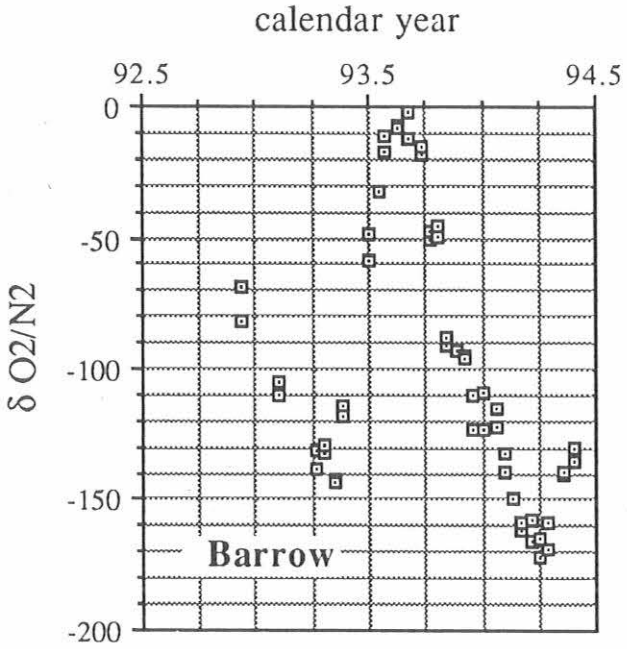

Fig. 1. The O_2/N_2 ratio as measured at the BRW station from late 1992 until mid 1994. The ratio is given as a difference (in units of per meg) from some arbitrary standard. At each point in time, two flasks are filled. The analysis of each flask's contents is shown on the plot, giving some indication of the overall reproducibility of the procedure. The seasonal cycle has an amplitude of ~170 per meg. The interannual decrease of O_2 also seems to be visible, but is not yet quantifiable.

effects at the air-sea boundary, and the terrestrial biosphere, different cycles in the northern and southern hemispheres are to be expected.

With longer records at all of the collection sites, we will be better able to constrain short-term interannual variation and the long-term consumption of O_2 due to human activities, as well as the distribution of carbon sources and sinks, terrestrial and oceanic. We look forward to the extension of this record in the coming years.

Acknowledgment. We wish to thank Dan Endres at BRW, Mark Winey at SMO, John Chin at MLO, and Duane Kitzis of the Boulder Carbon Cycle Division for the collection of the samples and standards used in this investigation.

References

Keeling, R.F. and S.R. Shertz, Seasonal and interannual variations in atmospheric oxygen and implications for the global carbon cycle, *Nature, 358*, 723-727, 1992.

Keeling, R.F., R.P. Najjar, M.L. Bender, and P.P. Tans, What atmospheric oxygen measurements can tell us about the global carbon cycle, *Global Biogeochem. Cycles, 7*(1), 37-67, 1993.

Latitudinal Profiles of Selected Trace Gases

DONALD R. BLAKE AND F. SHERWOOD ROWLAND
Department of Chemistry, University of California, Irvine California, 92717

INTRODUCTION

Atmospheric trace gas concentrations are important as both signals and agents for change during the coming decades. These changes include perturbation of the stratospheric ozone layer by chlorine atoms released in the upper atmosphere from the destruction of organochlorine compounds; exacerbation of the greenhouse effect long attributed to increasing concentrations of CO_2, and now known to involve important contributions from additional trace gases; and variations in the oxidative capacity of the global atmosphere through HO radical perturbations.

The source strengths of CFC gases such as CCl_3F (CFC-11), CCl_2F_2 (CFC-12) and CCl_2FCClF_2 (CFC-113) are known well enough to establish that the atmospheric lifetime of each exceeds 50 years, and that tropospheric losses other than diffusion to the stratosphere are of negligible importance. With negligible loss to tropospheric sinks, both CCl_3F and CCl_2F_2 serve as essentially inert tracers and have been used as calibration gases for atmospheric transport on a global scale in models ranging in sophistication from very simple one-box models to full-scale 3-D transport models.

Tropospheric HO is produced by the reaction of H_2O with $O(^1D)$ atoms released by solar ultraviolet photolysis of ozone. Atmospheric chemistry models clearly show that HO removal of hydrocarbons and hydro-halocarbons is much faster in the tropics than in polar regions. It is also more rapid during summer than winter in temperate zones.

METHOD

This research group has been monitoring the tropospheric concentrations of several halocarbons since November 1977 [*Tyler*, 1983; *Gilpin*, 1990; *Wang*, 1993] and of methane beginning early in 1978 [*Blake and Rowland*, 1988]. Since the mid 1980s measurements of carbon monoxide and numerous nonmethane hydrocarbons (NMHCs) have been added to our routine analysis [*Blake and Rowland*, 1986; *Hurst*, 1990]. Quarterly collections centered around the beginning of each season occur at approximately 40 remote land sites distributed throughout the Pacific region in the latitude range between 71°N and 47°S. The CMDL stations at Barrow, Alaska, and American Samoa are part of the sampling network. Gas chromatography utilizing either flame ionization or electron capture detection are the methods used for all sample analysis. Samples exhibiting numerous large, unidentified peaks may undergo further analysis using GC-MS detection.

RESULTS

Our CFC measurements have been useful in providing data to follow the temporal changes in the global mixing ratios and interhemispheric gradients of these important gases during periods when their production and emissions are changing [*Wang*, 1993]. Other halocarbons routinely assayed provide data critical for estimating their source and sink strengths.

To date, relatively little information has been obtained from actual atmospheric measurements of tropospheric trace gases to show the seasonal and latitudinal variations in their source and sink strengths. However, our measurements of the seasonal variations in tropospheric C_2H_6 concentrations do demonstrate a decrease by a factor of 3 from winter to summer in the northern hemisphere and by a factor of 2 in the southern hemisphere, together with a strong preference for emission in the northern hemisphere [*Blake and Rowland*, 1986]. These results are in reasonable agreement with various measurements and 3-D atmospheric models [*Rudolph et. al.*, 1989; *Kanakidou et al.*, 1991; *Penkett et. al.*, 1993].

REFERENCES

Blake, D.R. and F. S. Rowland, Continuing world-wide increase in tropospheric methane, 1978-1987, *Science, 239*, 1129-1131, 1988.

Blake D. R. and F. S. Rowland, Global atmospheric concentrations and source strength of ethane, *Nature, 321*, 231-233, 1986.

Gilpin, T.M., Global concentrations of three chlorofluorocarbons, 1984-1988, Ph.D. dissertation, 355 pp., University of California, Irvine, 1990.

Hurst, D.F., Seasonal variations in the latitudinal distribution of tropospheric carbon monoxide, 1986-1988, 267 pp., Ph.D. dissertation, Univrsity of California, Irvine 1990.

Tyler, S.C., Chlorinated hydrocarbons in the troposphere, Ph.D. dissertation, Univeristy of California, Irvine, 1983.

Wang, C.J.-L., Global concentrations of selected halocarbons, 2988-1992, Ph.D. dissertation, Uniersity of California, Ivine, 1993.

Antarctic UV Spectroradiometer Monitoring Program: Contrasts in UV Irradiance at the South Pole and Barrow, Alaska

C. R. BOOTH, T. B. LUCAS, J. R. TUSSON IV, J. H. MORROW, AND T. MESTECHKINA
Biospherical Instruments Inc., San Diego, California 92110-2621

INTRODUCTION

The Antarctic ultraviolet spectroradiometer monitoring network was established by the U.S. National Science Foundation (NSF) in 1988 in response to predictions of increased UV radiation in the polar regions. The network consists of several automated, high-resolution spectroradiometers; five are placed in strategic locations in Antarctica and the Arctic (Table 1), and one is established in San Diego to collect data and serve as a training and testing facility. The network makes essential measurements of UV spectral irradiance and provides a variety of biological dosage calculations of UV exposure. Biospherical Instruments Inc., under contract to Antarctica Support Associates (ASA), directed by NSF, is responsible for operating and maintaining the network and distributing data to the scientific community.

The spectroradiometers used in the system are Biospherical Instruments, Inc. model SUV-100. Each instrument contains an irradiance diffuser, a double-holographic grating monochromator, a photomultiplier tube, and calibration lamps. A vacuum-formed Teflon diffuser serves as an all-weather irradiance collector, and it is heated by the system to deter ice and snow accumulation. Tungsten-halogen and mercury-vapor calibration lamps are used for automatic internal calibrations of both responsivity and wavelength that occur two to four times daily. All instrument functions, calibration activities, and data acquisitions are controlled by an MS DOS-compatible computer. Further details on the spectroradiometers can be found in *Booth et al.* [1994].

UV RADIATION CLIMATE AT THE AMUNDSEN-SCOTT SOUTH POLE STATION, AND BARROW, ALASKA

The South Pole and Barrow, Alaska, installations of the network are in locations that also have CMDL installations. Therefore, the balance of this report will focus on these two sites. The South Pole site is uniquely suited to examinations of radiative transfer including the effects of ozone on UV radiation. This site is located away from the influence of mountains in a region of almost constant albedo. Cloud cover is relatively infrequent and it is generally thin when it does occur. The very small hourly change in the solar zenith angle at the South Pole supports examination of changes in total column ozone (as estimated by UV irradiance) at hourly resolution.

Barrow can be contrasted with the South Pole in that it is located where a significant change in surface albedo occurs because of both the springtime snowmelt [*Dutton and Endres*, 1991] and changes in sea-ice coverage. Also, Barrow experiences significant changes in incident irradiance because of Arctic storms. The contrast in irradiances between Barrow and the South Pole can be seen in Figure 1*b*, which depicts the integrated noontime irradiances over the UV-A spectrum (320-400 nm) from January 1992 through December 1993.

The large changes in total-column ozone encountered at the South Pole make it an ideal site to examine the relationship between ozone depletion and enhanced UV irradiance. For example, in Figure 1*a*, a substantial *decrease* is seen in the 300 nm irradiance around

TABLE 1. Installation Sites

Site	Latitude	Longitude	Established	Location
South Pole	90.00°S	0°	February 1988	Clear Air Building
McMurdo	77.51°S	166.40°E	March 1988	Arrival Heights
Palmer	64.46°S	64.03°W	May 1988	Clean Air Building
Ushuaia, Argentina	54.49°S	68.19°W	November 1988	CADIC*
Barrow, Alaska	71.18°N	156.47°W	December 1990	UIC-NARL**
San Diego, California	32.45°N	117.11°W	October 1992	Biospherical Instruments Inc.

*CADIC: Centro Austral de Investigaciones Cientificas, Argentina.
**Ukpeagvik Inupiat Corporation-National Arctic Research Laboratory

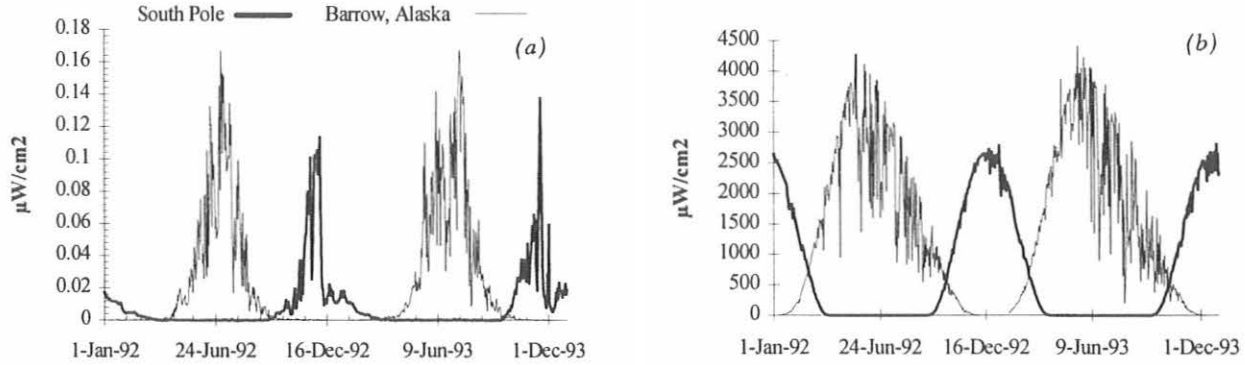

Fig. 1. Noontime irradiance at Barrow, Alaska, and the South Pole from January 1992 through December 1993. Panel *a* (left) shows the irradiance at 300 nm and is contrasted with panel *b* (right) that illustrates the integrated UV-A (320-400 nm) irradiance. The higher irradiance values at Barrow are due to the higher sun elevation. Note that the irradiances at Barrow peak in June, while the irradiances at the South Pole normally peak in December.

December 6, 1992. Meanwhile, Total Ozone Mapping Spectrometer (TOMS Nimbus-7) data report that the ozone column over the South Pole *increased* from 193 DU on December 5 to 292 DU on December 7, 1992. Similarly, a substantial *increase* in the 300 nm irradiance occurred between November 15 and November 20, 1993. As shown in Figure 2, this rise corresponded with a *decrease* of approximately 70 DU in the TOMS data.

By comparing the strongly depleted, springtime ozone levels over the Pole with the higher ozone levels observed at summer solstice, observations can be made regarding the impact of changes in ozone on UV irradiance - most other conditions (i.e., cloud cover, albedo, and solar zenith angle) being equal. Figure 2 contrasts integrated UV measurements with data from the TOMS satellite and corresponding solar zenith angles for September through December of 1993. As expected, ozone concentration and UV appear to be inversely correlated. Notice that as the season progressed toward summer solstice in December, the increase in solar angle (i.e., decrease in solar zenith angle) and small decreases in ozone resulted in a dramatic increase in UV (i.e., "radiation amplification"). Evaluation and calculation of the exact amplification factor of ozone on UV are described in *Madronich* [1993] and in *Booth and Madronich* [1994].

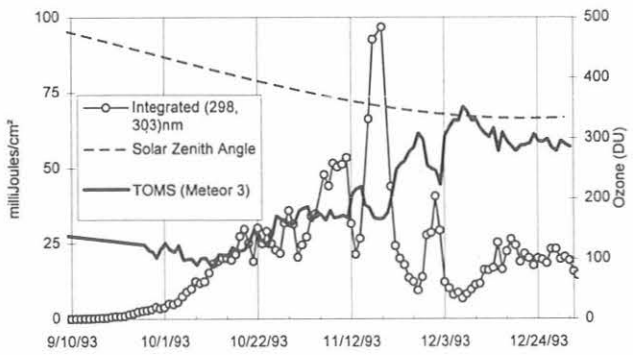

Fig. 2. Daily flux in milliJoules cm^{-2} integrated over the spectral region of 298 to 303 nm at the South Pole during the spring of 1993. Also shown is the Nimbus-7 TOMS reported total column ozone values in DU. TOMS data courtesy of Rich McPeters of GSFC, NASA.

SUMMARY

High spectral resolution scanning UV spectroradiometers were established at six sites and are successfully providing multi-year data sets. Resulting data were used to test radiative transfer models [*Lubin and Frederick*, 1990, 1991, 1992; *Lubin et al.*, 1989, 1992; and *Smith et al.*, 1991, 1992*a*, *b*, *c*], derive ozone concentrations [*Stamnes et al.*, 1990, 1991, 1992], and examine the biological impact of enhanced UV [*Lubin et al.*, 1992; *Cullen et al.*, 1992; and *Smith et al.*, 1991, 1992*b*, *c*; *Setlow*, 1974].

The data discussed here and all other data recorded by the NSF UV monitoring network are available to all qualified researchers. The data are divided into three classes. Level 1 data are in their original, uncorrected binary form and level 2 data were referenced to beginning-of-season calibration constants. These two classes are available only to NSF-sponsored researchers upon special request. Level 3 data are referenced to both beginning- and end-of-season calibration constants. These data are distributed on CD-ROM and are available to any researcher. For more information, please contact: C.R. Booth at Biospherical Instruments Inc., 5340 Riley St., San Diego, CA 92110 (Fax: (619) 686-1887, or Internet: booth@biospherical.com).

Acknowledgments. This research and monitoring activity was funded by contract A1T-M1743 from Antarctic Support Associates under the direction of Polly Penhale at the National Science Foundation, Office of Polar Programs. B. Mendonca of CMDL

assisted in providing operators and support for the installations at Barrow. R. McPeters of NASA/GSFC provided TOMS Total Ozone data for comparison purposes. TOMS Update CD-ROM is available from the National Space Science Data Center (NSSDC), Goddard Space Flight Center. Barrow operators include D. Norton (Arctic Sivumnun Ilisagvik College), D. Endres and B. Halter (CMDL). The Ukpeagvik Inupiat Corporation of Barrow provided assistance in the installation. Operators at Palmer and McMurdo were provided by ASA. Special thanks go to John Gress of ASA who has been invaluable in the operation of the network.

REFERENCES

Booth, C.R., T.B. Lucas, T. Mestechkina, J.R. Tusson IV, D.A. Neuschuler, and J.H. Morrow, *NSF Polar Programs UV Spectroradiometer Network 1991-1993 Operations Report*, 218 pp., Biospherical Instruments Inc., San Diego, CA, 1994.

Booth, C.R., and S. Madronich, Radiation amplification factors-improved formulation accounts for large increases in ultraviolet radiation associated with Antarctic ozone depletion, in *Ultraviolet Radiation in Antarctica: Measurements and Biological Effects, Antarctic Res. Series*, Vol. 62., Am. Geophys. Union, pp. 39-42, 1994.

Cullen, J.C., P.J. Neale, and M.P. Lesser, Biological weighting function for the inhibition of phytoplankton photosynthesis by ultraviolet radiation, *Science, 258*, 646-650, 1992.

Dutton, E.G., and D.J. Endres, Date of snowmelt at Barrow, Alaska, U.S.A., *Arctic Alpine Res., 23(1)*, 115-119, 1991.

Lubin, D. and J.E. Frederick, Column ozone measurements at Palmer Station, Antarctica: variations during the austral springs of 1988 and 1989, *J. Geophys. Res., 95*, 13,883-13,889, 1990.

Lubin. D. and J.E. Frederick, The ultraviolet radiation environment of the Antarctic Peninsula: the roles of ozone and cloud cover, *J. Appl. Met., 30*, 478-493, 1991.

Lubin, D., and J.E. Frederick, Observations of ozone and cloud properties from NSF ultraviolet monitor measurements at Palmer Station, Antarctica, *Ant. J. U. S., 25(5)*, 241-242, 1992.

Lubin, D., J.E. Frederick, C.R. Booth, T.B. Lucas, and D.A. Neuschuler, Measurements of enhanced springtime ultraviolet radiation at Palmer Station, Antarctica, *Geophys. Res. Lett., 16(8)*, 783-785, 1989.

Lubin, D., Mitchell, B.G., J.E. Frederick, A.D. Alberts, C.R. Booth, T.B. Lucas, and D.A. Neuschuler, A contribution toward understanding the biospherical significance of Antarctic ozone depletion, *J. Geophys. Res., 97*, 7817-7828, 1992.

Madronich, S. UV Radiation in the natural and perturbed atmosphere, in *UV-B Radiation and Ozone Depletion*, edited by M. Tevini, pp. 17-19, Lewis Pub., Boca Raton, FL, 1993.

Setlow, R.B., The wavelengths in sunlight effective in producing skin cancer: a theoretical analysis, *Proceedings of the Nat. Academy of Science*, USA, 71(9), 3363-3366, 1974.

Smith, R.C., K.S. Baker, D. Menzies, and K. Waters, Biooptical measurements from the IceColors 90 cruise 5 October-21 November 1990, *SIO 91-13*, 121 pp., Scripps Institution of Oceanography, La Jolla, CA, 1991.

Smith, R.C., B.B. Prezelin, R.R. Bidigare, D. Karentz, and S. MacIntyre, IceColors'90: Ultraviolet radiation and phyto-plankton biology in Antarctic waters, *Science, 255*, 952-959, 1992*a*.

Smith, R.C., B.B. Prezelin, K.S. Baker, R.R. Bidigare, N.P. Boucher, T. Coley, D. Karentz, S. MacIntyre, H.A. Matlick, D. Menzies, M. Ondrusek, Z. Wan, and K.J. Waters, Ozone depletion: Ultraviolet radiation and phytoplankton biology in Antarctic waters, *Science, 256*, 952-959, 1992*b*.

Smith, R.C., Z. Wan, and K.S. Baker, Ozone depletion in Antarctica: Modeling its effect under clear-sky conditions, *J. Geophys. Res., 97*, 7383-7397, 1992*c*.

Stamnes, K., J. Slusser, and M. Boden, Derivation of total ozone abundance and cloud effects from spectral irradiance measurements, *Appl. Opt., 30*, 4418-4426, 1991.

Stamnes, K., Z. Jin, J. Slusser, C.R. Booth and T.B. Lucas, Several-fold enhancement of biologically effective ultraviolet radiation levels at McMurdo Station, Antarctica, during the 1990 ozone hole, *Geophys.Res. Lett., 19*, 1013-1017. 1992.

Stamnes, K., J. Slusser, M. Bowen, C.R. Booth, and T.B. Lucas, Biologically effective ultraviolet radiation, total ozone abundance, and cloud optical depth at McMurdo Station, Antarctica, September 15, 1988, through April 15, 1989, *Geophys. Res. Lett., 17*, 2181-2184, 1990.

Examination of the Mauna Loa Robertson-Berger Meter Data for Calibration Inconsistencies

J. DELUISI
NOAA Air Resources Laboratory, Boulder, Colorado 80303

This investigation was concerned with the stability of the calibrations done by Temple University on the Robertson-Berger (R-B) meter [*Berger*, 1976] instrumentation at MLO.

A demonstration of the R-B meter stability and a demonstration of a drift in the calibration can be seen in the data obtained at MLO that is operated by CMDL. Clear skies were determined by continuous direct-sun radiometer measurements made routinely at the observatory. A Dobson instrument operated at the station supplied the total ozone data [*Komhyr et al.*, 1989]. Figure 1 is the calculated ratio of the calibrated MLO R-B meter data to the model calculated irradiance (scaled to a convenient magnitude) and Figure 2 is the ratio using the uncalibrated R-B meter data. The large variations seen in the clustered groups of points reflect calibration and instrumental problems requiring several replacements in the early part of the record, therefore, rendering the data unfit for the *Scotto et al.* [1988] analysis. Attention is called to the record after 1979; the period when the calibrated data ratio showed a downward trend of roughly 10% between 1979 and 1988. It is our understanding that *Scotto et al.* [1988] used a linear interpolation method to remove the discontinuities between calibration periods and this is why calibration jumps do not appear in the calibrated data previous to 1988. Apparently, this was not done in 1987 when an upward jump appeared. The uncalibrated data ratio showed virtually no trend, remaining remarkably uniform, and thereby demonstrating the stability of a meter and the soundness of our approach. During this period, the instrument operated without an incident that would require replacement. Considering the exceptional quality of the MLO site for viewing the sky radiation, there is no reasonable explanation for the downward trend seen in the calibrated ratio data other than a calibration error.

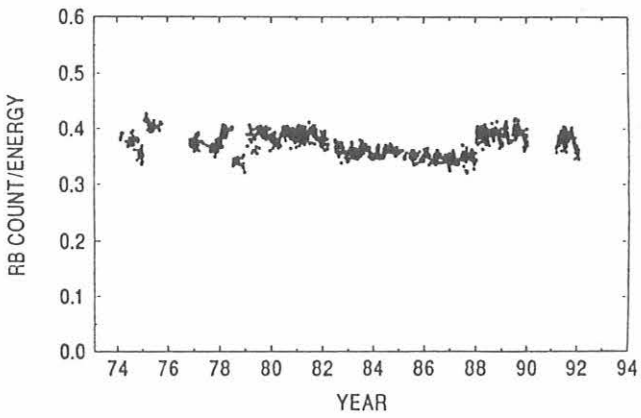

Fig. 1. Ratio of calibrated MLO R-B meter data to model calculated iradiance. The R-B meter data is the half-hour value sum 11:00-11:30 a.m. for clear days between 1974 and 1992.

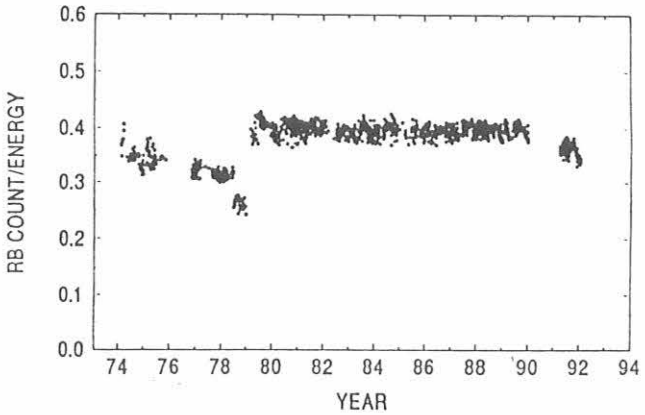

Fig. 2. Ratio of uncalibrated Mauna Loa R-B meter data to model calculated irradiance as in Figure 1.

The eruption of El Chichon occurred in the spring of 1982 and a short data gap exists near this time in the R-B meter record. Nevertheless, the ratio hardly varies after 1981 indicating little sensitivity to the stratospheric aerosol that was still significant after the data gap. The aerosol optical depth ranged between 0.1 and 0.2 or roughly 10 times greater than background [see *DeLuisi et al.*, 1989]. A maximum stratospheric aerosol optical depth of slightly more than 0.1 from El Chichon occurred over the U.S. in January 1983 [e.g., *DeLuisi et al.*, 1989]. Strong forward scattering and minimal absorption of UV radiation by the stratospheric aerosols are believed to be responsible for the UV irradiance. On the basis of this result, it seems unlikely that a significant effect would be seen over the U.S. The experience with the Mauna Loa data led us to proceed with a similar analysis of the data used by *Scotto et al.* [1988] in search of a pattern that might be attributed to possible calibration inconsistencies. A paper is being prepared summarizing the results of examining the calibrations of instruments operating in the U.S. network.

References

Berger, D., The sunburning ultraviolet meter: design and performance, *Photochem. Photobiol. 24*, 187-192, 1976.

DeLuisi, J.J., D.U. Longenecker, C.L. Mateer, and D.U. Wuebbles, An analysis of northern middle-latitude Umkehr measurements corrected for stratospehric aerosols for 1979-1986, *J. Geophys. Res., 94(D7)*, 9837-9846, 1989.

Komhyr, W.D., R.D. Grass, R.K. Leonard, Calibration of primary standard Dobson spectrophotometer No. 83 and total ozone trends at Mauna Loa Observatory, Hawaii, and American Samoa, South Pacific, in *Ozone in the Atmosphere*, edited by R.D. Bojkov and P. Fabian, 85-87, A. Deepak, Hampton, Virginia, 1989.

Scotto, J., G. Cotton, F. Urbach, D. Berger, and T. Fears, Biologically effective ultraviolet radiation: surface measurements in the United States, 1974-1985, *Science, 293*, 762-764, 1988.

Comparison of Mauna Loa Observatory And Hilo Radiosonde Meteorological Measurements

ELEANOR FOLTZ*
Kwajalin High School, Kwajalin Atoll, P.O. Box 929, APO AP 96555

INTRODUCTION

This report compares meteorological measurements taken automatically at Mauna Loa Observatory (MLO) with twice daily concurrent Hilo radiosonde measurements. Hilo is 25 km upwind of MLO. It is well known that MLO nighttime downslope winds and daytime upslope winds do not relate well to free tropospheric wind flow in the region of the Mauna Loa massive. The regular downslope winds bring nocturnal upper level air to the observatory site that allows MLO to make background atmospheric composition measurements most days of the year. Less well known is the fact that other surface meteorological measurements (such as temperature and dewpoint) may also differ considerably from free atmosphere (radiosonde) measurements at or near to the same altitude. For this study, it is assumed that both the radiosonde and MLO meteorological instruments are accurate and thus the data from each fully comparable. The MLO and Hilo radiosonde data for 1992 were acquired from the MLO data base maintained in Hilo.

MLO had an average station pressure of 680 mb during 1992. For ease of comparison, radiosonde data for the 700 mb level for 0 and 12 GMT (0200 LST and 1400 LST) soundings were compared to the MLO hourly average data for the same hours grouped by month. According to the Smithsonian Meteorological Tables, the 20 mb offset between MLO and the radiosonde data would produce a maximum temperature error of 1.5°C in dry air (i.e., cooler at MLO) and a lesser difference in wet air. One would expect little difference in humidity between MLO and the radiosondes at the same altitude and no difference in wind speed and direction due solely to the 20 mb height differential. But, the mass of the mountain and its dark color considerably distorts the MLO surface meteorological readings as shown below. This report should be considered as an early step towards quantifying and understanding some of these effects.

WIND DIRECTION

The effect of the mountain on wind direction was as previously known: air flow at MLO was northerly during the day and southerly at night, fairly independent of the free tropospheric air flow patterns (Figures 1 and 2). These results are considered a reality check and suggest that the MLO surface data was processed in a correct manner. From the radiosonde data alone it may be observed that winds were most often flowing from an easterly direction night and day, but that there are diurnal effects in the 700 mb free atmosphere winds.

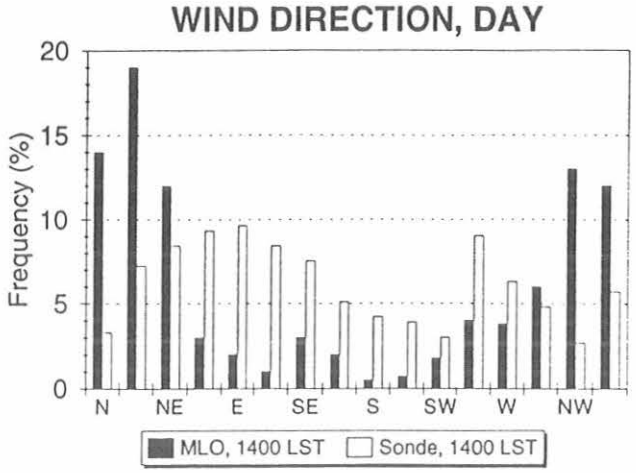

Fig. 1. Monthly average frequency of 700 mb winds measured at 1400 LST by the Hilo radiosonde in the free troposphere and the corresponding winds at MLO measured at 2 m above ground and 680 mb.

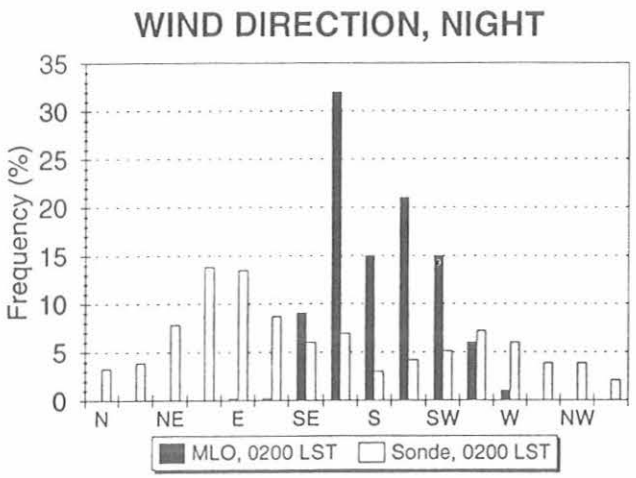

Fig. 2. Monthly average frequency of 700 mb winds measured at 0200 LST by the Hilo radiosonde in the free troposphere and the corresponding winds at MLO measured at 2 m above ground and 680 mb.

Again this is nothing new and serves more as a confirmation that the radiosonde data was acquired and processed in a reasonable manner rather than a presentation of new science.

The daytime upslope winds at MLO presented in Figure 1 (hourly average winds at 1400 LST) are mainly from the northeast through northwest that slip under the free troposphere. It is worthy of note that the free troposphere winds over Mauna Loa are not exclusively easterly in direction.

At night (Figure 2) the downslope southeast through southwest winds dominate in a narrow 90° arc with negligible winds recorded in the northeast through northwest directions at 0200 LST. Like the upslope flows, these downslope winds slip under the free tropospheric flow and rush down the mountainside passing the observatory on a regular and highly predictable pattern.

Air Temperatures

The monthly average air temperatures at 0200 and 1400 LST recorded at 2 m above the surface at MLO compared to the concurrent radiosonde measurements are presented in Figure 3. From Figure 3 it may be observed that the MLO monthly average temperatures were 2-4°C warmer at 1400 LST and 2-5°C cooler at 0200 than the temperatures of the corresponding free atmosphere. There is a small diurnal cycle in the radiosonde data with slightly higher temperatures during the day and slightly cooler temperatures at night. The higher daytime temperatures at MLO are explained by the fact that the dark lava heats up during the generally cloud-free days that occur above the temperature inversion some 1200 m below the level of MLO. This warming drives the daily upslope flows that must be warmer than the free tropospheric air or they would not be rushing up the mountain each day. Both the surface heating effects and the warm air movements combine to produce the warmer daytime temperatures at MLO.

At night, the dark lava radiates heat to the clear sky and cools the air above it. This cooling drives the nightly downslope winds as the cool, dense air flows down the mountain slope. As observed in Figure 2, these downslope winds are pervasive, thus indicating that the air is always cooler at night at the surface at MLO than in the corresponding free atmosphere.

Dewpoint Temperatures

The dewpoint temperatures at MLO (Figure 4) exhibit a pattern of higher dewpoints in the day (i.e., more moisture in the air) than at night when the dry downslope air dominates. The relatively moist (and adiabatically cooling) upslope flow indicates that air influenced by the marine boundary layer is reaching the observatory during the day. It may also be observed in Figure 2 that the daytime radiosonde dewpoint temperatures are also generally slightly higher than the nighttime values. This is to be expected as the dewpoint temperature tendencies follow temperature in conservative, non-precipitating meteorological situations.

Conclusions

Monthly average measurements of 1400 and 0200 LST wind directions, air temperatures and dewpoints at MLO are unrepresentative of the true state of the free atmosphere at the altitude of MLO. Thus, one should be cautious in using MLO surface meteorological data for climatological purposes. Follow-up studies should correct each data point for the 20 mb difference between the true air pressure at MLO and the standard

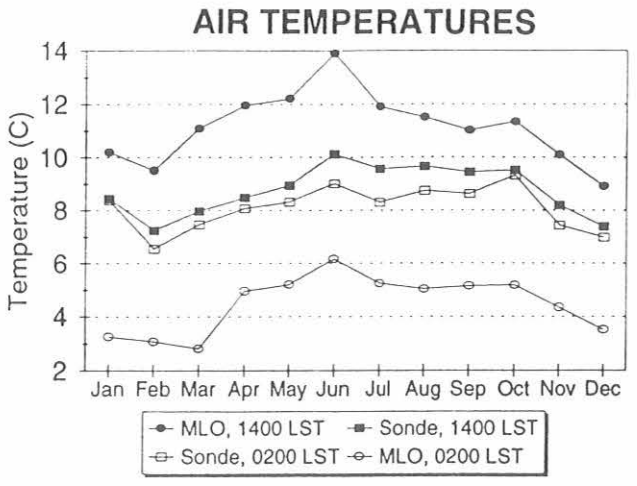

Fig. 3. Monthly average air temperatures at 0200 and 1400 LST measured by the Hilo radiosonde at 700 mb in the free troposphere and at 680 mb and 2 m above ground level at MLO.

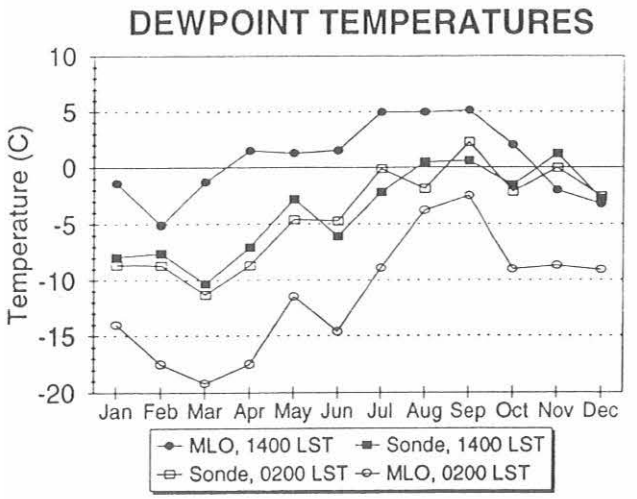

Fig. 4. Monthly average dewpoint temperatures at 0200 and 1400 LST measured by the Hilo radiosonde at 700 mb in the free troposphere and at 680 mb and 2 m above ground level at MLO.

700 mb level radiosonde data. For the purposes of the current study, this 20 mb offset did not unduly obscure nor accentuate the much larger effects on meteorology produced by the mountain's topography and physiography.

*Eleanor was a student in the 1994 Hawaii Student Science Training Program held each year at the University of Hawaii, Hilo. She conducted her 10-day off campus research project at MLO under the supervision of Drs. John Barnes and Russ Schnell. Eleanor had completed grade 11 at the time of the study and plans on entering engineering school at MIT in the fall of 1995.

Intercomparison of Stable Isotope Measurements of CO_2

R.J. FRANCEY, C.E. ALLISON, L.P. STEELE, R.L. LANGENFELDS, AND E.D. WELCH
CSIRO Division of Atmospheric Research, Aspendale, Victoria, Australia

J.W.C. WHITE AND M. TROLIER
University of Colorado, Institute of Arctic and Alpine Research, Boulder, Colorado 80309

P.P. TANS AND K.A. MASARIE
NOAA, Climate Monitoring and Diagnostics Laboratory, Boulder, Colorado 80303

INTRODUCTION

Over the last decade the two most extensive, high-precision measurement programs measuring the $\delta^{13}C$ of CO_2 [*Keeling et al*, 1989; *Whorf et al.*, 1993; *Francey et al.*, 1990] have resulted in data that have very different implications for the global carbon budget over the period [*Francey et al.*, 1995*a*]. The $\delta^{13}C$ data are primarily used to partition the uptake of fossil carbon emissions between ocean and terrestrial plant reservoirs. The requirement for high precision in these measurements was emphasized by *Enting et al.* [1993, 1994] and *Tans et al.* [1993] and the requirement for extensive spatial coverage by *Ciais et al.* [1994]. The recent advent of isotopic measurements on the extensive CMDL flask network has added stimulus for a number of improvements in the intercalibration of isotope measurement programs. This report gives preliminary results from one such program where a subset of CMDL flasks filled at Cape Grim, Tasmania, were analyzed with both CSIRO and INSTAAR mass spectrometer facilities. The results were compared to the long running CSIRO in situ CO_2 extraction program at Cape Grim [*Francey et al.*, 1995*b*].

The normal mass spectrometric measurement of $\delta^{13}C$ in atmospheric CO_2 requires the simultaneous measurement of ion currents because of three mass-to-charge ratios (m/e) at 44, 45, and 46. The m/e 46 is primarily measured so that any ^{17}O contribution to the m/e 45 can be calculated and removed in order to obtain the actual ^{13}C contribution. With some precautions, a bonus is a record of the $\delta^{18}O$ in atmospheric CO_2, a useful tracer in its own right. An explanation that described the global distribution of this species was first presented by *Tans et al.* [1986] and *Francey and Tans* [1987], and subsequently further expounded by *Farquhar et al.* [1993]. An intercomparison of the measurements of $\delta^{18}O$ in CO_2 shows considerable systematic influence, but the preliminary data are included for completeness.

METHODS

The isotopic analysis of air collected in CMDL flasks filled at Cape Grim commenced in December 1991 and still continues; data are presented for samples collected to the end of 1993. The 2.5-L glass flasks are flushed for 5 minutes at 8 L min^{-1}, then pressurized to around 0.4 bar above ambient. The air is sealed using Teflon O-ring valves. For details of the sample collection procedure for flasks in the CMDL-INSTAAR network see *Conway et al.* [1994] and associated references.

A subset of the flasks (Table 1) is routed through the CSIRO/DAR Global Atmospheric Sampling Laboratory (GASLAB) in Aspendale, where about 150 bar-mL of air is used for the duplicate determinations of CO_2, CH_4, CO, H_2, and N_2O by gas chromatography. Comparisons of results from Aspendale and Boulder for these species will be the subject of a separate report (*Steele et al.*, in preparation, 1994). An additional 30-50 bar-mL of the flask air provides $\delta^{13}CO_2$ and $\delta^{18}CO_2$ using a Finnigan MAT 252 mass spectrometer with MT Box-C accessory for the extraction of CO_2 from the air.

Flasks are then returned to Boulder, Colorado, for analysis by CMDL and INSTAAR. The CMDL Carbon Cycle Division analyzes the air for the mixing ratio of CO_2 using a non-dispersive infrared analyzer and for mixing ratios of CH_4, CO, and H_2 by gas chromatography [*Conway et al.*, 1994, *Steele et al.*, 1987, *Novelli et al.*, 1992]. The Stable Isotope Laboratory at INSTAAR uses ~700 bar-mL of the sample to determine the $\delta^{13}C$ and $\delta^{18}O$ of the CO_2 using a Vacuum Generators SIRA Series II mass spectrometer that is equipped with a "triple-trap" assembly to cryogenically separate CO_2 from the air sample (*M. Trolier et al.*, Monitoring the stable isotopic composition of atmospheric CO_2: measurements from the CMDL global network, in preparation, 1995).

TABLE 1. Annual Average and Standard Deviation of $\delta^{13}C$ for the Cape Grim In Situ Method and for Corrected GASLAB and INSTAAR Measurements

$\delta^{13}C$	In situ	GASLAB	INSTAAR
1992	-7.756	-7.759	-7.752
(n = 2)	(0.031)	(0.028)	(0.038)
1993	-7.759	-7.758	-7.765
(n = 44)	(0.030)	(0.029)	(0.044)

Calibration strategies for the mass spectrometer raw data and correction strategies for the isotopic determinations are critical considerations. This reflects the fact that the scientific requirement is for an inter-laboratory precision in average $\delta^{13}C$ values close to, or better than, the instrument internal precision on an individual analysis. In this intercomparison it was found necessary to consider the following factors: (a) the assumed isotopic composition of the primary international reference materials, (b) the methodology used to determine the isotopic composition of secondary or working standards, (c) the algorithms employed to calculate the ^{13}C and ^{17}O contributions to the m/e 45 ion beam intensity (the ^{17}O correction), (d) the constants and trace gas concentration calibration scales used in the estimation of the N_2O contribution to the m/e 44 ion beam current, (e) modification of the isotopic composition of the working standard CO_2, (f) isotopic fractionation in the extraction of CO_2 from whole air samples, and (g) mixing of sample and working standard CO_2 in the mass spectrometer ion-source region.

Points (a), (b), and (c) have recently been addressed in detail [*Allison et al.* 1994*a*,*b*, *Allison and Francey*, 1994]. Summarizing, both the CSIRO and INSTAAR mass spectrometer values were corrected using the same recommended values for the isotopic composition in the hypothetical V-PDB international isotope standard, and both laboratories have related the measured δ^{45}, and δ^{46} of samples to the primary standard by the measured δ^{45}, and δ^{46} of intermediate standards to avoid propagation of errors associated with the ion corrections. The same assumption about the relationship between ^{17}O and ^{18}O [*Craig*, 1957] is then applied in the conversion of the final ratios to $\delta^{13}C$, $\delta^{18}O$.

Point (d) uses a correction involving the ratio of N_2O/CO_2 in the sample and a relative ionization efficiency of the two gases in the mass spectrometer source [*Mook et al.*, 1983]. At DAR a relative ionization efficiency of 0.72 ± 0.01 has been measured (C.E. Allison, private communication, 1994). The CO_2 concentrations used to determine the N_2O/CO_2 ratio in the sample are the GASLAB measured values for the flask, calibrated against a suite of standards, linked in 1993 to the CMDL scale to better than 0.1 ppmv. For N_2O a nominal 310 ppbv was employed; the annual average value at Cape Grim in 1992 is estimated at 310 ppbv [*Montzka et al.*, 1993]. At INSTAAR, the relative ionization efficiency of N_2O/CO_2 has been measured at 0.754 ± 0.010 on the SIRA Series II instrument [*Gemery*, 1993]. The CO_2 mixing ratios used in the N_2O correction for each flask are the values measured by CMDL on the same flasks. The N_2O mixing ratios are approximated from global mean values determined at CMDL, taking the global mean for January 1, 1993, to be 310 ppbv, with a linear growth rate of about 0.66 ppbv yr^{-1} [*Montzka et al.*, 1992].

A typical N_2O correction to $\delta^{13}C$ is -0.2‰, and an error of 1% in N_2O or CO_2 concentration results in a $\delta^{13}C$ error of <0.003‰, considered negligible in the present case. There are potential differences because of errors in the determination of the relative N_2O/CO_2 ionization efficiency, but they are relatively small. For example, a +5% error translates into changes of -0.006‰ and -0.009‰ for $\delta^{13}C$ and $\delta^{18}O$, respectively.

Point (e), the modification of standard CO_2 during analysis, refers to a fractionation of the CO_2 gas in the standard reservoir during bleed through the capillaries or waste line. At GASLAB a fractionation of about 0.0028‰ per hour in $\delta^{13}C$ of CO_2 in the standard reservoir is measured; the effect is twice as large for $\delta^{18}O$. This is documented by *Allison et al.* [1994*a*] for the MAT252 and a correction automatically applied to the data; in practice the standard reservoir is automatically refilled every four to six samples. For the MAT252 analysis of the CMDL flask data set, the average "bleed" correction amounted to 0.011 ± 0.009‰ in $\delta^{13}C$ and 0.023 ± 0.018‰ in $\delta^{18}O$, corresponding to a mean bleed time of 3.9 hours. The correction is made implicitly at INSTAAR by measuring a working standard (whole air) at the beginning and end of every analysis run, and linearly interpolating to account for all instrument drifts. The observed drifts are variable but are typically less than 0.05‰ for $\delta^{13}C$ (over 8 hours); they are probably dominated by instabilities in the VG SIRA mass spectrometer.

Point (f) addresses potentially significant differences arising from the different CO_2 extraction methods. The GASLAB MAT252 MT Box-C was supplied with a capillary to drop the sample pressure for cryogenic drying and CO_2 extraction in cold traps. In a typical flask analysis, about 30 bar-mL of air is bled through the capillary and two -180°C cold traps in series. The trap pressure rises from 0 to around 200 mb during this process in which the H_2O, CO_2, and N_2O are retained in the traps and the remaining air components are pumped away. In a succession of distillations, H_2O is then retained at -100°C and the mobile CO_2 and N_2O finally collected in a third cold trap at -180°C; maximum pressure in these transactions (the yield) is a few mb and about 0.5 μmol of CO_2 is collected. From here the sample CO_2 (and N_2O) is fed to the mass spectrometer changeover valve for analysis. The cryogenic separation scheme at INSTAAR is rather different. Because of the larger volume of air required for analysis, and the consequent drop in backing pressure within the sample flask, a mass flow controller is used instead of a capillary to limit the flow through the extraction system. The air is drawn through a high capacity glass trap held at -90°C to remove water (common to all samples), then through a stainless-steel trap at -196°C to remove CO_2 (N_2O). A flow rate of 60 bar-ml min^{-1} is used; the pressure in the traps during this process is typically a few mb. The yield of CO_2, about 12 μmol, is released to the mass spectrometer by expansion after warming the CO_2 trap.

On April 28, 1993, the GASLAB MT Box-C was modified to permit the analysis of very small (ice core)

samples and operating parameters optimized for the small sample analyses. The influence of the modifications on the routine measurements of flask samples is discussed below. The results from both the INSTAAR and GASLAB trapping boxes are compared to an independent manual system operated at Cape Grim as part of the long running in situ program [*Francey et al.*, 1995]. This system uses an air flow of 300 mL per minute over 2 hours, with trapping at a maximum pressure of 20 mb. The collected CO_2 is stored in 50 mL glass bulbs with a Teflon O-ring tap for analysis at Aspendale on the MAT252 mass spectrometer through the normal inlet variable volume.

Finally, point (g) brings up the potential for systematic errors arising from the mixing of sample and standard gases in the source region of the mass spectrometer. Similar effects were discussed by *Mook and Grootes* [1973] and were documented in the MAT252 (C. Flehoc et al., Systematic influences in the high precision stable isotope measurements of atmospheric trace gases, in preparation, 1995). They are emphasized by having a standard CO_2 with isotopic ratio very different from the sample CO_2 or by insufficient evacuation of the source region during normal sample-standard switching. The effect can be manifested as a sample size dependence in δ, but more importantly, a sample value biased towards the working standard isotopic ratio.

Calibration Strategies

Different calibration strategies are employed by the two groups. At GASLAB all isotopic values are routinely expressed relative to the one working-standard (high-pressure cylinder "HC453" CO_2) used in the reference reservoir of the MAT252. The working standard isotopic value is monitored each measurement session by prior calibration against an independent sub-sample of the working gas. The small difference of around 1‰ in $\delta^{13}C$ between ambient air and standard, minimizes possible sample-standard mixing effects. The calibration is also monitored by analysis of a high-pressure cylinder containing "standard" Cape Grim air, before, in the middle, and at the end of automatic sequences of sample analyses (typically 10 samples and 1 to 2 additional low pressure air standards). Generally, the air standard data has not been used to modify sample results, an exception being the so-called "APC correction" discussed below.

INSTAAR uses a different routine calibration strategy. INSTAAR's working standard is CO_2 in whole air, just as the samples are. The CO_2 gas in the mass spectrometer's standard reservoir is used only to relate samples to the working standard within the same analysis run, not as an isotopic reference material as is the routine at GASLAB. Several aliquots of the working standard are used at the beginning and end of each analysis run (typically 10-20 samples). The isotopic composition of the working standard is monitored monthly by intercalibration with other CO_2-in-air and pure CO_2 secondary standards.

Results

The results of the intercomparison are shown in Figure 1(*a*) and (*b*) for $\delta^{13}C$ and $\delta^{18}O$, respectively. The main features of the $\delta^{13}C$ intercomparison are:

(a1) The flask record defines the seasonality of the in situ record faithfully in 1993 but not so well in 1992. This appears to be due to increased scatter in the early flask data.

(a2) The agreement between the annual mean levels of all three records is surprisingly good, particularly

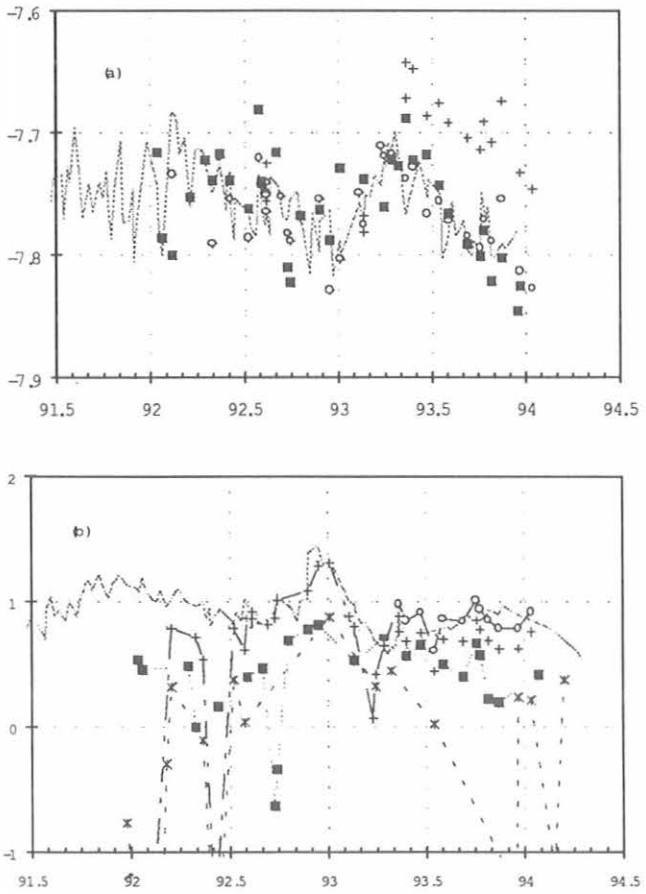

Fig. 1. (*a*) The $\delta^{13}C$ of Cape Grim CO_2 measured in CMDL flasks by GASLAB (+: uncorrected, o: with "APC" correction) and INSTAAR (filled squares). The line connects measurements at GASLAB on CO_2 extracted in situ at Cape Grim. (*b*) The $\delta^{13}O$ of Cape Grim CO_2 measured in CMDL flasks. Symbols are as for $\delta^{13}C$, except that INSTAAR values are given separately for unflagged data (filled squares) and flagged data (stars). In this case the "APC/idle time" adjustment is not independently corrected, rather maintains the 1992 relationship with the in situ data (see text).

in view of the independent calibration of standards between the two laboratories. The annual averages and standard deviations for each year are summarized in Table 1. There is excellent agreement between the in situ and CMDL mean values. All values agree within one standard deviation (which include the seasonality). Taking only flasks analyzed on both GASLAB and INSTAAR instruments, the mean difference is negligible though this may be somewhat fortuitous as the scatter remains comparable to that in the annual averages.

$$\Delta\delta^{13}C(\text{GASLAB-INSTAAR}) = -0.004 \pm 0.034‰$$

(a3) The very good agreement in $\delta^{18}C$ is only achieved after all GASLAB analyses after April 28, 1993, are corrected by -0.081‰. At this time, the MT Box-C extraction line on the GASLAB MAT252 was modified to permit analysis of very small (ice core) air samples and operating parameters optimized. The capillary connecting the flask manifold to the cryogenic traps was by-passed (connected in parallel) with an "Automatic Pressure Flow Controller" (APC). Recent removal of the APC resulted in no change in calibration, and the step change in April 1993 is attributed to a change in mass spectrometer "idle time" which was increased from 12 to 20 seconds at that time (*C. Flehoc et al.*, Systematic influences in the high precision stable isotope measurements of atmospheric trace gases, in preparation, 1995). The correction of -0.081 ± 0.010‰ was obtained from least squares regressions to the data obtained from the most frequently analyzed of our air standards (ALVZ861) before and after the APC installation and idle time change, though slightly larger uncertainty is obtained by averaging the results from several other air standards in use around this time (C.E. Allison, private communication, 1993). The comparison here supports the magnitude of the standard-derived correction, and highlights the potential for significant differences in $\delta^{13}C$ to arise from apparently minor changes to routine.

For $\delta^{18}O$, the situation is less satisfactory. This reflects the fact that the CMDL flasks are filled without drying of the sample air and so are susceptible to oxygen exchange between CO_2 and trace water inside the flask. Isotopic composition of the trace water (i.e., past flask history) is likely to be an important influence [*Gemery*, 1993]. It also reflects the fact that the GASLAB APC correction is not yet well defined by independent analyses of GASLAB air standards. For $\delta^{18}C$, most air standards are relatively stable and extrapolation of results from several standards gives a consistent correction. This is not the case for $\delta^{18}O$ where drifts are a common feature in the GASLAB tanks, and in particular in the tank in most use around the time of the APC installation. The small sample size employed in GASLAB almost certainly emphasizes the difficulty.

In Figure 1*b* an "APC adjustment" was applied to the GASLAB measurements that maintains the relationship between the flask and in situ measurements and between the GASLAB and INSTAAR measurements on the flasks. This determines an effective $\delta^{18}O$ APC correction for use in further study of the effect at GASLAB. The main features of Figure 1*b* are:

(b1) Despite several outliers, the flask data record features of the in situ $\delta^{18}O$ record (in which the opportunity for oxygen exchange in flasks is considered negligible).

(b2) The INSTAAR values are, on average, significantly lower than the GASLAB numbers. Excluding INSTAAR values, and using only pre-APC GASLAB data, only 5 points are available, for which:

$$\Delta\delta^{18}O(\text{GASLAB-INSTAAR}) = -0.443 \pm 181‰.$$

Allison et al. [1994*a*] have postulated that a slowly (1-2 year) converging difference in $\delta^{18}O$ between the new MAT252 and previous VG602D at GASLAB, was a readjustment of the isotopic content of trace water in the MAT252 instrument from closer to northern continental (depleted) to closer to southern ocean ambient water values. The present results are qualitatively in this sense, as is the sense of the outliers. The mean $\delta^{18}O$ of precipitation at INSTAAR is about -8‰, very similar to the values for Germany and UK, from where the various mass spectrometers originate. At Cape Grim latitudes around -4‰ is observed [*Yurtsever and Gat*, 1981], and the assumption is that the VG602D, purchased in 1976, had equilibrated towards this value because of exposure to room air during maintenance, power failures, etc. The outliers, when appearing in the results from both laboratories, presumably reflect oxygen isotope exchange between CO_2 and trace water condensed within individual flasks [*Gemery*, 1993]. Outliers in INSTAAR data alone could reflect exchange occurring during shipment of the flasks to Boulder. (b3) There is reasonable agreement in the temporal behavior between the majority of GASLAB flask samples and the in situ samples, and similarly between the GASLAB and INSTAAR measurements on individual flasks. This suggests that many of the CMDL flasks, despite the potential for contamination by water, are reflecting atmospheric values at Cape Grim.

Conclusions

Considering the very preliminary state of intercalibration between the two laboratories, and the potential for systematic error in both the CO_2 extraction and mass spectrometric isotope ratio determination, there is excellent agreement in $\delta^{13}C$ measured on Cape

Grim samples. The merging of data sets used by *Ciais et al.* [1994] for inversion studies is strongly supported by the data presented here.

The confirmation of the large shift in the GASLAB flask $\delta^{13}C$ compared to the in situ record and the CMDL flask results, accompanying relatively minor plumbing modification of the trapping box inlet, emphasizes the potential for serious interlaboratory discrepancies. The importance of calibrations using whole air standards, and redundancy in measurement and calibration strategies is obvious.

It is also clear that much more work is required to achieve similar consistency and compatibility in the measurements of $\delta^{18}O$ in CO_2, though there are quite encouraging sections of the intercomparison record.

Acknowledgments. The staff of the Australian Bureau of Meteorology/CSIRO Cape Grim Baseline Air Pollution Station are thanked for the conscientious sample collection. Pamela Gemery and Cyndi Brock are acknowledged at INSTAAR for their dedicated efforts in analyzing the CMDL flasks, and Marco Lucarelli at GASLAB for engineering support.

REFERENCES

Allison, C.E., and R.J. Francey, High precision stable isotope measurements of atmospheric trace gases, in *Report to I.A.E.A. Consultant's Meeting on Stable Isotope Standards and Intercalibration,* Vienna, Austria, December 1-3, 1993, International Atomic Energy Agency, Vienna, in press, 1994.

Allison, C.E, R.J. Francey, R.L. Langenfelds, and E.D. Welch, Comparison of high precision Cape Grim CO_2 stable isotope measurements using two mass spectrometers, in *Baseline Atmospheric Program (Australia) 1991,* edited by C. Dick and J.L. Gras, pp. 10-19, Bureau of Meteorology and CSIRO, Division of Atmospheric Research, Melbourne, Australia, 1994*a*.

Allison, C.E., R.J. Francey, and H.A.J. Meijer, Recommendations for the reporting of stable isotope measurements of carbon and oxygen in CO_2 gas, in *Report of I.A.E.A. Consultants' Meeting on Stable Isotope Standards and Intercalibration*, Vienna, Austria, December 1-3, 1993, International Atomic Energy Agency, Vienna, in press, 1994*b*.

Ciais, P., P. Tans, J.W. White, R. Francey, M.. Trolier, J. Berry, D. Randall, P. Sellers, J. Collatz, and D. Schimmel, The global carbon budget inferred from a new worldwide data set of $\delta^{13}C$ measurements in atmospheric CO_2, *J. Geophys. Res.*, in press, 1995.

Conway, T.J., P.P. Tans, L.S. Waterman, K.W. Thoning, D.R. Kitzis, K.A. Masarie, and N. Zhang, Evidence for interannual variability of the carbon cycle from the NOAA/CMDL global air sampling network, *J. Geophys. Res., 99*, 22,831-22,855, 1994.

Craig, H., Isotopic standards for carbon and oxygen and correction factors for mass-spectrometric analysis of carbon dioxide, *Geochim. Cosmochim. Acta., 12*, 133-149, 1957.

Enting, I.G., C.M. Trudinger, and R.J. Francey, A synthesis inversion of the concentration and $\delta^{13}C$ of atmospheric CO_2, *Tellus*, in press, 1994.

Enting, I.G., C.M. Trudinger, R.J. Francey, and H.Granek, Synthesis inversion of atmospheric CO_2 using the GISS tracer transport model, *Div. Atmos. Res. Tech. Paper No. 29,* 45 pp., CSIRO Melbourne, Australia, 1993.

Farqhuar, G.D., J. Lloyd, J.A. Taylor, L.B. Flanagan, J.P. Syvertsen, K.T. Hubick, S.Chin Wong and J.R. Ehleringer, Vegetation effects on the isotope composition of oxygen in atmospheric CO_2, *Nature, 363*, 439-443, 1993.

Francey, R.J., and P.P.Tans, The latitudinal variation in oxygen-18 of atmospheric CO_2, *Nature, 327*, 495-497, 1987.

Francey, R.J., F.J. Robbins, C.E.Allison, and N.G. Richards, The CSIRO global CO_2 isotope survey, in *Baseline Atmospheric Program (Australia) 1988*, edited by S.R. Wilson and G.P. Ayers, pp. 16-27, Bureau of Meteorology and CSIRO, Division of Atmospheric Research, Melbourne, Australia, 1990.

Francey, R.J., P.P. Tans, C.E. Allison, I.G. Enting, J. White, and M. Trolier, Changes in the oceanic and terrestrial carbon uptake since 1982, *Nature*, in press, 1995*a*.

Francey, R.J., C. E. Allison, and E. D. Welch, The 11-year high precision in situ CO_2 stable isotope record from Cape Grim, 1982-1992, in *Baseline Atmospheric Program (Australia) 1992*, edited by C. Dick and P.J. Fraser, Bureau of Meteorology and CSIRO, Division of Atmospheric Research, Melbourne, Australia, in press, 1995*b*.

Gemery, P.A., Investigation of the source of deviation in oxygen isotope measurements made on atmospheric carbon dioxide, Ph. D. thesis, University of Colorado, Boulder, 1993.

Keeling, C.D., R.B. Bacastow, A.F. Carter, S.C. Piper, T.P. Whorf, M.. Heimann, W.G. Mook, and H. Roeloffzen, A three-dimensional model of atmospheric CO_2 transport based on observed winds: 1. Analysis of observational data, in *Geophys. Monograph 55, Aspects of Climate Variability in the Pacific and the Western Americas*, edited by David H. Peterson, pp. 165-236, American Geophysical Union, Washington, DC, 1989.

Montzka, S.A., J.W. Elkins, J.H. Butler, T.M. Thompson, W.T. Sturges, T.H. Swanson, R.C. Myers, T.M. Gilpin, T.J. Baring, S.O. Cummings, G.A. Holcomb, J.M. Lobert, and B.D. Hall, in *Climate Monitoring and Diagnostics Laboratory Summary Report 1992*, edited by J.T. Peterson and R.M. Rosson, pp. 60-67, NOAA Environmental Research Laboratories, Boulder, CO, 1993.

Mook, W.G., and P.M. Grootes, The measuring procedure and corrections for the high-precision mass-spectrometric analysis of isotopic abundance ratios, especially referring to carbon, oxygen and nitrogen, *Int. J. Mass Spectrom. Ion Phys., 12*, 273-298, 1973.

Mook, W.M., and S. Van der Hoek, The N_2O correction in the carbon and oxygen isotopic analysis of atmospheric CO_2, *Isotope Geosci., 1*, 237-242, 1983.

Novelli, P.C., L.P. Steele, and P.P. Tans, Mixing ratios of carbon monoxide in the troposphere, *J. Geophys. Res., 97*, 20,731-20750, 1992.

Steele, L.P., P.J. Fraser, R.A. Rasmussen, M.A.K. Khalil, T.J. Conway, A.J. Crawford, R.H. Gammon, K.A. Masarie, and K.W. Thoning, The global distribution of methane in the troposphere, *J. Atmos. Chem., 5*, 125-171, 1987.

Tans, P.P, R.J. Francey, and G.I. Pearman, Large Scale variations in $\delta^{18}O$ of Tropospheric CO_2, in *Baseline Atmospheric Program (Australia) 1983-84*, edited by R.J. Francey and B.W. Forgan, pp. 10-14, Bureau of Meteorology and CSIRO, Division of Atmospheric Research, Melbourne, Australia, 1986.

Tans, P.P., J.A Berry, and R.F. Keeling, Oceanic $^{13}C/^{12}C$ observations: A new window on ocean CO_2 uptake, *Global Biogeochem. Cycles, 7*, 353-368, 1993.

Whorf, T.P., C.D. Keeling, and D.M. Wahlen, in *Climate Monitoring and Diagnostics Laboratory Summary Report 1992*, edited by J.T. Peterson and R.M. Rosson, pp. 119-122, NOAA Environmental Research Laboratories, Boulder, CO, 1993.

Yurtsever, Y., and J.R. Gat, Atmospheric Waters, in *Stable Isotope Hydrology: Deuterium and Oxygen in the Water Cycle, IAEA Tech. Rpt. Ser. No. 210*, edited by J.R. Gat and R.Gonfiantini, pp. 103-142, International Atomic Energy Agency, Vienna, 1981.

Barrow, the Westernmost Magnetometer Site in the STEP Polar Network

K. HAYASHI
Department of Earth and Planetary Physics, The University of Tokyo, Tokyo 113, Japan

Within a global network system, we conducted an international program, the Solar Terrestrial Energy Program (STEP) with two types of magnetometer, fluxgates and search-coil types, distributed through the polar region of the northern hemisphere.

Both types of magnetometer detect variations in DC and AC magnetic fields caused mostly by fluctuation in the ionospheric currents and also by changes of magnetic fields in the magnetosphere. We placed both the fluxgate and search-coil magnetometers at 22 sites while eight sites had only search-coil magnetometers (Figure 1).

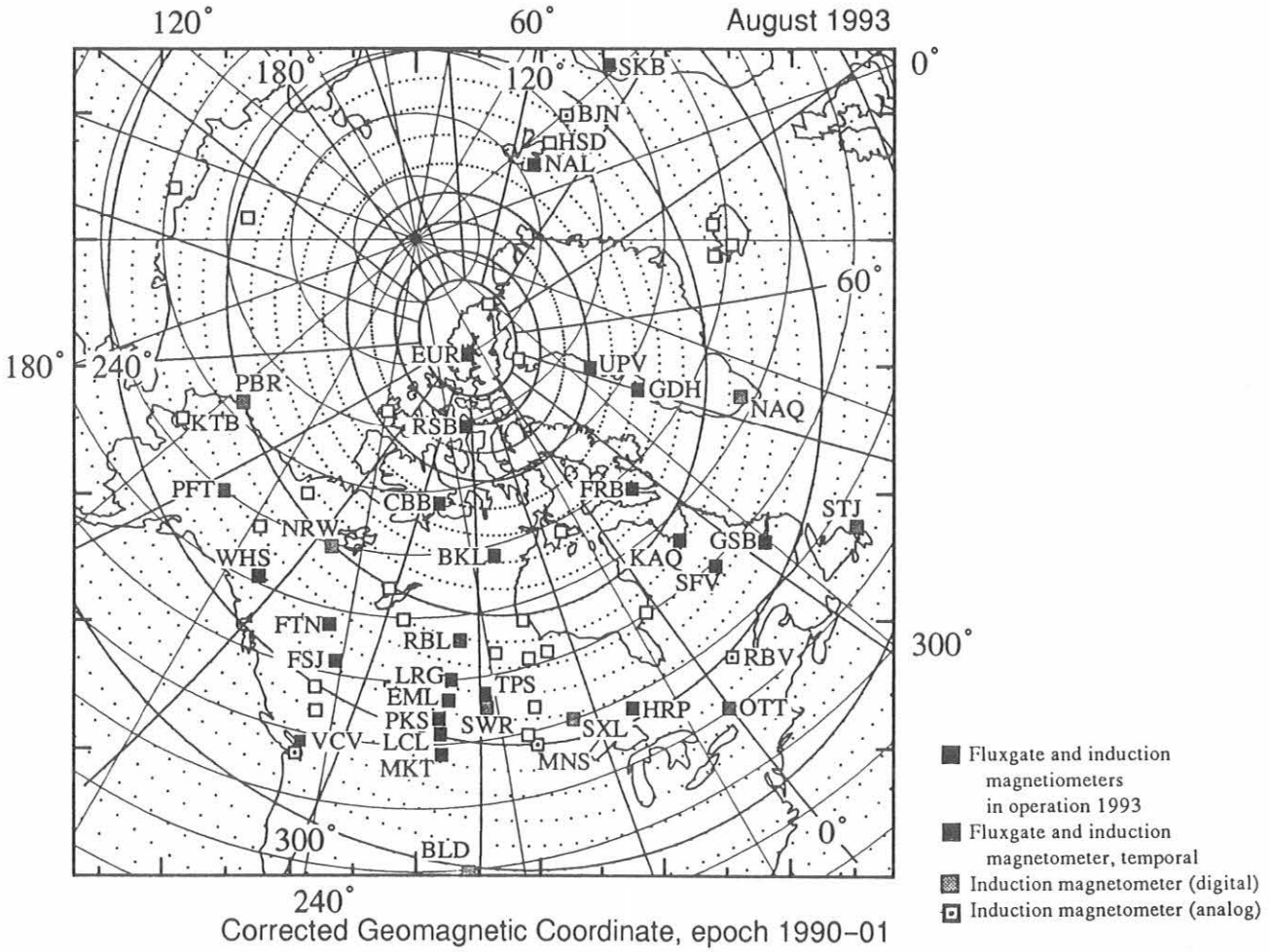

Fig. 1. Magnetometers in the STEP polar network.

The major objective of our network is to research magnetospheric disturbances in two-dimensional, dynamic nature mapped onto the ionosphere, especially in high-time resolution.

One search-coil magnetometer site operated courtesy of CMDL at Barrow, is situated at the key location of the westernmost location of our network station distribution.

The data acquisition at BRW started about 10 years ago and was intermittently activated. We plan to start a new data acquisition period at Barrow linked with the STEP program by the end of August 1994. A new datalogger capable of recording search-coil data of 10 Hz sampling rates continuously during a month will be shipped and installed before then.

Total Nitrate Variation at Mauna Loa

B.J. HUEBERT AND J.A. HEATH
Department of Oceanography, University of Hawaii, Honolulu, Hawaii 96822

INTRODUCTION

Much of the NO and NO_2 emitted into the atmosphere is converted to nitric acid vapor or aerosol nitrate before being removed by dry or wet deposition. This conversion to nitrate is largely complete within a few days of the odd-nitrogen's emission; therefore in remote areas such as at the Mauna Loa Observatory, the total nitrate concentration (vapor plus aerosol) represents a fair estimate of the total odd-nitrogen concentration [*Atlas et al.*, 1992].

With support from NSF, we have measured nitrate concentrations at MLO for several years to help identify the important sources of odd-nitrogen compounds in remote parts of the globe. We now measure total nitrate every night from the walkup tower in collaboration with the MLO staff.

MATERIAL AND METHODS

A Teflon/nylon filter pack method is used for collecting atmospheric nitrate. Since August 1988, one filter has been exposed each night, from 2000 LST to 0800 LST. Filters are returned to the University of Hawaii for extraction and analysis by ion chromatography.

The data from August 1991 to July 1992 was, unfortunately, treated somewhat differently from the remainder. These samples were all analyzed as a batch during a brief period between the return of our analytical laboratory from a field deployment in the Azores and its shipment to its new home at the University of Hawaii. Once it became apparent that this data looked very different from previous years, it was no longer possible to replicate the analytical conditions or the standards to resolve questions of its validity.

RESULTS AND DISCUSSION

Lee et al., 1993 published a description of gradient measurements of nitric acid and aerosol nitrate at MLO. This work showed that surface-active species like nitric acid often have large gradients near the surface at MLO, raising the potential for underestimating free tropospheric concentrations due to depletion of material upstream of samplers. The deposition velocity of nitric acid to the lava surface varied from 0.3 to 4 cm s^{-1}.

During our intermittent MLO sampling prior to September of 1988, we observed a sharp maximum in nitric acid and aerosol nitrate concentrations in the summer. The search for an explanation for this maximum continues to stimulate our science. The daily total nitrate values for 1993 are plotted in Figure 1. The lowest sustained concentrations are still evident in the winter, with a mix of high-concentration events and cleaner periods in the spring and late summer.

Figure 2 shows monthly averages of 2000 LST to 0800 LST total nitrate concentrations from September of 1988 to May of 1994. The questionable data from 1991 and 1992 (represented by smaller dots) is included for completeness, although we have serious questions about its validity. The 1993 data represent the lowest (defendable) concentrations we have observed during our sampling at MLO. They may represent a minimum, however, since early 1994 concentrations have returned to levels not seen since 1990.

The concentration of total nitrate at MLO is to a large extent controlled by precipitation scavenging of soluble material during transport from the continents [*Lee et al.*, 1994] so this interannual variability may be an indicator of changes in large-scale precipitation patterns. The

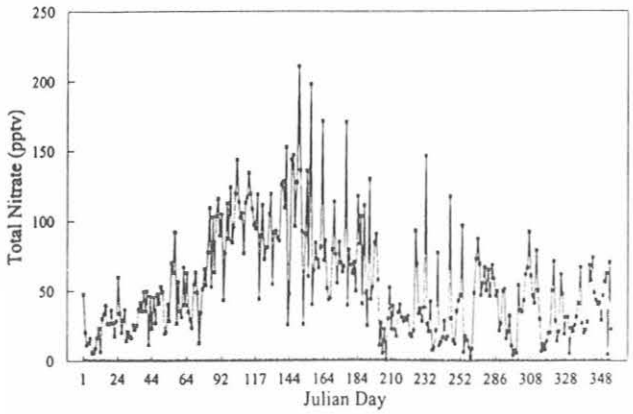

Fig. 1. Nightly concentrations of total nitrate in 1993.

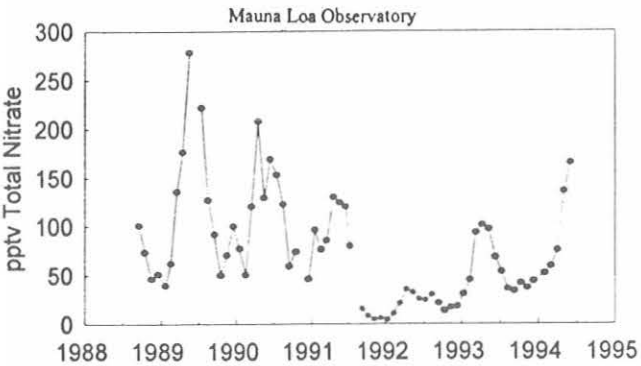

Fig. 2. Monthly average total (aerosol plus vapor) nitrate versus time.

apparently-monotonic decrease in summertime total nitrate from 1988 through 1991 suggests that a cyclic process, such as the southern oscillation, may be reflected in this record. It is certainly reasonable that the transport of continental materials like mineral aerosol and fixed nitrogen (which can be limiting nutrients in certain parts of the Pacific) should be sensitive to changes in large-scale atmospheric circulation patterns. Clearly we need to identify the climatological differences that cause this dramatic change in the annual cycle of nitrate from one year to the next since they may have impacts on phenomena as diverse as marine biological productivity and the earth's radiation budget.

Ongoing Research

We are continuing our inclusive nightly sampling from the tower with the help of the MLO staff. Although equipment failures and analytical problems have occasionally caused lapses in the data, a very interesting record is emerging. We intend to continue this total nitrate data record in the hopes of identifying those factors that control the form and the range of its annual cycle.

References

Atlas, E.L., B.A. Ridley, G. Hübler, M.A. Carroll, D.D. Montzka, B. Huebert, R.B. Norton, J. Walega, F. Grahek, and S. Schauffler, Partitioning and budget of NO_y species during MLOPEX, *J. Geophys. Res.*, *97*, 10,449-10,462, 1992.

Lee, G., L. Zhuang, B.J. Huebert, and T.P. Meyers, Concentration gradients and dry deposition of nitric acid vapor at Mauna Loa Observatory, Hawaii, *J. Geophys. Res.*, *98*, 12,661-12,671, 1993.

Lee, G., J.T. Merrill, and B.J. Huebert, Variation of free tropospheric total nitrate at Mauna Loa Observatory, Hawaii, *J. Geophys. Res.*, *99*, 12,821-12,831, 1994.

Trends of CO at Hawaii: Seasonal Cycles and Decreasing Concentrations

M.A.K. KHALIL AND R.A. RASMUSSEN
Global Change Research Center and Department of Environmental Science and Engineering
Oregon Graduate Institute, Portland, Oregon 97291

INTRODUCTION

The importance of carbon monoxide in global change science comes from its role in affecting, or perhaps controlling, the concentrations of tropospheric OH radicals. Tropospheric OH is the main oxidant in the vast non-urban atmosphere. Increases of CO, for instance, may trigger a decrease in the oxidizing capacity of the earth's atmosphere that could indirectly lead to global warming and stratospheric ozone depletion. That this would happen was indeed the current thinking since the concentrations of CO were observed to be increasing [*Khalil and Rasmussen*, 1985; *Levine et al.*, 1985; see also *Thompson and Cicerone*, 1986]. Recent data, however, show that CO concentrations have now begun to decline, eliminating this potentially significant reinforcement of climatic change.

This paper will discuss the data taken in Hawaii at two sites: Cape Kumukahi and Mauna Loa Observatory (21.08°N, 157.1°W) and, specifically, to evaluate the trends and seasonal cycles of CO at these sites. Both sites are located on the island of Hawaii. Mauna Loa is at an altitude of 3.4 km and Cape Kumukahi is nearby at sea level. The existence of two sites, so close to each other, provides a unique data set on the cycles and trends of trace gases in and above the boundary layer in the northern hemisphere tropics [see *Khalil and Rasmussen*, 1981].

SAMPLING AND ANALYSIS

Samples were collected in triplicate using a pump, in 0.8-L stainless-steel cans that are especially designed for the analysis of clean background air. The cans are internally passivated by a combination of processes that include eltropolishing. Each can is tested and certified before it is used in the field. Concentrations are stable for more than a year in these sampling containers [see *Rasmussen and Khalil*, 1980].

The samples were analyzed by a Carle 211 MS GC/FID and Trace Analytical HgO GC/RGD. Measurements before 1984 were by GC/FID and afterwards by both instruments. The detection limits are 5 ppbv (RGD) and 20 ppbv (FID). Triplicates usually agree within 1-2%. If one is more than about 20% different from the other two, it is eliminated (very few were discarded). The stability of the calibration standards is determined by periodic measurements. The records show no significant drifts [*Khalil and Rasmussen*, 1994].

CONCENTRATIONS, SEASONAL CYCLES AND TRENDS

Concentrations: Table 1 contains the seasonally averaged CO concentrations at the two sites (also shown in Figure 1). The most prominent feature of the record is the seasonal cycle (about 50-110 ppbv). This cycle is caused by three processes which, in the order of their importance, are the seasonal changes in the removal of CO by reaction with OH, seasonal changes in the emissions, and variations in transport.

Seasonal Cycles. The seasonal cycle is the largest source of the variability of CO during the year. During the course of the experiment the average monthly concentration of CO is calculated as: $\bar{C}_i = \Sigma\ C_{ij}/N$. Here $\bar{C}_i$ is the average concentration in month i (1...12) and C_{ij} is the average concentration in month i and year j (1,...,N). Since the trends are much smaller than the cycles, this calculation is an accurate representation of

TABLE 1. The Seasonal Average Concentrations of CO, and Their Variabilities at Mauna Loa Observatory and Cape Kumukahi, Hawaii

	CO Concentrations (ppbv)		Variability (ppbv)	
Month	Cape Kumukahi	MLO	Cape Kumukahi	MLO
Jan.	98.2 ± 5.8	84.0 ± 3.4	13.5	10.1
Feb.	98.4 ± 6.0	96.5 ± 4.7	18.7	16.9
March	105.7 ± 5.3	102.0 ± 2.7	10.6	17.2
April	107.4 ± 5.3	104.7 ± 1.9	10.7	12.2
May	94.2 ± 4.9	86.0 ± 3.5	10.6	12.1
June	78.7 ± 5.2	69.0 ± 1.3	8.4	8.0
July	60.0 ± 3.6	56.8 ± 2.0	6.3	7.3
Aug.	53.6 ± 6.0	48.8 ± 1.8	5.0	3.9
Sept.	61.2 ± 4.6	57.6 ± 1.6	6.2	7.0
Oct.	68.0 ± 6.1	60.5 ± 1.5	6.3	8.1
Nov.	73.6 ± 4.9	67.6 ± 19	8.0	14.3
Dec.	86.0 ± 5.4	76.2 ± 3.2	14.8	10.5

The ± values are 90% confidence limits of the mean concentrations. The last two columns show the variability in each month. It is defined as the average (over 12 years of data) of the monthly standard deviations.

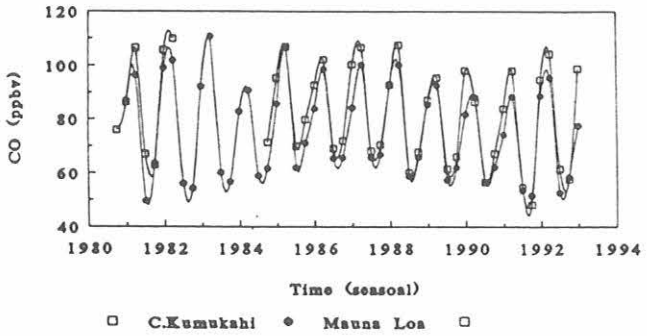

Fig. 1. Seasonally-averaged concentration of CO (ppbv) at Mauna Loa and Cape Kumukahi over a 12-year period. Concentrations at Cape Kumukahi are higher than at Mauna Loa at an average difference of 5 ppbv. The most significant variability is the seasonal cycle that is similar at the two sites.

the seasonal cycle (Table 2 and Figure 2*a*). In addition to the average cycle, the seasonal cycle of the variability can also be calculated as: $\overline{Sd_i} = \Sigma\ S_{ij}/N$, where S_{ij} is the standard deviation of the measurements in month i and year j. The results are shown in Figure 2*b*. The cycle of variability is highly correlated with the cycle of the concentration. In the winter, the concentrations of CO are the highest and so is the

TABLE 2. Seasonally-Averaged Concentations of CO (ppbv) at MLO and Cape Kumukahi From 1980-1993

Time	Cape Kumukahi	MLO	Time	Cape Kumukahi	MLO
1980 Fall	76	-	1987 Winter	100	84
1981 Winter	86	87	Spring	107	100
Spring	106	97	Summer	68	66
Summer	67	50	Fall	71	67
Fall	63	64	1988 Winter	93	93
1982 Winter	106	99	Spring	108	100
Spring	110	102	Summer	60	59
Summer	-	56	Fall	68	66
Fall	-	54	1989 Winter	87	86
1983 Winter	-	92	Spring	96	93
Spring	-	111	Summer	62	58
Summer	-	60	Fall	66	62
Fall	-	57	1990 Winter	98	82
1984 Winter	-	83	Spring	86	88
Spring	-	91	Summer	57	57
Summer	-	59	Fall	67	62
Fall	71	62	1991 Winter	84	74
1985 Winter	95	86	Spring	98	88
Spring	107	107	Summer	55	54
Summer	70	62	Fall	48	52
Fall	80	71	1992 Winter	95	89
1986 Winter	93	84	Spring	104	96
Spring	102	99	Summer	62	53
Summer	69	66	Fall	58	59
Fall	72	66	1993 Winter	99	78

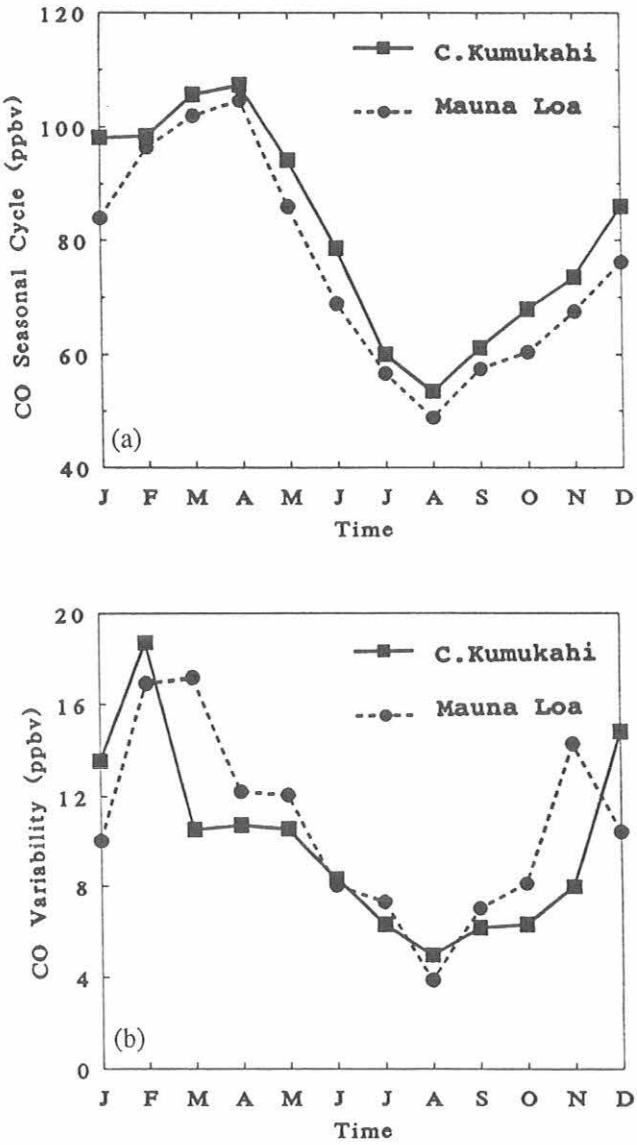

Fig. 2 (*a*). The average seasonal concentration of CO at Cape Kumukahi and Mauna Loa. The concentration at Cape Kumukahi (in the boundary layer) is higher than at Mauna Loa (above the boundary layer). The difference is about the same throughout the year. This feature is also observed for other trace gases. (*b*). The seasonal cycle of the variability of CO. The variability is defined as the average standard deviation of the monthly concentrations over the 12-year period of the record. The variability follows a pattern similar to the concentration. When the concentration is low the variability is low.

monthly variability. In the summer, the average concentrations and variability are the lowest.

Trends: In Figure 3, the 3-year running averages of the monthly concentrations of CO are plotted. By filtering the data over this period, most of the effect of the seasonal variations of CO (Figure 1) and other random variability are eliminated. The running

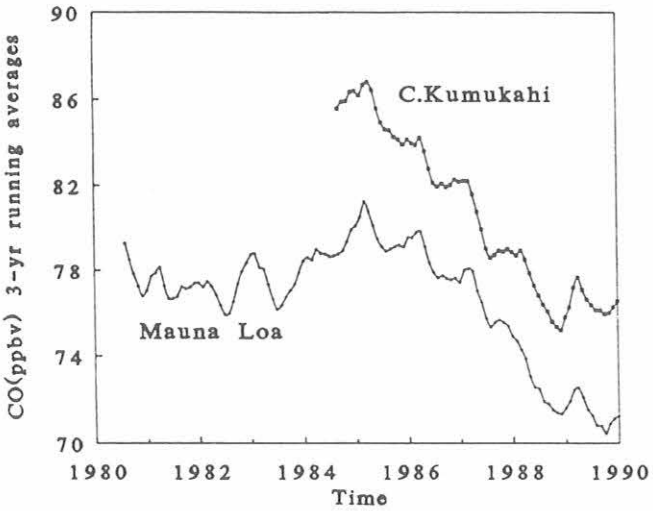

Fig. 3. Three-year running averages of CO concentrations (ppbv) based on monthly average concentrations. These calculations show the long term trends in which the effects of seasonal cycles are eliminated. The graphs show that CO may have been increasing in the beginning of the record and has been declining during the last 6 years or so at fairly rapid rates.

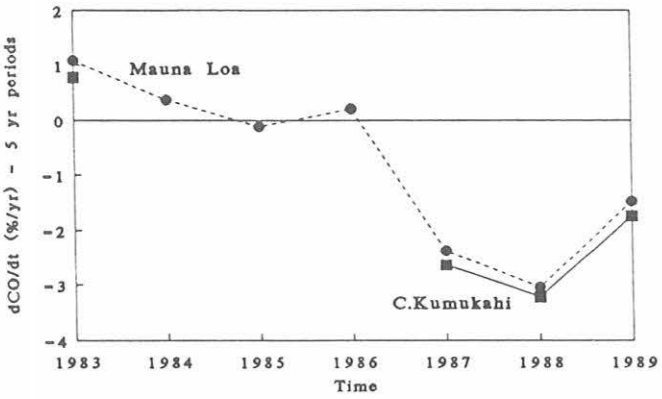

Fig. 4. The trends of CO. The trends are based on the annual averages of CO concentrations (see text). CO increased in the early part of the record and has declined in the recent 5 years. Both sites give the same results (note the trend at 1983 for Cape Kumukahi - for 1984-1986 there are no data to calculate the trends at this site).

averages are plotted in the middle of the time over which the average is taken. This figure suggests that CO was increasing between 1980-1985 and has decreased since then. Similar trends were observed at other sites around the world. The earlier global increases in CO and the recent decreases are reported by *Khalil and Rasmussen* [1984, 1988, 1994] and by *Novelli et al.* [1994].

By looking at the seasonal minima in Figure 1, it is apparent that the concentration of CO increased in the early part of the record and has been decreasing in recent times. The trends are estimated quantitatively as follows: First, annual averages of the seasonally averaged data were taken. The annual averages are not affected by the seasonal variation (on the average). Then, the trends were calculated as:

$$\text{Trend } (i+\delta/2) = \left([C(i+\delta) - C(i)] / [\overline{C}(i)\delta] \right) \times 100\%$$

where Trend (i) is the rate of change of concentration at time $i + \delta/2$, $C(i + \delta)$ is the annual average concentration at time $i + \delta$, C(i) is the annual concentration at time i, $\overline{C}(i)$ is the average concentration for the years between i and $i + \delta$. δ is taken to be 5 years for the calculation discussed here. These calculations are shown in Figure 4. The results show that CO was increasing at about 1% yr^{-1} in the early 1980s and has been decreasing in recent years at rates of -3% yr^{-1} or so. Similar declining trends are observed at other sites around the world [*Khalil and Rasmussen*, 1994; *Novelli et al.*, 1994].

Conclusions

Measurements of CO showed that between the 1950s and middle 1980s, the concentrations of CO were increasing. This increase may have gone on for longer times [*Khalil and Rasmussen*, 1988; *Rinsland et al.*, 1985]. Since then, however, the concentrations appear to be declining. Both of these observations are in accord with our understanding of the sources and sinks of CO. Anthropogenic emissions have been increasing over the last 50 years. Major anthropogenic sources include urban areas (with many sources such as automobiles) and biomass burning [see *Logan et al.*, 1981; *WMO*, 1986, 1991; *USEPA*, 1990]. Emissions of other hydrocarbons (including methane) may also have contributed to increasing trends. In recent years, however, the urban sources of CO in the United States and in Europe, have decreased rapidly because of air quality regulations. The decrease of CO in the southern hemisphere is most easily explained by a hypothesized decrease or a stabilization in tropical biomass burning. Whether biomass burning is decreasing awaits direct observational and statistical verification. In addition to the decreasing emissions, there are various possibilities that may have caused an increase of OH at some latitudes that would also lead to a decrease in CO [see *Madronich and Granier*, 1992]. All of these processes would lead to declining global concentrations of CO since it has a relatively short lifetime and responds quickly to changes in emissions or sinks. Yet at this time, it is impossible to say whether these declining trends will continue. It is clear, however, that the current declining trend shows an improvement in global air quality.

Acknowledgments. Samples were collected by CMDL staff at Mauna Loa Observatory and for some of the time at Cape Kumukahi. Samples were analyzed in the laboratory by Don Stearns and others. Sporadic financial support was provided by NSF and DOE (DEFG06-85ER60313) for measurements of sampling of specific gases. Additional funding was provided by the resources of the Biospherics Research Corporation and the Andarz Co.

REFERENCES

Khalil, M.A.K., and R.A. Rasmussen, Differences in the concentrations of trace gases in and above the tropical boundary layer, *Pure Appl. Geophys., 119*, 990-997, 1981.

Khalil, M.A.K., and R.A. Rasmussen, Carbon monoxide in the Earth's atmosphere: Increasing trend, *Science, 224*, 54-56, 1984.

Khalil, M.A.K., and R.A. Rasmussen, Causes of increasing atmospheric methane: Depletion of hydroxyl radicals and the rise of emissions, *Atmos. Environ. 19*, 397-407, 1985.

Khalil, M.A.K., and R.A. Rasmussen, Carbon monoxide in the earth's atmosphere: Indications of a global increase, *Nature, 332*, 242-245,1988.

Khalil, M.A.K., and R.A. Rasmussen, Global decrease of atmospheric carbon monoxide, *Nature, 370*, 639-641, 1994.

Levine, J.S., C.P.Rinsland and G.M.Tenille, The photochemistry of methane and carbon monoxide in the troposphere 1950 and 1985, *Nature, 318*, 254-257, 1985.

Logan, J.A., M.J. Prather, S.C., Wofsy, and M.B.McElroy, Tropospheric chemistry: A global perspective, *J. Geophys. Res. 86*, 7210-7254, 1981.

Madronich, S., and C. Granier, Impact of recent total ozone changes on tropospheric ozone photodissociation, hydroxyl radicals and methane trends, *Geophys. Res. Lett. 19*, 465-467, 1992.

Novelli, P.C., K.A. Masarie, P.P. Tans, and P.M. Lang, Recent changes in atmospheric carbon monoxide, *Science*, 263, 1587-1590, 1994.

Pinto, J.P., and M.A.K. Khalil, The stability of tropospheric OH during ice ages, inter-glacial epochs and modern times, *Tellus, 43B*, 347-352, 1991.

Rasmussen, R.A., and M.A.K. Khalil, Atmospheric methane (CH_4): Trends and seasonal cycles, *J. Geophys. Res., 86*, 9826-9832, 1981,

Rasmussen, R. A., and M.A.K. Khalil, Atmospheric methane (CH_4): Trends and seasonal cycles, *Proceedings, NATO Advanced Study Institute on Atmospheric Ozone*, edited by A.E. Aikin, Dept. Trans., Washington, DC., 1980.

Rinsland, C.P. and J.S.Levine, Free tropospheric carbon monoxide in 1950 and 1951 deduced from infrared total column amount measurements, *Nature, 318*, 250-254, 1985.

Thompson, A.M. and R.J.Cicerone, Possible perturbations of CO, CH_4 and OH, *J.Geophys. Res. 91*, 10,853-10,864, 1986.

USEPA (U.S. Environmental Protection Agency) Air Quality Criteria for Carbon Monoxide, EPA, 551 pp., Washington, D.C., 1990.

WMO (World Meteorological Organization), *Scientific Assessment of Ozone Depletion:1991*, 211 pp., WMO, Geneva, 1991.

WMO (World Meteorological Organization), *Atmospheric Ozone 1985*, 1094 pp., WMO, Geneva, 1986).

Radioactivity in the Surface Air at BRW, MLO, SMO, and SPO During 1993

RICHARD J. LARSEN AND COLIN G. SANDERSON
Environmental Measurements Laboratory, U.S. Department of Energy, New York 10014-3621

INTRODUCTION

High-volume air filter samples are routinely collected by CMDL personnel at BRW, MLO, SMO, and SPO for EML's Surface Air Sampling Program (SASP). The primary objective of this program is to identify and study the temporal and spatial distribution of specific anthropogenic and natural radionuclides in the lower troposphere. The naturally occurring radionuclides ^{7}Be and ^{210}Pb are of particular interest since they serve as excellent tracers for air masses of upper and lower tropospheric origin. Beryllium-7 ($T_{1/2}$ = 53.2 d) is produced by cosmic-ray interactions in the upper troposphere and the stratosphere, and ^{210}Pb ($T_{1/2}$ = 22.3 years) is a decay product of ^{222}Rn, a noble gas that diffuses from soils.

MATERIAL AND METHODS

Weekly air filter samples are continuously collected using Dynaweb filter material. The air samplers move ~1700 m^3 of air per day through a 20.3-cm diameter filter. The weekly filter samples collected at BRW and MLO are analyzed by gamma-ray spectrometry using a high-purity germanium (HPGe) detector with a 1.5-cm diameter well. The individual weekly samples from SMO and SPO are not routinely analyzed. Monthly composite samples for each site are formed by adding together one half of each of the weekly filter samples. These monthly composite samples are compressed into 45-cm^3 plastic planchets and are routinely analyzed for several gamma-ray emitting radionuclides using either n-type low-energy coaxial, HPGe detectors or p-type coaxial high-resolution, germanium lithium or HPGe detectors. Detailed information on SASP is periodically published [*Larsen and Sanderson*, 1991].

RESULTS

The results of the analyses of several radionuclides and the total gamma-ray activities for the monthly composite samples from filters collected at BRW, MLO, SMO, and SPO during 1993 are reported in Table 1. The total gamma-ray activities are reported in units of counts per minute (cpm) per cubic meter of sampled air referenced to 15°C and 1 Atm. The surface air concentrations of ^{7}Be and ^{210}Pb are reported in millibecquerels (mBq) per standard cubic meter of air, and ^{95}Zr, ^{137}Cs, and ^{144}Ce are reported in microbecquerels (μBq) per cubic meter of air referenced to 15°C and 1 Atm. The concentrations are reported as corrected for radioactive decay to the midpoint of the month of collection. Unfortunately, the bulk of the air filter samples collected at SPO during 1993 have been "lost" during transit to EML.

Table 1. Monthly Surface Air Concentrations of Radionuclides at BRW, MLO, SMO, and SPO during 1993

Site	Jan.	Feb.	March	April	May	June	July	Aug.	Sept.	Oct.	Nov.	Dec.
						Nuclide: Gamma (cpm m^{-3})						
BRW	<0.01	<0.01	<0.01	<0.01	<0.01	<0.01	<0.01	<0.01	<0.01	<0.01	<0.01	<0.01
MLO	<0.01	<0.01	<0.01	<0.01	<0.01	<0.01	<0.01	<0.01	<0.01	<0.01	<0.01	<0.01
SMO	<0.01	<0.01	<0.01	<0.01	<0.01	<0.01	*	<0.01	<0.01	<0.01	<0.01	<0.01
SPO	<0.01	*	*	*	*	*	*	*	*	*	<0.01	*
						Nuclide: ^{7}Be (mBq m^{-3})						
BRW	1.4	1.4	1.6	2.3	1.8	0.6	0.8[a]	0.5	0.9	1.6	1.7	2.5
MLO	4.7	8.0	7.5	7.1	7.2	7.1	7.0	5.5	5.0	6.0	7.2	7.0
SMO	1.3	2.2	1.3	0.8	2.0	2.5	*	2.5	3.2	3.7	2.5	2.0
SPO	6.8	*	*	*	*	*	*	*	*	*	5.9	*
						Nuclide: ^{95}Zr (mBq m^{-3})						
BRW	<6.2	<3.3	<4.4	<1.1	<37.	<5.1	<29.	<3.6	<5.1	<7.3	<5.7	<13.
MLO	<5.4	<8.9	<12.	<6.9	<12.	<2.5	<45.	<19.	<14.	<2.7	<11.	<14.
SMO	<7.6	<6.5	<7.7	<9.3	<20.	<14.	*	<4.6	<5.7	<4.8	<4.9	<4.7
SPO	<30.	*	*	*	*	*	*	*	*	*	<11.	*

Table 1. Monthly Surface Air Concentrations of Radionuclides at BRW, MLO, SMO, and SPO during 1993—Continued

Site	Jan.	Feb.	March	April	May	June	July	Aug.	Sept.	Oct.	Nov.	Dec.
					Nuclide: ^{137}Cs (mBq m^{-3})							
BRW	<1.3	<0.9	<1.1	0.9a	<1.9	<0.5	<0.6	<0.7	<1.1	<2.0	<0.6	<1.7
MLO	<1.2	<2.1	<2.0	<2.0	<1.4	<0.8	<4.1	<3.4	<2.5	<0.8	<3.1	<3.6
SMO	<2.2	<2.3	<1.4	<1.6	<1.3	<1.6	*	<0.9	<1.3	<1.2	<1.6	<1.8
SPO	<1.2	*	*	*	*	*	*	*	*	*	<2.0	*
					Nuclide: ^{144}Ce (mBq m^{-3})							
BRW	<5.5	<3.3	<4.6	<2.1	<11.	<2.1	<3.6	<2.5	<4.5	<9.0	<3.0	<9.2
MLO	<5.3	<9.9	<8.0	<8.1	<6.7	<3.4	<18.	<18.	<12.	<3.1	<13.	<18.
SMO	<9.3	<11.	<6.5	<6.9	<7.2	<8.2	*	<3.9	<5.4	<5.8	<6.6	<7.6
SPO	<5.8	*	*	*	*	*	*	*	*	*	<9.4	*
					Nuclide: ^{210}Pb (mBq m^{-3})							
BRW	0.78	0.80	0.67	0.38	0.26	0.05	0.11	0.06	0.09	0.23	0.35	0.59
MLO	0.17[c]	0.31	0.49	0.54	0.43	0.49	0.27[a]	0.18	0.23	0.26	0.22	0.21
SMO	0.03[c]	0.05[a]	0.02[b]	0.02[b]	0.05[a]	0.04[a]	*	0.05[c]	0.09	0.08	0.08	0.05
SPO	0.03[c]	*	*	*	*	*	*	*	*	*	0.03[a]	*

*No data

Uncertainty is < 20% except:

[a]Uncertainty is between 20% and 50%

[b]Uncertainty is between 50% and 100%

[c]Uncertainty is > 100%

DISSCUSSION

During 1993 there was one reported significant release of anthropogenic radionuclides into the atmosphere. On April 6, 1993, radioactivity was accidentally released into the atmosphere during an explosion and fire at a reprocess-ing plant in the Tomsk-7 military nuclear complex located 16 km north of the Siberian city of Tomsk. Details about the release of nuclear materials from this accident and the atmospheric transport and detection of the debris have been previously reported [*Lee et al.*, 1993; *Larsen et al.*, 1994]. We suggest that the detection of ^{137}Cs at BRW during April (see Table 1) represents traces of the Tomsk-7 debris released during this accident [*Larsen et al.*, 1994].

The seasonal cycles of ^{7}Be and ^{210}Pb continue to follow those observed in previous years *[Feely et al.*, 1989; *Larsen and Feely*, 1986].

Acknowledgment. We wish to thank the CMDL staff at BRW, MLO, SMO, and SPO for the collection of air filter samples for SASP.

REFERENCES

Feely, H.W., R.J. Larsen and C.G. Sanderson, Factors that cause seasonal variations in Beryllium-7 concentrations in surface air, *J. Environ. Radioact.*, *9*, 223-249 (1989).

Larsen, R. J. and H. W. Feely, Seasonal variations of ^{210}Pb and ^{7}Be at Mauna Loa and Barrow, in *Geophysical Monitoring for Climatic Change, No. 14, Summary Report 1985*, edited by R.C. Schnell and R.M. Rosson, pp. 127-130, NOAA Environmental Research Laboratories, Boulder, Colorado, 1986.

Larsen, R. J. and C. G. Sanderson, EML surface air sampling program, 1989 data, *U.S. DOE Report EML-541* (available from NTIS, Springfield, VA) 1991.

Larsen, R. J., C. G. Sanderson, H. N. Lee, K. M. Decker and H. L. Beck, Fission products detected in Alaska following the Tomsk-7 accident, *J. Environ. Radioactivity*, Letter to Editor, *23*. 1994.

Lee, H. N., R. J. Larsen and C. G. Sanderson, Tomsk-7 debris at BRW: detection and transport, in *Climate Monitoring and Diagnostics Laboratory No. 21 Summary Report 1992*, edited by J.T. Peterson and R.M. Rosson, pp. 102-103, NOAA Environmental Research Laboratories, Boulder, CO, 1993.

Exposure Experiment, South Pole

J.E. MAK
Lawrence Livermore National Laboratory, Livermore, California 94551-9900

C.A.M. BRENNINKMEIJER
Max Planck Institut fur Chemie, Mainz, Germany

J.R. SOUTHON
Center for Accelerator Mass Spectrometry, Lawrence Livermore National Laboratory, Livermore, California 94551-9900

The scope of this project is to directly detect and quantify the production rate of atmospheric ^{14}C. Carbon-14 is not only used for dating organic materials, it can also be used as a tracer of OH chemistry (in the form of ^{14}CO). In the latter case, if the inventory of ^{14}CO is measured and the production rate known, then the sink rate, which is oxidation by OH, can be calculated. Although cascade calculations have constrained the ^{14}CO production rate to ±20%, it is of interest to measure this rate directly.

^{14}CO is produced from the reaction:

$$^{14}N + n \rightarrow {}^{14}C + p$$

which is immediately followed by

$$^{14}C + O_2 \rightarrow {}^{14}CO + O \ (>90\% \text{ yield}).$$

The methodology takes advantage of gas handling techniques previously developed by these authors. A known amount of CO carrier gas was mixed in with zero air and compressed into a suite of cylinders, some of which were placed 1 m above the surface at SPO. There they sat, exposed to incoming cosmic rays. The cylinders were removed about 11 months later and brought back to the isotope laboratory in New Zealand where the CO was extracted and measured for ^{14}C content at Lawrence Livermore's Center for Accelerator Mass Spectrometry. During the same period, cylinders were exposed at Scott Base, on Mount Cook, New Zealand, and at various heights on the Boulder Atmospheric Observatory tower in Colorado. The latter was to constrain the surface effect that is known to cause an increase in the thermal neutron flux for a distance of about 150 m.

Monte Carlo simulations are currently being performed at LLNL to estimate any effects from the mass of the cylinders used as well as the ground effect. These simulations indicate that the effect from the cylinders is small. The experimental results are still being analyzed, and preliminary analyses show that the amounts of ^{14}C produced at the South Pole would be easily detectable for an exposure time of about 6 months. To our knowledge, this is the second time direct ^{14}C detection was achieved and the first time a ground effect was accounted for by direct measurement. This is an ongoing cooperative project.

Correlations in Short-Term Variations in Atmospheric Oxygen and Carbon Dioxide at Mauna Loa Observatory

ANDREW C. MANNING AND RALPH F. KEELING
Scripps Institution of Oceanography, UCSD, La Jolla, California 92093-0236

Since January 1991, SIO has measured atmospheric O_2 and CO_2 from flask samples collected by station personnel at MLO at roughly 2-week intervals. Samples were collected in triplicate in 5-L glass flasks, which were flushed overnight and closed off the next day, then shipped back to La Jolla where they were analysed for O_2 and CO_2 concentrations. The results of this program, from January 1991 through to the end of 1993, are shown in Figure 1.

Keeling and Shertz [1992] and *Keeling et al.* [1993] have discussed various aspects of these O_2/N_2 and CO_2 data, including reasons for the observed seasonal cycles in both CO_2 and O_2/N_2; the larger seasonal amplitude in O_2/N_2 than CO_2; the interannual decrease in O_2/N_2; and the resultant implications of these phenomena to the global carbon cycle. In 1992, after slightly more than 1 year of data had been collected, *Keeling and Shertz* [1991] pointed out that there appeared to be greater relative short-term variability in O_2/N_2 at MLO than at other sites, but were unsure of the cause. This paper will try to establish whether the residuals of the flask data from the smooth curves fitted through the data are due to experimental artifacts or real atmospheric variability; that is, whether there is some problem with the sampling procedure used to collect the air samples at MLO or whether there are one or more natural processes affecting the air at MLO, and in a manner not seen at other SIO stations.

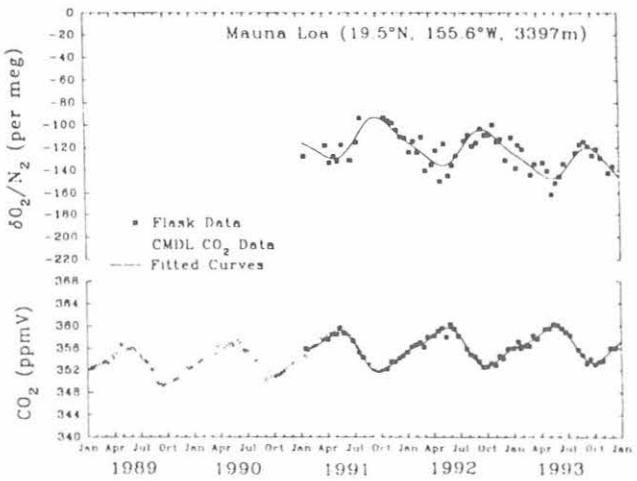

Fig. 1. Measurements of $d(O_2/N_2)$ and CO_2 from air samples collected at Mauna Loa. O_2 concentration changes are reported as changes in the O_2/N_2 ratio of the air sample. We report this ratio relative to a reference as:

$$\delta\,(O_2\,/\,N_2) = \left(\frac{(O_2\,/\,N_2)_{sample}}{(O_2\,/\,N_2)_{reference}} - 1 \right),$$

and multiply this by 10^6 and express the result in units of "per meg". In these units, 4.8 per meg is equivalent to 1 ppmV. Flask concentrations for a given date (usually three flasks per date) were averaged resulting in a single concentration for each sample date. The scale of the axes were adjusted in such a way that visually, differences in CO_2 can be directly compared with differences in O_2 on a mole fraction basis. For CO_2, supplementary data from CMDL flasks are shown going back to 1989, with some overlap when the sampling program first began. The curves shown (from which all residuals are calculated) were calculated with a least-squares fit to a function of two harmonics (annual and semi-annual periodicity) and a stiff Reinsch spline.

The sampling procedure at MLO is slightly different from that at our other sites. Because samples are collected at an altitude of about 3400 m, a back pressure regulator is used to ensure that our flask samples are pressurized to 760 torr, consistent with samples collected at our sea-level sites. Despite this procedural difference, however, we have found evidence to suggest that a significant fraction of the short-term variability in O_2/N_2 at MLO is due to real atmospheric variability.

This evidence comes from looking at short-term covariations in O_2/N_2 and CO_2. As a measure of short-term variability, we have computed the residuals in O_2/N_2 and CO_2 relative to smooth curves through the data. The curves consist of a two-harmonic fit to account for seasonality and a stiff, *Reinsch* [1967] spline to account for interannual variations. A correlation plot of these residuals is shown in Figure 2, and although there is some scatter, a clear negative correlation can be seen. Statistically speaking, the linear least-squares fit line shown gives an r^2 value of 0.37; thus a minimum of 37% of the variance in the O_2/N_2 residuals can be explained by the variance in the CO_2 residuals. The probability of these data being a random collection of points, and still resulting in an r^2 of 0.37, is less than 0.001.

This statistically significant correlation between O_2/N_2 and CO_2 could either be caused by real atmospheric variations in O_2/N_2 and CO_2, or by systematic flask sampling problems which are influencing both O_2/N_2 and CO_2 simultaneously. This latter possibility can be eliminated by a comparison of our CO_2 data with concurrent data measured by a continuous infrared CO_2 analyzer at MLO operated by C.D. Keeling's group. We calculated residuals of the steady CO_2 data obtained from that instrument relative to the same smooth curves that are fitted to our CO_2 data and correlated those residuals with our own CO_2 residuals. This correlation resulted in an r^2 value of 0.78, showing that almost 80% of the variability in our CO_2 data was also seen in the C.D. Keeling data, hence suggesting that most of the short-term variability in our CO_2 data is due to real atmospheric variations.

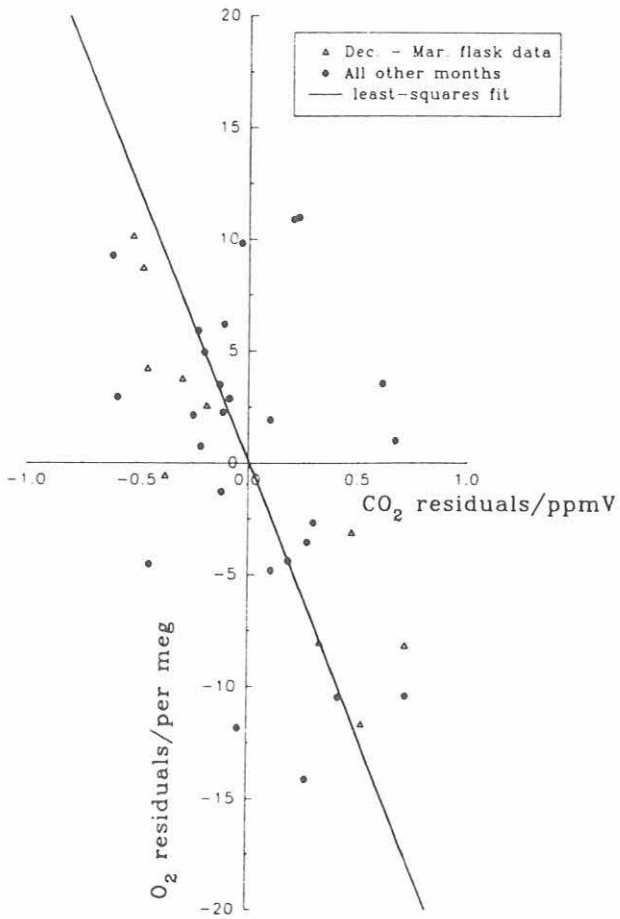

Fig. 2. CO_2 and O_2/N_2 residuals of the flask data from the smooth curves of Figure 1 are shown plotted against each other. Samples were included only if they were collected during a period of steady CO_2 concentration, as defined by C.D. Keeling's group using their continuous CO_2 analyzer at MLO; as a result only 37 sampling dates, from an original 59, were used. A clear negative correlation can be seen.

Additionally, a correlation of our O_2/N_2 data with C.D. Keeping's CO_2 data produced an r^2 value of 0.36. This is almost identical to the correlation with our own CO_2 data that had the advantage of being taken from the same flask samples as the O_2/N_2 data.

Having shown that a significant fraction of the short-term variability in O_2/N_2 and CO_2 at MLO is due to atmospheric changes, we now ask the question: what may be causing these background variations? *Heimann et al.* [section 5.5, 1989] have shown that a significant fraction of the CO_2 variability at MLO is related to changing synoptic weather patterns in the area. Particularly important may be variations in north-south transport, since for much of the year, due to both seasonal and anthropogenic differences, air masses to the north of MLO have large differences in O_2/N_2 and CO_2 concentrations relative to air masses to the south. *Keeling, et al.* [section 2, 1989] have also shown that the zonal mean CO_2 concentration at the latitude of MLO is almost identical to the actual CO_2 concentration measured at MLO, hence further suggesting that longitudinal variations are not as important as north-south variations. Although there is no direct measurement of these north-south gradients at MLO, their magnitude can be estimated based on the differences in O_2/N_2 and CO_2 that exist between midlatitude sites in each hemisphere; La Jolla, California, at 32.9°N, and Cape Grim, Tasmania, at 40.7°S. Curves for these sites are shown in Figure 3.

If variations in north-south transport are in fact causing the short-term variability at MLO, then we would expect the ratio of the instantaneous O_2/N_2 and CO_2 gradients (shown in Figure 3) to be roughly equal to the ratio of the short-term covariations in O_2/N_2 and CO_2. In other words, we would expect the ratio of the two vertical lines shown in Figure 3 to be roughly equal to the slope of the envelope of the flask residuals shown in Figure 2, for the same time period. In the period from December through March, when the ratio of the north-south gradient is at its most stable, the average absolute value of this north-south O_2/N_2 versus CO_2 ratio is 15 ± 3 per meg $ppmV^{-1}$, while a least squares fit to the flask residuals over this period results in a slope of 17 ± 4 per meg $ppmV^{-1}$. This agreement suggests that the north-south transport may indeed be implicated as a source of variability at MLO. However, this analysis is hardly conclusive because we have only 3 years worth of data to work with, and we are close to the level of our experimental uncertainty. Also, the rapid seasonal variations in the interhemispheric gradient complicates the analysis.

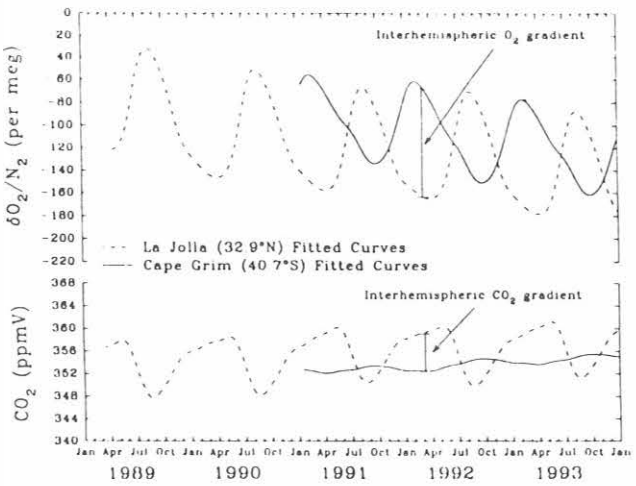

Fig 3. Seasonal patterns of O_2/N_2 and CO_2 as observed at La Jolla, California, and Cape Grim, Tasmania, Australia. The curves are fits to flask data (not shown) similar to those shown in Figure 1 for MLO, except that the seasonality is represented here by four harmonics instead of two. The difference between O_2/N_2, and CO_2 concentrations at these two sites can be taken as a measure of the interhemispheric gradient between the middle latitudes in the northern and southern hemispheres. The vertical lines show examples of the north-south gradient in O_2/N_2 in the top plot, and CO_2 in the bottom plot. These gradients change rapidly with time, due to opposing seasonal changes in the two hemispheres.

In conclusion, we have shown that a significant fraction of the short-term variability in our CO_2 and O_2/N_2 data at MLO can be explained by real atmospheric variability rather than by artifacts of our flask sampling procedure or analysis. We have suggested that this variability may be related to seasonal north-south concentration gradients that exist in the tropics as a result of opposing seasonal variations at middle latitudes in either hemisphere and have given statistical evidence to support this. If we are correct, we would expect to see high variability at other tropical sites as well. We have recently started collecting flask samples at two additional tropical sites supported by NOAA personnel, one at Cape Kumukahi, also in Hawaii, but at sea level, and another in American Samoa, at a latitude of 14.3°S. The Cape Kumukahi site should help to eliminate the parameter of variable altitude, which can have an effect on results obtained, as shown for CO_2 in *Keeling et al.*, [section 2, 1989]. These new sites, along with the continuing MLO data should, over time, help to clarify the interpretations put forward in this paper.

References

Heimann, M., C.D. Keeling, C.J. Tucker, A three dimensional model of atmospheric CO_2 transport based on observed winds: 3. Seasonal cycle and synoptic time scale variations, in *in the Pacific and the Western Americas*, edited by D.H. Peterson, pp. 277-303. American Geophysical Union, Washington, DC, 1989.

Keeling, C.D., S.C. Piper, and M. Heimann, A three dimensional model of atmospheric CO_2 transport based on observed winds: 4. Mean annual gradients and interannual variations, in *Geophysical Monograph 55, Aspects of Climate Variability in the Pacific and the Western Americas*, edited by D.H. Peterson, pp. 305-363, American Geophysical Union, Washington, DC, 1989.

Keeling, R.F., and S.R. Shertz, Variations in atmospheric molecular oxygen at Mauna Loa, in *Climate Monitoring and Diagnostics Laboratory, No. 20, Summary Report 1991*, edited by E.F. Ferguson and R.M. Rosson, pp. 103-104, NOAA Environmental Research Laboratories, Boulder, CO, 1992.

Keeling, R.F., and S.R. Shertz, Seasonal and interannual variations in atmospheric oxygen and implications for the global carbon cycle, *Nature, 358*, 723, 1992.

Keeling, R.F., R.P. Najjar, M.L. Bender, and P.P. Tans, What atmospheric oxygen measurements can tell us about the global carbon cycle, *Global Biogeochem. Cycles, 7*, 37-67, 1993.

Reinsch, C.H., Smoothing by spline functions, *Numer. Math., 10*, 177-183, 1967.

York, D., Least squares fitting of a straight line, *Can. J. Phys., 44*, 1079, 1966.

Artificial Windshielding of Precipitation Gauges in the Arctic

RICHARD J. MCCLURE
Soil Conservation Service, Anchorage, Alaska 99508-4362

INTRODUCTION

Precipitation gauges can provide good measurements of the water equivalent of snow precipitation, provided the gauge is protected or shielded from wind effects. Unfortunately, there are no standards for collecting snow precipitation. Gauges located in exposed and windy areas may be totally unshielded, partially shielded by one or more buildings, or equipped with one of several types of artificial shields. The various shielding options in common use, therefore, produce a wide range of gauge catch efficiency. Also, the various studies of artificial shields in the United States and Canada have produced a wide range of results. This must be, in part, due to the wide range of weather conditions under which the various studies have been conducted. A lingering problem is applying the results to the local conditions of Alaska's tundra regions.

METHODS

A study of the windshield alternatives, under the unique conditions of Alaska's Arctic coastal region, was set up at the CMDL facility at Barrow during September 1989. Snowfall catches from four newly installed precipitation storage gauges were compared with that from an existing storage gauge protected by a Wyoming shield [*Hanson, 1988*]. Two of the new gauges were shielded—one with a Nipher shield [*Goodison et al., 1983*] and the other with an Alter shield [*Alter, 1937*]—and two were unshielded. One of the unshielded gauges was serviced on an event basis, the same as the three shielded gauges. The other unshielded gauge was treated as if it were a remote gauge, allowing rime to build up and dissipate naturally to see what effects rime had on the overall catch. The four newly installed gauges are 20.3 cm in diameter × 100 cm tall, mounted with the orifice 2 m above the normal ground surface. The existing Wyoming-shielded gauge is 30.5 cm in diameter × 2-m tall and is equipped with a Leupold-Stevens water-level recorder.

RESULTS

The 1992-1993 winter season total precipitation is available for comparison of the 5 gauges. The results for the period October 2, 1992 through May 6, 1993 are as follows: The Wyoming-shielded gauge caught a total of 105.7 mm of snowfall precipitation during the period. The Nipher-shielded gauge caught 100.8 mm or 95% of the Wyoming-shielded gauge. The Alter-shielded gauge caught 38.1 mm or 36% of the Wyoming-shielded gauge. The unshielded but serviced gauge caught 19.3 mm or 18% of the Wyoming-shielded gauge. The unshielded and non-serviced gauge caught 14.2 mm or 13% of the Wyoming-shielded gauge. The results continue to confirm the Alter-shielded and unshielded gauges catch one-third or less of the catch of the Wyoming-shielded and Nipher-shielded precipitation gauges.

Acknowledgment. Appreciation is expressed to D. Endres, Station Chief, Barrow, Alaska, who serviced the precipitation gauges and collected the snow samples.

REFERENCES

Alter, S.C., Shield storage precipitation gauges, *Mon. Weather Rev.*, 65, 262-265, 1937.

Goodison, B.E., V.R. Turner, and J.E. Metcalfe, A nipher-type shield for recording precipitation gauges, *Proceedings, 5th Symposium on Meteorological Observations and Instrumentation*, Toronto, Ontario, Canada, pp. 2-126, American Meteorological Society, Boston, 1983.

Hanson, C.L., Precipitation measured by gauges protected by the Wyoming shield and the dual-gauge system, *Proceedings, 56th Western Snow Conference*, Kalispell, Montana, pp. 174-177, Colorado State University, Fort Collins, CO, 1988.

Lidar Measurements of Stratospheric Ozone, Temperature, and Aerosol Profiles at Mauna Loa

I. STUART MCDERMID, MARTHA SCHMOE, ERIC W. SIRKO, AND T. DANIEL WALSH
Jet Propulsion Laboratory, California Institute of Technology, Table Mountain Facility, Wrightwood, California 92397-0367

1. INTRODUCTION

Mauna Loa Observatory (MLO) has been designated as a primary site within the Network for the Detection of Stratospheric Change (NDSC) and as such, will eventually host a complement of instruments for stratospheric observations. JPL has developed and operated a lidar system for NDSC to measure stratospheric profiles of ozone, temperature, and aerosols at its Table Mountain Facility (TMF) in southern California [*McDermid et al.*, 1990*a*, 1991]. The TMF lidar has been in continuous operation since 1988 and has undergone extensive testing and validation [*McDermid et al.*, 1990*b,c,d*]. Based on the success of the TMF lidar a new, and somewhat improved, system was constructed for deployment at MLO. This new lidar is housed in a transportable facility and was built and tested at TMF before being moved intact to MLO in June 1993 in advance of the new NDSC facility being completed there.

2. INSTRUMENTATION

The new lidar is substantially similar to that at TMF and has been fully described elsewhere [*McDermid et al.*, 1990*a*, 1991]. The major improvements for the MLO lidar are the addition of Raman receiver channels at 332 nm and 385 nm [*McGee et al.*, 1993], and an optical chopper to reduce signal-induced-noise. The Raman channels are used to obtain ozone and temperature profiles in regions of aerosol layers, a measurement that was not possible with the TMF implementation. The aerosol backscatter ratio profile is also obtained from comparison of the lidar returns at 353 nm and 385 nm, thus eliminating the need for a reference atmospheric density profile.

3. RESULTS

The lidar measurements are made at night as the cloud conditions permit. Typically measurements were obtained about three nights per week. The incidence of high altitude cirrus clouds is a limiting factor in the total number of measurements that can be achieved.

3.1. OZONE

Three separate ozone profiles are generated from the high intensity Rayleigh/Mie DIAL pair, low intensity Rayleigh/Mie pair, and Raman pair. These profiles are then combined, taking into account the location of aerosol layers and the relative errors for each profile, to make a single ozone profile that can extend from about 15 km to 60 km altitude. An example is shown in Figure 1. The error bars at the bottom of the profile are relatively large because this region is obtained from the Raman pair that has the weakest signal but is not affected by the aerosol layers.

3.2. TEMPERATURE

Temperature profiles are obtained in the same manner as with the TMF lidar except that additional information is available using the 385 nm Raman channel. This data can be used to extend the temperature profile downwards to almost 20 km altitude. As for the ozone profile, the error bars from the Raman data are relatively large but temperature profile information is obtained in a region where it was not previously possible from lidar measurements. Figure 2 shows an example of a temperature profile obtained with the MLO lidar.

3.3. AEROSOLS

The Raman-channel data at 385 nm provides a measure of the atmospheric relative density profile.

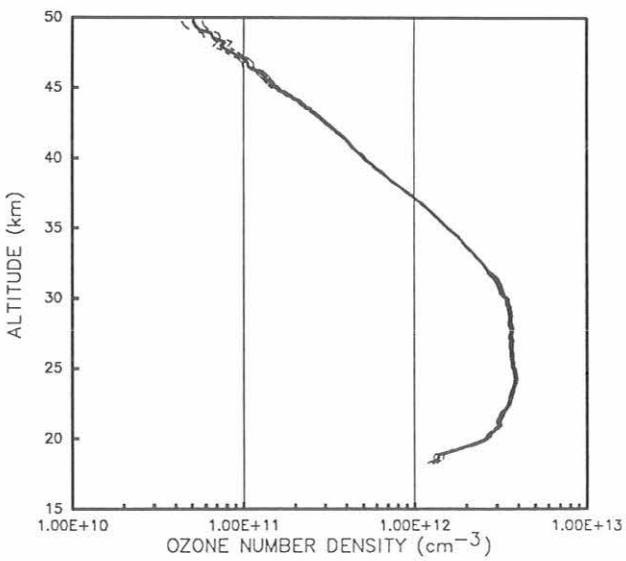

Fig. 1. MLO ozone profile for January 27, 1994.

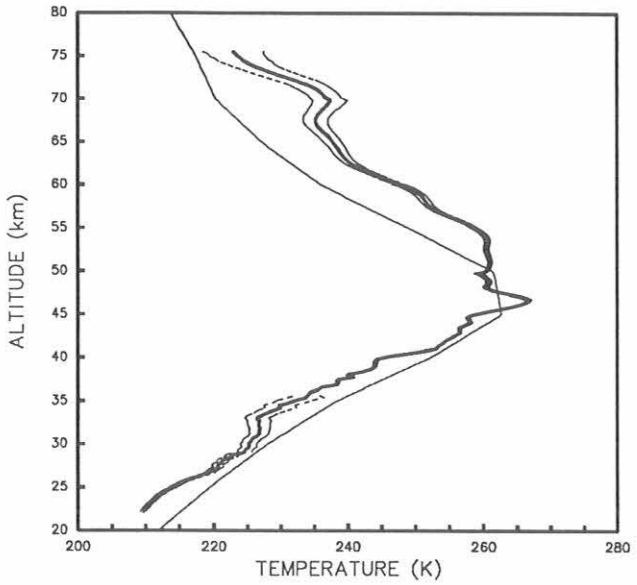

Fig. 2. MLO temperature profile for January 27, 1994. Dashed line is the CIRA reference atmosphere model.

This can be used, together with the Rayleigh/Mie scattered data at 353 nm, to calculate a backscattering ratio that does not depend on an atmospheric model such as is typically the case. If the relative density profile is normalized, for example by using results from a coincident balloon sonde, then absolute backscatter cross sections can be deduced. Figure 3 shows an example of an aerosol backscatter ratio profile. At the latitude of MLO there are still considerable aerosol layers up to at least 30 km altitude.

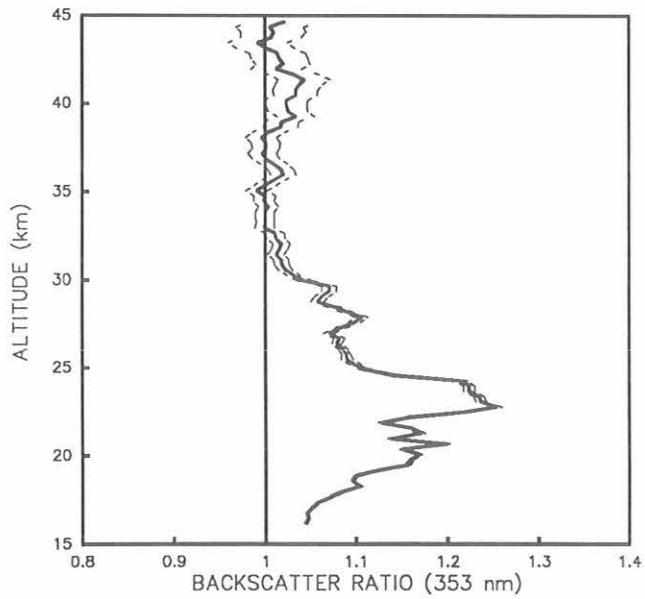

Fig. 3. MLO aerosol profile for January 27, 1994.

3.4. Intercomparisons

Figure 4 shows an example where the lidar ozone profile has been converted from number density versus absolute altitude to mixing ratio versus pressure altitude using both the lidar and CIRA model atmospheric temperature/pressure profiles and then compared with results from UARS-MLS. The two closest MLS profiles are used. For these two examples, the ozone profile has a slightly different shape but the agreement between the lidar and MLS is very good in both cases and over the entire range of the lidar measurement. This provides confidence in the Raman augmentation and in both the temperature and density measurements since both are required for the conversion to mixing ratio and pressure altitudes.

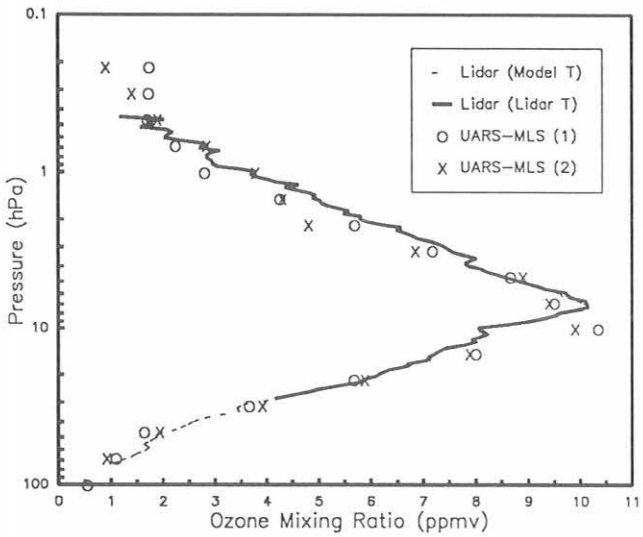

Fig. 4. Lidar MLO ozone profile converted to mixing ratio and comparison with two closest UARS overpasses (January 19, 1994).

Acknowledgments. The work described here was carried out by the Jet Propulsion Laboratory, California Institute of Technology, under an agreement with the National Aeronautics and Space Administration. We are grateful to the staff at MLO for their extensive efforts in preparing a site for the lidar facility and for their continuing support of this program.

4. References

McDermid, I. S., S. M. Godin, and L. O. Lindquist, Ground-based laser DIAL system for long-term measurements of stratospheric ozone, *Appl. Opt., 29*, 3603-3612, 1990*a*.

McDermid, I. S., S. M. Godin, P. H. Wang, and M. P. McCormick, Comparison of stratospheric ozone profiles and their seasonal variations as measured by lidar and SAGE II during 1988, *J. Geophys. Res., 95*, 5606-5612, 1990*b*.

McDermid, I.S., S.M. Godin, L.O. Lindquist, T.D. Walsh, J. Burris, J. Butler, R. Ferrare, D. Whiteman, and T.J. McGee, Measurement intercomparison of the JPL and GSFC stratospheric ozone lidar systems, *Appl. Opt., 29*, 4671-4676, 1990*c*.

McDermid, I.S., S.M. Godin, R.A. Barnes, C.L. Parsons, A. Torres, M.P. McCormick, W.P. Chu, P. Wang, J. Butler, P. Newman, J. Burris, R. Ferrare, D. Whiteman, and T.J. McGee, Comparison of ozone profiles from ground-based lidar, ECC balloon sonde, ROCOZ-A rocket ozonesonde, and SAGE II satellite measurements, *J. Geophys. Res., 95*, 10,037-10,042, 1990*d*.

McDermid, I.S., D.A. Haner, M.M. Kleiman, T.D. Walsh, and M.L. White, Differential absorption lidar systems for tropospheric and stratospheric ozone measurements, *Opt. Eng., 30*, 22-30, 1991.

McGee, T.J., M.R. Gross, R.A. Ferrare. W.S. Heaps, and U.N. Singh, Raman lidar measurements of stratospheric ozone in the presence of volcanic aerosols, *Geophys. Res. Lett., 20*, 955-958, 1993.

Strontium-90 Deposition at SMO and MLO Through 1990

M. MONETTI
Environmental Measurements Laboratory, U.S. Department of Energy, New York, NewYork 10014-3621

INTRODUCTION

Deposition samples have been collected at American Samoa (SMO) since 1965 and Mauna Loa, Hawaii (MLO) since 1959 for the Environmental Measurements Laboratory's (EML) Global Fallout Program. Sampling at both locations has been supported by CMDL for the majority of these years through a cooperative agreement. These samples, along with others collected in our global network, were regularly analyzed for ^{90}Sr. Strontium-90 is a radioactive fission product, and most of the ^{90}Sr measured in deposition samples were produced as a result of atmospheric nuclear weapons testing. Strontium-90 is an important radionuclide from a health perspective because it has a long half-life (28 years), is produced in relatively large quantities during nuclear fission reactions, and has a high bio-accumulation potential. The data generated by this program are used to determine the distribution and inventories of ^{90}Sr deposited on the earth's surface. Many factors controlling the transport and fate of atmospherically released radionuclides have been revealed by this program. The results are periodically published in EML reports [*Monetti and Larsen*, 1991].

MATERIAL AND METHODS

Deposition samples have been collected at MLO and SMO using two different collectors, either an ion-exchange column or a 23-L polyethylene bucket. Using either method, the collectors are exposed to bulk (wet and dry) atmospheric deposition, and a new sample is collected each month. The ion-exchange columns were used at MLO and at SMO until 1976. The column was packed with Dowex-50W ion-exchange resin that efficiently removes ^{90}Sr and other cations from the aqueous phase of the sample, while the particulates are trapped in the paper pulp. The column was placed in a wooden housing unit, and a polyethylene funnel with a diameter of 30 cm was attached to the top of the column. Presently, an open 23-L polyethylene bucket with a diameter of 29 cm is being used as a deposition sampler at both locations. The precipitation samples collected are shipped to EML and are passed through an ion-exchange column. The contents of the columns are analyzed for ^{90}Sr using established radiochemical procedures [*Chieco et al.*, 1992].

RESULTS

The annual ^{90}Sr deposition data through 1990 for MLO and SMO are summarized in Figure 1. The deposition is reported in units of activity per unit area (Bq ^{90}Sr m^{-2}). Samples were not collected at SMO prior to 1965, therefore, no data are shown in the corresponding positions on the graph. In all other instances, a lack of data indicates that the samples contained ^{90}Sr activities that were below the detection limit.

DISCUSSION

The trend of ^{90}Sr deposition at MLO, shown in Figure 1, is characteristic of the depositional history throughout most of the world [*Larsen*, 1984]. There is generally a 1963 maximum value as a result of the large number and high fission yield of the 1962 weapons tests. Reduced ^{90}Sr deposition is observed at both locations for the years 1965 to 1986. The depositional trends during these years were similar at both MLO and SMO, however ^{90}Sr deposition was apparently higher at SMO. Little ^{90}Sr was deposited at either sampling site following the last atmospheric weapons test conducted by China late in 1980. Strontium-90 resulting from the Chernobyl accident in April of 1986 was not found at either location due to the regional nature of this event and its related contaminant transport. Any ^{90}Sr deposited after 1982 is apparently due to resuspension

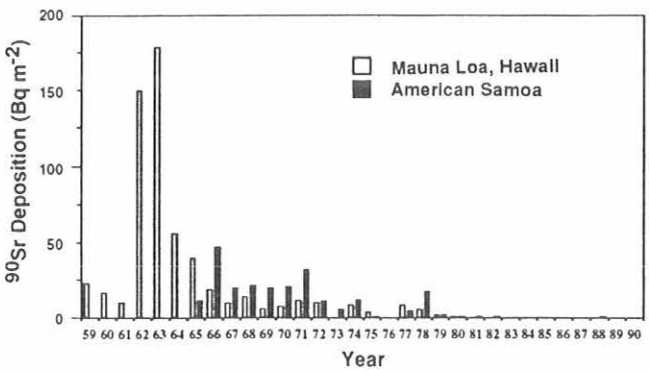

Fig. 1. Annual ^{90}Sr deposition at Mauna Loa, Hawaii, and American Samoa from 1959 to 1990.

processes and is insignificant compared to historic deposits. The ^{90}Sr inventory at the end of 1990 determined from the MLO deposition data is 290 Bq m^{-2}. A total inventory cannot be calculated for SMO because there is no SMO data available during the peak deposition period prior to 1965. MLO and SMO are just two sites of the many locations where deposition samples are collected for EML's Global Fallout Program. Using data from all the sampling stations enables us to determine the global distribution and magnitude of ^{90}Sr deposition .

Acknowledgment. I wish to thank the CMDL staff at MLO and SMO who have continued to provide EML with deposition samples for all of the years our program has been in operation.

REFERENCES

Chieco, N.A., D.C. Bogen, and E.O. Knutson (eds.), EML Procedures Manual, 27th Edition, *HASL-300*, Vol. 1, pp. 4.5-195 to 4.5-236, U.S. Department of Energy, Environmental Measurements Laboratory, New York, 1992.

Larsen, R.J., Graphic presentation of quarterly ^{90}Sr fallout data 1954-1982, *EML-424*, 186 pp., U.S. Department of Energy, Environmental Measurements Laboratory, New York, 1984.

Monetti, M.A., and R.J. Larsen, Worldwide Deposition of Strontium-90 through 1986, *EML-533*, 31 pp., U.S. Department of Energy, Environmental Measurements Laboratory, New York, 1991.

Results from the Mauna Loa Ultrahigh Resolution Infrared Solar Spectrometer

FRANK J. MURCRAY, SHELLE J. DAVID, RONALD D. BLATHERWICK,
DAVID G. MURCRAY, AND AARON GOLDMAN
University of Denver, Department of Physics, Denver, Colorado 80208

CURTIS P. RINSLAND
NASA Langley Research Center, Hampton, Virginia 23681

INTRODUCTION

The Network for Detection of Stratospheric Change (NDSC) ultrahigh resolution infrared solar spectrometer system continued operation in 1993 with only minor problems. The instrument and data analysis technique were described in the 1991 Summary Report [*Ferguson and Rosson, 1992*]. The instrument is operated once per week (usually Wednesdays) at sunrise by the MLO staff. The spectra cover two regions: 750 to 1250 cm^{-1} (8 to 13 μm) and 2500 to 3100 cm^{-1} (3.1 to 4 μm). University of Denver personnel visited the site three times during the year to make special measurements and carry out adjustments.

The spectrometer system began routine operation in November, 1991, so we now have 2 years of data. This is sufficient to begin the study of seasonal cycles and trends.

RESULTS AND DISCUSSION

We are currently analyzing the infrared spectra for total column amounts of several gases. In some cases, altitude information can also be recovered. Although this instrument is intended primarily for monitoring of stratospheric chemistry, many tropospheric gases are also observed. An example of this is ethane (C_2H_6). Ethane is released from the surface in a variety of processes, some of them related to human activity. Destruction of ethane in the troposphere is due to oxidation by OH radicals. The ethane concentration falls off rapidly in the stratosphere. This, coupled with the high tropopause over MLO, means that total column amounts measured by infrared solar absorption spectra are almost entirely tropospheric.

Spectra were analyzed for the vertical column amount of ethane using an absorption feature at 2976.77 cm^{-1}. An example spectrum and a fit are shown in Figure 1. The spectral fitting routine adjusts several parameters, including amounts of interfering gases like ozone and methane. Spectra from 71 days have been processed, and the results are shown in Figure 2. The seasonal effect is expected, and the model prediction of *Kanakidou et al.* [1991] is shown on the figure for 3 months.

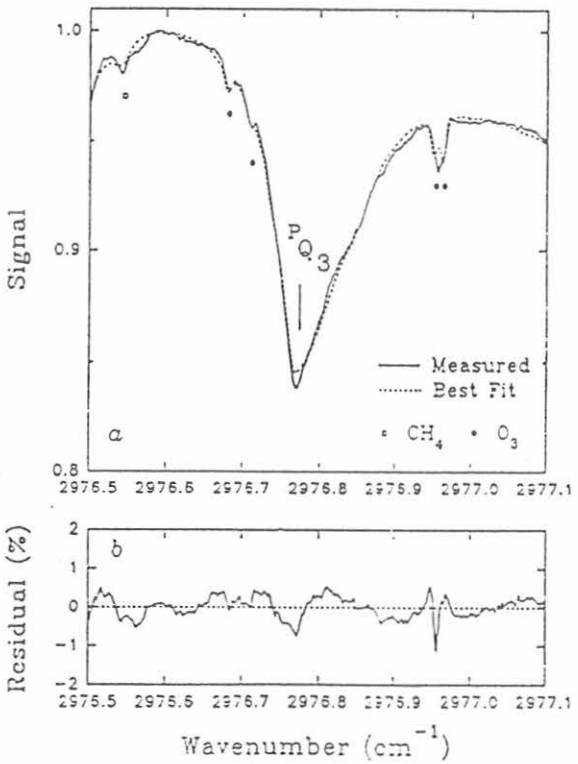

Fig. 1. A small section of an infrared solar absorption spectrum is shown in the top panel (dotted line) along with the best fit modeled spectrum (solid line). The absorption marked P_{Q3} is due to ethane, the smaller features are methane or ozone as indicated. The bottom panel shows the experimental spectrum minus the calculated on an expanded scale.

HNO_3 is one of the stratospheric gases that is routinely monitored. The total vertical column of HNO_3 over the period from November 1991 to October 1993 is shown in Figure 3. Mount Pinatubo erupted in July 1991, shortly before routine operation of the instrument began. Also shown in the figure is the aerosol loading of the stratosphere (as observed by the SAGE satellite) during the same period. The effect of the Mount Pinatubo aerosol on the HNO_3 column is clear, indicating that significant reactions are occurring on the aerosol surface. We also show the ozone amount

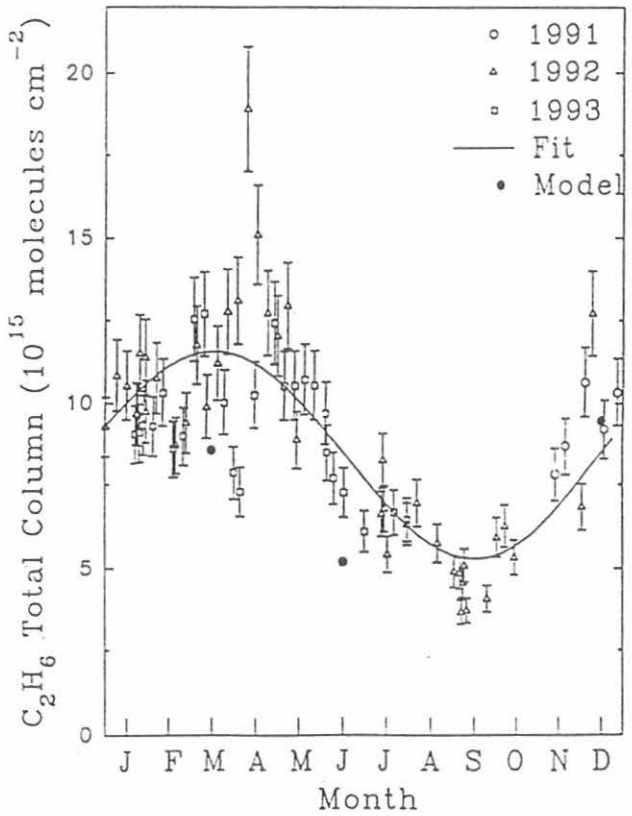

Fig. 2. Vertical column amounts of ethane determined from the infrared spectra. Error bars show the random component of uncertainties in the measurement. The best fit curve (solid line) is a cosine with amplitude 0.37 and maximum in mid-March, added to the average column of 8.44×10^{15}. Model values are from *Kanakidou et al.*, 1991.

in this figure to indicate that no large change in ozone column occurred, although our data is not sufficient to determine small changes. The observed change in HNO_3 agrees well with similar observations from New Zealand [*Koike et al.*, 1994].

Continued operation of the instrument is planned for next year.

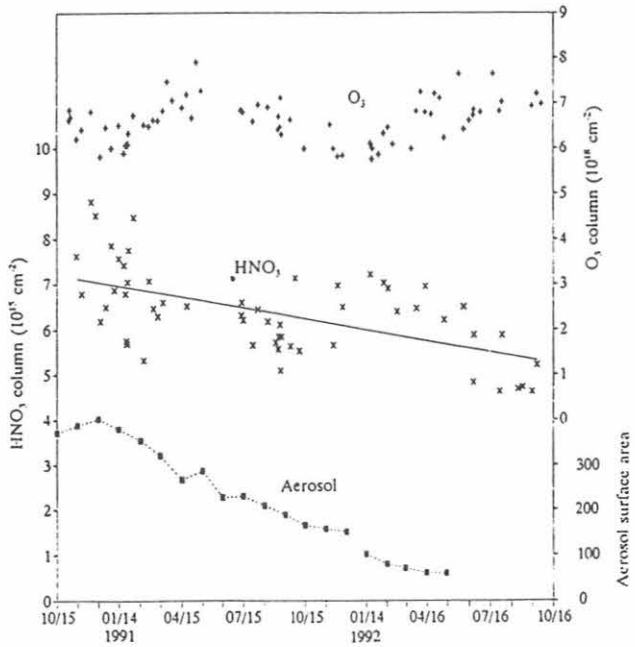

Fig. 3. Vertical column amounts of ozone and HNO_3 over MLO, along with the monthly mean total aerosol loading ($\mu m^2 km/cm^3$) observed by SAGE in the 15 to 35 km region between 10°N and 20°N. The solid line through the HNO_3 values has a slope of 15% per year.

Acknowledgments. We continue to be particularly grateful to the MLO staff for the dedication and skill in operating our instrument.

REFERENCES

Ferguson, E.E. and R.M. Rosson (Eds.), *Climate Monitoring and Diagnostics Laboratory No. 20: Summary Report 1991*, pp 115-116, NOAA Environmental Research Laboratories, Boulder, CO, 1992.

Kanakidou, M., H.B. Singh, K.M. Valentin and P.J. Crutzen, A two dimensional study of ethane and propane oxidation in the troposphere, *J. Geophys. Res., 97(D8)*, 15,395-15,413, 1991.

Koike, M., N.B. Jones, W.A. Matthews, P.V. Johnston, R.L. McKenzie, D. Kinnison and J. Rodriguez, Impact of Pinatubo aerosols on the partitioning between NO_2 and HNO_3, *Geophys. Res. Lett., 21*, 597-600, 1994.

UV-B Optical Depths at Mauna Loa: Relative Contribution of Ozone and Aerosols

PATRICK J. NEALE, DAVID L. CORRELL, VERNON R. GOODRICH, AND DOUGLASS R. HAYES, JR.
Smithsonian Environmental Research Center, Edgewater, Maryland 21037

Our laboratory has been monitoring surface spectral UV-B irradiance at Mauna Loa since fall of 1984. The instrument is similar to a radiometer in operation in Edgewater, Maryland [*Correll et al.*, 1992]. The instrument measures UV-B irradiance in a series of eight, 5-nm band passes (290-325 nm) and records 1-minute averages. Operation is continuous except for an annual break of about 1 month when the instrument is returned to Maryland for calibration. Our primary objective is to monitor long-term changes in incident solar UV-B irradiance. To accomplish this, a complete review of instrument calibrations over the period of operation is underway. Publication of our UV-B record will await the completion of this review.

While a record of absolute irradiance is presently not available, we nevertheless undertook preliminary analyses to assess the utility of the data set in regard to increasing our understanding of how different atmospheric factors control the intensity of surface UV-B. This was accomplished by calculating a relative optical depth for UV-B irradiance and statistically analyzing the relationship between such optical depth and parallel records of primary properties affecting atmospheric transparency to UV-B: total column ozone and aerosol optical depth.

Sunphotometers are commonly used for measurements of total optical depth, but usually are not designed to operate in the UV-B spectral region. On the other hand, the SERC radiometer measures total global irradiance as opposed to direct normal beam irradiance that is typically used for calculation of optical depth via Beer's law. Even so, an approximate optical depth can be estimated using the relationship:

$$I(\lambda) = I_0(\lambda)\cos(\theta_s)\exp(-\tau \sec\theta_s) \qquad (1)$$

where $I(\lambda)$ is surface irradiance, $I_0(\lambda)$ is direct normal irradiance at the top of the atmosphere, θ_s is the solar-zenith angle, and τ is total optical depth. Operationally, τ can be estimated as the slope of a linear regression of $log(I(\lambda)/cos(\theta_s))$ on $sec\ \theta_s$. Since the diffuse (sky) component of $I(\lambda)$ does not completely obey eq. (1) [*Box and Deepak*, 1979], the regression slope is termed "relative optical depth." The differences between relative and true optical depth are further discussed below.

For the analysis we chose measurements from morning to midday, for θ_s <54°. The analysis was done on days for which (1) morning to midday data were recorded, (2) clear sky conditions prevailed, (3) aerosol optical depth (τ_a) at 500 nm was measured (data kindly provided by CMDL and further described in *Dutton et al.* [1994]), and (4) total column ozone was measured on the same day or day immediately before and after, i.e., by the MLO Dobson spectrometer. If ozone was not measured on the same day, it was estimated by interpolation. Clear sky conditions were ascertained by the lack of deviations from a log-linear relationship, additionally τ_a at 500 nm was generally only estimated for clear sky mornings [*Dutton et al.*, 1994]. No slope was estimated unless at least 50 1-minute averages could be entered into the regression analysis.

We focused on two parts of the record with contrasting conditions in terms of aerosol optical depth, a period from mid-1984 through 1985 when aerosol optical depth was low, i.e., near historic background levels, and 1991 through mid-1992 during which aerosol turbidity markedly increased due to the eruption of Mt. Pinatubo [*Dutton et al.*, 1994]. A total of 208 days during these two periods met the criteria for analysis.

A time-series of regression slopes for channels with nominal center wavelengths between 300 and 325 nm is shown in Figure 1. The results show several expected features for UV-B optical depths. First, optical depths vary by almost an order-of-magnitude over this spectral range with the largest depths associated with the shortest wavelengths. Second, there is significant seasonal variation of about 20-30% around the annual mean that is in phase with the seasonal variation in total ozone concentration (data not shown). Third, optical depths increase following the eruption of Mt. Pinatubo in June 1991 cf. [*Dutton et al.*, 1994].

The quantitative relationship between our estimated relative optical depth, ozone, and aerosol turbidity was analyzed via multiple linear regression. This is based on the assumption that total optical depth is the sum of components due to Rayleigh scattering, ozone, and aerosols, the last two components being time variable. By analogy, relative optical depth would be explained by the model:

$$\tau_\rho = A[O_3] + B\tau_a + C \qquad (2)$$

where τ_ρ is relative optical depth, $[O_3]$ is total column ozone and τ_a is aerosol turbidity at 500 nm, and A, B, and C are constants. The results of the regression analysis applied to τ_ρ estimated from the 1984-1992 SERC UV-B radiometer record are given in Table 1. The proportion of variation in τ_ρ explained by the regression varied from 50% at 325 nm to 77% at 305 nm. All regressions were highly statistically significant, and all coefficients were significantly

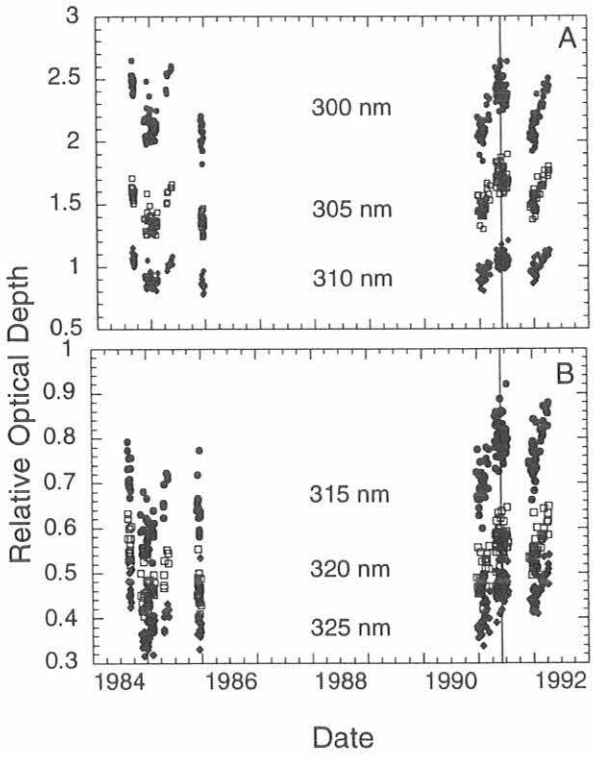

Fig. 1. Time series of relative optical depths in six UV-B bands (5 nm full bandwidth at half maximum) as estimated from morning-midday data recorded on the SERC UV-B radiometer. Upper (A) graph for 300-, 305-, and 310-nm bands, bottom (B) graph for the 315-, 320-, and 325-nm bands. Note the different abscissa scales. Although data has been recorded more-or-less continuously since 1984, only periods between 1984-1986 and 1991-1992 were used in the present analysis. Vertical line indicates date of Mt. Pinatubo eruption.

different from zero, except for the coefficient of τ_a for τ_ρ at 300 nm. The coefficient A is analogous to $a_{o\lambda}$, the spectral absorption coefficient for ozone. Estimates for the coefficient A were approximately equal to or exceeded effective $a_{o\lambda}$, Table 1, [*Molina and Molina*, 1986], except at 300 nm. The estimate for A may generally be greater than $a_{o\lambda}$ when τ_ρ has been estimated from total (direct plus diffuse) irradiance. Attenuation of the diffuse component of $I(\lambda)$ will be over longer mean optical paths than for the direct beam irradiance, e.g., *Perliski and Solomon* [1993]. The estimate of A for the 300-nm channel may be less than $a_{o\lambda}$ at 300 nm due to the probable red-shift of effective center wavelength of this channel with respect to the filter center wavelength (300.6 nm) as discussed by *Correll et al.* [1992].

The coefficient B is interpreted as an overall proportion between τ_a at 500 nm and aerosol optical depth in each of the UV-B bands. Generally, aerosol optical depth obeys an inverse power law (Ångstrom)

TABLE 1. Results of Regression Analysis of t_r Using Eq. 2

λ	a_{ol}	A	B	C	R^2
300.6	9.34	6.17	NS	0.63	68
304.8	5.42	5.04	0.76	0.19	77
310.7	2.45	2.72	0.51	0.24	66
314.6	1.46	2.66	0.66	0.08	63
320.1	0.68	1.45	0.43	0.13	57
325.2	0.33	1.12	0.38	0.12	50

Wavelength (λ) is the computed center wavelength for the band interference filter. a_{ol} is the absorption coefficient for total column ozone (units, atm^{-1} cm at NTP). A, B, and C are the fitted coefficients of eq. 2, and R^2 is the coefficient of determination (given in %). Ozone absorption is estimated from the spectral integrals of *Molina and Molina* [1986] assuming a stratosphere temperature of -40°C and normal surface temperature of 18°C. All regressions were significantly different from zero, n = 208. NS = not significant.

relationship with wavelength, arising from a Junge-type size distribution of aerosols [*Ångstrom*, 1961]. Thus it may be surprising at first sight to find that estimated B in all bands is less than one. However, the variation of τ_a at MLO was dominated by Mt. Pinatubo stratospheric aerosols, at least during the selected period [*Dutton et al.*, 1994]. These aerosols were inferred to have a narrow size range, in contrast with the Junge-type distribution of background aerosols [*Dutton et al.*, 1994]. Furthermore, our regression analysis (eq. 2) does not explicitly consider that relative airmass (m_r) for aerosol attenuation will be decreased at the altitude of MLO. This was not attempted since we did not have a basis to estimate m_r, i.e., vertical distributions of aerosols. However, we would expect m_r to range between $sec\ \theta_s$ and 0.67 $sec\ \theta_s$, the latter being the altitude adjusted Rayleigh m_r using the expression of *Bird and Riordan* [1986].

Finally, the constant term in the regression model, C, represents all time-constant contributions to optical depth, primarily attenuation due to Rayleigh (molecular) scattering. However, the estimated Cs are very much lower than the theoretical Rayleigh contribution at these wavelengths [*Bird and Riordan*, 1986]. Again, this is expected since our estimation of τ_ρ includes diffuse irradiance, which mainly arises from Rayleigh scattering.

Overall, the results of the regression analysis conform to expectations given the approximate nature of the model. Thus we conclude that our record can provide an indication of the relative importance of ozone and aerosol variation in causing variations in incident solar UV-B. One quantitative indicator of the relative importance of these two variables is the proportion of variance in τ_ρ explained by each variable in the regression eq. (2). The fractional contribution of each factor was obtained by (1) performing a second regression including A but omitting B (i.e., the term for

τ_a); the R^2 of this equation is the variance explained by ozone alone, and (2) the difference between the former R^2 and the R^2 for the full equation is the variance explained by τ_a. Such a "step-wise" approach can be used because variations in ozone and aerosol optical depth in this record are not correlated. The results are shown in Figure 2. Aerosol optical depth is seen to have a significant, though secondary, contribution to UV-B optical depth with the importance of aerosols increasing (and importance of ozone decreasing) at the longer wavelengths. Between 315 and 325 nm, aerosol optical depth accounts for almost 20% of the variation in total optical depth at MLO.

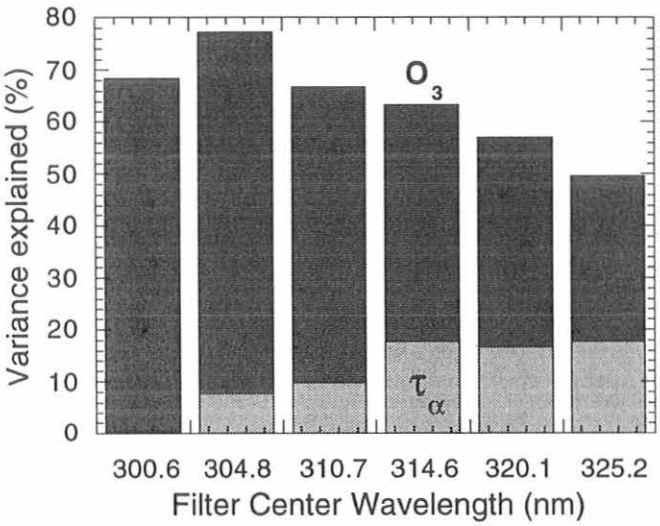

Fig. 2. Partitioning of the total coefficient of determination (R^2) for the regression of relative optical depth against total column ozone and aerosol optical depth at 500 nm. The dark, upper bar is the variance explained by total column ozone; the light, lower bar is the variance explained by aerosol optical depth.

This preliminary analysis of our record of UV-B measurements at MLO suggests that volcanic aerosols can contribute significantly to the variation in UV-B irradiance. Aerosol-forced variation in UV-B is probably of less importance during periods inbetween eruptions, due to the high-altitude, pristine nature of the MLO site. These pristine conditions actually make it easier to detect an aerosol-related event when it does occur such as documented by [*Dutton et al.*, 1994]. An understanding of the interaction between aerosols, ozone, and UV-B will assist in the analysis of trends at sites with more complex variations in atmospheric conditions such as at our Maryland site. Thus in the future we will be extending this preliminary analysis over the complete MLO record.

References

Ångstrom, A., Technique of determining the turbidity of the atmosphere, *Tellus, 13*, 214-231, 1961.

Bird, R.E., and C. Riordan, Simple solar spectral model for direct and diffuse irradiance on horizontal and tilted planes at the Earth's surface for cloudless atmospheres, *J. Clim. Appl. Meteorol., 25*, 87-97, 1986.

Box, M.A., and A. Deepak, Atmospheric scattering corrections to solar radiometry, *Appl. Opt., 18*, 1941-1949, 1979.

Correll, D.L., C.O. Clark, B. Goldberg, V.R. Goodrich, D.R. Hayes Jr., W.H. Klein, and W.D. Schecher, Spectral Ultraviolet-B radiation fluxes at the earth's surface: long-term variations at 39°N, 77°W, *J. Geophys. Res., 97*, 7579-7591, 1992.

Dutton, E.G., P. Reddy, S. Ryan, and J.J. DeLuisi, Features and effects of aerosol optical depth observed at Mauna Loa, Hawaii: 1982-1992, *J. Geophys. Res., 99*, 8295-8306, 1994.

Molina, L.T., and M.J. Molina, Absolute absorption cross sections of ozone in the 185- to 350- nm wavelength range, *J. Geophys. Res., 91*, 14,501-14,508, 1986.

Perliski, L.M., and S. Solomon, On the evaluation of air mass factors for atmospheric near-ultraviolet and visible absorption spectroscopy, *J. Geophys. Res., 98*, 10,363-10,374, 1993.

Advanced Global Atmospheric Gases Experiment (AGAGE)

R.G. PRINN
Massachusetts Institute of Technology, Cambridge, Massachusetts 02139

R.F. WEISS
Scripps Institution of Oceanography, University of California, La Jolla, California 92093

F.N. ALYEA AND D.M. CUNNOLD
Georgia Institute of Technology, Atmospheric Sciences, Atlanta, Georgia 30332

P.J. FRASER AND L.P. STEELE
CSIRO, Division of Atmospheric Research, Victoria, Australia 3195

P.G. SIMMONDS
University of Bristol, School of Chemistry, Bristol, United Kingdom BS8 1TS

INTRODUCTION

Continuous high frequency gas chromatographic measurements of two biogenic/anthropogenic gases (CH_4, N_2O) and five anthropogenic gases ($CFCl_3$, CF_2Cl_2, CH_3CCl_3, $CF_2ClCFCl_2$, and CCl_4) are being carried out at globally-distributed sites in order to quantitatively determine the source and sink strengths and circulation of these chemically and radiatively important long-lived gases. The current station locations are Cape Grim, Tasmania (41°S, 145°E), Point Matatula, American Samoa (14°S, 171°E), Ragged Point, Barbados (13°N, 59°W), and Mace Head, Ireland (53°N, 10°W). Stations also previously existed at Cape Meares, Oregon (45°N, 124°W) and Adrigole, Ireland (52°N, 10°W). The current Mace Head station replaced the Adrigole station and a station is planned at Trinidad Head, California (41°N, 124°W) to replace Cape Meares. The program, which began in 1978, is conveniently divided into three parts associated with three changes in instrumentation: the Atmospheric Lifetime Experiment (ALE) that utilized Hewlett-Packard HP5840 gas chromatographs, the Global Atmospheric Gases Experiment (GAGE) that utilizes HP5880 gas chromatographs, and the Advanced (AGAGE) phase that has recently begun using a new fully-automated system from the Scripps Institution of Oceanography (SIO) containing a custom-designed sample module and HP5890 and Carle Instruments gas chromatographic components. Finally, a new Finnigan gas chromatograph-mass spectrometer system for measuring hydrochlorofluorocarbons (HCFCs) and hydrofluorocarbons is being installed at Mace Head with another planned for Cape Grim.

1993-1994 UPDATE

The data for the seven long-lived gases measured in GAGE during 1993-1994 continue to be generally of good quality. Some significant conclusions have been made over the past year as a result of analyzing the data. First, 13 years of ALE/GAGE CCl_3F and CCl_2F_2 measurements have been analyzed and published [*Cunnold et al.*, 1994]. Comparisons are made against shipboard measurements made by SIO and archived air samples collected at Cape Grim, Tasmania, since 1978. CCl_3F in the lower troposphere was increasing at an average rate of 9.2 ppt yr^{-1} over July 1978 to June 1988. CCl_2F_2 was increasing at an average 17.3 ppt yr^{-1} in the lower troposphere over the same period. However, between July 1988 and June 1991 the increases of CCl_3F and CCl_2F_2 in this region have averaged just 7.0 ppt yr^{-1} and 15.7 ppt yr^{-1}, respectively. The rate of increase has been decreasing 2.4 ppt yr^{-2} and 2.9 ppt yr^{-2} over this 3-year period. Based on recent scenarios of the worldwide releases of these compounds and using the calibration scale SIO 1993, the equilibrium lifetimes are estimated to be 44^{+17}_{-10} years and 180^{+820}_{-81} years for CCl_3F and CCl_2F_2 respectively. Using these lifetime estimates and a two-dimensional model, it is estimated that global releases of these two chlorofluorocarbons (CFCs) in 1990 were $249 \pm 28 \times 10^6$ kg for CCl_3F and $366 \pm 30 \times 10^6$ kg for CCl_2F_2. It is also estimated that combined releases of these chlorofluorocarbons in 1990 were 21 ± 5% less than those in 1986.

Second, recent analysis of 15 1/2 years of ALE/GAGE CH_3CCl_3 data (1978-1993) has shown that global concentrations are decreasing rapidly and are approximately consistent with reported industrial emissions decreases [*Prinn et al.*, 1994]. The concentration decreases (about 12% globally) began in 1991 in the northern hemisphere and in 1992-1993 in the southern hemisphere consistent with the predominantly northern hemisphere industrial emissions and expected interhemispheric mixing times. Interpretation of the data using optimal estimation inverse techniques, together with new SIO 1993 calibrations for this gas and recent estimates of

industrial CH_3CCl_3 emissions, indicate a tropospheric lifetime of about 4.85 years which is a significantly lower lifetime than that reported previously [*Prinn et al.*, 1992] that was based on 12 years of data and the old (17% greater) calibration.

Operations at SMO will soon make the transition from the GAGE instrument to the new AGAGE system, with the actual schedule depending upon plans for the replacement of the existing laboratory building at this site. During 1993-1994 the GAGE HP5880 continued to be operated by the CMDL station personnel in collaboration with SIO. Operations were quite smooth and uneventful during this period, with most problems being of a routine maintenance and repair nature. Through the results obtained at SMO where ambient atmospheric water vapor concentrations are high, we have become aware that the quality of the HP5880 electron capture chromatography is sometimes degraded by poor performance of the Nafion drier [*Foulger and Simmonds*, 1979] configuration used in GAGE, in which pellets of molecular sieve are used to absorb water in the space surrounding the drier tube. As a result, in 1994 we modified all of the GAGE driers to use the same Nafion drier method used for the AGAGE instruments, in which the drier tube is surrounded by a countercurrent flow of dry "zero air."

The new instrument systems for AGAGE represent a significant technological advance. All operations and data acquisition are by a Sun Microsystems workstation computer using custom runfile architecture, signal processing and integration routines, and storing all the data and chromatograms digitally. The instrument measures its own non-linearity for all the AGAGE gases on a regular basis using a pressure-programmed constant-volume injection system and a single gas standard. All channels of the instrument are fitted with precolumns to avoid column contamination by late-eluting gases, and as a result the frequency of measurement has been increased three-fold versus GAGE. Precision is also greatly improved over the GAGE instruments with 1σ relative precisions on the order of 0.05% for the rapidly eluting gases CH_4, CCl_2F_2, N_2O, and CCl_3F. The system works interactively with its uninterruptible power supply so that controlled shutdown and startup of the entire instrument and sampling system are assured when there are extended power outages. The new AGAGE instruments are now operational at Cape Grim and at Mace Head, and the remaining instruments will be installed at the other stations within the coming year.

Another major component of the AGAGE program is the development of new absolute calibration scales. This work is being done using an extension of the "bootstrap" calibration method used earlier at SIO. In the AGAGE work, an all-metal high-vacuum system is used to mix gravimetrically determined aliquots of pure CFCs with about 12 L of gravimetrically determined pure nitrous oxide. This mixture is prepared at roughly the ambient atmospheric mole ratios of these gases. A small aliquot (~0.4 cm^3) of this mixture is then introduced using a separate pressure/vacuum system, fitted with a high-pressure chromatographic sampling valve, into a 35-L electropolished stainless steel canister to which about 10 torr of water vapor has been added to reduce wall reactions and adsorption. The canister is then filled with about 40 atmospheres of re-purified "zero air" to bring the nitrous oxide mole fraction to a near-ambient value. The resulting nitrous oxide concentration is then calibrated gas chromatographically against existing SIO standards, and the CFC concentrations are determined by multiplying the measured nitrous oxide mole fraction by the gravimetric CFC nitrous oxide ratios of the original mixture. In this way, we have been able to obtain improved accuracy for all AGAGE gases, but especially for the lower vapor pressure and more adsorptive gases. AGAGE and CMDL are now engaged in an active intercalibration program for all the AGAGE gases as well as for methyl halides and some HCFCs.

Data Access

The ALE/GAGE/AGAGE data are archived at the DOE Carbon Dioxide Information Analysis Center at Oak Ridge and are available to interested scientists. Potential users of the data should contact CDIAC (Internet: CDP@ORNL.GOV).

Acknowledgments. The AGAGE is supported by NASA grants NAGW-732 and NAGW-2034, NOAA Contract NA85-RAC05103, CSIRO, Australian Bureau of Meteorology, the U.K. Department of Environment, and the Alternative Fluorocarbons Environmental Acceptability Study. We thank the CMDL staff at Samoa for their continued excellent local support of our instrumentation there.

References

Cunnold, D.M., P.J. Fraser, R.F. Weiss, R.G. Prinn, P.G. Simmonds, B. R. Miller, F. N. Alyea, and A. J. Crawford, Global trends and annual releases of CCl_3F and CCl_2F_2 estimated from ALE/GAGE and other measurements from July 1978 to June 1991, *J. Geophys. Res., 99*, 1107-1126, 1994.

Foulger, B.E., and P.G. Simmonds, Drier for field use in the determination of trace atmospheric gases, *Anal. Chem., 51*, 1089-1090, 1979.

Prinn, R., D. Cunnold, P. Simmonds, F. Alyea, R. Boldi, A. Crawford, P. Fraser, D. Gutzler, D. Hartley, R. Rosen, and R. Rasmussen, Global average concentration and trend for hydroxyl radicals deduced from ALE/GAGE trichloroethane (methyl chloroform) data, *J. Geophys. Res., 97*, 2445-2461, 1992.

Prinn, R.G., R.F. Weiss, B.R. Miller, J. Huang, F.N. Alyea, D.M. Cunnold, D.E. Hartley, P.J. Fraser, and P.G. Simmonds, Global weighted-average concentration and trend for OH based on 15 1/2 years of ALE/GAGE CH_3CCl_3 data, paper presented at the 2nd IGAC 8th CACGP Symposium, Fuji-Yoshida, Japan, September 5, 1994.

The $^{13}C/^{12}C$ of Atmospheric Methane

PAUL QUAY, JOHN STUTSMAN, AND DAVID WILBUR
School of Oceanography, University of Washington, Seattle, 98195

INTRODUCTION

For the past 6 years we have been measuring the $^{13}C/^{12}C$ of atmospheric CH_4 on air samples collected at three CMDL sites (BRW, MLO, and SMO) and on the Washington coast at 48°N 126°W.

The $^{13}C/^{12}C$ of atmospheric CH_4 is a tracer that can distinguish between CH_4 input from bacterial and non-bacterial CH_4 sources. Bacterial CH_4 is microbially produced in anoxic environments likes swamps, bogs, rice paddies, and the rumens of cows. Non-bacterial CH_4 sources include thermogenically produced natural gas and CH_4 produced during the incomplete oxidation of plant material during biomass burning. Bacterial CH_4 has a $\delta^{13}C$ of about -60‰ (versus PDB) whereas the $\delta^{13}C$ of natural gas and CH_4 produced from biomass burning are about -40 and -27‰, respectively [*Quay et al.*, 1991].

The spatial and temporal variations in the $^{13}C/^{12}C$ of atmospheric CH_4 depend on the variations of the relative strength and $^{13}C/^{12}C$ of the CH_4 sources and sinks. Over interannual time scales the trends in the $^{13}C/^{12}C$ of atmospheric CH_4 indicate changes in the source composition, i.e., the relative strength of bacterial versus non-bacterial CH_4 sources. Because CH_4 will likely contribute about 15% of the radiative forcing during the next century [*Wigley and Raper*, 1992], it is important to quantify the strength of the individual CH_4 sources, currently known to about ±50% and to determine whether the CH_4 source strengths are changing with time. This latter point has been underscored by the recently observed slowdown in the rate of CH_4 increase in the atmosphere [*Dlugokencky et al.*, 1994].

METHODS

The air samples are collected at approximately 2-week intervals, using pre-evacuated stainless steel flasks either 15- or 30-L in volume. The CH_4 is extracted from air in our laboratory using the procedure developed by *Stevens and Rust* [1982]. Briefly, the air is metered into a high-vacuum extraction line through a series of liquid nitrogen traps to remove H_2O, CO_2, and N_2O. The air then passes through a bed of Schutze's reagent, I_2O_5 on silica, to oxidize CO to CO_2 that is trapped cryogenically. Then the CH_4 in the air is combusted over platinized silica at 800°C to CO_2 which is then trapped cryogenically. The yield of the procedure, determined from standards, is 100 ± 2% (n = 114). The $^{13}C/^{12}C$ of the CO_2 derived from CH_4 is measured on a Finnigan MAT 251 gas ratio isotope mass spectrometer. The overall measurement precision is about ±0.1‰. We obtain a $\delta^{13}C$ of -41.73‰ (versus PDB) for NBS-16.

RESULTS AND DISCUSSION

The seasonal cycle in the $\delta^{13}C$ of CH_4 is greatest at 71°N (BRW), with an amplitude of ~0.6‰, and decreases southward to 14°S (SMO) where we measure no significant seasonal trend, i.e. <0.1‰ (Figure 1). The seasonal trends at 71°N and 48°N can be approximated roughly by a single harmonic with an annual period. Episodes of high CH_4 concentrations associated with very depleted $\delta^{13}C$ values occur at these two sites in September-October of each year and are due to input of bacterial methane. Generally, at the northern hemisphere sites the lowest $\delta^{13}C$ values occur in the fall and the highest values occur in the summer. This trend toward higher summertime $\delta^{13}C$ values is expected if CH_4 oxidation by OH primarily controls the seasonal cycle because the $^{12}CH_4$ molecules react at a slightly faster rate (1.0054×) than the $^{13}CH_4$ molecules [*Cantrell et al.*, 1990]. The annual mean $\delta^{13}C$ values increase southward from about -47.8‰ at 71°N to -47.3‰ at 14°S.

We calculate a global average $\delta^{13}C$ of CH_4 of approximately -47.5‰. The mean global $\delta^{13}C$ value, when combined with the ^{14}C content of atmospheric CH_4, yields estimates of the proportion of bacterial, non-bacterial, and fossil CH_4 source strengths [*Quay et al.*, 1991]. We estimate that bacterial CH_4 sources contribute ~70%, fossil CH_4 sources ~20%, and biomass burning ~10% of the total CH_4 input.

Although the seasonal cycle in $\delta^{13}C$ dominates the time-series measurements in the northern hemisphere, there is evidence for a slight interannual increase up until 1992. Measurements at all four time-series locations indicate an increase in $\delta^{13}C$ and, when combined and area weighted, yield an average rate of approximately 0.04 ± 0.02‰ per year. A $\delta^{13}C$ increase indicates the ratio of bacterial to non-bacterial CH_4 source strength is decreasing. In 1993, however, there has been a leveling of the $\delta^{13}C$ trend at the northern sites and a decrease at SMO. This trend is similar to the recent $\delta^{13}C$ decrease observed at Baring Head, New Zealand (41°S) and Scott Base, Antarctica (78°) by *Lowe et al.* [1994], who attribute the decrease to a reduction of the CH_4 released from biomass burning. Measuring the interannual change in the $\delta^{13}C$ of atmospheric CH_4 at several sites over the longer term will be a useful indicator of changes in the proportion of

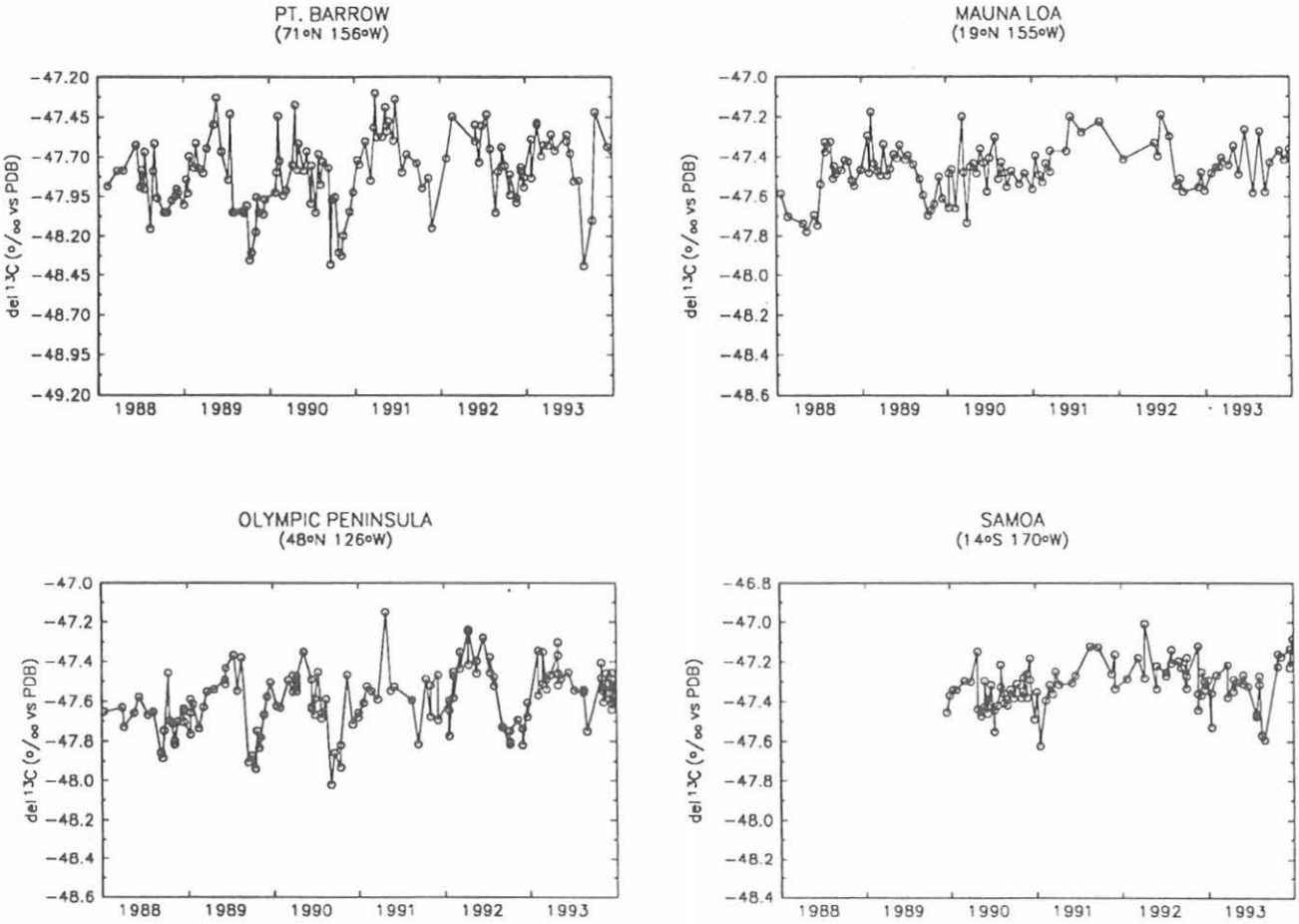

Fig. 1. The time series of the $\delta^{13}C$ of atmospheric CH_4 measured at BRW, Olympic Peninsula, MLO, and SMO since 1988.

bacterial and non-bacterial CH_4 inputs. These isotopic records should help us determine why the rate of methane increase has slowed so dramatically over the last few years.

References

Dlugokencky, E.J., K.A. Maserie, P.M. Lang, P.P. Tans, L.P. Steele and E.G. Nisbet, A dramatic decrease in the growth rate of atmospheric methane in the northern hemisphere during 1992, *Geophys. Res. Lett.*, *21*, 45-48, 1994.

Cantrell, C.A., R.E. Shetter, A.H. McDaniel, J.G Calvert, J.A. Davidson, D.C. Lowe, S.C. Tyler, R.J. Cicerone and J.P. Greenberg, Carbon kinetic isotope effect in the oxidation of methane by the hydroxyl radical, *J. Geophys. Res.*, *95*, 22,455-22,462, 1990.

Lowe, D.C., C.A.M. Brenninkmeijer, G.W. Brailsford, K.R. Lassey, A.J. Gomez and E.G. Nisbet, Concentration and ^{13}C records of atmospheric methane in New Zealand and Antarctica: evidence for changes in methane sources, *J. Geophys. Res.*, *99*, 16,913-16,920, 1994.

Quay, P.D., S.L. King, J. Stutsman, D.O. Wilbur, L.P. Steele, I. Fung, R.H. Gammon, T.A. Brown, G.W. Farwell, P.M. Grootes, and F.H. Schmidt, Carbon isotopic composition of atmospheric methane: Fossil and biomass burning source strengths, *Global Biogeochem. Cycles*, *5*, 25-47, 1991.

Stevens, C.M. and F.E. Rust, The carbon isotopic composition of atmospheric methane, *J. Geophys. Res.*, *87*, 4879-4882, 1982.

Wigley, T.M.L. and S.C.B. Raper, Implications for climate and sea level of revised IPCC emission scenarios, *Nature*, *357*, 293-300, 1992.

Point Barrow Geomagnetic Observatory

J.F. SCARZELLO
Naval Surface Warfare Center, Electromagnetic Fields Branch, Silver Spring, Maryland 20903-5640

As part of the U.S. Navy's Ice Experiment 1-91, a permanent Geomagnetic Observatory was established at Point Barrow, Alaska, on March 21, 1991. The Point Barrow Geomagnetic Observatory (PBGMO) was designed and established by Naval Surface Warfare Center (NSWC), Electromagnetic Fields Branch, to be a permanent facility that acquires ambient noise using state-of-the-art and experimental magnetic sensors. This program is sponsored by the Office of Naval Research, Ocean, Atmosphere, and Space Science Technology Department. The observatory was established to measure the high level geomagnetic activity (1991 to 1993) generally associated with sunspot maximum periods and to provide data for at least the next decade. The PBGMO sensors are located on U.S. Air Force property, near the NOAA Climate Monitoring and Diagnostics Laboratory that provides support and housing for the observatory electronics. The U.S. Geological Survey's geomagnetic observatory is about 1/2 km west and uses less sensitive proton precession magnetometers.

The PBGMO has three helium-3 magnetometers and three triaxial fluxgate magnetometers arranged to form two orthogonal gradiometer axes, north-south and east-west magnetic with baselines of 152 m (500 feet). The sensor and its electronics are mounted on a tray inside a PVC tube that is put inside a 203-mm (8-inch) diameter fiberglass waterproof housing. The fiberglass tube has a welded aluminum pipe shield (open ends) and is put inside a non-magnetic wooden box. A non-magnetic wooden fence was built around the sensor to mark its location and protect it from animals and adventuresome snowmobilers. Two RG-8/U cables are required to provide power to and obtain signals from each sensor. The six cables are routed to the CMDL facility building where NOAA has provided NSWC with a table in a corner of one room and access to a phone line. The U.S. Air Force Long Range Radar Site provides space for storage, lodging, and other logistical support.

Data from the Point Barrow helium-3 and fluxgate sensors are recorded on magnetic tape cartridges (March 1991 to January 1994) and most recently, (January 1994 to present) on optical disk storage medium because of the volume of data obtained from continuously sampling the ambient noise and to easily access data records. Data tapes and cartridges have been shipped to NSWC, White Oak site by NOAA personnel.

The PBGMO electronics were originally designed to pump the helium-3 sensors once a day, assuming the helium-3 nuclear magnetic resonance magnetometer T2 times would be greater than 24 hours. Unfortunately, only one of the three worked reliably greater than 24 hours, so a 12-hour repump time was programmed, resulting in a 10-minute loss of data from an otherwise continuous data record. Trips to repair one helium-3 sensor and up-grade software, electronics, and assure that sensors have greater than 12 hours T2 time were made on September 30, 1991, and again in January 1994. The helium-3 magnetometers, designed and built by Texas Instruments, Inc., McKinney, Texas, have a noise level of nominally 1 picotesla. (1 picotesla = 10^{-8} Oersted= 10^{-3} nanotesla = 10^{-3} gamma).

All observatory functions are controlled by a type 386 personal computer with a magnetic tape drive and a Ricoh Optical Drive, uninterruptable power supply, modem phone line for program control, and instant access from White Oak. An electronics power supply sensor interface cabinet contains three power supplies that power each sensor separately.

THE DATA

The initial measured data contained some glitches and incomplete data records that have been corrected resulting in almost continuous data records from April 1991 to the present. Each data file contains all sensor information sampled at 2.34 Hz and identified by year (last digit), month (2 digits), day (2 digits) hours Zulu (2 digits) and tens of minutes to define the standard half hour file. The helium-3 NMR magnetometer measures the absolute value of the total ambient field, and at this location it is nominally 57,450 nT with slight variations associated with sensor location, i.e., sensor no. 1 measures 35 nT more than sensor no. 3, and sensor no. 2 is 10 nT less than sensor no. 3.

In addition to the total field helium sensor information, each of the three sensors has a fluxgate magnetometer. Activity indices are computed from the triaxial fluxgate magnetometers over a 23-hour period. The indices are the change in component field amplitude in nanotesla measured in a 2.5-minute period. Display software has been developed to plot the field value from all sensors and components and the gradient field from each sensor pair, i.e., 1-2, 2-3, and 1-3 for one 30-minute data segment.

THE FUTURE

The present plan is to operate the PBGMO for at least the next decade. Some upgrading is planned for the helium-3 and fluxgate magnetometers, enhancing data recording reliability, and testing experimental sensors and systems. Data reduction, which includes transferring magnetic tape cartridge data to optical disks, appears to be the most efficient storage and distribution mechanism and will be done in FY95. Software development has been started to define a set of geomagnetic noise parameters, to automatically scan through the archived data, and to select out data segments of interest for further examination.

USGS Barrow Observatory

JACK TOWNSHEND
U.S. Geological Survey, College Obesrvatory, Fairbanks, Alaska 99775-5160

The Barrow Magnetic Observatory is the northernmost of this agency's (U.S. Geological Survey) 12 continuously-recording, digital magnetic observatories. As such, it serves as a singularly important site in a global network of observing stations whose combined data define the planetary magnetic field and track its secular change. Ground stations such as the Barrow Observatory are controls for field modeling by harmonic analysis, essential reference stations for airborne and satellite surveys, and absolute calibration locations for field survey instrumentation.

The primary instrumentation operated is an EDA FM-100BR Triaxial fluxgate magnetometer, an EDA PPM-105 proton free-precession magnetometer, an Observatory Magnetometer Interface System (OMIS), and several pier-mounted instruments for absolute control observations.

In August 1993 the USGS and NOAA negotiated a Memorandum of Agreement (MOA) to have CMDL personnel at Barrow service the USGS BRW equipment, make instrument observations, and provide some logistic support.

The principal investigator for the Barrow Observatory in 1993 was Jack Townshend. The coinvestigator in 1993 was Robert Hammond. In 1994, Johnny Dickey is the coinvestigator. The Barrow Magnetic Observatory receives its authorization to operate from the USGS Branch of Earthquakes and Geomagnetic Information in Golden, Colorado.

Parts of the NOAA-USGS MOA are presented below to provide some history and background of our joint Barrow operations.

For many years, the Naval Arctic Research Laboratory (NARL) was the source of electrical power, road maintenance, transportation, and lodging support. Effective October 1, 1984, this support was no longer assured as the Navy began the process of transferring ownership of NARL to the Ukpeagvik Inupiat Corporation (UIC).

Individual withdrawal applications for land occupied by each agency's project was approved by BLM and published in the Federal Register. Withdrawal file numbers are NOAA-F-81469 and USGS-F-81490. Transfer of the land to the USGS and NOAA was made effective April 2, 1991, and published in the *Federal Register*, Volume 56, Number 63, page 13413, dated April 2, 1991.

A third-party agreement was set up between NOAA, USGS, and the Department of the Air Force, now located at 11TCW/LG0X, 6900 9th St. Suite 301, Elmendorf AFB, Alaska 99506-2270, to provide support for electrical power, road service, transportation, vehicle repair, lodging, and meals through their DEW System Station at Barrow, Alaska (Pow-Main). This agreement (Inter-Agency MOA between NOAA and USGS) will be an attachment to the "Support Agreement" between USAF, NOAA and USGS. NOAA is authorized by the USGS to be signatory to the "Support Agreement" with the USAF, since they want only one signature on the document.

Subsequently NOAA and USGS agreed to get power from the Barrow Utilities and Electric Co-op, Inc., (BUEGI), through the Ukpeagvik Inupiat Corporation/Northern Arctic Research Laboratory (UIC/NARL) facility.

NOAA and the USGS shall continue to acquire electrical power from the Barrow Utilities and Electric Co-op., Inc. (BUECI). During emergencies and times then when power is not available from BUECI, it is the intent of NOAA and USGS to receive electrical power from the Air Force DEW Line.

Under the terms of the MOA, NOAA agrees to have the CMDL personnel at Barrow do the following:

Weekly

Check facilities for any noticeable damage or unusual conditions and report anything that may seem out of the ordinary to the College Observatory, Fairbanks, check the Observatory instruments and equipment, and make routine rotations on specific forms supplied.

Monthly

Make six sets of magnetic absolute observations with a Declination Inclination Magnetometer (DIM); make one set of Scale Value Observations on the Observatory Magnetometer Interface System (OMIS) Fluxgate Magnetometer; change digital magnetic, and analog paper tapes; and send all data, computations, observations, and tapes to the USGS office.

Unscheduled

Perform minor trouble shooting and make adjustments to equipment when USGS technical personnel provide instructions by telephone.

For the services supplied by NOAA in the previously mentioned items, the USGS will reimburse NOAA for the time required to perform the work, travel time required to get to and from USGS facilities and instruments, and a reasonable amount for unplanned circumstances because of emergencies, weather, etc. Supplies and materials are not included in this agreement. USGS will pay for or reimburse NOAA for supplies or materials needed.

A New Rugged High Sensitivity Radon Monitor for Remote Stations

STEWART WHITTLESTONE
Australian Nuclear Science and Technology Organization, Menai NSW 2234, Australia

STEVE RYAN
NOAA Mauna Loa Observatory, Hilo, Hawaii 97621-0275

INTRODUCTION

The radon detector which was operated for ANSTO by MLO, was installed in April 1989 to provide a full year of radon concentrations to assess the utility of such information to the CMDL baseline monitoring program. After a year the data proved to be of interest, and the instrument was easy to operate so it was left in place. Over the 5 years to April 1994, several publications have drawn on data from the radon program [*Whittlestone*, 1985, 1990, *Whittlestone et al.*, 1991, 1992, 1993; *Gras and Whittlestone*, 1992]. Radon has been established as a valuable measurement for characterizing air masses and should continue to be measured at MLO.

Scientifically it would be desirable to expand CMDL's radon measurement program to other stations. The major inhibition to this process has been financial, but there was also concern that the instrument was more complex than would be desirable at some stations. MLO is environmentally relatively benign and, because of its size, has the technical capability to maintain a relatively complex instrument. Simply installing a duplicate of the first MLO radon detector would not guarantee success at another observatory. ANSTO has, therefore, been developing an instrument better suited to more remote sites.

MLO has provided an excellent opportunity to assess the requirements of a radon detector, partly because it has much in common with other stations that could benefit from radon measurements, and partly because it has two radon detectors (ANSTO's and EML's), each with different characteristics. ANSTO's new design is superior in all ways to its old one, and it incorporates some of the better qualities of the EML instrument. In line with the design objectives, the main respects in which the new instrument is superior to either of the others is in initial cost, simplicity, low power consumption, and freedom from routine maintenance.

In April 1994 the ANSTO radon detector at MLO was re-built to become the second detector of its type. The first was installed at Cape Grim in February 1994. Prior to this, only a small laboratory prototype had been operated. It is therefore pleasing to be able to report that the new system has performed to specification and required no operator intervention between its installation and writing of this report (July 1994). A detailed report on the new design is being prepared by S. Whittlestone et al, 1994.

DETECTOR DESIGN

High-sensitivity radon detectors work on the "two-filter" principle. Five stages are involved: (1) All radon decay products are filtered from the inlet air by the first filter; (2) the air passes through a delay chamber where a known proportion of the radon decays; (3) the decay products, which have a concentration proportional to that of the radon, are collected on the second filter; (4) the decay of the radon decay products on the filter is converted to electronic pulses; and (5) a data acquisition and control system collects the data and monitors essential operating parameters.

For brevity the EML detector will be designated "E", the old ANSTO detector "A1" and the new one "A2". Little discussion is required of stage 1. All the instruments have similar filters for filter 1, but rather different flow rates, being 400-, 90-, and 40-L min^{-1} for E, A2 and A1 respectively.

Stage 2 involves important design considerations because it is necessary to stop the radon decay products from being plated out on the walls of the delay chamber. E uses the approach of moving the air so fast that the decay products do not have time to stick. In E's design this means that high flow rates (400 L min^{-1}) are needed in all flow paths, resulting in high pumping power. A1 had an aerosol injected into the air stream. The decay products became attached to the aerosol which was much less likely to plate out, so it was possible to use a low flow rate (40 L min^{-1}). A2 uses the high flow rate idea, but has an internal flow loop which means that the high flow is only through a very low impedance filter. The result is that A2 has the simplicity of E but an even lower pumping power than A1. At 25 watts, the power is about an order of magnitude less than E or A1.

In stage 3, the second filter, A2 again takes the simpler of the approaches used in E and A1. In this case it is A1's fixed filter that is used. But an important step is taken here by using a very fine wire screen that is just as effective as a filter for collecting the decay products, but offers much less flow impedance. This is the only part of the detector that requires routine maintenance, and it should be replaced or cleaned every 1 or 2 years.

The fixed filter has two advantages over the moving-filter design. One is the inherent simplicity. Nothing moves and no external control is required. The other advantage is that all the decay products on the filter are

counted, whereas in a moving-filter system, about half of them decay during sampling before the filter is moved to the counter. Fixed-filter detectors are, therefore, more efficient.

The disadvantage of the fixed filter is that the time response is slow. A1 took about 90 minutes to reach 50% of maximum count rate, whereas E indicates the concentration in well-defined half-hour intervals. A2 is much faster than A1 for reasons that are too complex to explain here. It reaches 50% of maximum response in 30 minutes.

There are applications where the slow response time of A1 makes it necessary to use design E. Many of those applications would be adequately served by design A2, making it unnecessary to compromise on efficiency and increase complexity, as E does, in order to gain the required time response. Stage 4, counting the decay products, is practically identical for all three systems. It involves a zinc sulfide screen scintillator with a photomultiplier to detect the alpha particles, followed by pulse amplifiers, and discriminators.

In the final stage, 5, which includes data acquisition and control, E and A1 need active control of moderately complex systems: a filter tape transport mechanism and particle counter respectively. A2 has no devices to control and in its simplest configuration needs to record only pulses from the alpha counter. Only a very simple device is needed. Real-time requirements could be met by a simple, robust data logger.

Results

Figure 1 is an example of the results obtained from the new detector (A2) and the EML detector (E). There is no question that A2 is measuring radon. However well a laboratory prototype works, performance must be obtained in the field. The agreement between the results will be considered first. Correlation analysis shows that overall, the correlation coefficient between them is 0.79. The data were grouped using different criteria: groups with a wide range of concentrations had the best correlations. The period shown with its concentration range of about 50 to 500 mBq m^{-3}, had a correlation coefficient of 0.87, whereas groups with ranges 50 to 300 typically had correlation coefficients of about 0.65. These are consistent with correlations observed between detectors E and A1 that ranged from 0.55 for narrow concentration ranges to 0.97 when the concentrations reached 1000 mBq m^{-3}. There is some evidence in this limited data set that the correlation is better between E and A2 than E and A1, as expected because of the improved time resolution of A2.

It is instructive to examine the differences between the results. At concentrations below 100 mBq m^{-3}, the agreement is poor, which can be attributed mainly to counting statistical error. At 60 mBq m^{-3} the error on a 1-hour value for E is 30% and for A2 is 15%. At higher concentrations, differences are smaller, but not as small as could be expected on the basis of counting statistics. These differences are attributed to the better time resolution of E.

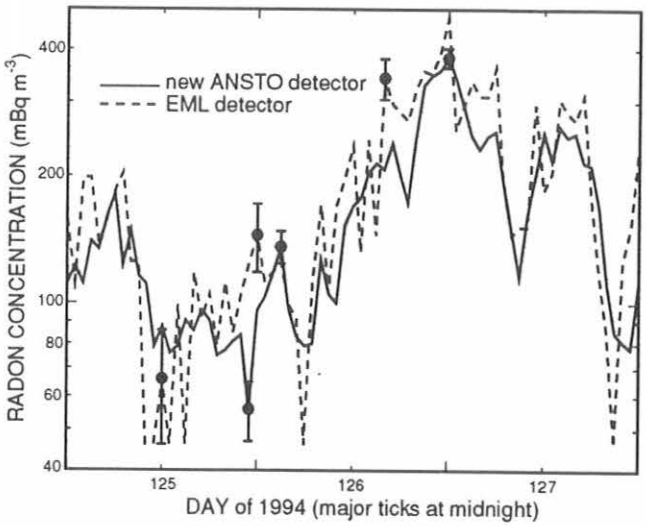

Fig. 1. Radon concentrations at MLO measured by ANSTO and EML instruments.

Conclusions

A new design of baseline radon detectors brought the cost and maintenance requirements down to about the cost of meteorological instruments. Given the power of radon measurements to characterize air samples at remote stations, it is recommended that such measurements be viewed as a necessary component of their basic instrumentation.

The new design has been proven in the field at MLO. It has achieved the same sensitivity as the previous ANSTO radon detector for about half the capital cost, a tenth of the power consumption, and reduction of routine maintenance from weekly to once per year. Because of the simplicity of the design, it is reasonable to expect that unscheduled breakdowns should be less frequent and diagnosis should be much easier.

While the new detector is superior to the old ANSTO design in all respects, the EML design would be preferred in situations when time resolution is of prime importance and concentrations of interest are more than 100 mBq m^{-3}. At MLO, where the demands of instrument maintenance can be met easily, it is desirable to have both detectors because there are rapid concentration changes, long periods when the concentration is more than 100 mBq m^{-3}, and periods when the concentration is lower than 100 mBq m^{-3} and higher sensitivity is necessary.

For a new installation at stations less well staffed than MLO and with a more demanding environment, the new design is to be preferred on cost and maintenance considerations. At Samoa, South Pole, and Barrow,

long periods of very low radon concentrations could be anticipated, which gives a scientific preference for the more sensitive instrument.

Acknowledgments. The authors are grateful to CMDL for housing the equipment and assisting with its operation. The radon detector upgrade kit was built by B. Stenhouse of ANSTO.

REFERENCES

Gras J., and S. Whittlestone, Radon and CN: Complementary tracers of polluted air masses at coastal and island sites, *J. Radioanal. Nucl. Chem., 161*, 293-306, 1992.

Whittlestone S., Radon measurements as an aid to the interpretation of atmospheric monitoring, *J. Atmos. Chem., 3*, 187-201, 1985.

Whittlestone S., Radon from distant continents detected at the Mauna Loa Observatory, in *Climate Monitoring and Diagnostics Laboratory No. 18 Summary Report 1989*, pp. 131-133, NOAA Environmental Research Laboratories, Boulder, CO, 1990.

Whittlestone S., L.P. Steele, and S. Ryan, Radon as a baseline selection criterion at Mauna Loa Observatory, in *Climate Monitoring and Diagnostics Laboratory No. 19 Summary Report 1990*, pp. 120-123, NOAA Environmental Research Laboratories, Boulder, CO, 1991.

Whittlestone S., S.D. Schery, and Y. Li, Separation of local from distant pollution at MLO using Pb-212", in *Climate Monitoring and Diagnostics Laboratory No. 21 Summary Report 1992*, pp. 116-118, NOAA Environmental Research Laboratories, Boulder, CO, 1993.

Whittlestone S., E. Robinson, and S. Ryan, Radon at the Mauna Loa Observatory: Transport from distant continents, *Atmos. Environ. 26A(2)*, 251-260, 1992.

7. International Activities, 1993

In July, Eldon Ferguson attended and participated in the International Symposium on Modern Chemistry in Beijing, China. In November, he lectured at the Department of Chemistry and interacted and collaborated on research in atmospheric ion chemistry and air-sea exchange of CO_2 at the University of Canterbury, Christchurch, New Zealand.

In April, Russ Schnell spent 1 week in northern Siberia at Cherskiy, Russia, co-leading a group of NOAA, EPA, and DOE scientists and administrators in a research logistics demonstration project. The group flew on chartered Russian aircraft including an AN-74 (jet), AN-26 (twin turboprop), and AN-2 (single engine biplane) to test the aircraft capabilities for future Arctic air research projects. Doug Guenther, also a member of the group, determined the feasibility of utilizing Russian aviation resources to carryout out flask sampling of trace gases. Russ Schnell attended the International Global Aerosol Program workshop in Geneva, June 28-July 2, 1993, as a member of two Expert Panels drafting the overall IGAP program plan. October 4-8 Russ Schnell attended and presented papers on AGASP and CMDL Arctic meteorological data sets at the International Symposium on the Ecological Effects of Arctic Air Contaminants, Reykjavik, Iceland.

Bernard Mendonca traveled to Geneva, Switzerland, in January to attend the first organizational meeting for the establishment of the WMO GAW stations. In March he traveled to Munich, Germany, to attend the Harmonization of Environmental Measurement (HEM) Programme and Technical Advisory Group Meeting as a member of the programme and technical advisory group of the United Nations Environment Programme (UNEP). In March and April Bernard traveled to Buenos Aires, Argentina, and Sao Paulo, Brazil, to continue in the organization and establishment of GAW stations. Bernard traveled to Geneva in June and again in October to aid the WMO Secretariat staff in station logistics and purchasing of equipment for the GAW stations.

In April and May, Dave Hofmann traveled to Oberpfaffenhofen, Germany, to discuss research results at the Institute for Atmospheric Physics. D. Hofmann presented a paper entitled "Twenty years of balloonborne tropospheric aerosol measurements at Laramie, Wyoming" at the First International Global Atmospheric Chemistry Program (ICAG) Scientific Conference in Eilat, Israel. Next, he visited the Institute for Atmospheric Environment Research in Garmisch, Germany, to conduct research and present a paper entitled "Possible impact of the commercial jet fleet on the upper tropospheric aerosol" at the XVIII General Assembly of the European Geophysical Society in Wiesbaden, Germany. D. Hofmann then visited the Max Planck Institute (MPI) in Heidelberg before attending the MPI sponsored IPCC WGI Workshop on The Impact on Climate of Ozone Change and Aerosols held in Hamburg.

D. Hofmann attended two WMO meetings. The first was the June meeting of the Stratospheric Aerosol working group of the International Global Aerosol Program at WMO headquarters in Geneva, Switzerland. The second meeting was comprised of authors for the United Nations Environment Program Ozone Trends Report and was held in September in Cambridge, England. In late October and early November, D. Hofmann attended a meeting at the CSIRO Cape Grim Baseline Air Pollution Station in Hobart, Tasmania, Australia.

H. Vömel participated in the NATO Advanced Study Institute on Low Temperature Chemistry of the Atmosphere in Maratea/Sapri, Italy. He presented a paper entitled "Balloon-borne observations of stratospheric and upper tropospheric water vapor in the tropics and over Antarctica." While in Europe, H. Vömel also visited Grossforschungsanlage in Jülich, Germany, to work with Dieter Kley on the use of their atmospheric test for calibrating ozonesonde pumps and the frost-point hygrometer. M. O'Neill accompanied H. Vömel to carry out balloonborne water vapor and ozone measurements from aboard the research vessel *John H. Vickers*.

Mike O'Neill visited Christmas Island, Republic of Kiribati, on March 18-29 and Terciera, Azores, on July 28-September 9 to discuss $CO_2/CH_4/CO$ sampling with local sample takers.

The University of Stockholm invited John Ogren to present a seminar "Measurements of the size-dependence of the scavenging efficiency of aerosol particles by fog droplets" in January. While in Sweden, John consulted with colleagues on the measurements done at the Swedish baseline station on Spitsbergen and worked with faculty and students on evaluation of cloud/aerosol measurement data.

In September, Sam Oltmans attended a workshop on European Ozonesonde Records and presented results on North American ozonesonde trends in Jülich, Germany.

B. Evans and W. D. Komhyr traveled to Hradec Kralove in the new Czech Republic to attend the Dobson Workshop and Intercomparison in May.

In June, W.D. Komhyr attended the High Latitude Optics Symposium in Tromsø, Norway, to present an invited paper entitled, "U.S.A. Dobson Spectrophotometer Total Ozone Program, 1962-1992." In November, W.D. Komhyr traveled to Thessaloniki, Greece, to participate in a WMO Meeting of Experts on Homogenizing Total Ozone Records for Ozone Assessments and Early Warning of Ozone Changes.

B. Bodhaine and J. Wendell traveled to the remote Sable Island Regional Climate Monitoring Station off the coast of Newfoundland, Canada, in July to install

new and to test and calibrate existing aerosol instrumentation. In late October, J. Wendell installed a new solar radiation data acquisition system at South Pole, Antarctica.

M. Lucarelli from Australia (CSIRO) and R. Knobben from New Zealand (NIWA) worked with D. Guenther from April to June to build four of the CMDL-design aircraft sampling apparatus. Under an agreement, CSIRO and NIWA each received a complete sampling system.

In May, L. Haszpra from the Institute for Atmospheric Physics in Budapest, Hungary, came to Boulder for 25 days. The purpose of the visit was to prepare a paper for presentation at the 4th International Conference on CO_2.

Pieter Tans, Jim Peterson, and Michael Trolier attended the WMO CO_2 Experts Meeting held on September 6-11 in Rome, Italy.

Peter Bakwin, Philippe Ciais, Jim Peterson, Pieter Tans, and Michael Trolier participated in the 4th International CO_2 Conference in Carqueiranne, France, on September 13-17. Each presented a paper (see Publications and Presentations).

The program to bring flask-sampling network personnel to Boulder was continued. In preparation for establishing a sampling site in Malta, H. Galea from the Ministry of Environment, Pollution Control Co-ordinating Unit, Vittoriosa, visited Boulder September 8-12. Likewise, H. Muñoz, Direcion Meteorologica de Chile, was invited to Boulder in connection with establishing a cooperative program for collecting air samples on Easter Island. Sampling began in January 1994. Taking advantage of his trip to Washington, DC, arrangements were made for D. Dagvadorj, Mongolian Hydro-Meteorological Research Institute, to make a side trip to Boulder on December 18-21 to discuss the results to date of sampling for about 2 years at Ulaan Uul.

The South China Sea air sampling aboard the Chevron tanker *Carla A. Hills* terminated in February after 19 months of continuous collections. The vessel's charter was not renewed by Caltex. The Blue Star Line vessels, *Wellington Star* and *Southland Star* were withdrawn from trans-Pacific service in July and August, respectively. L. Waterman traveled to Los Angeles to join the Blue Star Line vessel *California Star* on October 16-31 to train ship's officers to collect air samples and to restart Operation Pacific Air that had been in hiatus since August. The practice of collecting samples at 5° latitude intervals will be continued and a single pair in the middle of the Tasman Sea for each crossing was added to the protocol. L. Waterman disembarked at Botany Bay, NSW, and visited Glass Expansion Pty. Ltd., Hawthorn, Victoria, and CSIRO, Aspendale, Victoria, on November 2. Glass Expansion manufacturers one of the best glass o-ring seal valves currently on the market. From November 12-26, L. Waterman sailed on the *Great Promise* from Singapore to Hong Kong and return to restart the South China Sea program. The protocol for collecting pairs of evacuated samples every 3° of latitude on all runs, north and south, was reestablished.

P. Novelli continued intercomparisons of CO standards begun in 1991. The current round of comparisons, begun in July, involves ten laboratories in eight countries and will be completed in January 1995. Four cylinders of standard gases are being sent from one collaborator to the next in Australia, Brazil, Germany, Hong Kong, Japan, New Zealand, South Africa, and the United States (Colorado, Maryland, and Virginia). The objective of the intercomparisons, sponsored by NASA, is to create an internally consistent set of ground based measurements to which measurements from space can be compared.

8. Publications and Presentations by CMDL Staff, 1993

Bakwin, P.S., Measurements of carbon dioxide on a very tall tower, paper presented at the 4th International Conference on CO_2 sponsored by WMO Global Atmosphere Watch, Carqueiranne, France, September 13-17, 1993.

Bodhaine, B.A, The U.S. aerosol monitoring program in Antarctica, Proceedings, 4th Workshop Italian Research on Antarctic Atmosphere, Porano, Italy, October 21-23, 1991, Italian Physical Society, Bologna, Italy, 15-25, 1993.

Bodhaine, B.A., and E.G. Dutton, A long-term decrease in Arctic Haze at Barrow, Alaska, *Geophys. Res. Lett., 20*, 947-950,1993.

Bodhaine, B.A., B.I. Nazarov, and A.K. Shukurov, Comparison of aerosol concentrations at Fedchenko Glacier and Dushanbe, in *JOINT SOVIET-AMERICAN EXPERIMENT ON ARID AEROSOL*, G.S. Golitsyn (ed.), Hydrometeoizdat, St. Petersburg, Russia, 181-184, 1993.

Bojkov, R., W.D. Komhyr, A. Lapworth, and K. Vanicek, Dobson data re-evaluation handbook, *NOAA Tech. Report NESDIS 74*, 140 pp., 1993.

Butler, J.H., J.E. Elkins, T.M. Thompson, B.D. Hall, J.H. Lobert, T.H. Swanson, V. Korapalov, poster presentation at the Biannual Meeting of the Oceanographic Society, Seattle, WA, April 2-16, 1933.

Cess, R.D., S. Nemesure, E.G. Dutton, J.J. DeLuisi, G.L. Potter, and J.-J. Morcrette, The impact of clouds on the shortwave radiation budget of the surface-atmosphere system: Interfacing measurements and models, *J. Clim., 6(2)*, 308-316, 1993.

Chiou, E.W., M.P. McCormick, L.R. McMaster, W.P. Chu, J.C. Larsen, D. Rind, and S. Oltmans, Intercomparison of stratospheric water vapor observed by satellite experiments: Stratospheric Aerosol and Gas Experiment II versus Limb Infrared Monitor of the Stratosphere and Atmospheric Trace Molecule Spectroscopy, *J. Geophys. Res., 98(D3)*, 4875-4887, 1993.

Chu, W.P., E.W. Chiou, J.C. Larsen, L.W. Thomason, D. Rind, J.J. Buglia, S. Oltmans, M.P. McCormick, and L.M. McMaster, Algorithms and sensitivity analyses for Stratospheric Aerosol and Gas Experiment II water vapor retrieval, *J. Geophys. Res., 98(D3)*, 4857-4866, 1993.

Ciais, P., P. Tans, M. Trolier, and J.W.C. White, Global carbon cycle modeling: The distribution of the sources and sinks of CO_2 from ^{13}C isotope measurements in the remote troposphere, paper presented at the 4th International Conference on CO_2 sponsored by WMO Global Atmosphere Watch, Carqueiranne, France, September 13-17, 1993.

Conway, T.J., L.P. Steele, and P.C. Novelli, Correlations among atmospheric CO_2, CH_4 and CO in the Arctic, March 1989, *Atmos. Env., 27A(17/18)*, 2881-2894, 1993.

Davidson, C.I., and R.C. Schnell, Introduction: On arctic air, snow, and ice chemistry, *Atmos. Env., 27A(17/18)*, 2695-2699, 1993.

Davidson, C.I., J.-L. Jaffrezo. B.W. Mosher, J.E. Dibb, R.D. Borys, B.A. Bodhaine, R.A. Rasmussen, C.F. Boutron, U. Gorlach. H. Cachier, J. Ducret, J.-L. Colin, N.Z. Heidam, K. Kemp, and R. Hillamo, Chemical constituents in the air and snow at Dye 3, Greenland: I, Seasonal variations, *Atmos. Env., 27A*, 2709-2722, 1993.

Davidson, C.I., J.-L. Jaffrezo. B.W. Mosher, J.E. Dibb, R.D. Borys, B.A. Bodhaine, R.A. Rasmussen, C.F. Boutron, U. Gorlach. H. Cachier, J. Ducret, J.-L. Colin, N.Z. Heidam, K. Kemp, and R. Hillamo, Chemical constituents in the air and snow at Dye 3, Greenland: II, Seasonal variations, *Atmos. Env., 27A*, 2723-2737, 1993.

DeLuisi, J.J., D.U. Longenecker, C.L. Mateer, and W.P. Chu, Estimation of solar backscatter ultraviolet albedo using ground-based Umkehr measurements, *J. Geophys. Res., 98(D2)*, 2985-2993, 1993.

Dlugokencky, E.J., J.M. Harris, Y.M. Chung, P.P. Tans, and I.Y. Fung, The relationship between the methane seasonal cycle and regional sources and sinks at Tae-ahn Peninsula, Korea, *Atmos. Environ., 27A*, 2115-2120, 1993.

Dlugokencky, E.J., P.M. Lang, K.A. Masarie, L.P. Steele, and E.G. Nisbit, A dramatic decrease in the growth rate of atmospheric methane in the Northern Hemisphere during 1992, paper presented at the Fall American Geophysical Union Meeting, San Francisco, CA, December 10, 1993.

Dutton, E.G, An extended comparison between LOWTRAN7 computed and observed broadband thermal irradiances: Global extreme and intermediate surface conditions, *J. Atmos. Oceanic Technol., 10(3)*, 326-336, 1993.

Elkins, J., Facts and myths over ozone depletion and the CFCs, paper presented at the NOAA Sea Grant Meeting-New England Region, Durham, NH, November 9, 1993.

Elkins, J.W., T.M. Thompson, T.H. Swanson, J.H. Butler, B.D. Hall, S.O. Cummings, D.A. Fisher, and A.G. Raffo, Decrease in the growth rates of atmospheric chlorofluorocarbons 11 and 12, *Nature, 364*, 780-783, 1993.

Ferguson, E.E, Processes associated with stratospheric ozone decrease: homogeneous chemistry, in *The Role of the Stratosphere in Global Change*, M.-L. Chanin (ed.), NATO ASI Series, Vol. 18, Springer-Verlag, Berlin Heidelberg 47-64, 1993.

Gillette, D.A., and B.A. Bodhaine, U.S. results from a joint US/USSR experiment for the study of desert dust and its impact on local meteorological conditions and climate, in *JOINT SOVIET-AMERICAN EXPERIMENT ON ARID AEROSOL*, G.S. Golitsyn (ed.), Hydrometeoizdat, St. Petersburg, Russia, 7-22, 1993.

Gillette, D.A., B.A. Bodhaine, and D. Mackinnon, Transport and deposition of desert dust in the Kafirnigan River Valley (Tadzhikistan) from Shaartuz to Esanbay: Measurements and a simple model, *Atmos. Env., 27A(16)*, 2545-2552, 1993.

Gleason, J.F., PK. Bhartia, J.R. Herman, R. McPeters, P. Newman, R.S. Stolarski, L. Flynn, G. Labow, D. Larko, C. Seftor, C. Wellemeyer, W.D. Komhyr, A.J. Miller, and W. Planet, Record low global ozone in 1992, *Science, 260*, 523-526, 1993.

Goldan, P.D., W.C. Kuster, F.C. Fehsenfeld, and S.A. Montzka, The observation of a C_5 alcohol emission in a

North American pine forest, *Geophys. Res. Lett., 20(11)*, 1039-1042, 1993.

Gunter, R.L., A.D.A. Hansen, J.F. Boatman, B.A. Bodhaine, R.C. Schnell, and D.M. Garvey, Airborne measurements of aerosol optical properties over south-central New Mexico, *Atmos., Env., 27A(8)*, 1363-1368, 1993.

Hansen, A.D.A., R.C. Schnell, A.V. Polissar, and G.S. Golitsyn, Aerosol measurements over the East Siberian Sea, paper presented at the 5th Symposium on Arctic Air Chemistry, Copenhagen, Denmark, September 8-10, 1992, *NERI Tech. Report. No. 70*, National Environmental Research Institute, Roskilde, Denmark, 1993.

Hansen, A.D.A., V.N. Kapustin, V.M. Kopeikin, D.A. Gillette, and B.A. Bodhaine, Optical absorption by aerosol black carbon and dust in a desert region of Central Asia, *Atmos. Env., 27A*, 2527-2531, 1993.

Hansen, A.D.A., V.N. Kapustin, V.M. Kopeikin, D.A. Gillette, and B.A. Bodhaine, Optical absorption by aerosol black carbon and dust in a desert region of Central Asia, in *JOINT SOVIET-AMERICAN EXPERIMENT ON ARID AEROSOL*, G.S. Golitsyn (ed.), Hydrometeoizdat, St. Petersburg, Russia, 195-105, 1993,

Herbert, G.A., P.S. Sheridan, R.C. Schnell, M.Z. Bieniulis, B.A. Bodhaine, Analysis of meteorological conditions during AGASP-IV, March 30-April 23, 1992, *NOAA Tech Memo ERL CMDL-5*, 118 pp., 1993.

Herbert, G.A., R.C. Schnell, B.J.B. Stunder, B.A. Bodhaine, S.J. Oltmans, and M.Z. Bieniulis, Meteorology and aerosol distribution during AGASP-III: The "Haze" flights (March 16-30, 1989), *NOAA Tech. Memo. ERL CMDL-6*, 103 pp., 1993.

Hewitt, C.N., and W.T. Sturges (eds.), *Global Atmospheric Chemical Change*, Elsevier, London, 470 pp., 1993.

Hofmann, D.J, Twenty years of balloon-borne tropospheric aerosol measurements at Laramie, Wyoming, *J. Geophys. Res., 98(D7)*, 12,753-12,766, 1993.

Hofmann, D.J., Possible impact of the commercial jet fleet on the upper tropospheric aerosol, paper presented at the WVII General Assembly of the European Geophysical Society in Wiesbaden, Germany, Institute for Atmospheric Environment Research in Garmisch, Germany, May 3-7, 1993.

Hofmann, D.J., and S.J. Oltmans, J.M. Harris, W.D. Komhyr, J.A. Lathrop, T. DeFoor, and D. Kuniyuki, Ozonesonde measurements at Hilo, Hawaii, following the eruption of Pinatubo, *Geophys. Res. Lett., 20(15)*, 1555-1558, 1993.

Johnson, J.E., V.M. Koropalov, K.E. Pickering, A.M. Thompson, N. Bond, and J.W. Elkins, SAGA-3 Experiment: Overview and meteorological and oceanographic conditions, *J. Geophys. Res., 98(D9)*, 16,893-16,908, 1993.

Kahl, J.D.W., D.J. Charlevoix, N.A. Zaitseva, R.C. Schnell, and M.C. Serreze, Absence of evidence for greenhouse warming over the Arctic Ocean in the past 40 years, *Nature, 361*, 335-337, 1993.

Kahl, J.D.W., M.C. Serreze, R.S. Stone, S. Shiotani, M. Kisley, and R.C. Schnell, Tropospheric temperature trends in the Arctic: 1958-1986, *J. Geophys. Res., 98(D7)*, 12,825-12,838, 1993.

Kaufman, Y.G., S.S. Khmelevtsov, and T.E. DeFoor, Lidar measurements of stratospheric aerosols during the SAGA 3 expedition, *J. Geophys. Res., 98(D9)*, 16,909-16,913, 1993.

Keeling, R.F., R.G. Najjar, M.L. Bender, and P.P. Tans, What atmospheric oxygen measurements can tell us about the global carbon cycle, *Glob. Biogeochem. Cycles*, 7, 37-67, 1993.

Khalsa, S.J., J.R. Key, R.C. Schnell, J.D. Kahl, M.C. Serreze, and J. Bates, Final Report: Development and trend analyses of an Arctic TOVS temperature sounding record, Report to NASA, Contract NA26GP0186, 28 pp., (available from CIRES, University of Colorado, Boulder), 1993.

Komhyr, W.D., U.S.A. Dobson Spectrophotometer Total Ozone Program, 1962-1992, paper presented at the High Latitude Optics Symposium in Tromsø, Norway, June 1993

Komhyr, W.D., C.L. Mateer, and R.D. Hudson, Effective Bass-Paur 1985 ozone absorption coefficients for use with Dobson ozone spectrophotometers, *J. Geophys. Res., 198(D11)*, 20,451-20,465, 1993.

Larsen, J.C., E.W. Chiou, W.P. Chu, M.P. McCormick, L.R. McMaster, S. Oltmans, and D. Rind, A comparison of the Stratospheric Aerosol and Gas Experiment II tropospheric water vapor to radiosonde measurements, *J. Geophys. Res., 98(D3)*, 4897-4917, 1993.

Lobert, J.M., and D.H. Scharffe, N_2O-and CH_4-emissionen aus biomasseverbrennung, in *EMISSIONEN DER TREIB-HAUSGASE DISTICKSTOFFOXID UND METHAN IN DEUTSCHLAND*, M. Schön, R. Walz, G. Angerer, K. Bätcher, E. Böhm, T. Hillenbrand, H. Hiessl, and J. Reichert (eds.), Erick Schidt Verlag, Berlin, 110-132, 1993.

Lobert, J.M., and J. Warnatz, Emissions from the combustion process in vegetation, in *Fire in the Environment: The Ecological Atmospheric, and Climatic Importance of Vegetation Fires*, P.J. Crutzen and J.G. Goldammer (eds.), Wiley, New York, 15-37, 1993.

McCormick, E.W. Chiou, L.R. McMaster, W.P. Chu, J.C. Larsen, D. Rind, and S. Oltmans, Annual variations of water vapor in the stratosphere and upper troposphere observed by the Stratospheric Aerosol and Gas Experiment II., *J. Geophys. Res., 98(D3)*, 4867-4874, 1993.

Miller, J.M., J.L. Moody, J.M. Harris, and A. Gaudry, A 10-year trajectory flow climatology for Amsterdam Island, 1980-1989, *Atmos. Env., 27A(12)*, 1909-1916, 1993.

Montzka, S.A., M. Trainer, P.D. Goldan, W.C. Kuster, and F.C. Fehsenfeld, Isoprene and its oxidation products, methyl vinyl ketone and methacrolein, in the rural troposphere, *J. Geophys. Res., 98(D1)*, 1101-1111, 1993.

Montzka, S.A., R.C. Myers, J.H. Butler, and J.W. Elkins, Global tropospheric distribution and calibration scale of HCFC-22, *Geophys. Res. Lett., 20(8)*, 703-706, 1993.

Noone, K.B., K.J. Noone, J. Heintzenberg, J. Ström, and J.A. Ogren, In situ observations of cirrus cloud microphysical properties using the counterflow virtual impactor, *J. Atmos. Oceanic Technol., 10*, 294-303, 1993.

Ogren, J. Measurements of the size-dependence of the scavenging efficiency of aerosol particles by fog droplets, seminar presented at the University of Stockholm, Sweden, January 1993.

Oltmans, S.A, Climatology of Arctic and Antarctic tropospheric ozone, in *The Tropospheric Chemistry of Ozone in the Polar Regions,* H. Niki and K.H. Becker (eds.), Springer-Verlag, Berlin Heidelberg, 25-40, 1993.

Oltmans, S.J, Climatology of the Arctic and Antarctic tropospheric ozone, in *The Tropospheric Chemistry of Ozone in the Polar Regions,* H. Niki and K.H. Becker (eds.), *NATO ASI Series, 17,* Springer-Verlag, Berlin, 25-40, 1993,

Oncley, S.P., A.C. Delany, T.W. Horst, and P.P. Tans, Verification of flux measurement using relaxed eddy accumulation, *Atmos. Environ., 27A*, 2417-2426, 1993.

Pachenko, M.V., S.A. Terpugova, B.A. Bodhaine, A.A. Isakov, M.A. Sviridenkov, I.N. Sokolik, E.V. Romashova, B.I. Nazarov, A.K. Shukurov, E.I. Christyakova, and T.C. Johnson, Optical investigations of dust storms during U.S.S.R.-U.S. experiments in Tadzhikistan, 1989, *Atmos. Env., 27A(16)*, 2503-2508, 1993.

Parungo, F., C. Nagamoto, G. Herbert, J. Harris, R. Schnell, P. Sheridan, and N. Zhang, Individual particle analyses of Arctic aerosol samples collected during AGASP-III, *Atmos. Env., 27(17/18)*, 2825-2837, 1993.

Penner, J.E., R.J. Charlson, J.M. Hales, N. Laulainen, R. Leifer, T. Novakov, J. Ogren, L.F. Radke, S.E. Schwartz, and L. Travis, Quantifying and minimizing uncertainty of climate forcing by anthropogenic aerosols, *DOE/NBB-0092T UC-402*, U.S. Department of Energy, Washington, DC, 53 pp., 1993.

Peterson, J.T., and R.M. Rosson (eds.), *Climate Monitoring and Diagnostics Laboratory No. 21 Summary Report 1992*, Environmental Research Laboratories, Boulder, CO 131 pp., 1993.

Peterson, J.T., K.W. Thoning, and P.P. Tans, Continuous atmospheric carbon dioxide measurements at Barrow, Alaska, 1973-1992, paper presented at the 4th International Conference on CO_2 sponsored by WMO Global Atmosphere Watch, Carqueiranne, France, September 13-17, 1993.

Proffitt, M.H., K. Aikin, J.J. Margitan, M. Loewenstein, J.R. Podolske, A. Weaver, K.R. Chan, H. Fast, and J.W. Elkins, Ozone loss inside the northern polar vortex during the 1991-1992 winter, *Science, 261*, 1150-1154, 1993.

Rind, D., E.-W. Chiou, W. Chu, S. Oltmans, J. Lerner, J. Larsen, M.P. McCormick, and L. McMaster, Overview of the Stratospheric Aerosol and Gas Experiment II water vapor observations: method, validation, and data characteristics. *J. Geophys. Res., 98(D3)*, 4835-4856, 1993.

Russell, P.B., J.M. Livingston, E.G. Dutton, R.F. Pueschel, J.A. Reagan, T.E. DeFoor, M.A. Box, D. Allen, P. Pilewskie, B.M. Herman, S.A. Kinne, and D.J. Hofmann, Pinatubo and pre-Pinatubo optical depth spectra: Mauna Loa measurements, comparisons, inferred particle size distributions, radiative effects, and relationship to lidar data, *J. Geophys. Res., 198(D12),* 22,969-22,985, 1993.

Salawitch, R.J., S.C. Wofsy, E.W. Gottlieb, L.R. Lait, P.A. Newman, M.R. Schoberl, M. Loewenstein, J.R. Podolske, S.E. Strahan, M.H. Proffitt, C.R. Webster, R.D. May, D.W. Fahey, D.Baumgardner, J.E. Dye, J.C. Wilson, K.K. Kelly, J.W. Elkins, K.R. Chan, and J.G. Anderson, Chemical loss of ozone in the Arctic polar vortex in the winter of 1991-1992, *Science, 261*, 1146-1149,1993.

Schnell, R.C., Are biological ice nuclei important in drought processes, past thoughts, present perspectives?, paper presented at Sixth International Conference on Biological Ice Nuclei, Univ. of Wyoming, Laramie, August 4-16, 1993.

Schnell, R.C., P.J. Sheridan, B.A. Bodhaine, E.G. Dutton, and J.D. Kahl, Arctic gas and aerosol data sets from AGASP and the Barrow Baseline Station, Proceedings, Int. Symposium, Ecological Effects of Arctic Airborne Contaminants, Reykjavik, Iceland, 25 pp., USA CRREL Special Report 92-93, October 4-8, 1993.

Sheridan, P.J. R.C. Schnell, W.H. Zoller, N.D. Carlson, R.A. Rasmussen, J.M. Harris, and H. Sievering, Composition of Br-containing aerosols and gases related to boundary layer ozone destruction in the Arctic, *Atmos. Env., 27A(17/18)*, 2839-2849, 1993.

Sheridan, P.J., C.E. Quincy, and R.C. Schnell, Optical properties of aerosols in the Kuwait oil fire smoke plume, May-June 1991, *NOAA Data Report, ERL, CMDL-10*, NOAA, Boulder, CO, 154 pp., 1993.

Sheridan, P.J., R.C. Schnell, and D.W. Garvey, Analytical electron microscope analysis of aerosol sampled over White Sands Missile Range, NM, 1989, *Atmos. Environ., 27A(8),* 1169-1183, 1993.

Sheridan, P.J., R.C. Schnell, J.D. Kahl, J.F. Boatman, and D.M. Garvey, Microanalysis of the aerosol collected over south-central New Mexico during the ALIVE field experiment, May-December, 1989, submitted, *Atmos. Environ., 27A*, 1169-1183, 1993.

Sheridan, P.J., R.C. Schnell, W.H. Zoller, N.D. Carlson, R.A. Rasmussen, J.M. Harris, and H. Sievering, Composition of Br- containing aerosols and gases related to boundary layer ozone destruction in the Arctic, *Atmos. Environ., 27A*, 2839-2849, 1993.

Stone, R.S., J.R. Key, and E.G. Dutton, Properties and decay of stratospheric aerosols in the Arctic following the 1991 eruptions of Mount Pinatubo, *Geophys. Res. Lett., 20(21)*, 2359-2362, 1993.

Sturges, W.T, Halocarbons in the Arctic and Antarctic Atmosphere, in *The Tropospheric Chemistry of Ozone in the Polar Regions*, H. Niki, and K.H. Becker (eds.), Springer-Verlag, New York, 117-130, 1993.

Sturges, W.T., and J.W. Elkins, The use of adsorbents to collect selected halocarbons and hydrohalocarbons of environmental interest from large air volumes, *J. Chromatogr., 642*, 123-134, 1993.

Sturges, W.T., C.W. Sullivan, R.C. Schnell, L.E. Heidt, and W.H. Pollock, Bromoalkane production by Antarctic ice algae, *Tellus, 45B*, 120-126, 1993.

Sturges, W.T., J.F. Hooper, L.A. Barrie, and R.C. Schnell, Stable lead isotope ratios in Alaskan Arctic aerosols, *Atmos. Environ., 27A*, 2865-2837, 1993.

Sturges, W.T., R.C. Schnell, G.S. Dutton, S.R. Garcia, and J.A. Lind, Spring measurements of tropospheric bromine at Barrow, Alaska, *Geophys. Res. Lett., 20(2)*, 201-204, 1993.

Sturges, W.T., R.C. Schnell, S. Landsberger, S.J. Oltmans, J.M. Harris, and S.-M. Li, Chemical and meteorological

influences on surface ozone destruction at Barrow, Alaska, during spring 1989, *Atmos. Env., 27A(17/18)*, 2851-2863, 1993.

Tans, P., The carbon cycle, paper presented at the State-of-the-Art Symposium on Environmental Chemistry National American Chemical Society Meeting, Denver, CO, March 29, 1993.

Tans, P.P., An observational strategy for assessing the role of terrestrial ecosystems in the global carbon cycle: Scaling down to regional levels, in *Scaling Physiological Processes* J.R. Ehleringer and C.B. Field (eds.), pp. 179-190, Academic Press, 1993.

Tans, P.P., J.A. Berry, and R.F. Keeling, Oceanic $^{13}C/^{12}C$ observations, a new window on CO_2 uptake by the oceans, *Glob. Bioeochem. Cycles, 7*, 353-368, 1993.

Tans, P.P., T.J. Conway, D.R. Kitzis, K.A. Masarie, M. Stavish, L.S. Waterman, J.C. White, and N. Zhang, Evidence for interannual variability of the carbon cycle for measurements of the CMDL Cooperative Global Flask Network, paper presented at the 4th International Conference on CO_2 sponsored by WMO Global Atmosphere Watch, Carqueiranne, France, September 13-17, 1993.

Trolier, M., J.W.C. White, P.P. Tans, and P.A. Gemery, Monitoring the stable isotopic composition of atmospheric CO_2: Data from NOAA/CMDL flask sampling network, paper presented at the 4th International Conference on CO_2 sponsored by WMO Global Atmosphere Watch, Carqueiranne, France, September 13-17, 1993.

Vömel, H., Balloon-borne observations of stratospheric and upper tropospheric water vapor in the tropics and over Antarctica, paper presented at the NATO Advanced Study Institute on Low Temperature Chemistry of the Atmosphere in Maratea, Sapri, Italy, April 1993.

Webster, C.R., R.D. May, D.W. Toohey, L.M. Avallone, J.G. Anderson, P. Newman, L.Lait, M.R. Schoeberl, J.W. Elkins, and K.R. Chan, Chlorine chemistry on polar stratospheric cloud particles in the arctic winter, *Science, 261*, 1130-1134, 1993.

9. Acronyms and Abbreviations

AASE	Airborne Arctic stratospheric Expedition
ACATS	Airborne Chromatograph for Atmospheric Trace Species
AEC	Atomic Energy Commision
AGASP	Arctic Gas and Aerosol Sampling Program
AL	Aeronomy Laboratory, Boulder, Colorado (ERL)
ALE/GAGE	Atmospheric Lifetime Experiment/Global Atmospheric Gases Experiment
ALIAS	aircraft laser infrared absorption spectrometer
ALT	Alert, Northwest Territories, Canada
ANSTO	Australian Nuclear Science and Technology Organization
AOML	Atlantic Oceanographic and Meteorological Laboratory, Miami, Florida (ERL)
ARL	Air Resources Laboratory, Silver Spring, Maryland (ERL)
ARM	Atmospheric Radiation Measurement program
ASA	Antarctic Support Associates, Inc.
ASASP	Active Scattering Aerosol Spectrometer Probe
ASHOE	Airborne Southern Hemisphere Ozone Experiment
ASL	above sea level
ASR	aerosol solar radiation
ATLAS	airborne turnable laser absorption spectrometer
ATMOS	Atmospheric Trace Molecule Spectroscopy
BAO	Boulder Atmospheric Observatory
BC	black carbon
BSRN	Baseline Surface Radition Network
BRW	Barrow Observatory, Barrow, Alaska (CMDL)
CAF	Clean Air Facility
CAMS	Control and Monitoring System
CART	Cloud And Radiation Testbed
CD-ROM	compact disk-read only memory
CFC	chlorofluorcarbon
CFC-11	trichlorofluoromethane
CFC-12	dichlorodifluoromethane
CGO	Cape Grim, Tasmania, baseline station
CIRES	Cooperative Institute for Research in Environmental Sciences, University of Colorado, Boulder
CMDL	Climate Monitoring and Diagnostics Laboratory (ERL)
CN	condensation nuclei
CNC	condensation nucleus counter
CSIRO/DAR	Commonwealth Scientific and Industrial Research Organization/Division of Atmospheric Research, Australia
CSU	Colorado State University, Fort Collins, Colorado
DAS	data acquisition system
DB	direct-beam [irradiance]
DEW	distant early warning
DMS	dimethyl sulfide
DOE	Department of Energy
DOY	day of year
DU	Dobson units
ECC	electrochemical concentration cell
ECD	electron capture detector
EC-GC	electron capture-gas chromatograph
ECMWF	European Center for Medium-Range Weather Forecasts
EML	Environmental Measurements Laboratory
ENSO	El Niño/Southern Oscillation
ERL	Environmental Research Laboratories, Boulder, Colorado (NOAA)

FID	flame ionization detector
FPD	flame photometric detector
FTIR	Fourier transform infrared (spectroscopy)
FTS	File Transfer System
FW	filter wheel
GAGE	Global Atmospheric Gases Experiment
GAW	Global Atmosphere Watch
GC	gas chromatograph
GE	General Electric
GMT	Greenwich Mean Time
GOES	Geostationary Operational Environmental Satellite
GSA	General Services Administration
HAO	High Altitude Observatory
HCFC	hydrochloroflurocarbon
HCFC-22	$CHClF_2$
HCFC-141b	CH_3CCl_2F
HDFC-142b	CH_3CClF_2
H-1211	$CBrClF_2$
H-1301	$CBrF_3$
HFC	hydroflurocarbon
HP	Hewlett-Packard
HST	Hawaii standard time
INSTAAR	Institute for Arctic and Alpine Research, University of Colorado, Boulder
IR	infrared
ISWS	Illinois State Water Survey
JPL	Jet Propulsion Laboratories
KUM	Cape Kumukahi, Hawaii
LAN	local area network
LEADEX	Leads Experiment
LEAPS	Low Electron Attachment Potential Species
LES	Lincoln Experimental Satellite
LLNL	Lawrence Livermore National Laboratories
LOWESS	Locally Weighted Least Squares
LPM	liters per minute
LST	local standard time
MAKS	Martin and Kitzis Sampler (portable air sampler)
MAESA	Measurements for Assessing the Effects of Stratosperic Aircraft
METOP	Meteorological Operational Mission (polar satellite series)
MLO	Mauna Loa Observatory, Hawaii (CMDL)
MLOPEX	MLO Photochemical Experiment
MOA	Memorandum of Agreement
MRI	Meteorology Research, Inc.
MS	mass spectrometer
MSL	mean sea level
NADP	National Atmospheric Deposition Program
NASA	National Aeronautics and Space Administration
NAVSWC	Naval Surface Warfare Center, Department of Defense
NCAR	National Center for Atmospheric Research
NDSC	Network for the Detection of Stratospheric Change
NDIR	non-dispersive infrared analyzer
NIP	normal incidence pyrheliometer
NOAA	National Oceanic and Atmospheric Administration (U.S. Department. of Commerce)
NOAH	Nitrous Oxide And Halocarbons Division (CMDL)
NSF	National Science Foundation

NWR	Niwot Ridge, Colorado
NWS	National Weather Service
NOS	National Ocean Service
o.d.	outside diameter
OGIST	Oregon Graduate Institute of Science and Technology
OH	hydroxyl radical
ONR	Office of Naval Research
PBL	planetary boundary layer
PC	personal computer
PI	Principal investigator
PMEL	Pacific Marine Environmental Laboratory (ERL)
PMOD	Physikalisch-Meteorologisches Observatorium Davos (World Radiation Center)
PSP	Precision Spectral Pyranometer
QBO	quasi-biennial oscillation
RASS	Radio Acoustic Sounding System
RITS	Radiatively Important Trace Species
RGA	reduction gas analyzer
RSD	residual standard deviation
RV	Recreational vehicle
SBUV	solar backscattered ultraviolet (satellite ozone instrument)
SCS	Soil Conservation Service, Anchorage, Alaska
s.d.	standard deviation
SESAME	Second European Stratospheric Arctic Middle Latitude Experiment
SEASPAN	SEAREX South Pacific Aerosol Network
SIO	Scripps Institution of Oceanography
SMO	Samoa Observatory, American Samoa (CMDL)
SOI	Southern Oscillation Index
SPADE	Stratospheric Photochemistry, Aerosols, and Dynamics Expedition
SPO	South Pole Observatory, Antarctica (CMDL)
SRB	surface radiation budget
SRF	Solar Radiation Facility (CMDL)
SRF	spectral response function
SST	sea-surface temperature
STP	standard temperature and pressure (0° and 1 atm)
TDLS	tunable diode laser spectroscopy
TOMS	Total Ozone Mapping Spectrometer
TSI	Thermo Systems Incorporated
TSL	Technical Services Laboratory
UARS	Upper Atmosphere Research Satellite
UCI	University of California, Irvine
UPS	uninteruptable power supply
URAS	[a commercial CO_2 analyzer]
URI	University of Rhode Island
USDA	United States Department of Agriculture
USGS	United States Geological Survey
UT	universal time
UV	ultraviolet
UVB	ultraviolet B spectral band
VMS	Virtual Memory System
WD	wind direction
WS	wind speed
WOCE	World Ocean Circulation Experiment
WHOI	Woods Hole Oceanographic Institute
WMO	World Meteorological Organization

*U.S. GOVERNMENT PRINTING OFFICE:1995-673-018/00075